Western Kentucky University

TopSCHOLAR®

Fall 2019

Influence of Spring Flow Reversals on Cave Dissolution in a Telogenetic Karst Aquifer, Mammoth Cave, KY

Chelsey Kipper

INFLUENCE OF SPRING FLOW REVERSALS ON CAVE DISSOLUTION IN A
TELOGENETIC KARST AQUIFER, MAMMOTH CAVE, KENTUCKY

A Thesis
Presented to
The Faculty of the Department of Geography and Geology
Western Kentucky University
Bowling Green, Kentucky

In Partial Fulfillment
Of the Requirements for the Degree
Master of Science

By
Chelsey Kipper

December 2019

INFLUENCE OF SPRING FLOW REVERSALS ON CAVE DISSOLUTION IN A TELOGENETIC KARST AQUIFER, MAMMOTH CAVE, KENTUCKY

Date Recommended _11/14/2019_

_____
Dr. Patricia Kambesis, Thesis director

_____
Dr. Jason Polk

_____
Dr. Rickard Toomey

_____
Dean, Graduate Studies and Research   Date
_11/26/19_

Dedication

To women in science

Together, we are powerful.

ACKNOWLEDGMENTS

You've helped me to be comfortable with who I am, and you taught me how to have fun again. As long as I have a truck, you'll always have a place to sit.

Lastly, to Brian. You were here with me through this whole process. From those blistering hot days, to the days where we couldn't feel our fingers, through the sweat, and the mud, the long, dark hikes, the conversations about whatever was on our minds, and lots and lots of bickering. There's no one else that I would rather have gone through this adventure with. You are my rock — and coming from a geologist, that's the highest praise.

TABLE OF CONTENTS

LIST OF FIGURES

LIST OF EQUATIONS

LIST OF TABLES

INFLUENCE OF SPRING FLOW REVERSALS ON CAVE DISSOLUTION IN A TELOGENETIC KARST AQUIFER, MAMMOTH CAVE, KENTUCKY

Chelsey Kipper   December 2019   189 Pages

Directed by: Pat Kambesis, Jason Polk, and Rick Toomey

Department of Geography and Geology   Western Kentucky University

An often overlooked connection between karst groundwater systems and surface water is spring flow reversal, the flow of river water into karst springs caused by changes in hydraulic gradient. Karst aquifers are subject to the intrusion of river water when the hydraulic head of a base level river is higher than the hydraulic head of a base level spring. When this occurs, the flow out of the spring reverses, allowing river water to enter base level conduits. River water thus becomes a source of recharge into karst basins, transporting both valuable nutrients and harmful contaminants into karst aquifers. The rapid recharge of meteoric water, brief groundwater residence times, and the interconnection of surface and subsurface waters through a variety of karst features necessitates studying groundwater and surface water in karst landscapes as a unified system. This study examines the influence of spring flow reversal on cave dissolution in a telogenetic karst aquifer in Mammoth Cave, Kentucky.

Spring flow reversals in Mammoth Cave National Park (MCNP) were first recorded nearly one-hundred years ago, but a high-resolution study measuring the effects of spring flow reversals on dissolution in MCNP, or any other telogenetic karst system, had not been conducted until recently. In this study, high-resolution data were collected for pH, SpC, temperature, and stage, as well as weekly samples for major ion concentrations, alkalinity, and carbon isotopes, from June 2018 to December 2018. Surface water and groundwater data were used to quantify the complex hydrologic

processes associated with the spring flow reversals, including seasonal changes in karst geochemistry and dissolution taking place between the Green River, River Styx Spring, and Echo River Spring. Data show distinct changes in geochemical parameters as flow reversals occur, with temperature being the principal indicator of flow direction change. During this study, all ten stable reverse flows coincided with increased discharge from the Green River Dam. The predominant drivers of dissolution in the River Styx and Echo River karst basins are storm events and seasonal changes in the hydrologic regime, rather than seasonal CO_2 production, normal baseflow conditions, or stable reverse flow events. Estimated dissolution rates generally show that stable reverse flows contribute no more to dissolution than normal baseflow conditions – the highest amount of dissolution during a single stable reverse flow was only 0.003 mm. This is contrary to flow reversal studies in an eogenetic karst system in Florida, which estimated 3.4 mm of wall retreat during a single spring flow reversal. These contrasting results are likely due to significant differences in pH of river water, matrix porosity of the bedrock, basin morphology, and flow conditions.

1. Introduction

Karst landscapes are formed due to the dissolution of underlying bedrock (Ford and Williams 2007). Karst landscapes typically occur in carbonates, such as limestone or dolostone, but may also occur in evaporites, such as gypsum and halite and, to a lesser extent, in other rocks. Approximately 20% of all land on ice-free continents is a karst landscape. These regions contain aquifers that store and transport large volumes of groundwater.

It is essential to fully understand karst groundwater chemistry and flow processes because karst landscapes are important sources of drinking water and are home to complex and sensitive ecosystems. Karst aquifers are the primary supply of water for 20-25% of the world's population (Ford and Williams 2007; Anaya et al. 2014). Furthermore, a variety of animals, insects, and microbes live in karst landscapes. These subterranean ecosystems are vulnerable to changes in water chemistry and water quality (Palmer 2007).

Karst groundwater flow processes are especially complex due to the rapid infiltration of surface water through sinkholes and, in the case of flow reversals, through springs. A spring is typically a point of discharge; but under certain conditions, its direction of flow may reverse, and the spring becomes a point of recharge. This phenomenon occurs when a spring discharges into a region's base level river.

This study focuses on spring flow reversals that occur between two springs, Echo River Spring and River Styx Spring, and the Green River, in South Central Kentucky's Mammoth Cave National Park (MCNP). Both springs are base level, conduit springs that discharge groundwater at nearly the same elevation from their respective drainage basins

into the Green River, the regional base level river. Flow reversals occur when the stage of the Green River rises, causing river water to backflow into the spring and into Mammoth Cave. The Green River stage varies depending on dam control, precipitation, and season.

Spring flow reversals can occur in both River Styx Spring and Echo River Spring for short periods of time in response to flash storm events. Additionally, sustained high-stage events of the Green River, commonly associated with the lowering of the Green River Lake stage or multiple precipitation events, can cause spring flow reversals to occur in River Styx Spring for prolonged episodes. Flow reversals that occur for extended periods of time (days to weeks) have been termed "stable reverse flows" (Trimboli et al. 2016; Trimboli and Toomey 2019). During stable reverse flows, river water flows into River Styx Spring, flows over a drainage divide between the River Styx and Echo River basins, then flows out of Echo River Spring, and flows back to the Green River.

This study quantifies the geochemical changes associated with flow reversals in the base level karst aquifer of Mammoth Cave National Park using high-resolution collection of hydrogeochemical parameters and the measurement of major ions and alkalinity. These data provide insights about the influence of spring flow reversals on dissolution and conduit enlargement in telogenetic karst systems. This study addresses the following questions:

- How does the geochemistry change in response to an individual flow reversal event in River Styx and Echo River Springs?

- How do spring flow reversals affect cave dissolution in a telogenetic karst system?

- What are the seasonal changes associated with flow reversals in River Styx and Echo River Springs?

- What are the major sources of carbon in the River Styx and Echo River karst basins?
  - Do carbon sources change seasonally or during flow reversals?

This information is particularly significant because spring flow reversals may be significant contributors to conduit enlargement and cave formation in telogenetic karst systems, as seen in eogenetic karst systems (Gulley et al. 2011; Gulley et al. 2013). Additionally, spring flow reversals affect cave ecosystems by adding dissolved organic carbon and oxygen into the groundwater, providing sources of food and energy, and introducing contaminants into the ecosystem (Trimboli and Toomey 2019).

2. Literature Review

2.1 Overview of Karst

Karst evolution can be characterized by the interactions of five major elements: rock, solvent, structure, gradient, and time. Rock is the lithologic element from which karst is formed. Carbonates (e.g. limestone and dolomite) are the most common karst-producing lithologies. Karst landscapes develop due to the dissolution of soluble rock. Dissolution occurs when a solvent interacts with minerals in the rock, (e.g. the mineral calcite, $(CaCO_3)$ in limestone) and causes the mineral components to go into solution. Climate, vegetation, and the chemical makeup of the lithological formations can all influence the pH of the solvent, therefore either increasing or decreasing solubility. The structural element controls how water flows through a landscape by defining preferential pathways along fractures, faults, joints, and bedding planes. Additionally, structural openings and dips in the lithology, as well as surficial topography, produce a hydraulic gradient. This hydraulic gradient influences the direction of flow. Both the structure and gradient elements govern the spatial distribution and geometry of karst landscapes. Lastly, karst development requires time. For example, karst development can be affected by climatic and fluvial changes on time scales of one-hundred-thousand to one million years or tectonic and stratigraphic changes on time scales of one million to one-hundred-million years (Palmer 2007). It is essential to consider the role that time plays in karst evolution, even though it is difficult to be precise regarding the timescale of karst evolution, because rates of denudation vary depending on climate and structural influences over time.

2.1.1 Eogenetic vs. Telogenetic Karst

The strata that comprise carbonate aquifers may contain both primary porosity and secondary porosity. Primary porosity is the amount of space in between the individual mineral grains of a rock matrix. Secondary porosity is porosity created in rocks by weathering (chemical or mechanical) or structurally controlled regional fracturing (Freeze and Cherry 1979; Hiscock 2005). A rock's percentage of primary porosity is affected by the composition, shape, and arrangement of the individual minerals; whereas rock's percentage of secondary porosity within the strata is dependent on time and extent of burial (Choquette and Pray 1970; Moore 1989). In carbonate aquifers, primary porosity controls the storage capacity of the aquifer; secondary porosity controls groundwater flow (Ford and Williams 2007). Water in an aquifer with high secondary porosity flows along fractures, faults, bedding plane partings, or solutionally enlarged conduits. This flow regime is turbulent; therefore, Darcy's law does not apply.

Porosity and permeability in carbonate aquifers are affected by time and burial. Choquette and Pray (1970) defined three stages of post-depositional carbonate porosity based on time and burial: eogenetic, mesogenetic, and telogenetic (Figure 2.1). The eogenetic stage describes carbonates that have not been buried and have had exposure to surficial processes shortly following deposition. The mesogenetic stage describes carbonates unaffected by surficial processes during deep burial. Karst development in mesogenetic carbonates have hypogenic origins. The telogenetic stage describes carbonate rocks that have been deeply buried and were later exposed to surficial processes. Most karst can be categorized as eogenetic or telogenetic, since 80-85% of karst landscapes develop due to surficial processes (Florea and Vacher 2006; Palmer

2007). Most karst in Florida is eogenetic karst landscape; whereas the karst of MCNP is an example of a telogenetic karst landscape.

Diagenetic stages in the evolution of a limestone
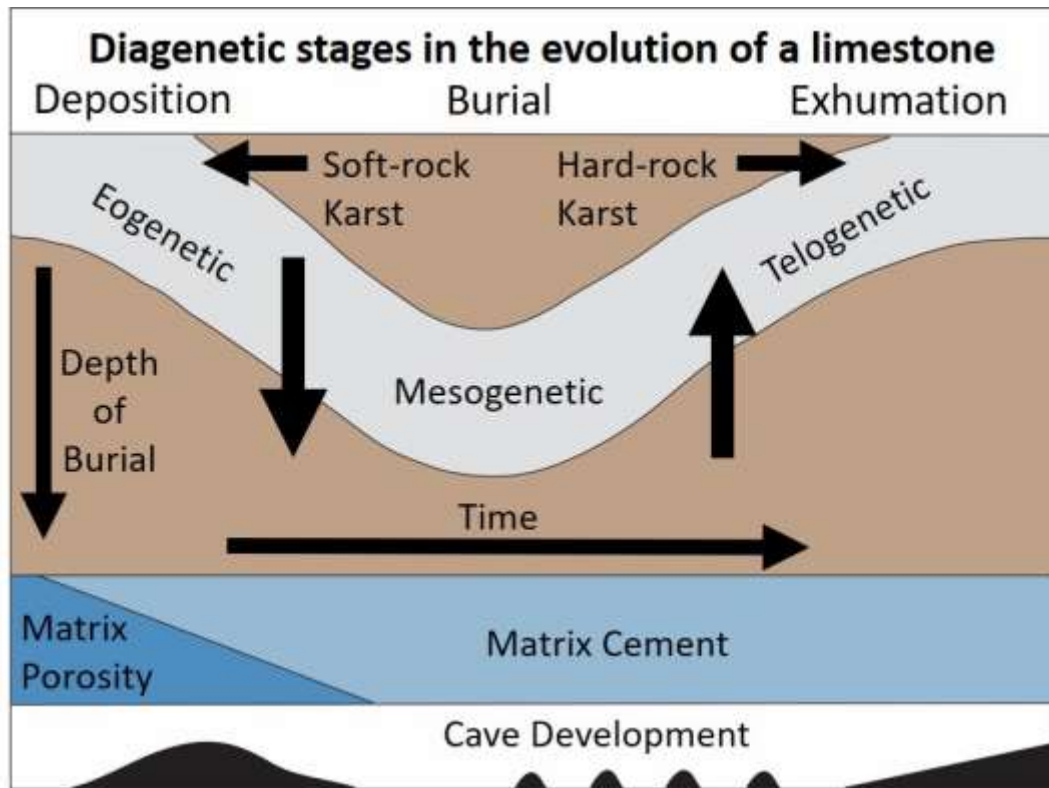
Figure 2.1 Stages of post-depositional porosity
(Modified from Grimes 2002)

Eogenetic karst aquifers have high porosities, ranging from 20-40% and permeabilities of $10^{-12} – 10^{-14}$ m^2 (Florea and Vacher 2006). The porosity and permeability of telogenetic aquifers are significantly lower. For example, the average porosity and permeability of the limestone that makes up Mammoth Cave are 2.4% and $10^{-17.7}$, respectively (Worthington et al. 2000). In eogenetic karst, the diagenetic processes of dissolution and cementation can transform matrix/primary porosity to secondary porosity. This transformation enhances the permeability of the aquifer by introducing an interconnected series of small cavities. In the Mammoth Cave Aquifer, matrix permeability is insufficient for groundwater flow. Solutionally enlarged structural

6

features (e.g. fractures and bedding plane partings) are the major control, accounting for 99% of total flow in the aquifer (Florea and Vacher 2006).

2.1.2 Groundwater Flow in Telogenetic Karst

Groundwater in telogenetic karst aquifers is recharged through the epikarst, sinkholes, and sinking and losing streams (Figure 2.2.2). The epikarst is an area, either covered by soil near the surface or exposed at the surface, where meteoric water is transported and stored in the vadose zone. The epikarst is characterized by solutionally enlarged fissures and pores due to infiltration of solutionally aggressive water through CO_2-rich soils. The soils in the epikarst store water during high precipitation events. As water is transported laterally to large vertical drains, the epikarst recharges karst aquifers (Palmer 2007; Jones 2013). Sinkholes are autogenic recharge sources, in which groundwater originates from precipitation directly onto the karst landscape. Sinking streams are allogenic recharge sources, in which the groundwater's origin is from non-karstic areas or karstic areas containing thin insoluble layers (e.g. chert, shale, or low-solubility limestones) and flows overland before encountering karst. Allogenic water tends to be more solutionally aggressive than autogenic water (Palmer 2007). Water in karst aquifers is piped through a network of underground conduits. The high velocities of these flows and the interconnectedness of karst systems allow surface water to drain into the aquifer rapidly; this makes karst groundwater especially vulnerable to contamination.
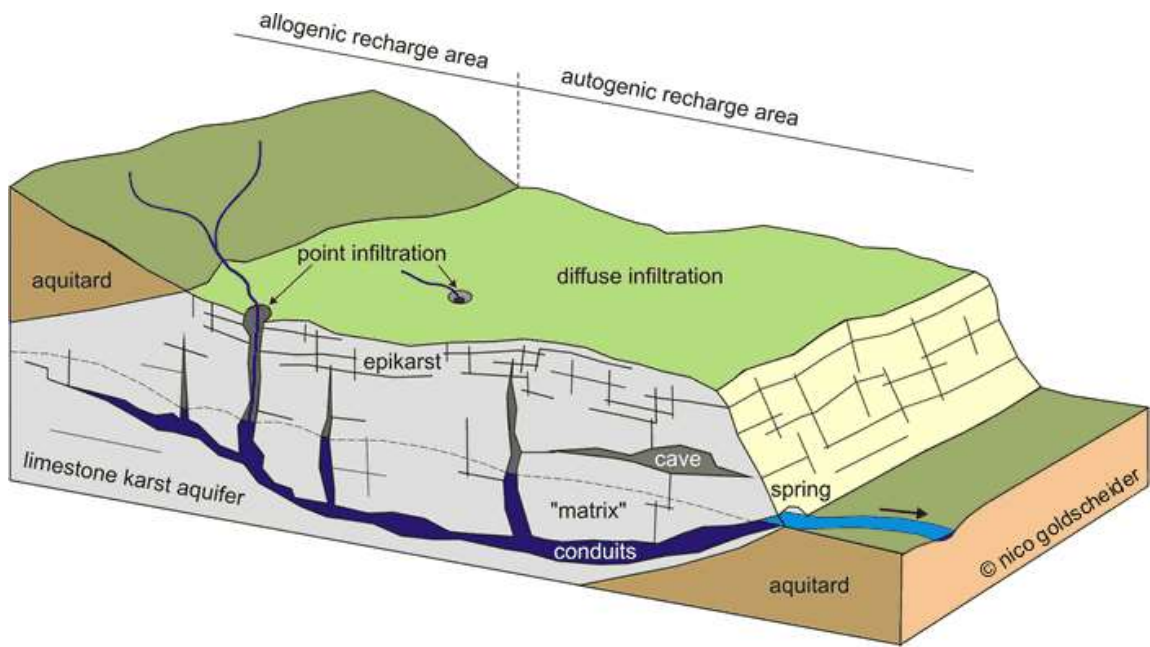
Figure 2.2 Diagram of a telogenetic karst aquifer
(Source: Goldscheider and Drew 2007)

Once groundwater enters the karst system, it travels through fractures, conduits, or cave passages until it eventually discharges from springs. Springs are points of discharge in groundwater basins that occur according to regional base level, stratigraphic contacts, or faults (Quinlan and Ewers 1989). Quinlan and Ewers (1989, 76) describe springs as "ephemeral, transient features" that "migrate to lower elevations as the base level is lowered" over time scales greater than thousands of years. Echo River Spring and River Styx Spring are only two of more than eighty-one springs that currently discharge into the Green River in South Central Kentucky (Hess et al. 1989). These springs are classified as base level springs, because they flow into the hydrologic base level of the area (Palmer 2007).

Flow in karst springs ranges from diffuse flow to conduit flow (Figure 2.3). Diffuse flow occurs through openings (e.g. fractures, joints, or bedding planes) that are small and measured in millimeters to centimeters. Diffuse flow generally is laminar.

Diffuse flow springs are more consistent over time regarding their temperature, water geochemistry, and discharge. Also, diffuse flow springs are only slowly affected by precipitation.

In contrast to diffuse flow, conduit flow is measured in centimeters to meters, and travels rapidly through solutionally enlarged openings. Conduit flow springs are characterized by a turbulent flow regime. A turbulent flow regime is characterized by chaotic, nonparallel flow (i.e. the formation of eddies). Precipitation affects conduit flow springs rapidly, causing substantial changes in discharge, temperature, and water chemistry (Shuster and White 1971; Hess et al. 1989; Ford and Williams 2007). Most of the springs that discharge into the Green River in MCNP, including Echo River and River Styx Springs, are conduit flow springs (Quinlan and Ewers 1989).
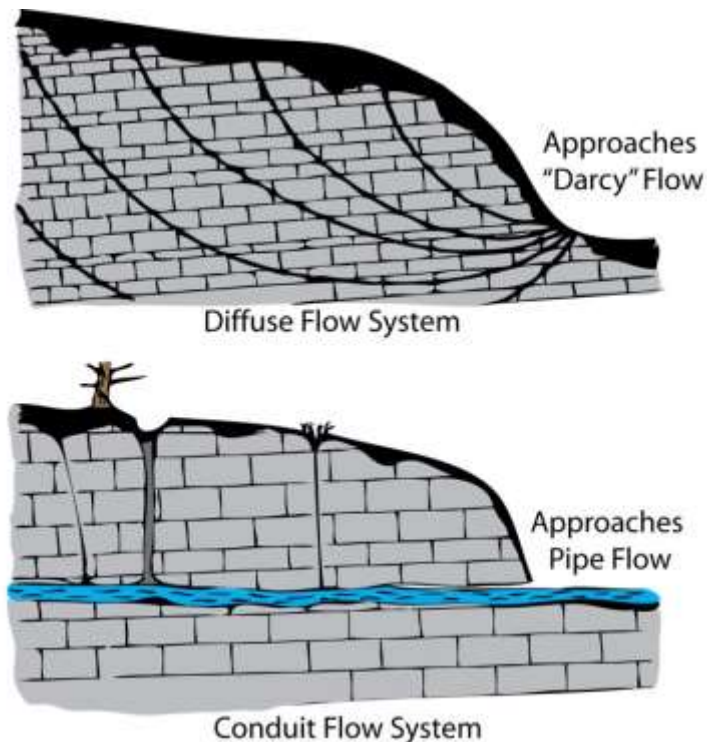
Figure 2.3 Diffuse flow and conduit flow systems
(Modified from Shuster and White 1971)

Sources of recharge in the Mammoth Cave karst aquifer (Figure 2.4) are:

1) sinking streams on the southeastern edge of the sinkhole plain; 2) precipitation collected in the southeastern sinkhole plain; 3) water from the perched Haney Limestone and Big Clifty Sandstone aquifers that discharges from springs along the edge of the caprock and flows into lower aquifers through vertical shafts; 4) precipitation in the karst valleys that is collected and transported by small sinkholes; 5) precipitation and surface water stored in the epikarst; 6) surface flow across areas underlain by the Big Clifty formation that sinks at limestone contact; 7) river water, as the Green River backfloods into base level aquifers; and 8) river water during spring flow reversal events (Hess et al. 1989; White and White 2017). Spring flow reversals occur when the hydraulic head of the river is greater than the spring (Hess et al. 1989; Ford and Williams 2007). This causes the flow direction of the spring to reverse, and river water to enter the karst system. Flow reversals occur when rivers and the springs that discharge into them are at similar elevations. When the hydraulic head of the Green River decreases below the hydraulic head of the spring, the spring returns to base flow, and the surface water returns to the river (Ford and Williams 2007).

Due to the significant differences in porosity and permeability, spring flow hydrographs of eogenetic karst vary significantly from those of telogenetic karst. For example, storm events in telogenetic karst have rapid responses when compared with eogenetic karst. Spring flow hydrographs of eogenetic springs in west-central Florida show little to no response to storm events; they do, however, show significant seasonal and decadal responses. This pattern of eogenetic spring flow response is due to the lack

of connectedness of conduits in this system and diffuse recharge from the surface (Florea and Vacher 2006).
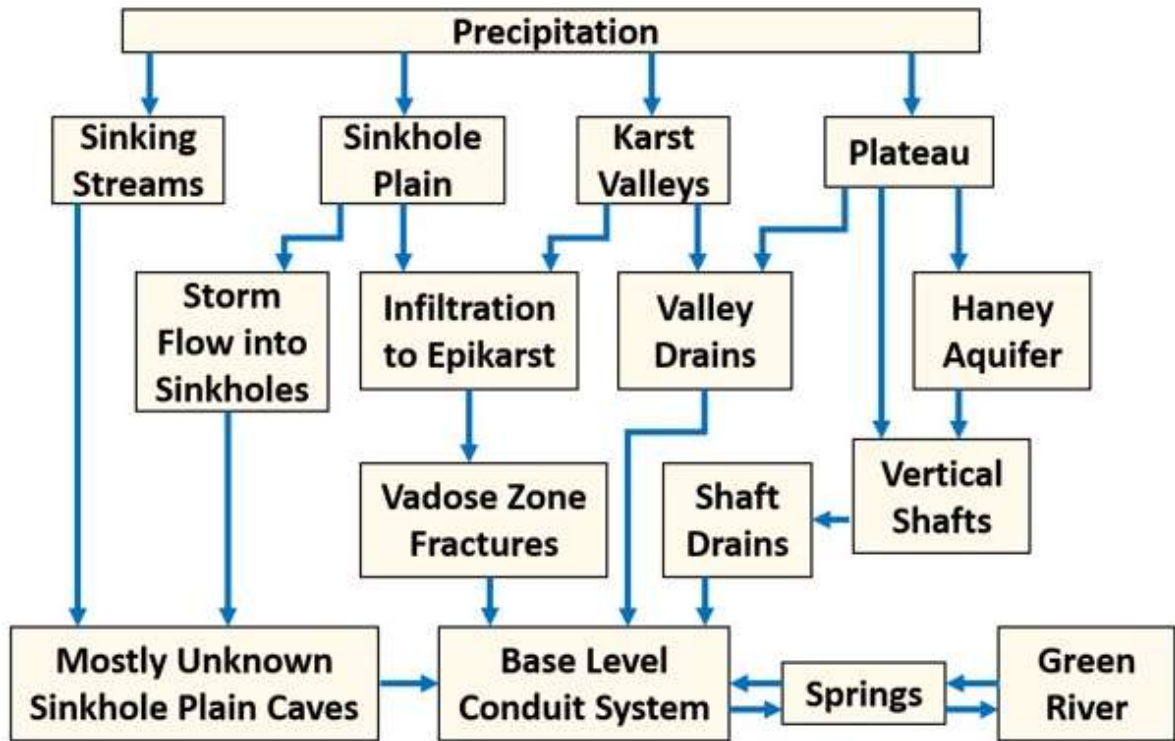
Figure 2.4 Conceptual model showing flow paths in the Mammoth Cave area Springs eventually discharge into the Green River, but the Green River can backflood into springs and recharge the aquifer (Modified from White and White 2017).

2.2 Mammoth Cave National Park

Well-developed karst underlies 25% of the state of Kentucky and approximately 55% of the state is underlain by carbonate rocks with karst forming potential (Kentucky Geological Survey 2013). Most of Kentucky's karst is concentrated in two areas of the state: the Inner Bluegrass karst area, located beneath the cities of Lexington and Frankfort; and the Western Pennyroyal karst area, which encompasses many cities in western and central Kentucky, including Fort Knox, Bowling Green, and Hopkinsville

(Figure 2.5). The Western Pennyroyal karst area lies on the edge of the Illinois Basin

(White 1989), a depositional basin developed in the Paleozoic era (Kolata and Nelson

1990). Mammoth Cave is located in the Western Pennyroyal karst area of south-central
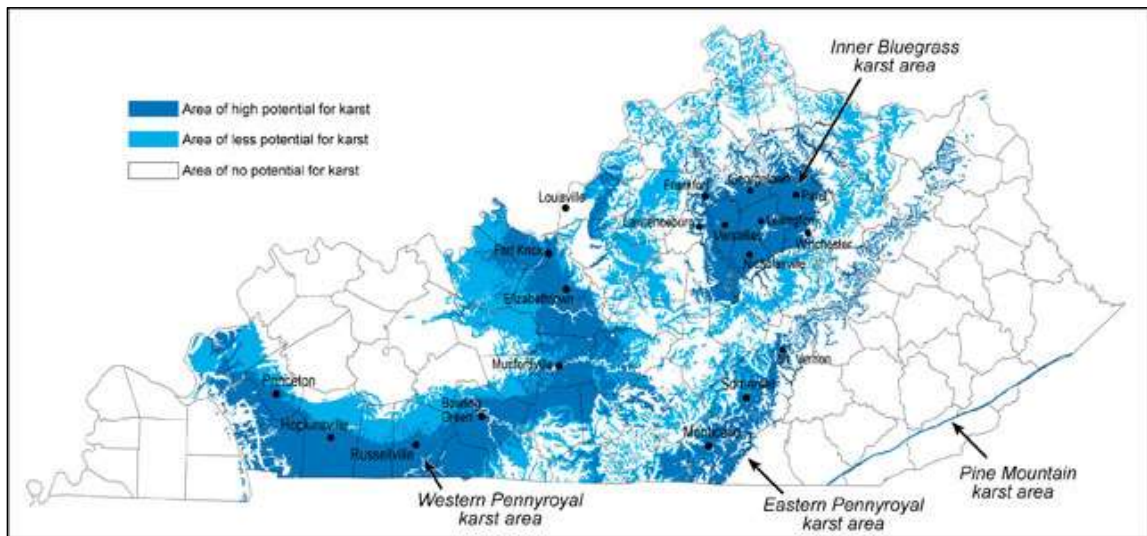
Kentucky.

Figure 2.5 Karst distribution in Kentucky
(Source: KGS 2013).

Mammoth Cave became a national park in 1941 and contains nearly 53,000 acres

of protected land. The park is located 145 kilometers south of Louisville and 30

kilometers northeast of Bowling Green, in one of the most cave-dense areas of the state

(Figure 2.6). MCNP became a World Heritage Site in 1981 and an International

Biosphere Reserve in 1990. Fifty-two troglobitic species, those that are adapted to cave

environments and spend their whole life inside caves, are present in Mammoth Cave

(Toomey et al. 2017). MCNP is characterized as a deciduous forest in a humid sub-

tropical climate (Hess and White 1989a; Meiman 2006).
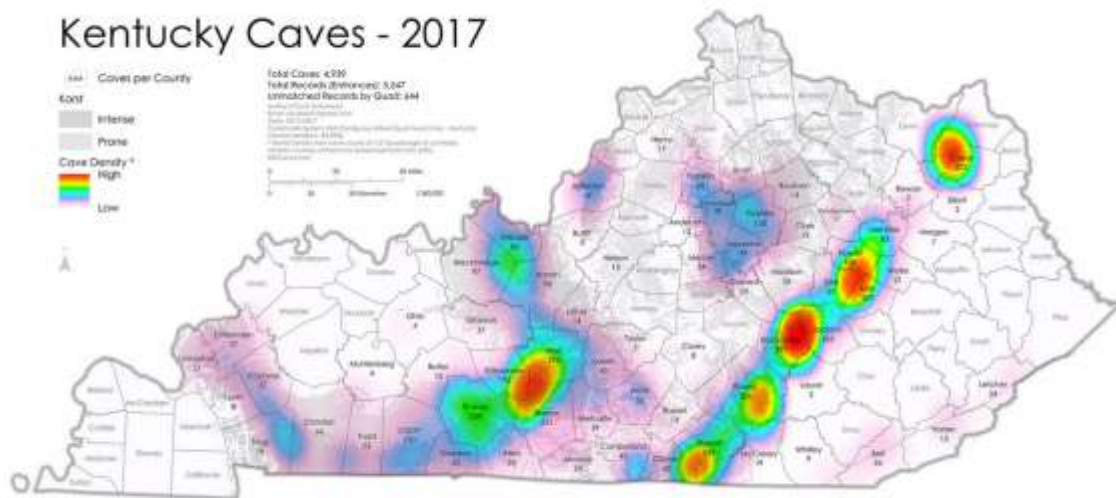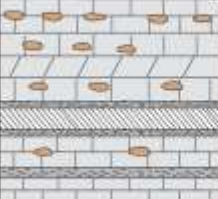
Figure 2.6 Cave density in Kentucky
MCNP is located in Edmonson, Hart, and Barren counties.
(Source: Sutherland 2017).

2.2.1 Geology of Mammoth Cave

South Central Kentucky is underlain by Mississippian age, Meramecian and
Chesterian series, sedimentary rocks (Figure 2.7). The Pennsylvanian age Caseyville
Sandstone can be found on ridge tops in some areas of South Central Kentucky (Hess et
al. 1989). These sedimentary rocks gently dip, less than one degree, northwest toward the
center of the Illinois Basin (Palmer 1981). The passages of Mammoth Cave developed in
the St. Louis, St. Genevieve, and Girkin Limestones.

Figure 2.7 Stratigraphy of South Central Kentucky
(Modified from Hess et al. 1989)

The St. Louis Limestone is a 60-meter-thick formation of interbedded fine to medium grained limestone, thin layers of shale, and beds of flat chert nodules (Palmer 1981; Hess et al. 1989; Soto and Pate 2016). The Lost River Chert is located near the top of the St. Louis formation and governs flow of sinking streams and sinkhole development in the Sinkhole Plain (Hess et al. 1989). The Corydon Ball Chert, within the St. Louis formation and just below the Lost River Chert, can also be seen in the Mammoth Cave area (May et al. 2005). Above the St. Louis Limestone is the St. Genevieve Limestone, a 35-meter-thick formation of interbedded, very fine to medium grained limestone and very fine-grained dolomite. The Girkin Limestone contains the uppermost levels of the cave.

14

The Girkin is a 40-meter-thick formation consisting of interbedded limestone, shales, and siltstones. The Girkin limestone is separated into upper fossiliferous layers and lower oolitic layers. The Big Clifty Sandstone is a 15 to 18-meter-thick formation consisting of interbedded sandstone, siltstone, and shale and is the lower portion of the resistant caprock that preserves the Mammoth Cave. The Haney Limestone is a carbonate unit above the Big Clifty Sandstone and contains perched aquifers, which are a source of recharge for the Mammoth Cave aquifer (Palmer 1981; Hess et al. 1989; Soto and Pate 2016).

The geomorphology of the Mammoth Cave area is dependent on its stratigraphy (Figure 2.8). Mammoth Cave is situated in the Chester Cuesta, a gently dipping plateau that ends in a steep slope called the Dripping Springs Escarpment. The Chester Cuesta, also known as the Chester Upland, is named because it is underlain by Chesterian rocks. The Green River has incised a large valley in the Chester Cuesta and is presently flowing through the lower St. Genevieve and upper St. Louis limestones. Smaller karst valleys are also present within the Chester Cuesta. During the Quaternary period, water was diverted by continental glaciers from the Teays River to the Ohio River Valley, causing rapid erosion of these steep walled karst valleys in the Chester Series siliciclastics (Granger et al. 2001). When the Green River exposed the underlying limestone, water from the adjacent rivers were pirated underground by sinkholes and the valleys became dry (Meiman 2006).
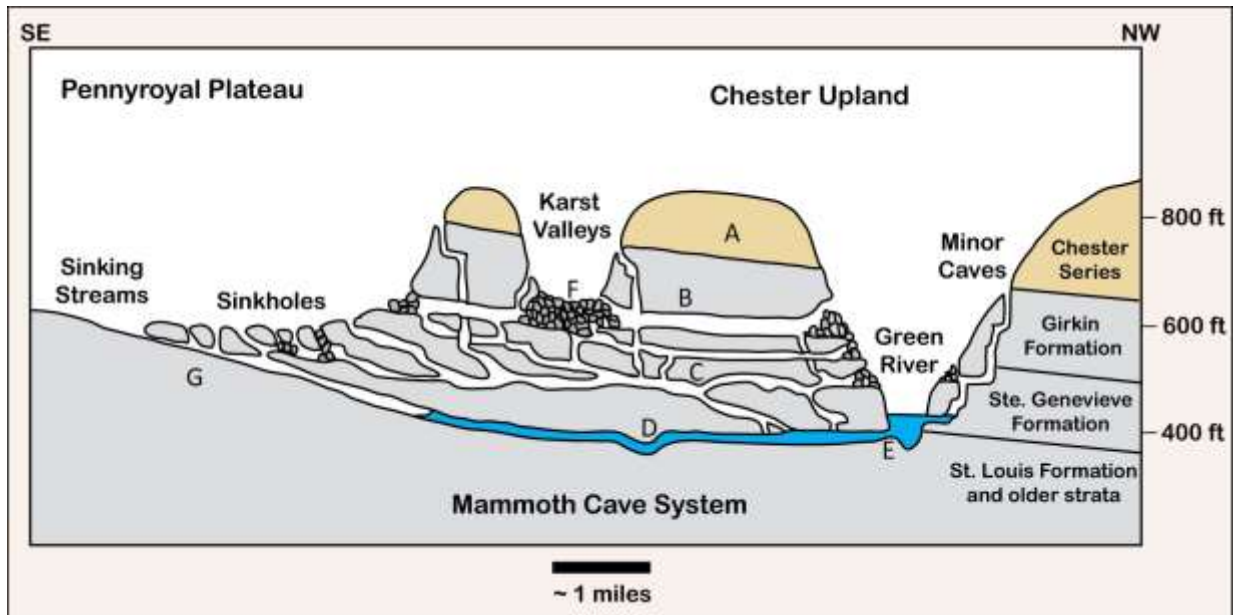
Figure 2.8 Profile of Mammoth Cave System
A) Big Clifty Sandstone (caprock) and Haney Limestone contain perched aquifers that discharge along the edge of the caprock. B) Upper cave levels that are partially filled with sediment. C) Lower cave levels. D) Water-filled or active conduits.
E) Backflooding can occur in base level springs discharging into the Green River.
F) Sinkholes draining karst valleys. G) The St. Louis Limestone and interbedded chert underlie the southeastern sinkhole plain (Modified from Palmer 1981).

The strata of South Central Kentucky dip 1°-2° towards the center of the Illinois Basin, in the northwest direction (Palmer 2016). Due to the dip of the rocks, the Girkin, St. Genevieve, and St. Louis Limestones are exposed south of the Dripping Springs Escarpment. This area is known as the Pennyroyal Plateau and has two physiographic settings: the Glasgow Uplands and the Sinkhole Plain. In the Glasgow Uplands, streams flow over the surface because the insoluble shale and thinly-bedded limestone units of the St. Louis act as confining units that prevent the flow of water into the karst aquifer. The surface streams flow in the northwest direction until meeting soluble units of the St. Louis limestone. At this point, the streams sink into the Mammoth Cave karst aquifer and become a significant source of recharge for many springs along the Green River. The

area between the Glasgow Uplands and the Dripping Spring Escarpment is the

Pennyroyal Sinkhole Plain, which is underlain by soluble limestones pitted with

sinkholes (Meiman 2006).

2.2.2 Karst Hydrogeology of Mammoth Cave

The Mammoth Cave Karst Aquifer is located in the Upper Green River drainage

basin (Hess et al. 1989; McClanahan 2014). The Green River is the regional hydrologic

base level of the area (Hess et al. 1989). Forty-two kilometers of the Green River flow

through MCNP and contain "one of the most diverse fish and mussel communities in the

state" (Meiman 2006, 1). The stratigraphic units that comprise the Mammoth Cave (the

Big Clifty sandstone and the Girkin, St. Genevieve, and St. Louis limestones) are incised

by the Green River. Mammoth Cave is a network of multi-level conduits in the Girkin,

St. Genevieve and St. Louis limestones (Palmer 1981; Granger et al. 2001; Soto and Pate

2016). Conduit development at Mammoth Cave is directly influenced by the Green River,

the regional base level of the Mammoth Cave Aquifer. The multiple levels in the cave are

attributed to the glacially-induced changes in base level of the Green River (Granger et

al. 2001).

According to Quinlan and Ewers (1989, 65), "No other karst area in the United

States has been as intensively studied by dye-tracing, cave mapping, potentiometric

surface mapping, and continuous monitoring of water quality and stage as the Mammoth

Cave area." Meiman et al. (2001, 179) states that the Mammoth Cave Karst Aquifer is

"the best understood conduit flow network in the world" with over five hundred dye

traces having been performed on the aquifer; however, due to Mammoth Cave's

complexity, more research is required to understand the interrelationships among the

numerous groundwater basins. Understanding these relationships will provide more

detailed information about MCNP's overall hydrogeology and important data regarding

contaminant transport by river water and groundwater.

Groundwater flow in South Central Kentucky's karst aquifers are "divisible into

groundwater basins and intervening interbasin areas" (Thrailkill 1985, 123). Groundwater

basins consist of a dendritic network of dissolved conduits, as shallow as tens of meters

to over one hundred meters below the surface. Groundwater basin divides do not align

with surface water divides (Quinlan and Ewers 1989). Flow in groundwater basins "often

passes beneath surface divides to emerge at low-level springs" (Thrailkill 1985, 179).

Furthermore, boundaries may shift or even disappear during flooding events, as water

from one groundwater basin overflows into neighboring groundwater basins (Quinlan

1989).

Mammoth Cave's groundwater basins have been delineated through dye tracing.

Most of the park's groundwater basins (Figure 2.9) were mapped using over five hundred

dye traces. The Mammoth Cave karst area includes three major basins: Hidden River

Basin, Turnhole Basin and Graham Springs Basin as well as several smaller basins,

including Echo River and River Styx. The groundwater basins of Echo River and River

Styx are small, relative to the major basins in the area, and drain the Mammoth Cave

Ridge and adjacent karst valleys south of the Green River (White and White 2017).
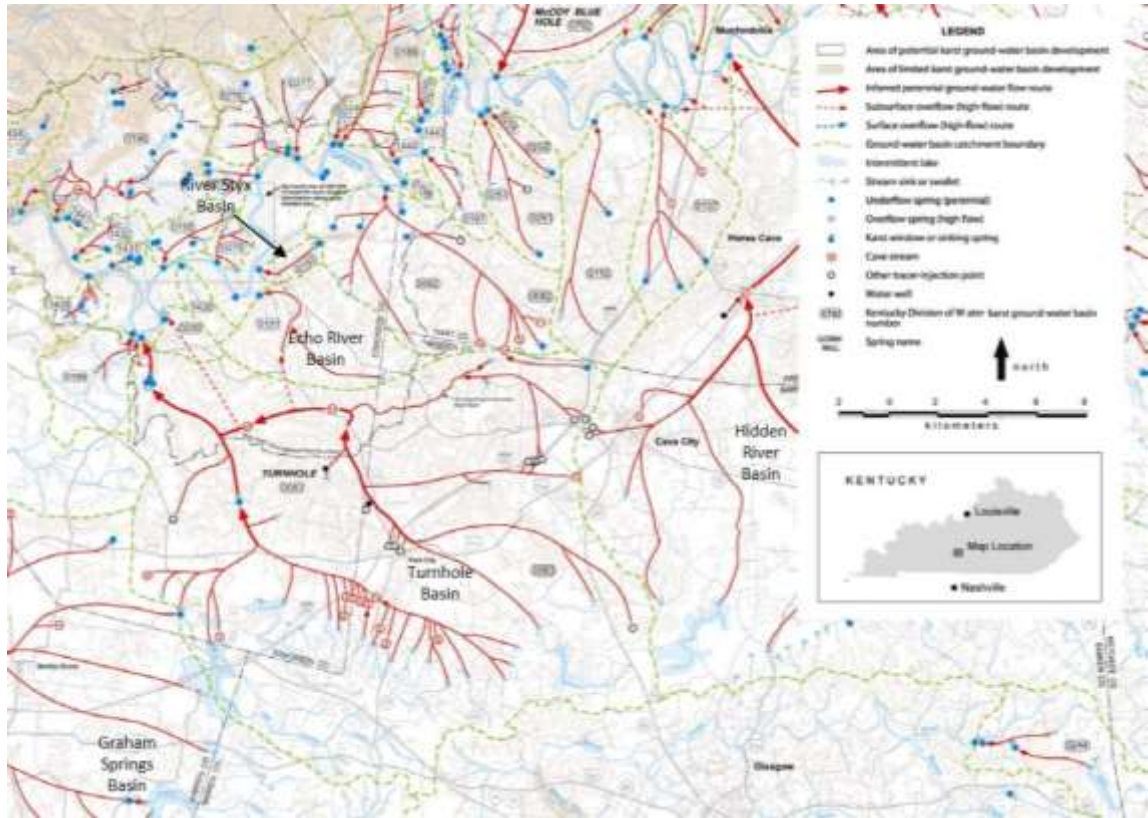
Figure 2.9 Groundwater basins of Mammoth Cave Area
(Modified from Glennon 2001)

2.3 Carbonate Geochemistry

2.3.1 Carbonate Dissolution

Karst landscapes develop due to the dissolution of soluble rock. Carbonates, (e.g. limestone and dolomite) and evaporites (e.g., gypsum) are common components of karst landscapes. Although gypsum can be found in MCNP, the geology is dominated by limestone bedrock. Limestone dissolution occurs when there is disequilibrium between the solid, liquid, and gas components involved in the dissolution reaction (White 1988; Ford and Williams 2007):

$$CaCO_3 + H_2O + CO_2 \leftrightarrow Ca^{+2} + 2HCO_3^- \hspace{3cm} \text{(Eq. 2.1)}$$

The solid component, calcite ($CaCO_3$), is the primary carbonate mineral that forms limestone. The liquid component is an aqueous solution of H_2O, dissolved ions, and dissolved gases. The primary gas component dissolved in the aqueous solution is carbon dioxide (CO_2), which increases the solubility of calcite in water (White 1988).

Calcite, a type of ionic salt, naturally dissociates into a calcium ion (Ca^{+2}) and a carbonate ion (CO_3^{-2}) when exposed to pure, deionized water (White 1988; Hess and White 1989b; Palmer 2007). However, the rate of dissociation in deionized water is low, about 14 mg/L at 25°C. The solubility of calcite in deionized water is comparable to the solubility of quartz, a silicate mineral that is very resistant to weathering, approximately 6-10 mg/L (White 1988; Ford and Williams 2007). For calcite to readily dissolve, the water must be undersaturated with respect to calcite. A solution is saturated with calcite when the products and reactants of the dissolution equation are in dynamic equilibrium. Karst waters are rarely in equilibrium; they are typically either undersaturated or supersaturated with respect to calcite (Ford and Williams 2007). Undersaturated water contains little to no calcite in solution. Undersaturated water is termed "aggressive" and will dissolve calcite. If the water is supersaturated with respect to calcite, i.e. the concentration of calcite is high, calcite will precipitate out of the solution and may form speleothems. A saturation index (SI) is used to determine whether the water is undersaturated or supersaturated. For calcite, the SI can be calculated using the equation:

$$SI_{cal} = log\frac{K_{iap}}{K_{sp}} \hspace{3cm} \text{(Eq. 2.2)}$$

where K_{sp} is calcite's solubility product, or equilibrium constant; and K_{iap} is the ion activity product, or equilibrium constant, of Ca^{+2} and CO_3^{-2} (White 1988; Anthony 1998;

20

Palmer 2007). The rate of dissolution or precipitation is related to the deviation of SI values from zero, or the chemical equilibrium (White 1988; Anthony 1998). If the saturation index of calcite is equal to zero, calcite is in equilibrium with the water and no dissolution or precipitation will occur. If the SI is negative, the water is undersaturated and dissolution will occur. If the SI is positive, the water is supersaturated and calcite precipitation will occur (Allaby 2013). Saturation with respect to calcite varies due to storm events and fluctuations in CO_2 partial pressure related to seasonal changes. Previous studies have shown waters discharging from River Styx and Echo River karst basins are generally undersaturated with respect to calcite (Hess and White 1993; White and White 2017).

Epigenic karst landscapes (e.g. the karst of MCNP) form due to the influence of surficial hydrologic processes. Limestone dissolution in epigenic karst typically occurs due to carbonic acid. Carbonic acid (H_2CO_3) forms when CO_2 gas dissolves in water (White 1988; Hess and White 1989b; Palmer 2007). Sources of dissolved CO_2 are the atmosphere and soil. As of January 2019, the concentration of atmospheric CO_2 was nearly 410 ppm, and continues to increase by approximately 3.5 ppm each year (Lindsey 2017; NOAA 2019). The concentration of soil CO_2 can be hundreds of times greater than atmospheric CO_2 due to biological activities in the soil, such as decomposition of organic material and microbial, root, and faunal respiration (Richey et al. 2002; Palmer 2007; Cuezva et al. 2010; Jackson 2017). Soil CO_2 concentrations vary depending on soil thickness, depth, composition, and structure, as well as climate, seasonal conditions, and soil ecology (Ford and Williams 2007).

The concentration of CO_2 dissolved in the water is measured by its partial pressure (pCO_2). Partial pressure of CO_2 can be calculated using alkalinity, temperature, and pH measurements with the following equation:

$$pCO_2 = \frac{(a_{HCO_3^-})(pH)}{(K_1)(K_{CO2})}$$ (Eq. 2.3)

where α_{HCO3^-} is the activity of bicarbonate (HCO_3^-); K_1 is the dissociation constant of carbonic acid; and K_{CO2} is the solubility constant of CO_2 in water (Ford and Williams 2007; Khadka et al. 2014). Both constants are temperature dependent; consequently, pCO_2 is also temperature dependent. The amount of pCO_2 in groundwater determines whether carbonate dissolution or precipitation occurs (Anthony 1998). Changes in the pCO_2 of groundwater can cause shifts in the saturation index (SI) causing calcite to dissolve or precipitate.

Anthony's (1998) study showed that dissolution along a karst flow is not constant and variations in the degree of dissolution and precipitation can occur. This was demonstrated in the Logsdon River, a large underground stream located in the Turnhole Basin of the Mammoth Cave Karst System. Values of pCO_2 in the Logsdon River were thirty-four times that of the atmosphere during the summer months, due to the increased CO_2 concentrations in the soil produced by biological activities. As water flowed along the river passage, CO_2 was outgassed, causing pCO_2 to decrease, the water to become supersaturated with respect to calcite, and SI_{cal} to shift to positive values. But as CO_2 increased near the middle of river's path, the water became undersaturated again, pCO_2 increased, and SI_{cal} shifted toward the negative. This increase in CO_2 can be attributed to the oxidation of organic material brought into the river during storm events from different conduits. This study demonstrated how variations in pCO_2 can cause longitudinal

changes in calcite dissolution and precipitation along a single flow path. Further study by

of carbonate dissolution in the Logsdon River demonstrated that most dissolution occurs

during storm events that flood the passage. These events increased the stage of the

Logsdon River less than 5% of the year but caused 63-100% of the dissolution. The range

varied due to the influence of sediment cover in the conduits (Groves and Meiman 2005).

2.3.2 Aqueous Geochemical Monitoring

Changes in karst waters caused by storm events and flow reversals can be

characterized by a variety of geochemical parameters. The most informative

measurements are temperature, pH, and specific conductivity. Temperature is particularly

significant because carbonate dissolution processes are temperature dependent. CO_2

dissolves readily into cool water; this increases the pCO_2. Conversely, as temperature

increases, CO_2 is outgassed and pCO_2 decreases (White 1988). Additionally, temperature

can be used to determine the timing of spring flow reversals — typically in the winter and

summer months (Gulley et al. 2013; Ballard et al. 2016; Trimboli and Toomey 2019).

However, the usefulness of temperature as proxy for reversals in MCNP during the

seasons of spring and fall is limited, as surface water temperatures and cave water

temperatures are similar (Trimboli and Toomey 2019).

Water's pH is the concentration of its hydrogen ions, or hydrogen ion activity.

(White 1988; Palmer 2007). This important geochemical parameter is used to determine

the water's acidity, and therefore how chemically aggressive the water is. Water's pH is

influenced by the amount of dissolved CO_2 it contains. Greater amounts of dissolved CO_2

will cause the pH to be low and the water to be more acidic. Seasonal changes in

vegetation can affect the pH of water that infiltrates through the epikarst. During the

summer, water infiltrating through soils react with CO_2 produced by biological processes, causing the water's pH to decrease. In the winter months, vegetation is generally dormant and microbial activity is low; therefore, there are lower CO_2 concentrations in the soil and the water's pH increases (Yang et al. 2012; Jackson 2017).

The pH of river water varies greatly and depends on several factors, including the CO_2 exchange at the air-water interface, the climatic setting, and the lithologic conditions beneath the river. The pCO_2 of river water is typically greater than the pCO_2 of the atmosphere, causing a disequilibrium between the river and atmosphere and degassing of CO_2 to the atmosphere (Richey et al. 2002). Most CO_2 dissolved in river water originates as soil-derived CO_2, which is dissolved and transported as groundwater flow or epikarstic interflow into the river (Khadka et al.2014). Flood events increase nutrient availability in soils, leading to an increase in microbial activity and CO_2 production. Khadka et al. (2014) demonstrated a decrease in the pH and increase of pCO_2 in the Santa Fe River in Florida associated with a midsummer flood in 2012. In portions of the river, the pH decreased from 6.6 (the average during low flow) to 4.6, and pCO_2 increased from approximately 16,700 µatm to nearly 41,000 µatm. The pH of river water can also be affected by factors other than CO_2. The water of the Suwannee River in Florida has pH values of 4.0-6.0 downstream of the Okefenokee Swamp (Crandall et al. 1999). The acidity of the water in this portion of the river can be attributed to high concentrations of humic and fulvic acids originating from organic materials in the swamp (Hull et al. 1981; Crandall et al. 1999). Another factor that affects the pH of river water is the underlying lithology. McClanahan (2014) and Osterhoudt (2014) studied the geochemistry of the Upper Green River basin at two sites upriver from MCNP. They demonstrated that the

pH of the river increased in the downstream direction as the bedrock under the river became dominated by more carbonate-rich rock.

Specific conductivity (SpC) is another geochemical parameter that is temperature dependent. Temperature affects a fluid's viscosity, and so affects the mobility of the dissolved ions in the solution (Miller et al. 1988; White 1988). SpC is a measure of the "concentration, charge, and mobility of the dissolved ions" in an aqueous solution (Miller et al. 1988, 3). In other words, SpC describes the electrical conductivity of a solution. In karst waters, concentrations of ions (such as Ca^{2+} and Mg^{2+}) increase as carbonate dissolution occurs; thus, SpC values of karst waters tend to be higher than meteoric water, especially in the summer months (Jackson 2017). McClanahan (2014) found that the average SpC of the Green River increased by nearly 75 µS/cm in the downstream direction. In this study, the lithology underlying the Green River changed from one region to another, from a mixture of silicates and carbonates upstream to carbonate-dominated downstream. The increase in SpC suggests that more dissolution was occurring in the carbonate-dominated region of the Green River than in the more resistant, silicate-dominated region (McClanahan 2014; Osterhoudt 2014).

2.3.3 Carbon Isotopes

In the karst systems, two additional aspects regarding carbonate dissolution are the carbon source and carbon transport. The dissolution reaction of carbonate minerals results in the transfer of inorganic carbon between all three phases: solid, liquid, and gas. Inorganic carbon is fixed in the crystal lattice of carbonate minerals in the solid phase; carbon is dissolved in water in the liquid phase; and carbon forms bonds in molecules of carbon dioxide in the gas phase. Sources of dissolved inorganic carbon (DIC) in river and

karst waters include dissolved atmospheric or soil CO_2, biological respiration in the water, and carbonate dissolution (Khadka et al. 2014).

Carbon isotopes can be used to determine carbon sourcing of DIC and provide further insight into carbonate dissolution dynamics, carbon flux, and organic processes that occur in the water. Carbon has two naturally occurring stable isotopes: ^{12}C and ^{13}C. In nature, 98.8% of stable carbon is ^{12}C and 1.2% of stable carbon is ^{13}C. For this reason, isotopes are expressed as ratios. The ^{13}C to ^{12}C ratio of a sample is compared with the international standard, written as the following equation (Clark and Fritz 1997; Palmer 2007; Fetter 2013):

$$\delta^{13}C\text{‰} = \frac{R_{sample} - R_{std}}{R_{std}} \times 1000 \qquad \text{(Eq. 2.4)}$$

where $\delta^{13}C$ is the apparent ratio of carbon isotopes in a sample (R_{sample}) compared with the standard (R_{std}) measured in parts per thousand ($^{0}/_{00}$). These values are multiplied by 1000 in order to sufficiently analyze differences in concentrations; the differences in isotopic ratios are generally small. For carbon isotopes, the international standard is the Vienna Pee Dee Belemnite (VPDB) of the Pee Dee Formation in South Carolina (Doctor et al. 2008; Fetter 2013). The VPDB standard is used as the relative benchmark; its ratio represents the "zero" value. Therefore, samples enriched in ^{13}C with respect to the VPDB have positive $\delta^{13}C$ values. Samples depleted in ^{13}C with respect to the VPDB have negative $\delta^{13}C$ values (Figure 2.10). The VPDB is the standard for $\delta^{13}C$ in all carbon compounds, including: carbonate minerals, CO_2, dissolved inorganic carbon (DIC), dissolved organic carbon (DOC), organic liquids, cellulose, and hydrocarbons (Clark and Fritz 1997).
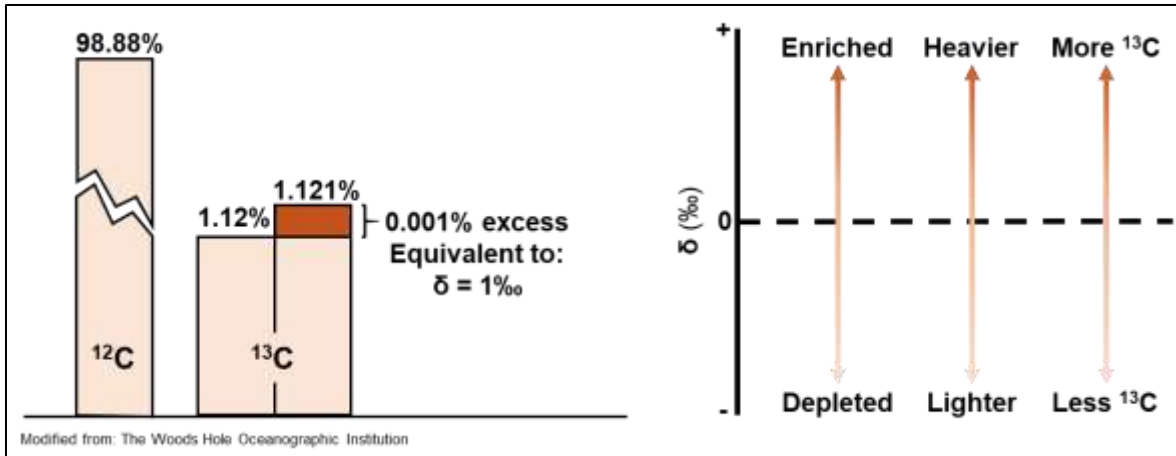
Figure 2.10 The ratio of ^{13}C to ^{12}C is expressed as $\delta^{13}C$‰
The 0 line indicates the VPDB, where positive values have relatively more ^{13}C and
negative values have relatively less ^{13}C.

Ratios of carbon isotopes are based on the process of fractionation, in which an

isotope of carbon is preferentially used in a chemical reaction or phase change based on

its mass. The differences in the masses of isotopes for lighter elements is large enough to

be distinguished in fractionation processes. Fractionation can occur through chemical,

physical, or biological processes (Drever 1997; Palmer 2007; Fetter 2013). Chemical

processes of fractionation involving carbon isotopes include the oxidation or reduction of

methane (CH_4) or organic matter, and the dissolution or precipitation of carbonate

minerals. A physical process of fractionation involving carbon isotopes is the dissolution

or degassing of CO_2. The major biological processes of carbon fractionation are

photosynthesis and respiration (Herczeg and Fairbanks 1987; Drever 1997; Doctor et al.

2008).

Chemical fractionation processes can be either equilibrium or kinetic (Clark and

Fritz 1997; Drever 1997). Reactions involving equilibrium fractionation minimize the

total energy in the system through preferential use of more labile isotopes. The bond

energy in carbon compounds slightly varies based on the mass of the isotope. ^{13}C has

27

stronger bonds and reacts slower than ^{12}C, therefore energy is minimized and ^{13}C

becomes enriched in certain compounds (Clark and Fritz 1997). Isotopic equilibrium is

not dependent on chemical equilibrium but is dependent on temperature (Fogel and

Cifuentes 1993).

Understanding equilibrium fractionation processes in the inorganic carbon

system, specifically between CO_2-HCO_3^-, is essential to understanding water-rock and

water-atmosphere interactions. In the CO_2-HCO_3^- system, isotopic equilibrium occurs

slowly (Fogel and Cifuentes 1993). The following equation describes the fractionation of

carbon between CO_2 and HCO_3^- (Herczeg and Fairbanks 1987; Fogel and Cifuentes

1993):

$$^{13}CO_2 \text{ (g)} + H^{12}CO_3^- \text{ (aq)} = {}^{12}CO_2 \text{ (g)} + H^{13}CO_3^- \text{ (aq)} \qquad \text{(Eq. 2.5)}$$
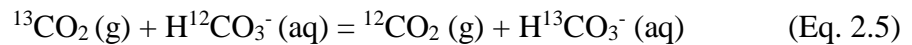
Because the activity coefficients are the same for ^{13}C to ^{12}C, the equilibrium constant can

be written as (Herczeg and Fairbanks 1987; Fogel and Cifuentes 1993):

$$\alpha \frac{HCO_3^-}{CO_2} = \frac{(^{13}C/_{12}C)_{HCO3^-}}{(^{13}C/_{12}C)_{CO2}} \qquad \text{(Eq. 2.6)}$$

where α is the equilibrium constant, also known as the fractionation factor. The

fractionation factor is used to compare the isotopic ratios in two compounds. If the bond

energies and distributions of ^{12}C and ^{13}C were equal, the ΔG for the reaction would be 0,

the reaction rates for each isotope would be equal, and the fractionation factor would

equal 1. However, bond energies differ for most isotopes, including ^{12}C and ^{13}C, so the

fractionation factor is not exactly 1 (Drever 1997; Fry 2006). The fractionation factor for

CO_2-HCO_3^- equilibrium is 0.9921 at 25°C, based on experimental exchange of CO_2 and

measured with mass spectrometry (Mook et al. 1974; Fogel and Cifuentes 1993). At this

temperature, the total energy in the system is minimized and little to no fractionation

occurs (Drever 1997; McClanahan 2014). Though concentrations of CO_2 and HCO_3^- in the system are dependent on pH, isotopic fractionation is only affected by temperature. As temperature decreases, the system diverges from equilibrium and fractionation increases (Drever 1997). Therefore, equilibrium is rare in low temperature aquifers (Geye 2000).

Kinetic isotope effect dominates fractionation when the system is not in equilibrium, generally due to the influence of biological processes. In kinetic fractionation, ^{12}C reacts more quickly than ^{13}C because it has less mass and forms weaker bonds (Drever 1997; McClanahan 2014). For example, ^{12}C is preferentially used in photosynthesis because the activation energy required to break the ^{12}C-O bond is less than the activation energy required to break the ^{13}C-O bond. For this reason, photosynthesis causes an enrichment of ^{12}C in organic matter (Fogel and Cifuentes 1993; Drever 1997). As in equilibrium processes, kinetic fractionation processes are temperature dependent. However; reaction rates and environmental factors also contribute to kinetic fractionation.

Most natural carbon-bearing materials (Figure 2.11) have $\delta^{13}C$ values between -100‰ and 20‰ VPDB (Hoefs 2018). The $\delta^{13}C$ values or "isotopic compositions" of different carbon sources vary due to fractionation (Clark and Fritz 1997; Drever 1997; Bullen and Kendall 1998). For example, equilibrium fractionation processes, such as precipitation of calcite, in the CO_2-HCO_3^--$CaCO_3$ system causes an enrichment of ^{13}C in marine carbonates (Hoefs 2018). Marine carbonates have $\delta^{13}C$ of 0 to 5‰, which is equal to or slightly more enriched in ^{13}C relative to VPDB (Clark and Fritz 1997; Bullen and Kendall 1998; Fetter 2013).
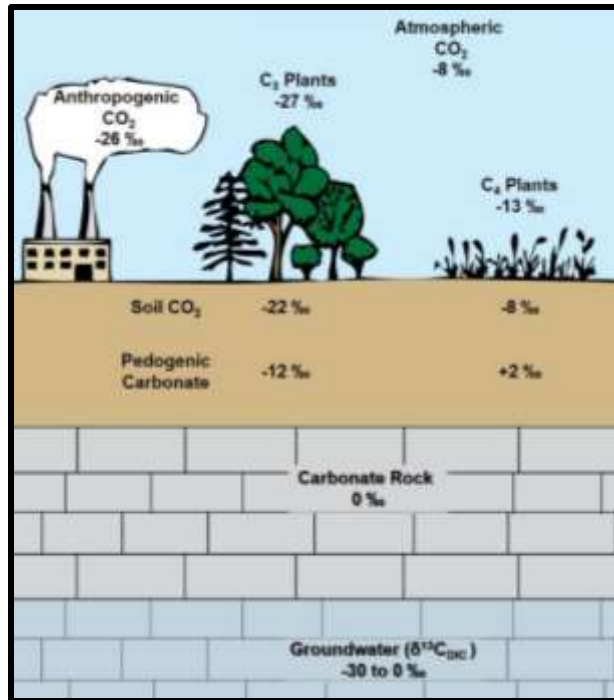
Figure 2.11 $\delta^{13}C$ values in various carbon sources
(Modified from Boutton 1991)

The $\delta^{13}C$ values of other carbon sources are typically depleted in ^{13}C relative to

VPDB and, therefore, have negative values. Current $\delta^{13}C$ of atmospheric CO_2 are

between -9‰ and -7‰ (Zhang et al., 1995; Clark and Fritz 1997; Zhang et al., 2015;

Graven et al. 2017). Atmospheric $\delta^{13}C$ values are affected by CO_2 exchange with the

ocean and anthropogenic CO_2. Soil CO_2 ranges between -28 and -5‰. $\delta^{13}C$ of soil CO_2

are affected by the exchange of CO_2 between the atmosphere and the upper 30 cm of the

soil (Boutton 1991). Soil CO_2 values are also affected by fractionation processes, such as

root respiration, microbial activities, decomposition of organic matter, and plant type

(Boutton 1991; Schulte et al. 2011).

The $\delta^{13}C$ values of plants are affected by photosynthesis, which is a kinetic

fractionation process that causes ^{12}C enrichment relative to the CO_2 source in its products.

Photosynthetic plants have two types of biochemical pathways, C3 and C4, which

determine the degree of fractionation (Drever 1997). C_3 plants (e.g. trees) and C_4 plants (e.g., grasses and corn) utilize carbon different because of difference in photosynthetic enzymes and the permeability of the plant cells. The cells of C_3 plants have higher permeabilities than C_4 plants, causing C_3 plants to have more exchange between cells. Therefore, C_3 plants are less effective at utilizing carbon without extensive fractionation (Hoefs 2018). For this reason, the $\delta^{13}C$ of C_3 plants ranges from -33‰ to -22‰ and the $\delta^{13}C$ of C_4 plants ranges from -20‰ to -10‰ (Bullen and Kendall 1998). Understanding how carbon fractionation processes contribute to the $\delta^{13}C$ values in natural materials allows for many applications of carbon isotopes including carbon sourcing and flux modeling.

Carbon isotopes can be useful tools in determining the source of waters and understanding weathering reactions. Many studies have used $\delta^{13}C$ values to identify carbon sources of dissolved inorganic carbon (DIC), which provides further insight about carbonate dissolution dynamics. Isotopic concentrations of DIC ($\delta^{13}C_{DIC}$) can change along a singular flow path due to the following fractionation processes: CO_2 degassing, temperature changes, mixing of waters, carbonate dissolution, and carbonate precipitation (Florea 2013; Khadka et al. 2014). By measuring $\delta^{13}C_{DIC}$ and comparing to the isotopic concentrations of known sources (i.e. soil gas, atmosphere, carbonates), the origin and chemical processing of carbon in river and karst waters can be determined (Khadka et al. 2014). Schulte et al. (2011) used $\delta^{13}C_{DIC}$ to show increased carbonate dissolution associated with waters discharging from an abandoned coal mine in Pennsylvania. A mixing model showed higher contributions of DIC from carbonate rocks in this area compared with areas not affected by coal mine drainage. Additionally, $\delta^{13}C_{DIC}$

contributions from carbonates in the mixing model decreased during the summer due to a higher input of biological fractionation processes. By understanding differences in fractionation processes, models can be developed to show the sources of water in a drainage basin, the mixing of such waters, and what processes affect the chemistry of the water.

2.4 Spring Flow Reversals

Only a few studies have been conducted on spring flow reversals, even though they are an important element in karst development (Gulley et al. 2011). Due to the interconnectedness of conduits and rapid infiltration into karst aquifers, the boundaries between groundwater and surface water systems at these locations can be difficult to distinguish. During periods of increased stage, water from a neighboring river can mix with groundwater and flood the karst aquifer, altering its chemistry. The study of the interconnection of river water and groundwater is especially important because this movement of water can lead to the transport of dangerous contaminants into fragile ecosystems (Gulley et al. 2011; Trimboli and Toomey 2019).

2.4.1 Flow Reversals in Florida

River water intrusion into caves was identified by cave divers in Florida, but the phenomenon has only been minimally studied by the "hydrologic and regulatory communities" (Kincaid 1998, 362). The most extensive work on this topic was conducted along the Suwanee River in North Central Florida. Martin and Screaton (2012) studied the effects of river water intrusion, how flow reversals affect dissolution, and the changes in hydraulic head during flow reversals.

The direction of groundwater flow in an aquifer is determined by hydraulic head (Hiscock 2005). Flow reversals occur when hydraulic head of the aquifer is lower than the hydraulic head of the river. Brown et al. (2014) and Hensley and Cohen (2017) analyzed variations in hydraulic head and found negative head differences, resulting in flow reversal. Because hydraulic head and discharge are proportional (Freeze and Cherry 1979), differences in discharge can be used to measure head differences. Q_{diff} is the difference in discharge between two gauges; one upstream and one downstream. Opsahl et al. (2005) recorded negative Q_{diff} values caused by flow reversals that were observed for extended periods of time (as many as ten days in one instance). Positive Q_{diff} values indicate normal flow conditions; negative Q_{diff} values indicate reversed flow conditions.

River water intrusion from the Sante Fe River into the aquifer in North Central Florida was characterized using radon (^{222}Rn) and oxygen isotopes (Kincaid 1998). ^{222}Rn is a gas that is present in Floridan groundwater at concentrations greater than surface water by at least an order of magnitude. The concentration of ^{222}Rn is lower in surface water because the radon gas rapidly dissipates into the air when exposed to the atmosphere. Oxygen isotopes (^{18}O and ^{16}O) also have different signatures in water depending on source due to isotopic fractionation. ^{18}O and ^{16}O have different masses, so they are used differently in chemical and physical reactions, such as evaporation and precipitation (Drever 1997). Kincaid (1998) observed infiltration of river water into the aquifer within two days of flooding events. Kincaid's study concluded that, due to rapid response to flooding events, there is little division between surface and groundwaters in the Upper Floridan aquifer of North Central Florida.

Crandall et al. (1999) used ionic, DOC, and isotopic sampling to provide hydrochemical evidence of river reversals into springs in the Upper Floridan aquifer. This study showed that Na, Mg, K, Cl, SO_4, and SiO_2 are not useful tracers for measuring river water and groundwater mixing in this area because the concentrations of these ions were similar in each water source. However, Ca, tannic acid, DOC, [222]Rn, and HCO_3 were all found to be effective tracers for quantifying mixing, because these tracers had distinct values when comparing river water and groundwater. Crandall et al. (1999) used these tracers and collected data to model the mixing of river water and groundwater during increased river stage.

Brown et al. (2014) investigated flow reversals at a karst spring in North Central Florida. Geochemical data were used to distinguish differences in river water and groundwater. They found that river water had low specific conductivity (SpC) and low concentrations of Ca^{2+}, NO_3^-, and HCO_3^-, but high concentrations of dissolved oxygen (DO), Na^+, and Cl^-. Furthermore, the river water had concentrations of dissolved organic carbon (DOC), Fe, and Mn "several orders of magnitude greater" than the groundwater (Brown et al. 2014, 58). Cl^- was used as a tracer of river-groundwater mixing, with the assumption that river water and groundwater were two end members with regard to Cl^- concentration. A mixing model was created with these data and used to estimate the effects of spring reversal effects on oxygen consumption, DOC oxidation, trace metal sequestration and mobilization, and calcite dissolution.

Processes that govern karst development in eogenetic karst aquifers (such as the Upper Floridan Aquifer) are not well understood (Gulley et al. 2011). Gulley et al. (2011) challenged the original theory of conduit development in eogenetic karst aquifers by

proposing that dissolution occurs during flood-induced flow reversals in the Floridan aquifer. Unlike the karst of Mammoth Cave, the karst in North Central Florida does not rely on interconnected, solutionally enlarged conduits to transmit water from points of recharge to points of discharge. Gulley at al. (2011) argues that this model does not work in eogenetic karst aquifers, because these karst systems are dominated by diffuse recharge and discrete recharge at sinking streams is uncommon compared to telogenetic karst systems. Additionally, groundwater in eogenetic karst aquifers is transmitted slowly, through conduits that are not connected or pinch out into the rock matrix, while exchanging flow with the matrix porosity. The unconnected nature of inputs and outputs in the Floridan Aquifer has been attributed to differences in dissolution associated with temporal changes in the water table (Florea and Vacher 2006). Gully et al. (2013) notes that flow reversals could not have been the original driver of cave formation because a "pre-existing cave void" is necessary to create the head gradient that causes reversals to occur.

Evidence to support Gulley's theory about eogenetic karst aquifers includes abrupt decreases in SpC, temperature, and SI_{cal} in the upstream direction of the conduit system. These abrupt decreases indicate that undersaturated river water, capable of dissolving calcite, is flowing into the conduit system during flow reversals. Additionally, solution scallops indicated the flow direction and velocity. Scallops are "shallow cuspate pockets," where the steep side of the scallop indicates the upstream direction of flow (White and Deike 1989). Gulley et al. (2011) noted the occurrence of solution scallops oriented in the upstream direction, indicating dissolution of the conduit walls from reversed flow. Additionally, Gulley et al. (2011) found that a single reversal event caused

3.4 mm of wall retreat. This evidence suggests that spring flow reversals are significant

contributors to the enlargement of preexisting eogenetic caves.

2.4.2 Flow Reversals at Mammoth Cave's Echo River and River Styx Springs

Mammoth Cave's River Styx Spring and Echo River Spring are both rise pools

that resurge beneath limestone ledges and flow to the Green River by short silt-floored

spring runs. River Styx and Echo River Springs formed in response to glacial-induced

changes in base level of the Green River. The Green River was previously lower than its

present elevation when these springs formed. As base level rose, sediment was deposited,

causing the Green River to be currently underlain by approximately 5-10 m of silt (White

and White 2017). Additionally, sediment filled the springs' channels causing River Styx

Spring and Echo River Spring to become alluviated (Palmer 1981). The River Styx and

Echo River groundwater basins (Figure 2.12) discharge groundwater from the Mammoth

Cave Ridge and neighboring karst valleys and are adjacent to one another, separated only

by a low sand bar (Figure 2.13) (White and White 2017; Trimboli and Toomey 2019).

Flow reversals have been directly observed at River Styx Spring and Echo River

Spring, during which the Green River flows into the springs (Hendrickson 1961; Hess

and White 1989a; Trimboli et al. 2016; Trimboli and Toomey 2019). Adding to the

complexity of the system, reverse flow at River Styx Spring can pass over the draininage

divide seperating the springs, and discharge at Echo River Spring (Figure 2.14). Meiman

(2006, 39) describes this phenomenon: "Water from the Green enters River Styx's spring

run, into the cave for perhaps one kilometer (uncharted), mixes with the karst

groundwater, and exits the cave (flowing for an additional kilometer) via Echo River

Spring." Because flow between River Styx Spring and Echo River Spring can last for

several weeks at a time, this phenomenon is known as "stable reverse flow" (Meiman 2006; Trimboli et al. 2016; Trimboli and Toomey 2019).
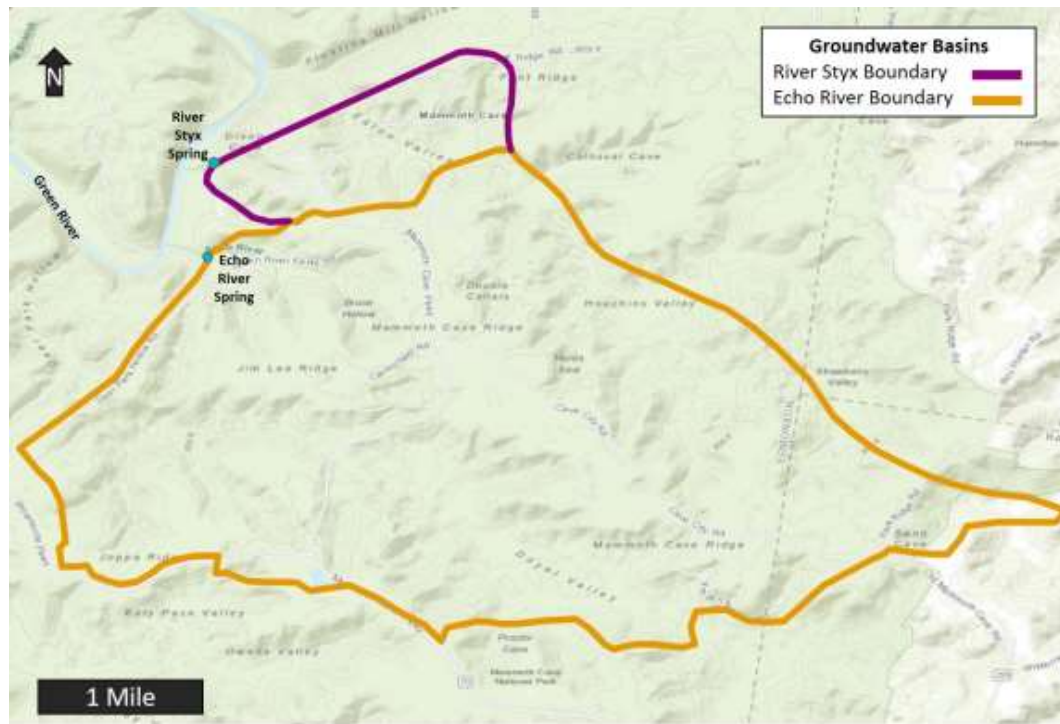
Figure 2.12 River Styx and Echo River groundwater basins
(Modified from Mammoth Cave International Center for Science and Learning 2012).
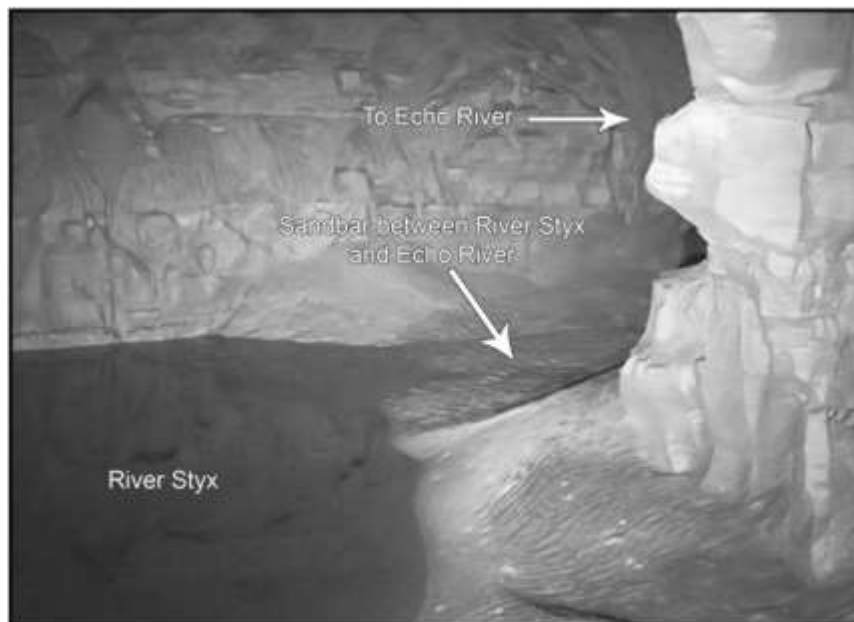
Figure 2.13 River Styx and Echo River are separated by a low sandbar
during normal flow conditions (Source: Trimboli and Toomey 2019).
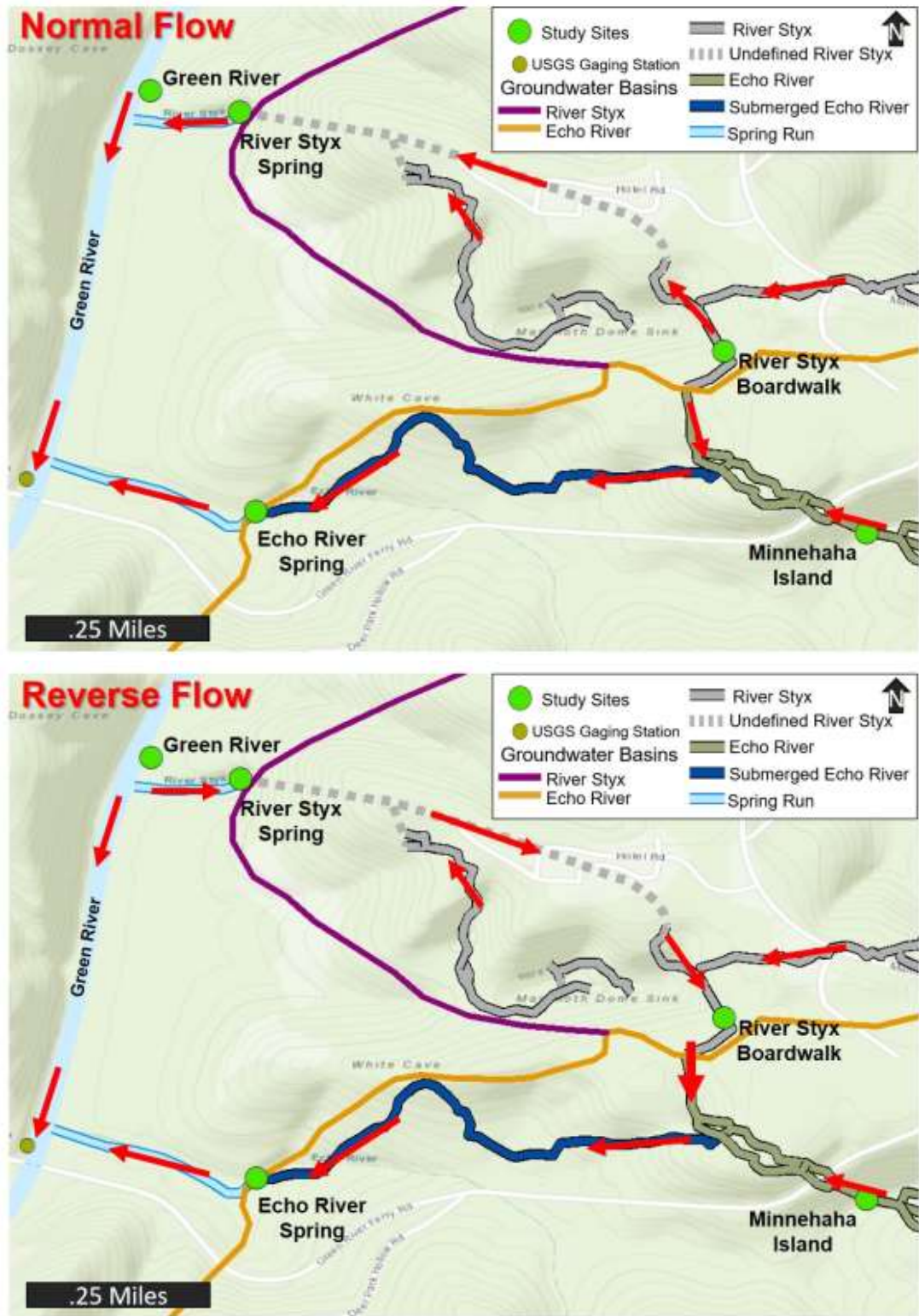
Figure 2.14 Normal and stable reverse flow paths
(Modified from Mammoth Cave International Center for Science and Learning 2012).

Little work has been completed on this phenomenon, even though the backflooding of the Green River into River Styx and Echo River was first documented over one-hundred years ago (Hovey 1912). One of the earliest attempts to study this phenomenon was by Hendrickson (1961), who measured chloride content, water temperature, and gauge height in an attempt to quantify reversals. Chloride content was a useful proxy during this time, because the the Green River was being contaminated by the Greensburg oil field, located upstream of Mammoth Cave. Oil production at the Greensburg site began in 1958 and was characterized by the extraction of large volumes of salt water along with the oil, at a ratio of 9:1 (Schwalb and Wilson 1972). Sinkholes and streams were used to dispose of the salt water, leading to contamination of the Green River. Prior to oil production in the area, the chloride content of the Green, Echo, and Styx Rivers was less than five ppm (Hendrickson 1961). Chloride content of the Green River increased substainally after the oil field went into production. Base level chloride content in Echo River and River Styx did not change, because these rivers are recharged by the sinkhole plain, which was not contaminated with oil field brines (Hendrickson 1961).

Hendrickson (1961) measured an increase in the chloride content of water at River Styx Spring and hypothesized that the chloride-rich water from the Green River had flowed back into the spring. Following local rain events, the chloride-rich waters in Echo River and Styx River were flushed out, resulting in abrupt drops in the chloride content. Periods of low precipitation were followed by a gradual decrease in chloride content, as chloride-rich waters were slowly diluted and transported out of the cave by normal groundwater flow. An increase in chloride content at Echo River was observed

39

within a day of a known flow reversal at River Styx Spring, which led to the conclusion that River Styx flowed into Echo River during increased stage events. During this study, dye testing was used to determine the time it would take for river water entering River Styx Spring to be present in Echo River. Dye injected at River Styx Spring was detected at Echo River Spring after about fifteen hours, when the stage of River Styx Spring was about 130.15 meters (Hendrickson 1961). Additionally, the degree of mixing between river water and groundwater was calculated at Echo River Spring based on chloride values. During a flow reversal event in March 1960, water entering River Styx Spring contained nearly 150 ppm of chloride and water discharging Echo River Spring contained about 60 ppm of chloride. These values, in conjunction with base flow chloride values, were used to determine that 60% of the water discharged at Echo River Spring during this event was groundwater and 40% was river water (Hendrickson 1961).

Gauge height varies seasonally and in response to precipitation events. Hendrickson (1961) documented that, due to an obstuction in the conduit, the gauge height of River Styx was regularly above 129.14 meters. At Echo and Green Rivers, the summer gauge heights were often below 128.6 meters. River Styx had normal flow when the Green River was below 129.14 meters. The flow reversed when the Green River was above 129.14 meters. Meiman (2006) later stated that reverse flow occurs when Green River's stage increases 1.5 to 3 meters above base flow. However, these values have likely changed, due to the removal of Lock and Dam No. 6 in April 2017 (MACA 2017; Trimboli and Toomey 2019). Prior to its removal, Lock and Dam No. 6 artificially increased the river stage upstream of the dam. Lock and Dam No. 6 is assumed to have

influenced flow reversals by causing the duration and frequency of these events to increase since its installment in 1906 (Meiman 2006; Edwards 2009).

In 2009, the Mammoth Cave International Center for Science and Learning, along with a group of middle school students, installed data loggers in an effort to teach the students about scientific practices and to understand stable reverse flow phenomenon at River Styx and Echo River Springs (Trimboli et al. 2011; Trimboli et al. 2016; Trimboli and Toomey 2019). The group used sets of HOBO data loggers at five locations (Echo River – in cave and spring, River Styx – in cave and spring, and the Green River) to measure the temperature of the river at two-hour intervals. Typically, base level cave streams remain at a consistent temperature with only minor fluctuations during storm events; however, the temperature of cave water varies significantly as river water enters the system. Cave stream temperatures increase during summer months and decrease during winter months during flow reversals. According to their data, from October 2009 to October 2012, reverse flows occurred at River Styx approximately 20% of the time – 17% were stable reverse flow events and 3% were backflooding events (Trimboli and Toomey 2019). Trimboli and Toomey (2019) showed that temperature was a useful proxy for flow reversals. However, low variations in temperature during the spring and fall make it difficult to identify reversals. Reversals can easily be identified during the summer and winter months because river and cave temperature are considerably different. However, during the spring and fall months, river and cave water temperatures differ minimally.

Ballard et al. (2016) attempted to understand cave dissolution, as well as carbon sourcing and transport, during flow reversals at River Styx Spring and Echo River

41

Spring. In this researcher's study, water samples were collected weekly at four sites (River Styx Spring, River Styx in cave, Echo River Spring, and the Green River) and were analyzed for isotopic values, alkalinity, cations, and anions. Additionally, spot data for pH, DO, and SpC were collected at each site. Ballard et al. (2016) also saw distinct changes in temperature in River Styx during flow reversals in the summer and winter months.

The discovery of river water intrusion from the Green River during reverse flow shows that River Styx and Echo River are susceptible to contamination (Meiman et al. 2001). River Styx and Echo River are home of the endangered Kentucky Cave Shrimp (Meiman 2006; White and White 2017) and flow reversals likely introduce contaminants from the Green River into the cave system. On the other hand, flow reversals may be essential to the cave ecosystems by providing organic matter to the food web (Helf and Olson 2017). The lack of high-resolution data and potential for contamination demonstrated the need to further study flow reversals in MCNP. This study expands on previous research in order to quantify the flow reversal phenomenon that occurs between River Styx Spring, Echo River Spring, and the Green River, and determine how flow reversals affect cave dissolution in a telogenetic karst system.

3. High-resolution Monitoring of Spring Flow Reversals at Mammoth Cave

3.0 Introduction

In karst landscapes, groundwater and surface water are inextricable, due to the rapid infiltration of meteoric water, short residence times, and the interconnectedness of the surface to subsurface through a variety of geomorphic features. An often-overlooked process that connects karst groundwater and surface water is spring flow reversal. Spring flow reversals can occur when a spring is located near a region's base level river. When the river's stage is higher than the spring's stage, the hydraulic gradient between a base level spring and river reverses, allowing river water to enter base level karst conduits.

In Mammoth Cave National Park (MCNP), where spring flow reversals were first recorded in River Styx Spring and Echo River Spring nearly one hundred years ago, karst aquifers are subject to the intrusion of river water from the Green River(Trimboli and Toomey 2019). Both springs are base level conduit springs that discharge groundwater from their respective drainage basins into the Green River, the regional base level. Flow reversals, during which the Green River flows into the springs, have been directly observed at both Echo River Spring and River Styx Spring (Hendrickson 1961; Hess and White 1989a; Trimboli et al. 2016; Trimboli and Toomey 2019). Under normal conditions, water flows out of these springs from their respective drainage basins and into the Green River. Flow reversals occur when the hydraulic head of the Green River rises above the head within the River Styx and Echo River karst basins, causing river water to flow into the cave through the spring mouths. Adding to the complexity of the system, the reverse flow at River Styx Spring can pass over a low draininage divide separating

River Styx and Echo River and then flow along the Echo River until finally discharging from Echo River Spring (Figure 3.1). This phenomenon, known as stable reverse flow, can last for days to several weeks at a time (Meiman 2006; Trimboli et al. 2016; Trimboli and Toomey 2019).

This area of study is important because spring flow reversals may have significant effects on telogenetic karst systems. They may be significant contributors to conduit enlargement and cave formation; studies suggest that spring flow reversals influence dissolution and cave development in eogenetic karst systems (Gulley et al. 2011; Gulley et al. 2013). Additionally, spring flow reversals can affect cave ecosystems. River Styx and Echo River are home to one species of cave crayfish, two species of eyeless cavefish, and the endangered Kentucky cave shrimp (Helf and Olson 2017; Trimboli and Toomey 2019). Spring flow reversals may benefit the ecosystem by adding dissolved organic carbon and oxygen into the groundwater and contributing sources of food and energy, such as non-troglobitic fish and plant matter (Ruhl 2005; Trimboli and Toomey 2019). Spring flow reversals can also be detrimental to the ecosystem by introducing contaminants, such as agricultural and residential pollutants, that enter the Green River upstream of MCNP.

Until recently, a high-resolution study measuring the geochemical response of spring flow reversals in MCNP (or any other telogenetic karst system) had not been conducted. Edwards (2009) used high-resolution geochemical sondes between May 2007 and November 2007 and Trimboli and Toomey (2019) utilized temperature loggers between October 2009 and October 2012 to record flow reversal events in River Styx and Echo River Springs. Results from both studies show that temperature is a useful proxy for

44

identifying spring flow reversals when the temperature of the Green River differs from groundwater temperatures. Using temperature data, Trimboli and Toomey (2019) determined that water from the Green River was entering River Styx approximately 20% of each year. These studies were conducted prior to the removal of Lock and Dam Number Six (located approximately 24 kilometers downstream of Echo River Spring on the Green River), which is believed to have potentially effected the timing and frequency of spring flow reversals.

This study examines the geochemical response of Mammoth Cave's River Styx and Echo River to the intrusion of river water through spring flow reversals. The duration, frequency, and other factors affecting spring flow reversals are identified to understand how the water's geochemistry responds to changes in flow direction. The combination of geochemical data and stage data provides details about hydraulic head dynamics between the Green River, the River Styx groundwater basin, and the Echo River groundwater basin. These karst springs are located at base level, where the hydraulic head of the karst aquifer is at its lowest. As a result, upstream changes in hydraulic head, both in the basin and in the base level river, control spring flow direction and velocity (Taylor and Greene 2008). Additionally, the rate of change and magnitude of hydrologic responses in karst springs is dependent on storm intensity, antecedent moisture conditions, and cave morphology. Hydrologic response times vary between karst springs due to lengths of flow paths from inputs to outputs, the size of individual basins, and the structure and geometry of the conduit network (White 1993). Possible factors affecting the hydraulic head dynamics between River Styx and Echo River karst basins and the Green River are: precipitation (rate, location, magnitude, and intensity);

antecedent moisture conditions; evapotranspiration rates; anthropogenic modifications to the hydrology (dams, impoundments, construction, removal of sediment); and the size and shape of the conduits within the basins (White 1993; Albéric᾽ 2004; Grubbs and Taylor 2004; Huawert and Sharp 2014; Brookfield et al. 2016; Compton et al. 2017; Trimboli and Toomey 2019).
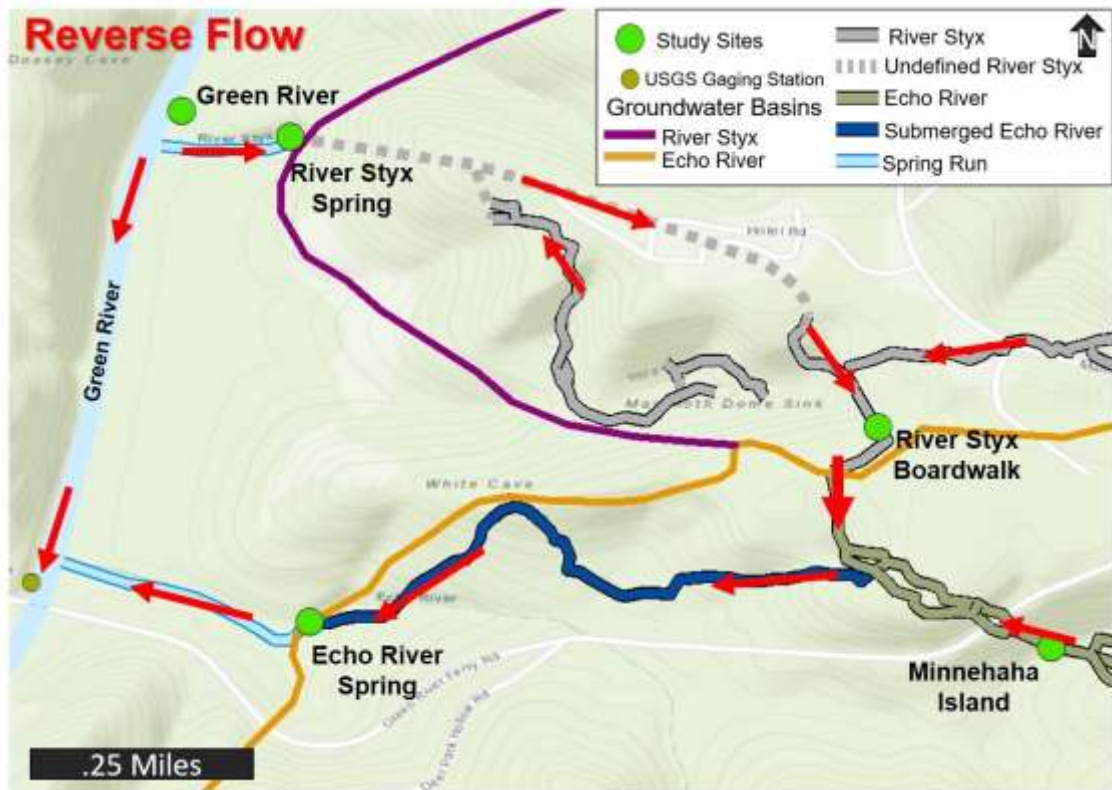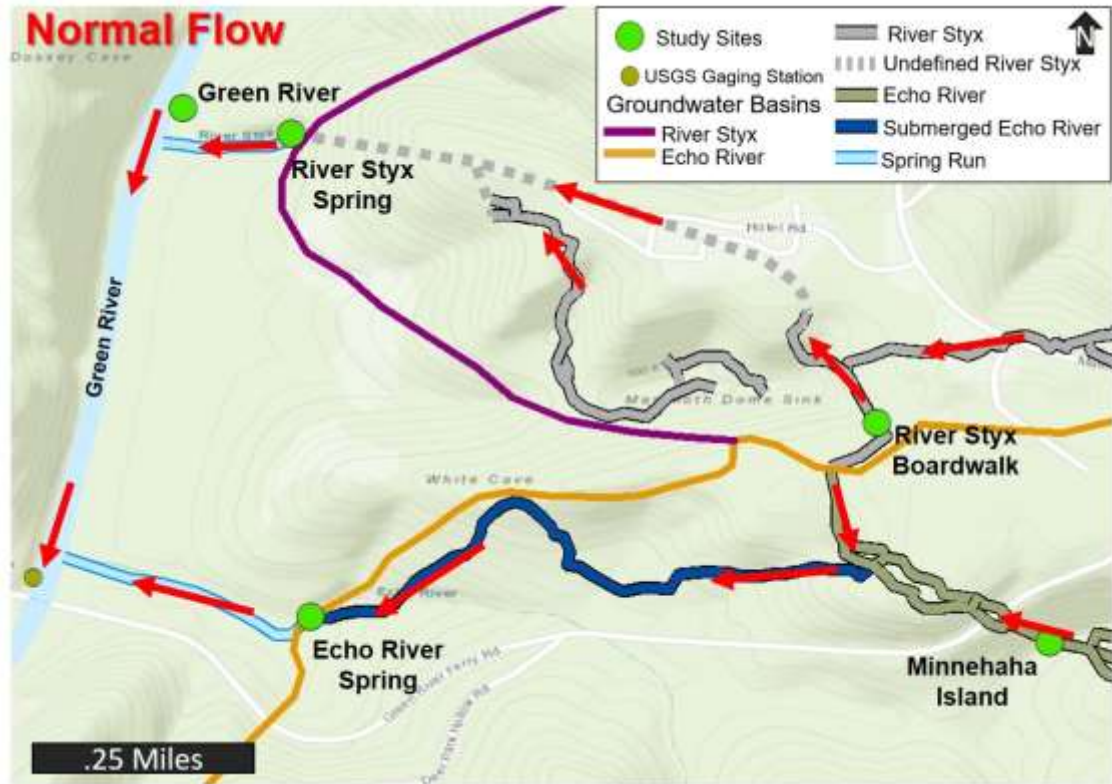
Figure 3.1 Green River, Echo River Spring, and River Styx Spring flow conditions
(Modified from Mammoth Cave International Center for Science and Learning 2012)

3.1 Study Area

The Western Pennyroyal karst area of South Central Kentucky, including MCNP (Figure 3.2), is one of the most explored and studied karst regions in the world (Palmer 1981; White 1989). The park is located 145 kilometers south of Louisville and 30 kilometers northeast of Bowling Green, in one of the most cave-dense areas of the state. MCNP is characterized as a deciduous forest in a humid, sub-tropical climate (Hess and White 1989; Meiman 2006). MCNP became a World Heritage Site in 1981 and an International Biosphere Reserve in 1990. Mammoth Cave is also home to fifty-two troglobitic species, creatures that have adapted to spend their entire lives in cave environments (Toomey et al. 2017).

South Central Kentucky is underlain by Mississippian age sedimentary rocks (Figure 3.3) that gently dip, less than one-degree northwest, toward the center of the Illinois Basin (Palmer 1981). The numerous passages of Mammoth Cave developed in an approximately 100 m-thick section of the St. Louis, St. Genevieve, and Girkin Formations. These formations are primarily limestones, containing minor beds of chert and dolomite. The Girkin Formation underlies the Big Clifty Formation, a 15 to 18 m-thick formation consisting of interbedded sandstone, siltstone, and shale. The Big Clifty Formation acts as a weather-resistant caprock that prevents rapid denudation of the Mammoth Cave System (Palmer 1981).
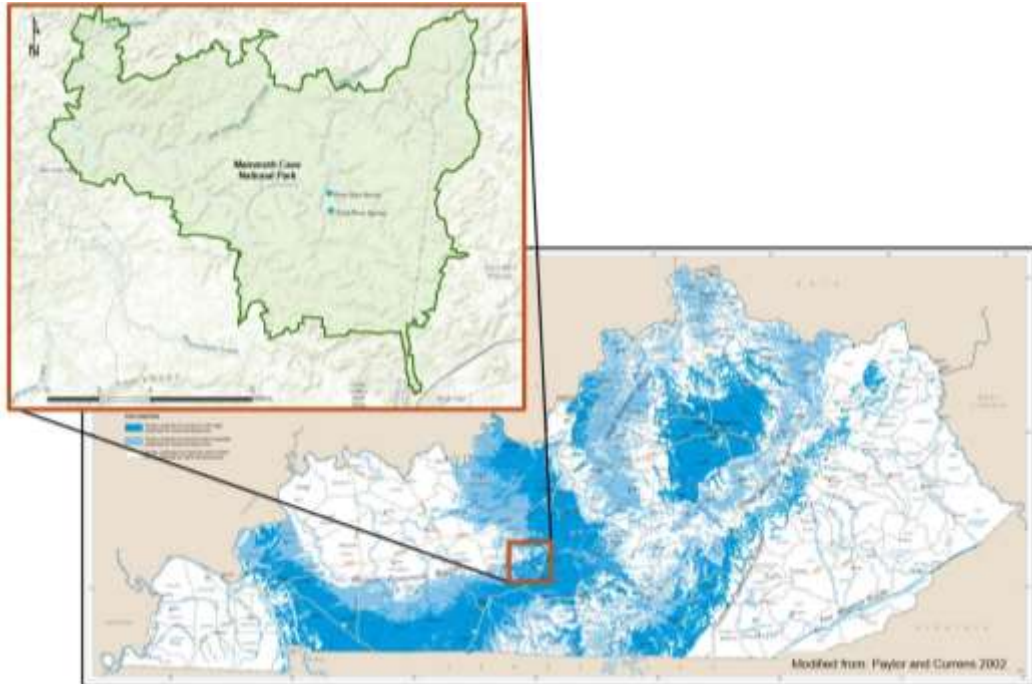
Figure 3.2 Mammoth Cave National Park
located in the Western Pennyroyal karst region
(Modified from Paylor and Currens 2002).

System	Series	Formation	Lithology	Thickness
Mississippian	Chesterian	Hardinsburg		18 m
		Haney		12 m
		Big Clifty		15-18 m
		Girkin		40-43 m
	Meramecian	St. Genevieve		34-37 m
		St. Louis		53-60 m

| Sandstone | Limestone | Gypsum | Shale | Chert | Dolomite |

Figure 3.3 South Central Kentucky geology
(Modified from Hess et al. 1989).

The Mammoth Cave Karst Aquifer is located in the Upper Green River drainage basin in South Central Kentucky. About 40 kilometers of the Green River flows through MCNP (Hess et al. 1989; Grubbs and Taylor 2004; McClanahan 2014). The Green River Dam is located 169 kilometers upstream of the Green River Ferry in MCNP and is a major control of the Green River's stage (Trimboli and Toomey 2019). River Styx and Echo River Springs are located in an area of the Green River that was previously influenced by the Lock and Dam Number Six. Lock and Dam Number Six, a low-head dam constructed in 1906 about 20 kilometers downstream of River Styx Spring and Echo River Spring, was decommissioned in the 1950s, breached in November 2016, and removed in 2017 (Meiman 2006; Grubbs and Taylor 2004; Compton et al. 2017). Conduit development at Mammoth Cave is directly influenced by the Green River. The multiple levels of the cave can be attributed to changes in the base level of the Green River during past glacial conditions (Granger et al. 2001). Current conduit development occurs primarily in passages at the elevation of the Green River in the St. Louis Formation and possibly the lower St. Genevieve Formation.

Mammoth Cave's River Styx Spring and Echo River Spring are both rise pools that resurge beneath limestone ledges and flow into the Green River by short, silt-floored spring runs. Echo River Spring and River Styx Spring formed in response to changes in the base level of the Green River. When Echo River Spring and River Styx Spring formed, the Green River was lower than its present elevation. As the base level increased, sediment was deposited, causing the Green River to currently be underlain by approximately 5-10 m of silt (White and White 2017). Sediment filled the springs' channels, causing Echo River Spring and River Styx Spring to become alluviated springs

(Palmer 1981). The Echo River (21.7 km^2) and River Styx (2.2 km^2) groundwater basins

(Figure 3.4) discharge groundwater from the Mammoth Cave Ridge and neighboring

karst valleys and are adjacent to one another, separated by only a low sandbar (White and

White 2017; Trimboli and Toomey 2019). During a stable reverse flow, water flows from

the Green River into River Styx Spring, flows opposite to its normal flow direction along

the trunk of River Styx, then passes over a low drainage divide between River Styx and

Echo River, flows into the Echo River, is discharged at Echo River Spring, where it

finally flows back into the Green River.
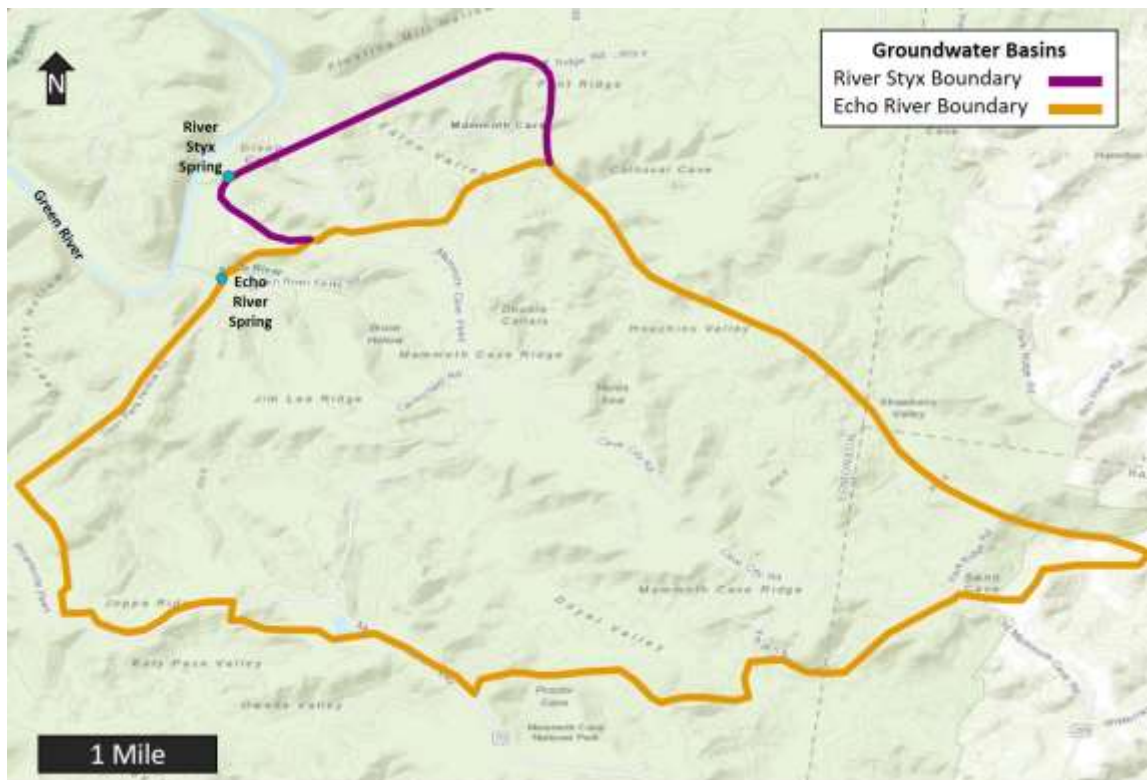
Figure 3.4 River Styx and Echo River groundwater basins
(Modified from Mammoth Cave International Center for Science and Learning 2012)

3.2 Methods

3.2.1 Site Selection and Setup

Four sites along the sustained flow reversal route were chosen for data collection: the Green River, River Styx Spring, the River Styx Boardwalk (River Styx, in cave), and Echo River Spring. Minnehaha Island (Figure 3.5), located upstream in Echo River, was the fifth and final site; it is outside of the sustained flow reversal route. Two PVC stilling wells were installed at each of the five sites. All stilling wells were drilled with multiple holes to allow water flow. The Green River stilling wells were screened with a wire mesh to prevent sediment buildup inside the wells. Due to limited access to vertical structures or surfaces, diagonal stilling wells were installed at River Styx Spring, Echo River Spring, Minnehaha Island, and the Green River. T-posts and trees were used as anchor points at these four sites. Vertical stilling wells were installed at River Styx Boardwalk and were anchored to the walkway's frame. A YSI EXO II was installed at the River Styx Boardwalk in a 7.6 cm stilling well. YSI 6920 V2 multiparameter sondes were installed at River Styx Spring, Echo River Spring, Minnehaha Island, and the Green River in 7.6 cm PVC stilling wells. HOBO pressure transducers were installed in 3.2 cm PVC stilling wells at all five sites.
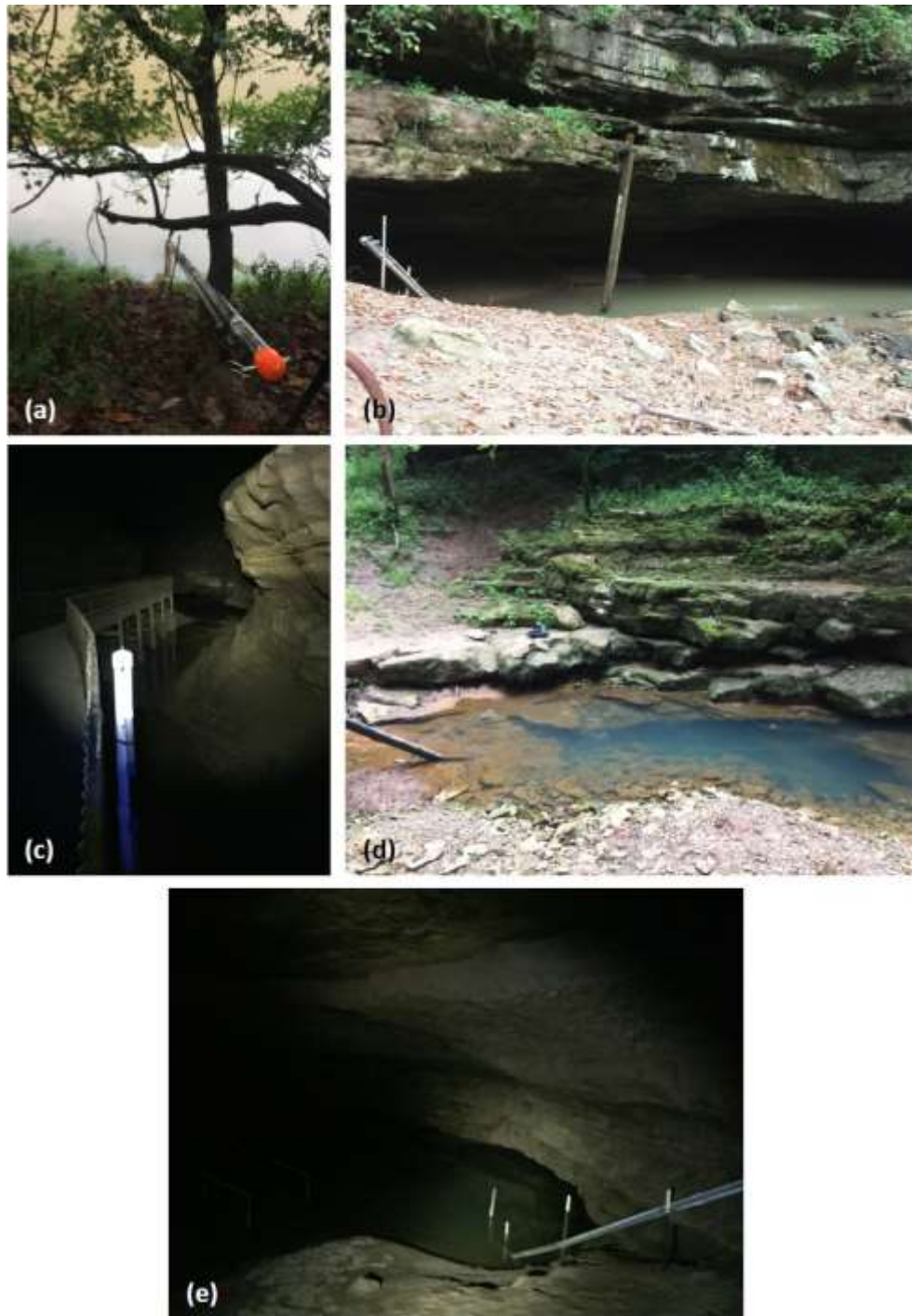
Figure 3.5 Stilling wells installed
(a) Green River, (b) River Styx Spring, (c) River Styx Boardwalk, (d) Echo River Spring,
and (e) Minnehaha Island.

3.2.2 Data Collection

YSI multiparameter sondes and HOBO pressure transducers were deployed at each of the five sites on June 9, 2018. The YSI multiparameter sondes were used to collect high-resolution data for pH, SpC, and temperature at ten-minute intervals. The HOBO pressure transducers were used to collect high-resolution water level and temperature data at two-minute resolution. Two additional pressure transducers were installed in-air: one on the surface at River Styx Spring and one in cave at Minnehaha Island. The in-air pressure transducers were used to collect barometric pressure data at two-minute resolution. Sites (when accessible) were visited weekly to verify the integrity of the installation, for maintenance, and to download data. The sondes (when accessible) were calibrated monthly to maintain accurate data collection and minimize drift. Precipitation rates (mm/hour) were collected from the National Park Service's gaseous pollutant and meteorological station located at Houchin Meadow. The stage height of the Green River was obtained from USGS gauging stations at the Green River Lake (03305990), the Green River near Campbellsville (03306000), Greensburg (03306500), Munfordville (03308500), Mammoth Cave (03309000), and Brownsville (03311505). Data from these gauging stations were used as a proxy to determine when water was released from the dam on Green River Lake. A YSI ProDSS multiparameter sonde and an Oakton PCTSTestr 35 were used to collect pH, SpC, and temperature data at each site during sample collection. Handheld multiparameter monitors were calibrated before each field day to ensure accuracy of the grab sample. Sampling sites were adjusted or omitted during storm events if the regular collection site had become inaccessible due to the increased stage of the Green River, River Styx, or Echo River.

3.2.3 Data Processing

All data were compiled in Excel and SigmaPlot spreadsheets. High-resolution measurement of water level data was calculated from the pressure transducer data using HOBOware software. Initial water levels, used as a reference, were measured with a tape measure. Barometric pressure data was removed from the total pressure data to increase the accuracy and reduce noise within the calculated water levels. The two-minute resolution was chosen because responses in the karst system occur rapidly, as shown in other studies (Lawhon 2014; Shelley 2019). Hydrochemical data obtained from the sondes (i.e. pH and SpC) were corrected for calibration drift and fouling in accordance with the USGS's Guidelines and Standard Procedures for Continuous Water-Quality Monitors: Station Operation, Record Computation, and Data Reporting using calibration values and grab sample data (Wagner et al. 2006). Graphs of high-resolution data regarding temperature, pH, SpC, and water level were analyzed to identify trends and relationships between sites.

3.3 Results and Discussion

Data analysis of seasonal and storm-event fluctuations in geochemical parameters and changes in water stage yields insights into the processes governing water flow in the Mammoth Cave Karst Aquifer. High-resolution geochemical and stage data were collected from June 9, 2018 to December 31, 2018; Julian Dates (JD) 160 to 365. Trends and extremes were used to characterize the geochemistry of the water and to identify flow reversals, specifically stable reverse flows that connect River Styx and Echo River. The beginning of each stable reverse flow was determined by identifying changes in the geochemistry at River Styx Spring. The end of the stable reverse flow was determined by

the return to geochemical base level conditions at Echo River Spring. Flow reversals

were identified by direct observation at springs and cave rivers and analysis of each site's

geochemical parameters. Over the course of the study period, ten stable reverse flows

connecting River Styx and Echo River were identified, as well as multiple, brief events

when flow direction could not be determined based on the data (Figure 3.6 to Figure

3.10).

3.3.1 Geochemical Response

Along the flow reversal route, changes in temperature, SpC, and pH at River Styx

Boardwalk and Echo River Spring occur within twenty-four hours of the initial

geochemical response at River Styx Spring. The differences in timing of flow reversal

responses at each of the sites can be attributed to differences in hydraulic head dynamics

between the Green River and the groundwater basins. In other words, the frequency,

intensity, and location of precipitation events, combined with discharge from the Green

River Dam, affect the direction and rate of groundwater flow in the River Styx and Echo

River groundwater basins. The fastest geochemical response associated with a stable

reverse flow was at Echo River Spring, approximately 7.5 hours after river water was

detected at River Styx Spring. The longest geochemical response associated with a stable

reverse flow was at Echo River Spring, approximately twenty-four hours after river water

was detected at River Styx Spring. Similarly, Hendrickson (1961) measured increases in

chloride content in Echo River Spring typically within twenty-four hours of reversals at

River Styx Spring. This suggests the spring response time of stable reverse flows has

experienced little to no change over the past seventy-nine years. However, Hendrickson's

study was conducted prior to the construction of the Green River Dam and the removal of

the Lock and Dam Number Six, which has modified the Green River's hydrology.
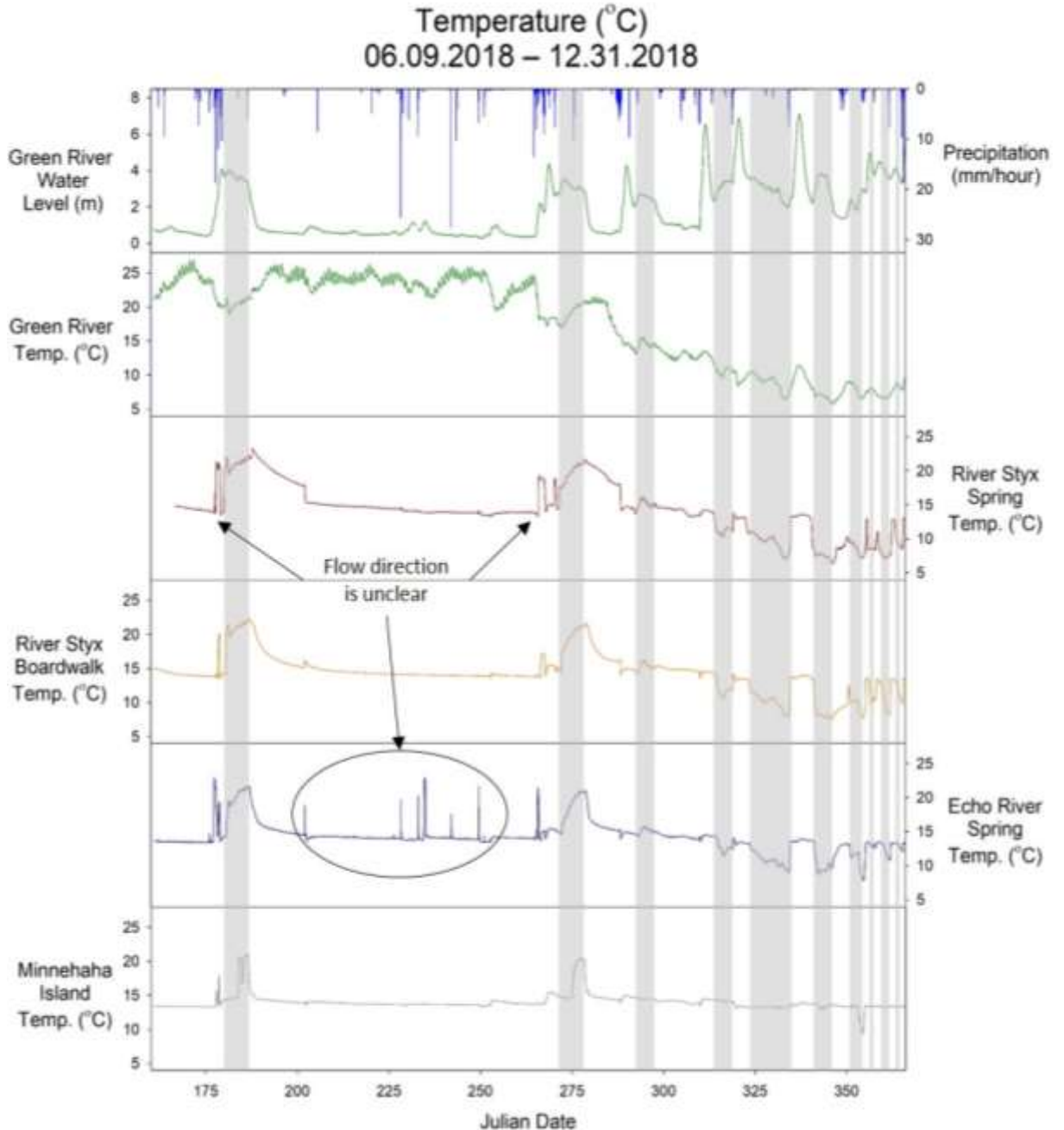
Figure 3.6 Temperature of the cave rivers and springs.
During flow reversals, temperature of the cave rivers and springs are reflective of Green River's temperature. Flow reversal events between River Styx and Echo River are shown by gray shading. Extreme temperature changes at Minnehaha Island indicate events where Green River water is backflooded upstream, outside of the flow reversal route.
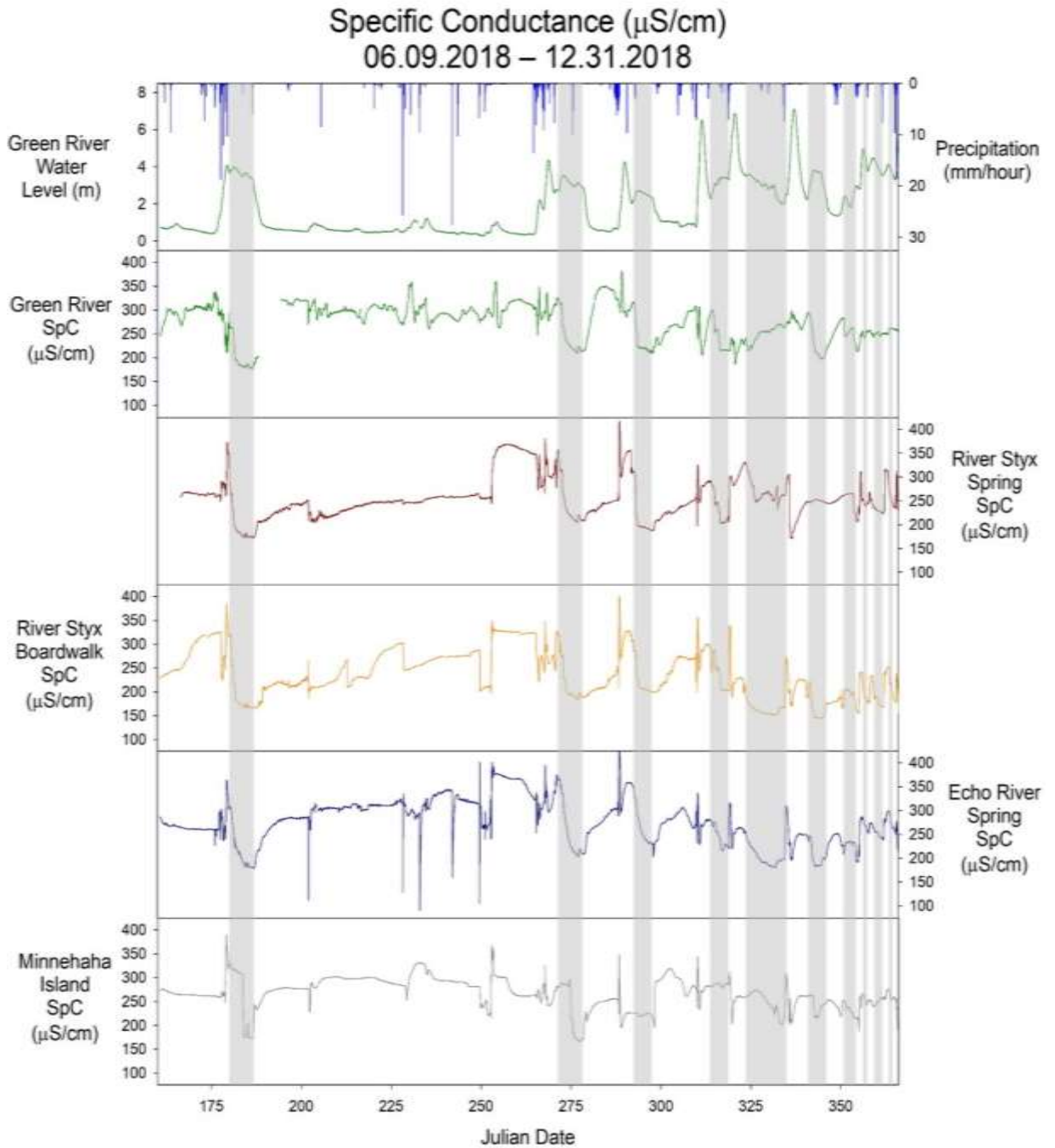
Figure 3.7 SpC
During flow reversals, SpC follows the same trend as the Green River's SpC.
Flow reversal events are shown by gray shading. Recognizing flow reversals with SpC
alone is difficult, because SpC varies widely over time, unlike temperature, which is
relatively stable.
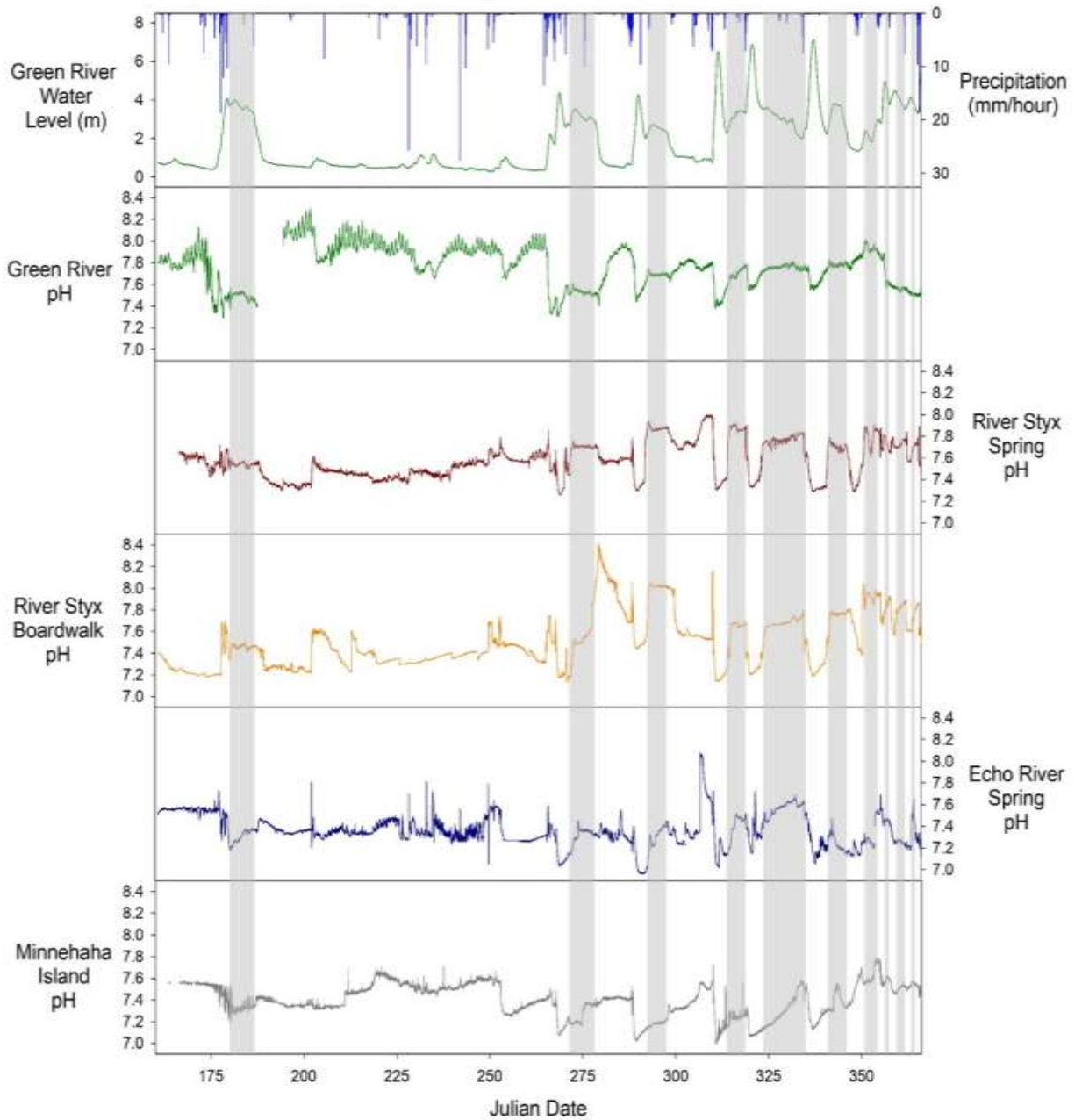
Figure 3.8 pH data

Identifying flow reversal events with pH is problematic; therefore, pH data were only used to supplement temperature and SpC data. However, pH was useful for showing clear seasonal trends in the Green River, with clear impacts from diel cycles in the summer and plateaus in pH values associated with dam releases.

(Flow reversals are indicated by gray shading)
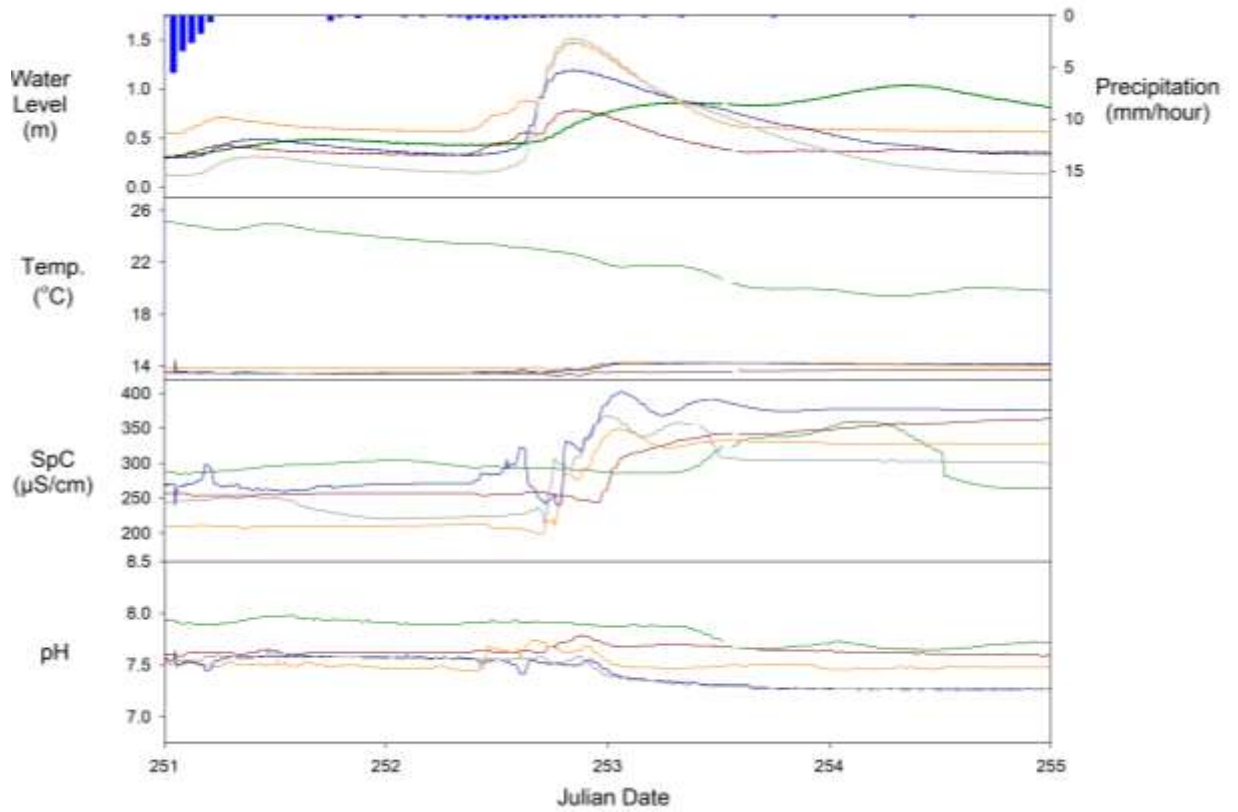
Figure 3.9 Geochemical Response to a Storm Event, September 7 – September 12
(JD 251-255)

This storm event represents the response of the River Styx and Echo River to a precipitation event. This event did not cause reverse flow. Temperature in the groundwater basins remained constant, while an increase in SpC and a slight increase in pH indicates a push of storage water through the system. During normal, storm flow conditions in the River Styx Karst Basin, the SpC, water level, and pH responses are seen first at River Styx Boardwalk, then at River Styx Spring. During normal, storm flow conditions in the Echo River Karst Basin, the water level response occurs at Minnehaha Island and Echo River Spring at nearly the same time and changes in SpC, pH, and sometimes temperature occur first at Echo River Spring. This suggests an input into Echo River after Minnehaha Island that causes rapid, short-term geochemical and hydrological changes at Echo River Spring.

60
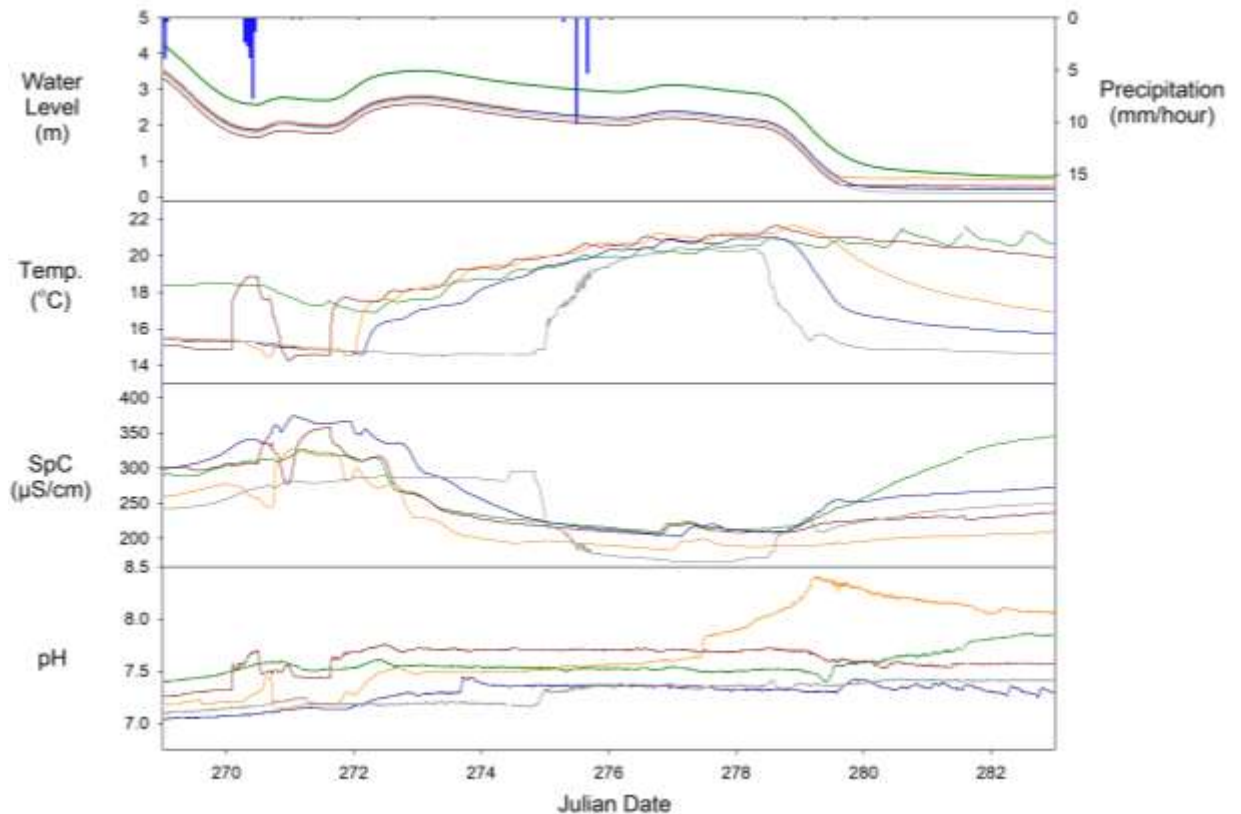
Figure 3.10 Geochemical Response to a Storm Event, September 26 – October 10 (JD 269-283). This storm event represents the response of the River Styx and Echo River to a stable reverse flow. Initially, geochemical responses are seen in River Styx Spring, then at River Styx Boardwalk, and lastly at Echo River Spring. Occasionally, river water backfloods upstream into Echo River, as seen in the increase in temperature at Minnehaha Island around Julian Date 275.

3.3.1.1 Temperature

For the purpose of this study, "season" was defined, not by its common astronomical definition, but based on the average daily water temperature in the Green

61

River and the average daily surface temperature at Houchin Meadow (
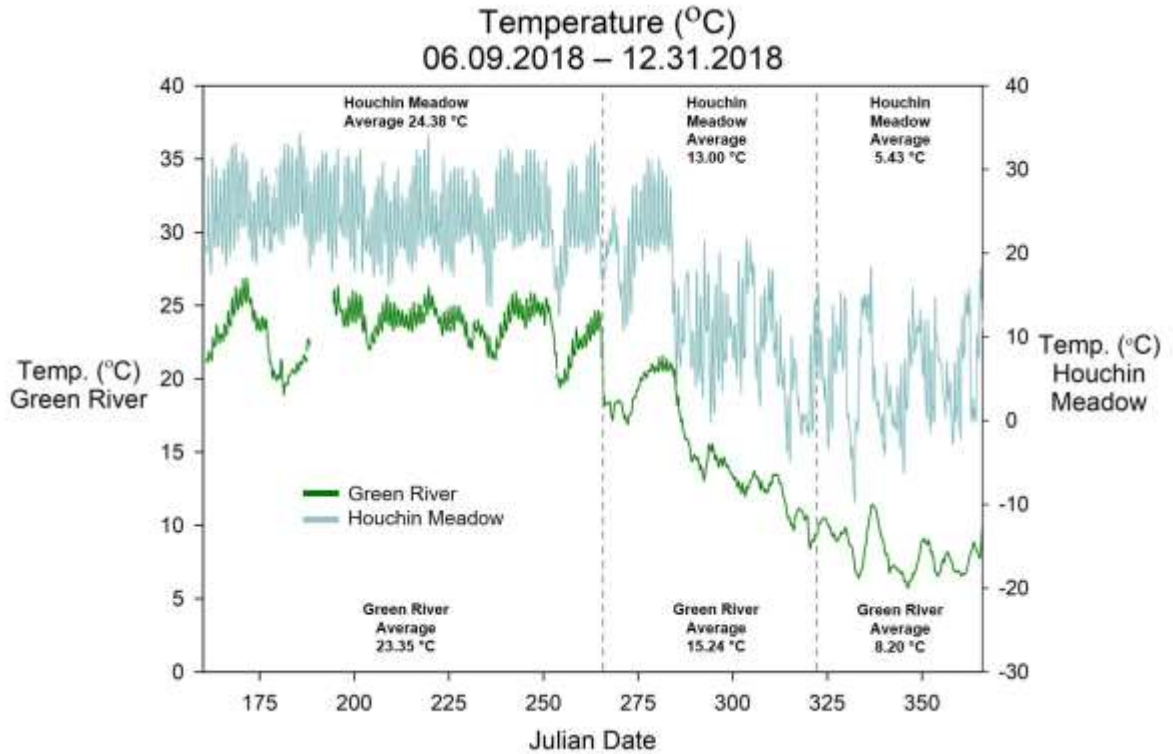
Figure 3.11). Summer was defined as the period from June 9 to September 22 (JD

160 to 265), when the average daily temperature of the Green River was consistently

above 20 °C. During that time, the average temperature of the Green River was 23.35 °C

and Houchin Meadow average surface temperature was 24.38 °C. Fall was defined as the

period from September 23 to November 17 (JD 266 to 321), when the average of the

Green River was consistently between 20 °C and 10 °C. During that time, the average

temperature of the Green River was 15.24 °C and Houchin Meadow average surface

temperature was 13.00 °C. Winter was defined as the period from November 18 to the

end of the study on December 31 (JD 322 to 365), when the average daily temperature of

the Green River was consistently below 10 °C. During that time, the average temperature

of the Green River was 8.20 °C and Houchin Meadow's average surface temperature was 5.43 °C.

Temperature can be used as a tracer of water flow and a valuable tool for monitoring exchanges between surface and groundwater reservoirs because the transfer of heat is simultaneous with the transfer of water (Constantz et al. 2008). The background temperatures of River Styx and Echo River show little variation over time. Temperatures during normal, storm flows don't change significantly, as seen in Figure 3.9. Despite increases in the water levels and changes in SpC, the temperature of the basin waters remains between 13 °C and 15 °C as the storm pulses through the basin. However, temperature can drastically change during flow reversal events. The average background temperature of the River Styx Spring, Echo River Spring, and the cave rivers ranged from 13.38 °C to 14.66 °C from June to December 2018, with little variation throughout the seasons. During flow reversals, spring and cave river water temperatures correlate closely with the Green River's temperature (Figure 3.6, Figure 3.10, and Figure 3.12).
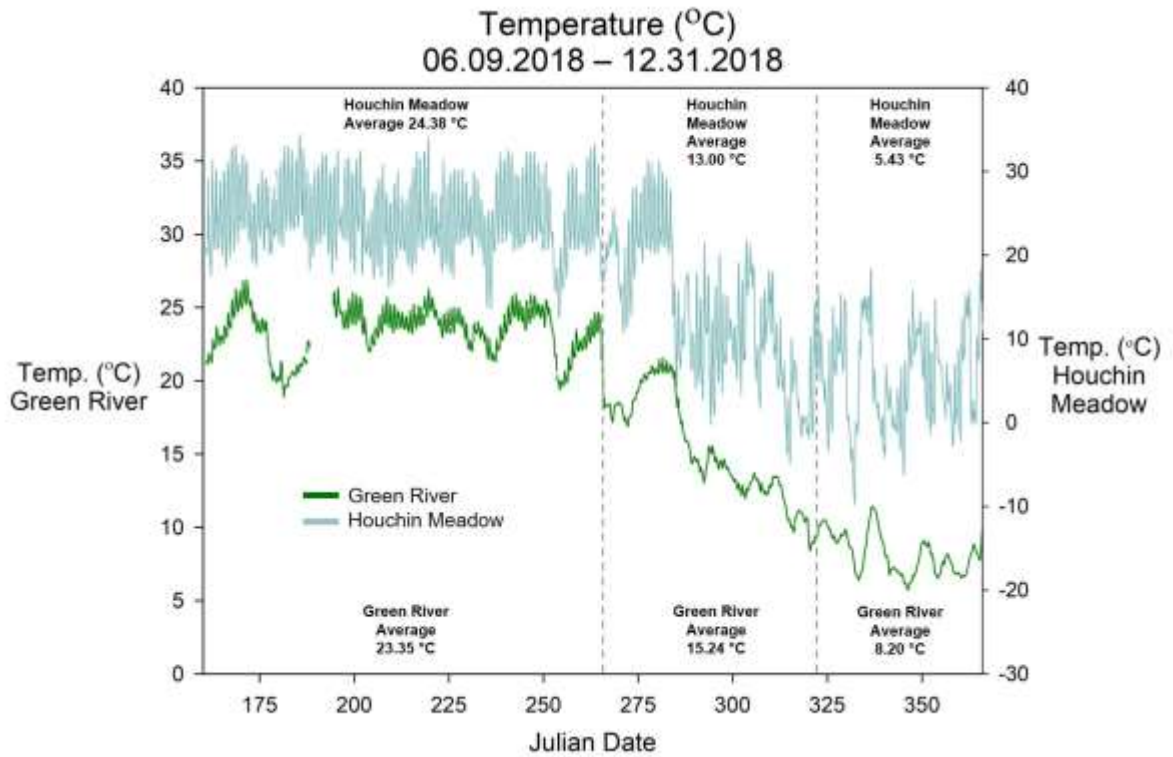
Figure 3.11 Distinct seasonal shifts in temperature of the Green River and at Houchin Meadow's weather station. Summer is September 23 to November 17 (JD 266 to 321). Fall is from September 23 to November 17 (JD 266 to 321). Winter is from November 18 to December 31 (JD 322 to 365).
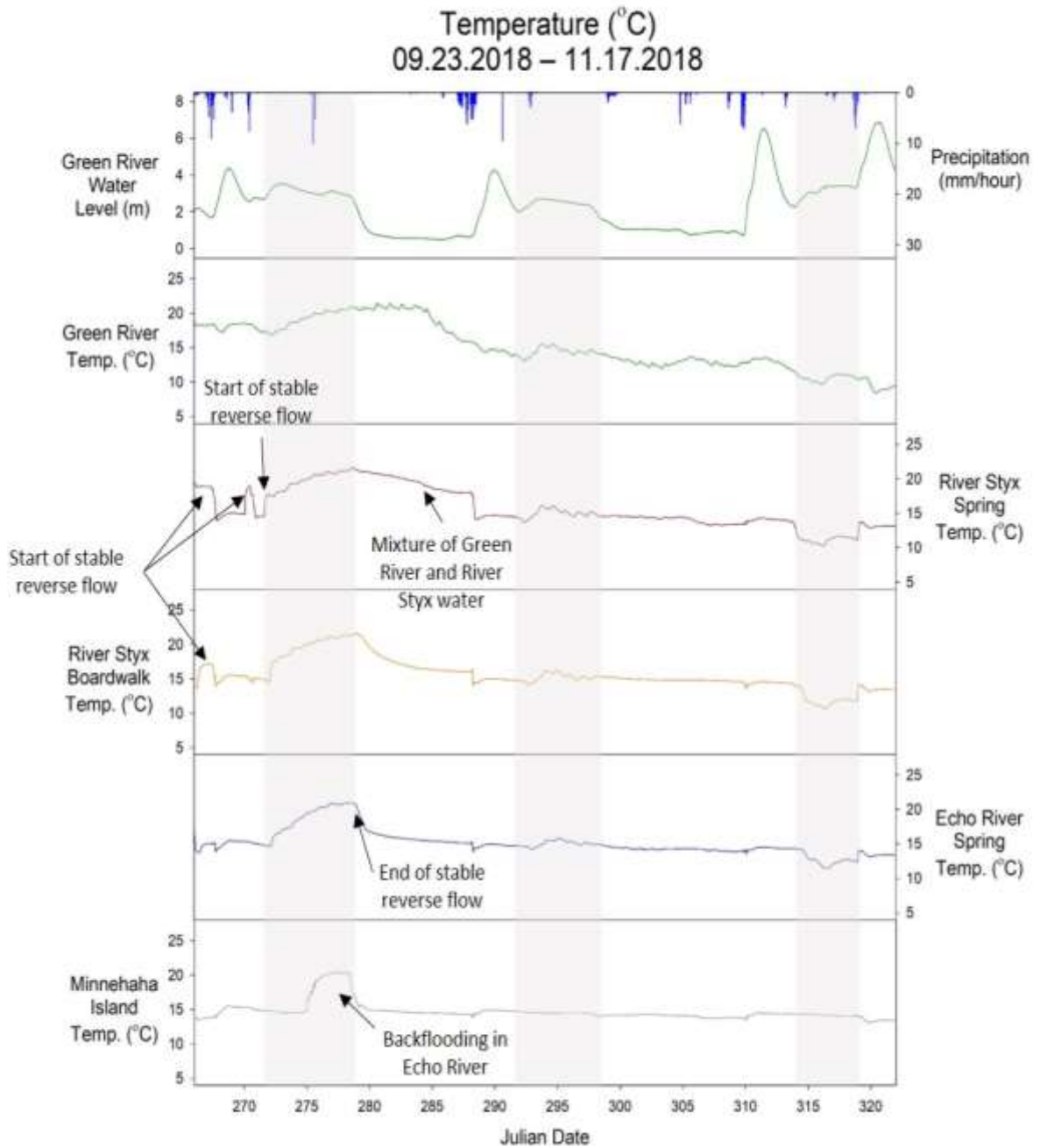
Figure 3.12 Flow reversal events during the fall season (JD 266-321)
Transitional river temperatures make flow reversals difficult to detect. Backflooding at
Minnehaha Island is indicated by an increase of temperature around day 275.

As river water flows along the flow reversal route, the addition of basin waters causes minor changes in the geochemical parameters. During reverse flow, water discharging from Echo River Spring is a mixture of Green River water and water from both the River Styx and Echo River basins. For this reason, the geochemistry of the water discharging from Echo River Spring during reverse flow represents a mixture of waters from at least three different sources. However, during flow reversals, the river water does not dwell in the subsurface long enough to become sufficiently mixed with cave waters or for thermal equilibration to cave temperatures; therefore, the water that enters River Styx Spring, flows past River Styx Boardwalk, and discharges from Echo River Spring, remains geochemically distinct from "normal" baseflow conditions, despite the addition of basin waters.

During the summer season, flow reversals were identified by warm river water entering River Styx Spring, when the average temperature of the Green River was 23.35 °C. During the one summer reversal, the maximum recorded temperature at River Styx Spring was 23.24 °C, indicating that water from the Green River was entering the spring (Figure 3.6). Additionally, temperature differences of the Green River show changes in temperature from day to night. These diurnal responses are more distinct during the summer and early fall seasons. The diurnal temperature fluctuations in the Green River are shown in temperature data at River Styx Spring, River Styx Boardwalk, and Echo River Spring during flow reversals of these seasons.

During the fall season, Green River water temperatures transition from being consistently above 20 °C in the summer to consistently below 10 °C in the winter. Three stable reversals occurred in the fall (Figure 3.12). The first (Figure 3.10) and third stable

reverse flows were reflective of the distinct temperature changes also found during the summer and winter months. The second stable reverse flow, however, was difficult to identify by temperature alone, because of the similarity between the water temperature of the Green River and River Styx Spring. On October 18 (JD 291), for example, the temperature of the Green River and River Styx Spring differed by only 0.3 °C. This reversal was identified by examining temperature trends, SpC, and pH. River Styx Spring followed the same temperature trend as water in the Green River — initially decreasing by 1.5 °C on October 18 (JD 291), followed by an overall increase in temperature by 2.5 °C until October 21 (JD 294), and then exhibiting diurnal fluctuations until October 24. Under normal flow, groundwater is thermally buffered and does not exhibit the variability evident in surface water. Therefore, identifying temperature trends can be a useful tool in identifying spring flow reversals, even during transitional seasons.

During the winter season, reversals were identified by cooler water entering River Styx Spring. The average Green River temperature during this time was 8.20 °C — noticeably lower than the average background temperature of the cave rivers. The minimum recorded temperature at River Styx Spring was 6.36 °C during a winter reversal, making the flow reversal event easily identifiable (Figure 3.6). Green River temperatures remained at least 1.5 °C lower than the average spring and cave water temperature throughout this season.

Temperature at Minnehaha Island was typically stable between 13 °C and 15 °C throughout most of the study period. Minnehaha Island is located upstream in Echo River, outside of the flow reversal route; therefore, river water did not reach this site during every reversal. River water did backflood to Minnehaha Island during three

events. This backflooding can be seen by the extreme temperature changes recorded following the flow reversal response at Echo River Spring (Figure 3.6 and Figure 3.10). The response times of backflooding at Minnehaha Island are slower than the response times at other locations along the flow reversal route. As seen in Figure 3.10, the temperature response at Minnehaha Island did not occur until approximately 64 hours after the initial response at Echo River Spring.

Backflooding at Minnehaha Island may have two distinct causes: Backflooding may be caused by flow reversal at Echo River Spring, as described by Trimboli and Toomey (2019). A second possibility is that the backflooding is caused by hydraulic head dynamics between the River Styx and Echo River groundwater basins and the Green River during a stable reverse flow. In this backflooding scenario, the large volume of water from the Green River and River Styx entering Echo River during a stable reverse flow is too great to be effectively discharged by the submerged Echo River conduit leading to the Echo River Spring. This causes a hydraulic damming of the basin waters in Echo River until, over time, river water backfloods farther upstream into the Echo River groundwater basin (Figure 3.13). As Green River levels subside, the hydraulic head of the Green River decreases below the hydraulic head of Echo River basin. Echo River then returns to its normal flow direction and the backflooded river water is discharged from Echo River Spring. During this study, there were no observations of reverse flow in Echo River Spring, and the geochemical data indicate flow reversals at Echo River Spring are short (less than twenty-four hours), when they do occur. Trimboli and Toomey (2019) indicated that backflooding events during their study period were often "sandwiched" between two stable reverse flows. The occurrence of backflooding in the middle of stable

68

reverse flows suggests that hydraulic damming is more likely than a change to reverse

flow in both springs. The collection of discharge data in future studies should reveal

which scenario causes backflooding in upstream Echo River.

Figure 3.13 Backflooding in Echo River

3.3.1.2 SpC

SpC is used as a proxy for the concentration of dissolved ions in solution (Drever

1997). In karst waters, SpC is affected by dissolution of carbonates and contributions

from meteoric water (Palmer 2007). On a seasonal scale, the average SpC of the Green

River decreases from June to December, with an average SpC of 290.7 μS/cm in the

summer; 268.9 μS/cm in the fall; and 251.1 μS/cm in the winter. Higher SpC

concentrations in the summer are associated with the seasonal hydrologic conditions.

Increased evapotranspiration rates and lower precipitation rates in the summer are associated with longer residence times and higher concentrations of Ca and Mg (Musgrove et al. 2010). The decrease in average SpC during the winter can be attributed to both seasonal influences controlling hydrologic conditions and dissolution. Vegetation and soil microbes enhance dissolution in the summer months by increasing soil CO_2 concentrations. Vegetation and soil microbe respiration slows during the winter months, decreasing soil CO_2 concentrations (Jackson 2017). SpC is likely influenced by the increased precipitation during the fall and winter seasons, causing the dilution of groundwater and surface water by meteoric water. Additionally, dam releases increase during the fall and winter months due to the increased precipitation and reduction to winter pool. Lake water released from the Green River Dam may have lower SpC levels by way of a self-purification processes. This has been found in other river basins where SpC decreased from inflow sites (e.g. rivers and streams) to outflow sites (e.g., lakes and dams) (Akindele and Indabawa 2015).

SpC of the Green River decreases after a precipitation event, as the water becomes diluted with meteoric water (Figure 3.7). This storm-scale change is followed, within forty-eight hours, by above average increases in SpC, as springs along the river flush storage water into the river. These "spikes" in SpC from the flushing of storage water can be seen in data from River Styx and Echo River as the precipitation event pushes through the system (Figure 3.9 and Figure 3.14). SpC decreases after each spike, as meteoric water flows through the basins and discharges into the Green River from the springs. Once the meteoric water has pushed through the system, SpC returns to baseflow conditions at the Green River. It slowly returns to baseflow conditions at River Styx and

Echo River, provided no flow reversal occurs. Increases in SpC in Echo River Spring prior to the SpC response from the storm pulse pushing through the basin suggest a rapid, epikarstic input close to the spring (Figure 3.9). This initial increase is not seen in at Minnehaha Island, so this secondary source of recharge to Echo River Spring inputs water into Echo River downstream of Minnehaha Island.

As with temperature, trends in SpC in the springs and cave rivers correlate with trends in the Green River during stable reverse flows (Figure 3.7, Figure 3.10, and Figure 3.14). SpC changes quickly in response to precipitation events, as storage and meteoric water causes extremes in SpC values that require days to weeks before "stable" baseflow conditions are achieved. For this reason, the SpC response during normal flow conditions in the Green River and springs can range between 100 µS/cm and 400 µS/cm. This variability in SpC does not allow for a clear response, either an increase in SpC or a decrease in SpC, associated with reverse flow; therefore, without temperature data, flow reversals would be difficult to identify based on changes in SpC alone.
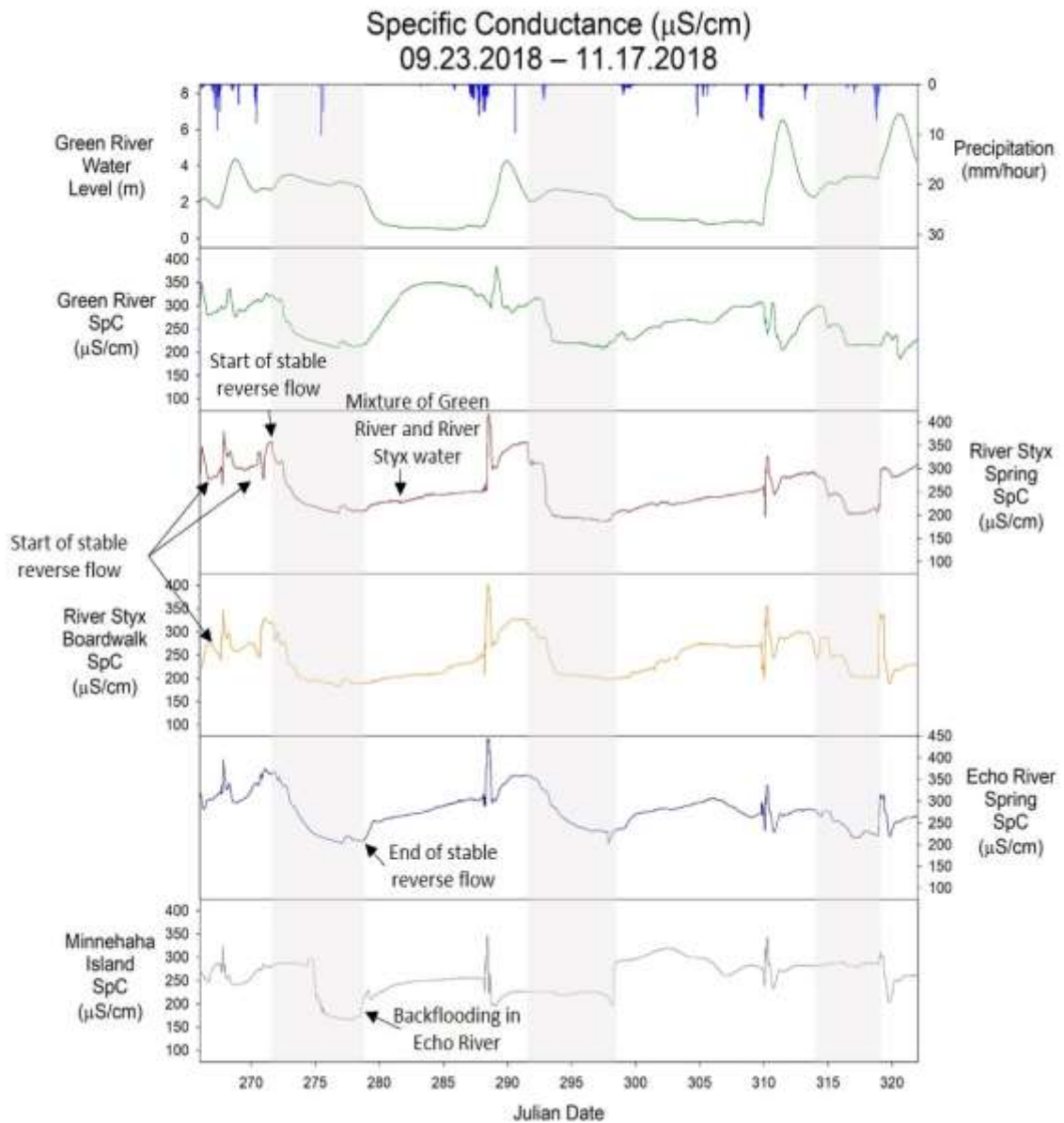
Figure 3.14 SpC response during the fall season (JD 266-321)
Three flow reversal events occurred during this transitional time as atmospheric and Green River temperatures transitioned from warm to cold. Stable reverse flows are indicated by gray shading. SpC response during flow reversals typically mirrors SpC of the Green River. One backflooding event occurred at Minnehaha Island during this time, noted by the extreme decline in SpC around day 275.

3.3.1.3 pH

The Green River's pH ranged from 7.29 to 8.30, with the average pH decreasing from 7.86 during the summer to 7.72 during the winter (Figure 3.8). Processes affecting fluctuations in pH values also show seasonal trends. During the summer season, the major influence on pH variability are diel cycles that may change the pH of the river up to 0.2 units in twenty-four hours. During these diel cycles, the pH of the Green River decreases to a minimum just before sunrise, then increases to its maximum around mid-afternoon. These diurnal fluctuations are caused by photosynthesis during the warmer months (Nimick et al. 2003). During the fall season, the Green River and surface temperature decreases by nearly 20 °C, causing photosynthetic organisms to slow or become dormant, and pH diel cycles to stop (Figure 3.15). On the shorter, storm-event scale, decreases in the Green River's pH occur in relation to precipitation events and increases in the Green River's stage.

During normal flow conditions, the average pH of the Green River's water was 0.34-0.49 pH units higher than the average pH at springs or in-cave sites. pH response to flow reversals was not as pronounced as the temperature or SpC response. However, small changes in the pH (often less than 0.3 pH units) did occur at each site, coinciding with river-induced changes in the temperature and SpC (Figure 3.10). pH values in River Styx were often distinct from the Green River's pH. This was likely due to the mixing of basin water with river water, causing slight changes in temperature and CO_2 concentrations. The pH values at Echo River Spring during stable reverse flows were 0.05-1.00 pH units lower than River Styx Spring and River Styx Boardwalk, due to mixing of Echo River basin water.
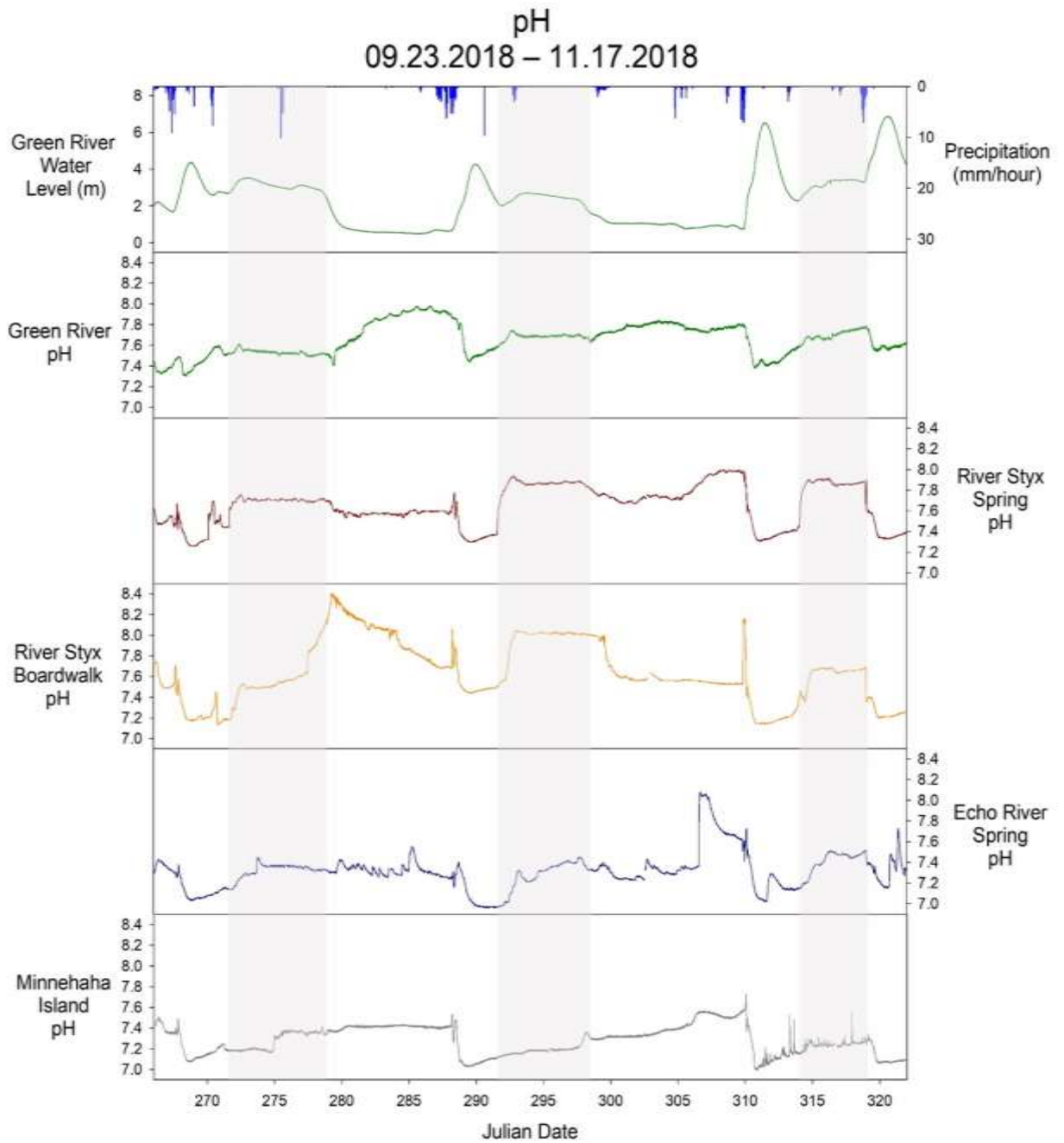
Figure 3.15 pH response during the fall season (JD 266-321)
pH alone was not a clear indicator of flow reversals, when compared with temperature
and SpC. However, pH can help identify flow reversals and provide insight about
geochemical changes in the water regarding dissolution.

3.3.2 Water Level Response

3.3.2.1 Basic Seasonal Precipitation and Discharge Description

The magnitude of the stage response to a particular precipitation event depends on several factors, including soil moisture conditions, seasonal weather conditions, and the intensity and location of the precipitation event. Periods with high rates of precipitation show greater magnitudes of stage response to individual events when compared with dry periods. The strong stage responses during these periods can be attributed to shorter recharge distances, an elevated water table, and more hydraulic conductivity caused by increased moisture in the vadose zone (Huawert and Sharp 2014; Brookfield et al. 2016).

Storm events of similar magnitude and intensity have different responses depending on the season. During the summer, the contribution of meteoric water to the water table is limited by high rates of evapotranspiration and canopy interception. During the winter, low rates of evapotranspiration and increased soil moisture allow meteoric water to reach the water table. Precipitation as snow (in contrast to rain) however, is slow to recharge the aquifer (Huawert and Sharp 2014; Brookfield et al. 2016). Seasonal changes in the hydrologic regime are seen in the response of water levels at the Green River, River Styx, and Echo River. Seasonal shifts in storm event frequency, higher soil moisture conditions, and lower evapotranspiration rates contribute to an increase in the frequency of stable flow reversal events during the winter (Figure 3.16).

During the summer season, on September 7 (JD 250), the Green River's water level (0.27 m) and discharge (15.69 m^3/s) were the lowest of the study period. Discharge remained below 17 m^3/s during the lowest flows of the summer season, from September 6 to September 8 (JD 249-251). According to historical data, a low-flow of this

magnitude and length is common, recurring nearly every year (Cushman et al. 1965). The total precipitation measured during the summer season at Houchin Meadow's weather station was 350.3 mm, or 3.33 mm/day. The combined monthly average precipitation from June through September for Mammoth Cave was 383.8 mm, or 3.15 mm/day (NOAA 2019), indicating that the summer season of this study had nearly average rates of precipitation.

During the fall season, on October 12 (JD 285), the Green River hit its minimum water level of 0.49 m and minimum discharge of 19.52 m^3/s. The maximum water level of 6.87 m and discharge of 523.03 m^3/s occurred on November 16 (JD 320). At the Houchin Meadow's weather station, a total of 305.9 mm, or 5.56 mm/day, of precipitation was recorded. This was higher than the average precipitation (215 mm, or approximately 3.51 mm/day) for this season (NOAA 2019).

During the winter season, on December 15 (JD 349), the Green River hit its minimum water level of 1.33 m and minimum discharge of 39.94 m^3/s. The maximum water level of 7.11 m and discharge of 562.31 m^3/s occurred on December 3 (JD 337). Houchin Meadow's weather station recorded a total of 178.8 mm, or 4.06 mm/day, of precipitation. These measurements are only slightly higher than the daily average of approximately 3.79 mm/day for November and December (NOAA 2019).

Precipitation and flow data from this study and historically-calculated averages indicate that the summer season was near average with respect to precipitation and discharge. Lower precipitation totals and low river flows in the summer suggest reverse flow events are typically less frequent in the summer than other seasons. The fall and winter seasons were slightly above average with respect to precipitation and discharge.

76

The frequency of reverse flow events may be predicted to be higher during the fall and winter seasons, if precipitation totals were the only variable. But precipitation alone is not a clear indicator of flow reversal frequency due to several factors such as antecedent moisture conditions, evapotranspiration, and dam releases from the Green River Lake Reservoir. Additionally, storm event intensity, frequency, and location can significantly change the hydrology and soil moisture conditions, which can drastically change surface water levels for brief periods in MCNP.

Anthropogenic modifications to base level karst rivers can also greatly impact the hydrology of an area. The removal of river rock and the subsequent lowering of stage in the River Loire was considered as a possible factor contributing to the change in frequency of spring flow reversals in Val d'Orléans karst system in France (Albéric' 2004). In MCNP, the Green River Dam is a major factor controlling frequency of flow reversals. The Green River Lake is located 160 kilometers upstream of the MCNP boundary and has a drainage area at the Green River Lake of approximately 1766 km^2 (USACE 2011). Storm events, occurring hundreds of river kilometers upstream and not recorded in the park, could induce stable reverse flows at River Styx Spring. Without high-resolution geochemical data, information regarding the complex hydraulic dynamics of the area, and a detailed analysis of the impact of anthropogenic modifications to the area's hydrology, it is difficult to determine the historical frequency and behavior of stable reverse flows.

3.3.2.2 Water Level Influence on Reversals

Measuring water level changes is essential to understanding flow reversals, since differences in water elevations create the hydraulic gradient that determines where water

will flow (Palmer 2007). Hendrickson (1961) indicated that an increase of only 0.27 m

above base level in the Green River's stage could cause a reversal. For this study, water

level and geochemical data from the Green River and River Styx Spring were recorded

from June to December 2018. During this time, the lowest water level of the Green River

at which a reversal was observed at River Styx Spring was 1.58 m, which was 0.7 m

above the average summer base level of 0.88 m. The Green River was below 1.58 m for

89% of the time during the summer season; 37% of the time during the fall season; and

7.67% of the time during the winter season (Figure 3.16).
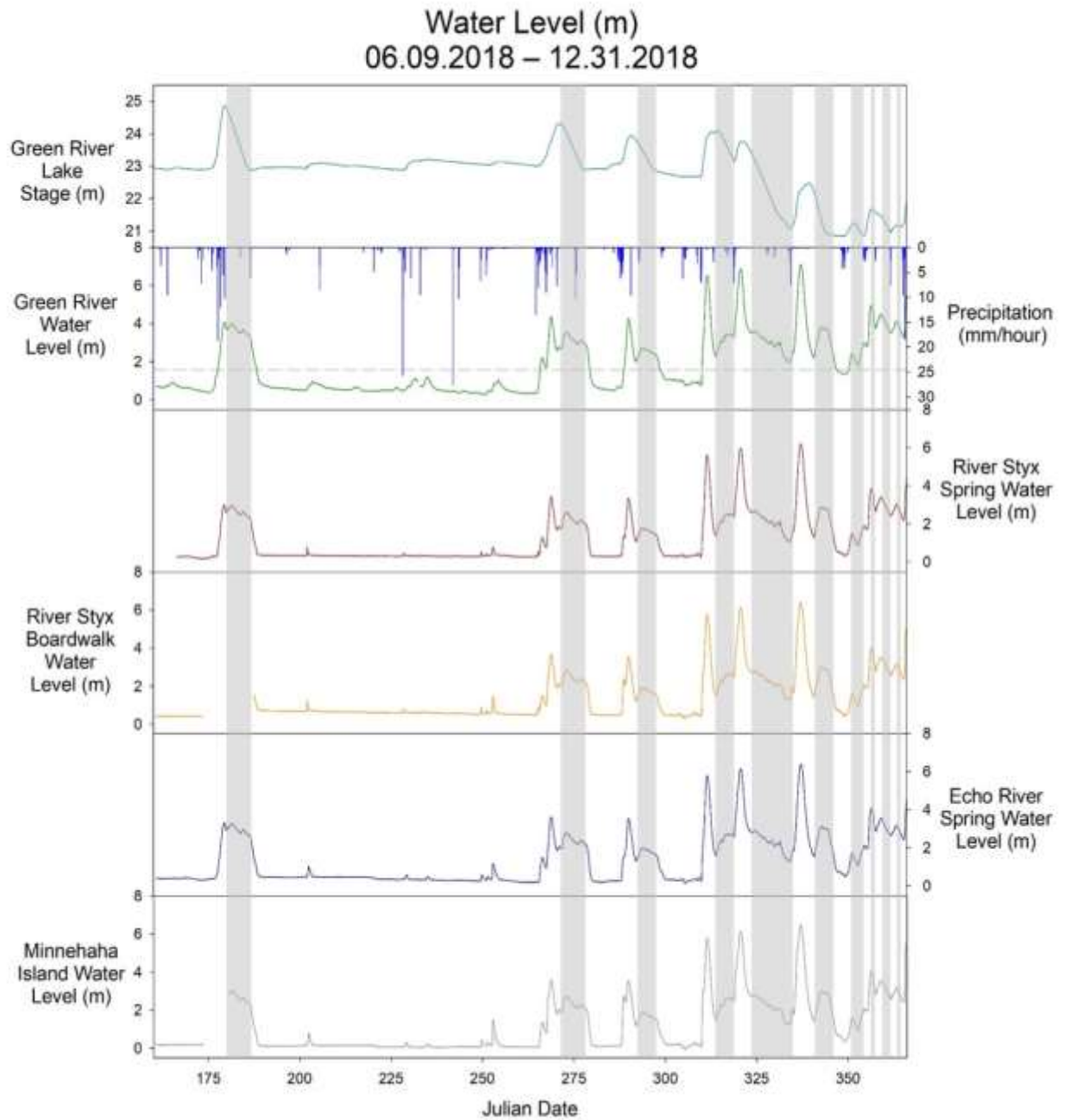
Figure 3.16 Water level of the Green River, River Styx, and Echo River
Water level of the springs and cave rivers are strongly reflective of the Green River.
Changes in water level occur almost simultaneously. The upstream dam on Green River
Lake significantly affects downstream Green River levels in MCNP.

Ten stable reverse flows were recorded during this study season; eight occurred after the initial peak Green River water level following a precipitation event (Figure 3.16). Flow reversal events can last from weeks to days at a time, because the water level of the Green River is sustained by dam releases from the lowering of the Green River Lake reservoir. Two stable reverse flows did not follow this pattern; they occurred near or at the Green River's peak water level following a dam release. These two reversals occurred during the winter, when the River Styx and Echo River were under a stable reverse flow regime for most of the time. In these two cases, precipitation events caused a return to normal flow conditions .

Stable flow reversals end by two different hydrologic processes. During this study, four of the ten stable flow reversals ended due to a reduction in the Green River's water level toward base level conditions following the end of a dam release at Green River Lake (Figure 3.16). The remaining six stable flow reversals ended due to storm events, which increased the elevation of the basin water above the Green River causing the hydraulic gradient to return to normal (Figure 3.16). However, the reversals resumed following the storm event, as the meteoric water from the basin discharged into the Green River, causing the basin's hydraulic head to be lower than the Green River's hydraulic head, once again changing the hydraulic gradient. Importantly, there is no precise stage at which a stable reverse flow will occur, due to the dynamics between Green River stage, storm event influences on the hydraulic head within the basin, and the influence of the Green River Dam (Table 3.1 Water Level data of the Green River).

The Green River Dam plays a major role in the hydrology and the ecology of MCNP. Dams can significantly modify rivers' geomorphology and hydrologic regimes

80

over considerable distances by reducing flood peaks, increasing the frequency of low

flows, and changing the timing and duration of peaks and low flows (Graf 2006).

Additionally, dams affect the hydraulic gradients and water table dynamics of an area by

artificially increasing the local head and base level elevations (Francis et al. 2010).

Before its removal, Lock and Dam Number Six impeded water flow, causing sections of

the river to be free of riffle, run, and pool habitats, affecting several mussel species and

the endangered cave shrimp (Meiman 2006; Grubbs and Taylor 2004). River Styx Spring

and Echo River Spring are located along a sixteen kilometer stretch of the Green River

that was considered an impounded flow regime before it transitioned to a free-flowing

regime following the removal of Lock and Dam Number Six (Meiman 2006; Grubbs and

Taylor 2004; Compton et al. 2017). Trimboli and Toomey (2019) found that, between

October 2009 to October 2012, River Styx Spring flowed backwards (including both

stable reverse flows and backflooding events) approximately 20% of the time; 29% of the

time from October 2009 to April 2010. From June to December 2018 (the period of this

study), River Styx Spring was in reverse flow approximately 34% of the time. Annual

precipitation amounts for 2018 were similar to those from 2009 to 2011 (Figure 3.17).

Although the total precipitation for these years are similar, further analysis of

evapotranspiration rates and precipitation intensity and duration are needed to adequately

compare the datasets of spring flow reversals pre- and post-removal of Lock and Dam

Number Six. The current study shows how water management at the Green River Dam

and subsequent changes of Green River stage are significant factors that influence stable

reverse flows in MCNP. Therefore, discharge from the Green River Dam should be

considered when comparing this dataset to previous datasets.
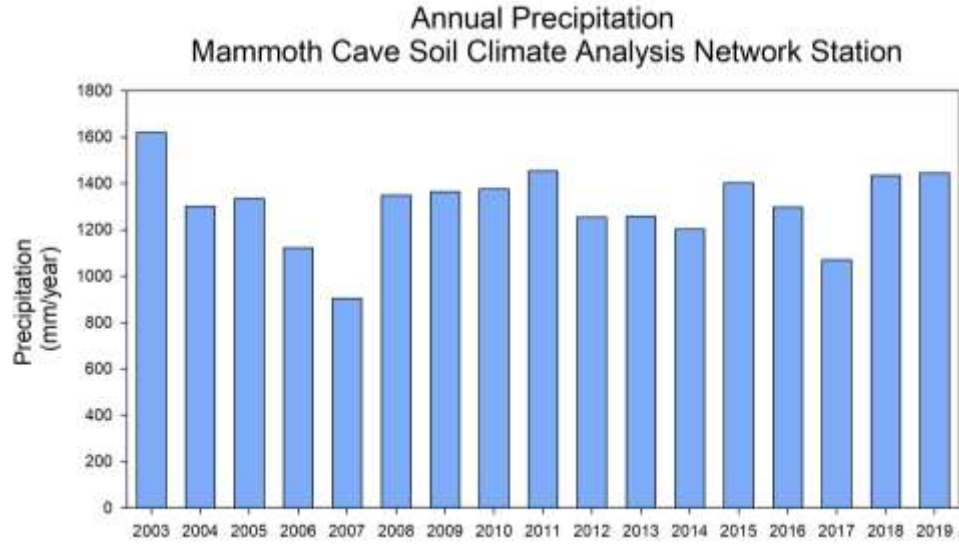
Figure 3.17 Annual Precipitation at Mammoth Cave

Reversal Dates (2018)	Starting Water Level (m)	Water Level Range (m)
06/29 – 07/05 JD 180-186	3.67	3.38 – 4.00
09/28 – 10/5 JD 271-278	2.71	2.71 – 3.54
10/18 – 10/24 JD 291-297	2.21	2.00 – 2.70
11/9 – 11/14 JD 313-318	2.28	2.27 – 3.43
11/18 – 11/30 JD 322-334	3.84	1.97 – 3.84
12/6 – 12/11 JD 340-345	2.41	2.23 – 3.82
12/16 – 12/20 JD 350-354	1.74	1.74 – 2.99
12/21 – 12/23 JD 355-357	3.66	3.66 – 4.98
12/24 – 12/27 JD 358-361	4.36	3.51 – 4.49
12/29 – 12/31 JD 363-365	4.08	3.29 – 4.13

Table 3.1 Water Level data of the Green River
Water Level data of the Green River during ten recorded stable reverse flows.

3.3.3 Natural and Artificial Processes Affecting Flow Reversals

Flow reversals in River Styx and Echo River Springs are caused by differences in hydraulic head between the Green River and the River Styx and Echo River karst basins. In this study, hydraulic head is defined by water pressure. In the Green River, water pressure can be treated as the elevation of the water because it is the hydrologic baselevel. In the River Styx and Echo River karst basins, hydraulic head is the pressure, or volume, of water pushing down on the basin. Because this is conduit flow, not diffuse flow, the elevation of the basin water changes rapidly during precipitation events, so elevation alone is not indicative of hydraulic head in the karst basins.

There are several factors that affect hydraulic head in the Green River and karst basins and, therefore, the occurrence and frequency of flow reversals in Mammoth Cave's River Styx and Echo River Springs. Some factors are natural processes — rainfall intensity and duration, rainfall location, antecedent moisture conditions, and evapotranspiration. Another major influence on flow reversals is the artificial control of the Green River Lake by the Green River Dam. Increases in discharge from the Green River Dam raise water levels downstream, causing sustained flows and high-water levels. This artificial process causes hydraulic head differences between the Green River and the karst groundwater basins that discharge into the Green River. These differences in hydraulic head lead to flow reversals. Figure 3.18 illustrates the possible relationship between the hydraulic heads of the Green River and River Styx Karst Basin that control flow direction from River Styx Spring.
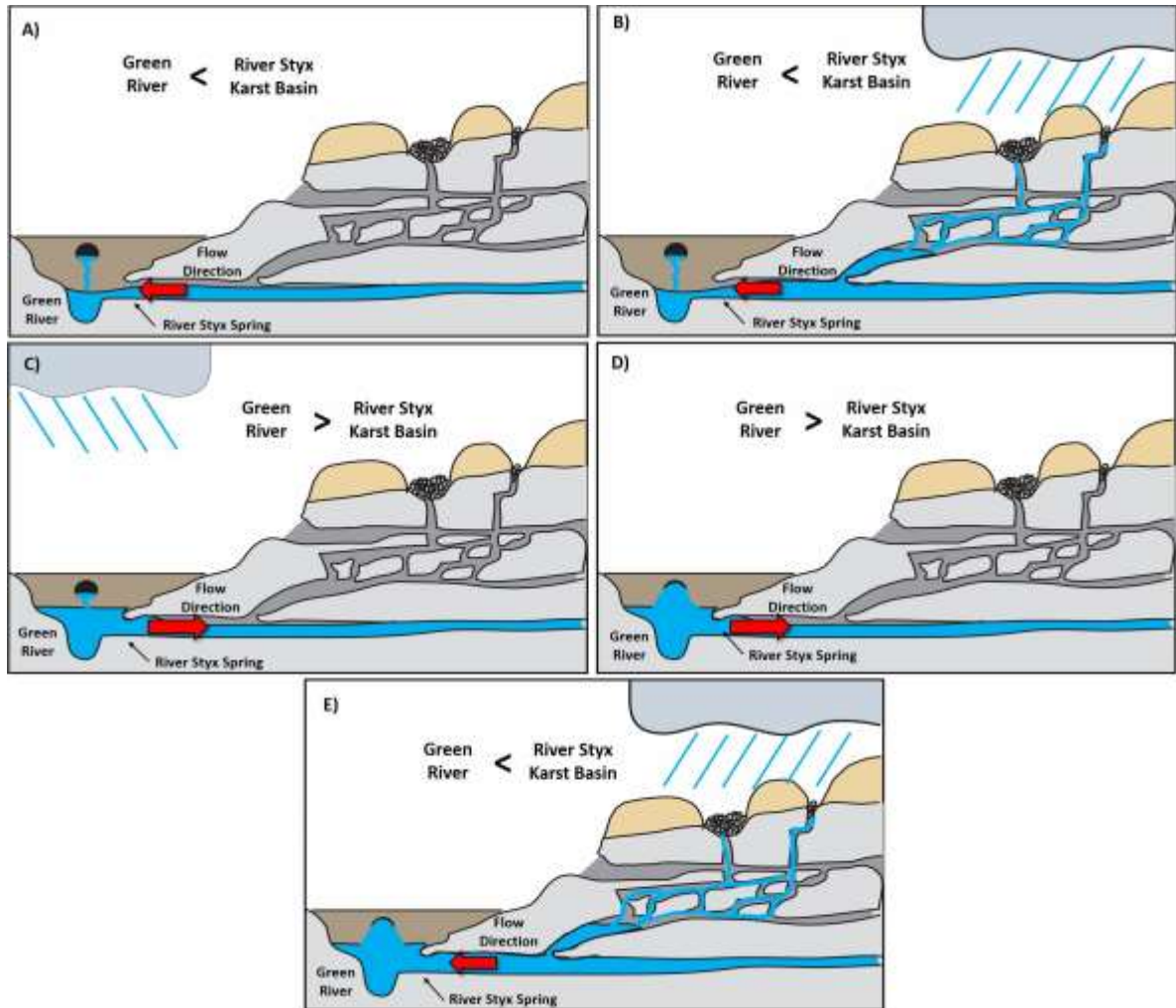
Figure 3.18 Model of hydraulic head conditions of the Green River and RSKB
A) Baseflow conditions – high evapotranspiration rates or no precipitation in either the
River Styx Karst Basin (RSKB) or upstream Green River (GR) and no increase in
discharge from the Green River Dam. Hydraulic head is greater in RSKB than GR and
flow from River Styx Spring (RSS) is normal. B) Storm flow conditions - precipitation
event in RSKB. Hydraulic head is greater in RSKB than GR and flow from RSS is
normal. C) Precipitation upstream of Mammoth Cave in the Green River Basin. High
rates of evapotranspiration or no/little precipitation in RSKB. Hydraulic head is greater in
GR than RSKB and flow at RSS is reverse. D) No precipitation in either RSKB or
upstream GR. Increased discharge from Green River Dam because of the lowering of the
Green River Lake to winter pool. Hydraulic head is greater in GR than RSKB and flow at
RSS is reverse. E) GR water level is high due to lowering of lake stage and increased
discharge from Green River Dam. An intense storm event in RSKB causes the hydraulic
head of RSKB to be greater than GR and flow from RSS is normal.
This figure is for conceptual purposes only and is not to scale.

84

The frequency of flow reversals is also influenced by seasonal variations. For example, only one stable reverse flow (JD 180-186) occurred during the summer season. This stable reverse flow was identified by a rapid increase in temperature and decrease in SpC, reflective of Green River water entering the system. Preceding that event, a total of 28.8 mm of precipitation was recorded at Houchin Meadow's weather station from June 21 to June 25 (JD 172-176). As the Green River's stage was increasing from that event, an additional 73.6 mm of precipitation fell from June 26 to June 28 (JD 177-179). The Green River's stage peaked at 4.08 m on June 28 (JD 179). The stage decreased until for approximately 18 hours and then began to increase. The Green River remained elevated, between 3.38 m and 4.00 m, due to increased discharge from the dam on Green River Lake. The river began returning to base level conditions on July 5 (JD 186; Figure 3.19). This was the only major dam release that occurred during the summer season. Two intense rainfall events (53.9 mm and 42.6 mm) were recorded in August over a forty-eight-hour period. Interestingly, these events increased the Green River's water level by only 0.2 – 0.3 m. It is likely much of the precipitation from these events did not reach the epikarst due to low antecedent moisture conditions in the soil, vegetation uptake, and the increased evapotranspiration rate during this time of the year.

Evapotranspiration rates can significantly affect the amount of recharge to a karst basin and, therefore, the depth of the water table. Seasonal fluctuations in the water table have been measured in other locations, with lows in the summer and highs during the winter (Cane and Clark 1999). In a water balance study taken over five hundred and five days, evapotranspiration accounted for 68% of precipitation entering the Edwards Karst Aquifer in South Central Texas. The remainder of the precipitation recharged the karst

aquifer, either through diffuse recharge (26%) or through discrete recharge (6%); however, 42% of the total precipitation during an intense individual storm event was discrete recharge because of the previously saturated conditions of the vadose zone. This study demonstrates the importance of antecedent moisture conditions to recharge rates (Huawert and Sharp 2014).
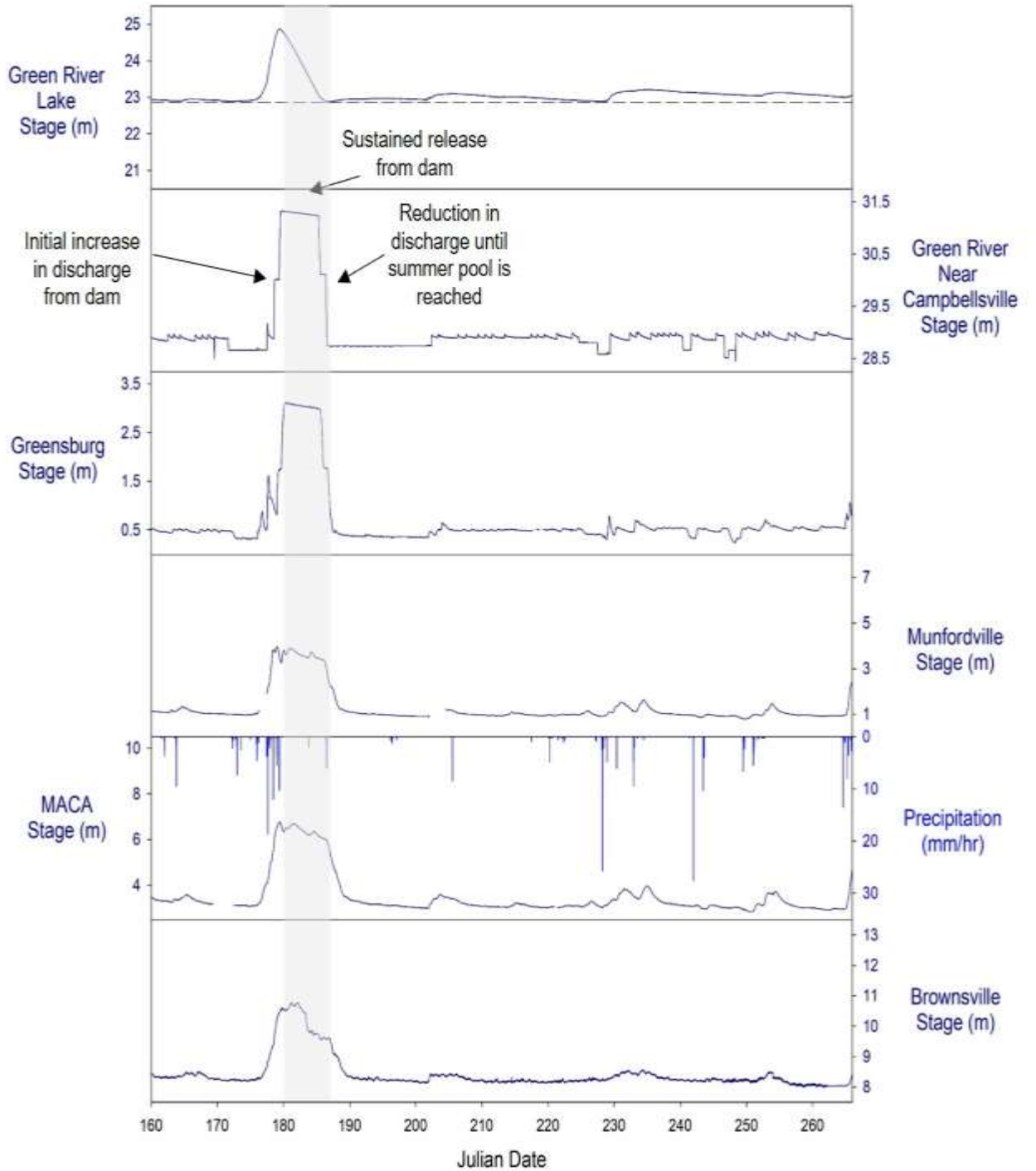
Figure 3.19 USGS gauging stations along the Green River during the summer
(JD 160-265) show how reductions in the Green River Lake increase river levels
downstream for extended seasons of time. Throughout the study, Green River Lake and
the downstream stations never reached flood stage.

87

Six stable reverse flows occurred during the winter season (Figure 3.20). Geochemical analysis indicates that, during this season, River Styx Spring was reversing 72.5% of the time, suggesting that stable reverse flow is typical during the winter season. Brown (1966) suggested that stable reverse flow conditions during the winter season were more common than normal flow conditions and that flow would only return to normal following local precipitation events in the River Styx catchment area. Similarly, all the stable reverse flows at this time, except for the reversal from December 6 to December 11 (JD 340-345), ended due to storm events that changed the hydraulic gradient in the system (Figure 3.18f). Data from the 2009-2012 study did not show the same frequency of stable reverse flow events in the winter (Trimboli and Toomey 2019). A closer comparison of these datasets is needed to understand the differences between these years that led to variability in reverse flow frequency. The frequency of stable reverse flows during the winter season of 2018 can be attributed to both anthropogenic dam control (reducing Green River Lake stage to winter pool conditions) and high rates of precipitation in the Green River basin upstream of MCNP (Figure 3.18). According to the Army Corp of Engineers, a 3 m reduction in lake stage is routinely scheduled for the month of November. But due to high rates of precipitation, the Green River Lake's stage remained higher than winter pool (a stage of 19.51 m at Green River Lake) despite increased discharge from the dam.

Precipitation duration and intensity, evapotranspiration, antecedent moisture conditions, and dam control also affect the elevation of the water table. Because the Green River is hydrologic baselevel of the Mammoth Cave area, the river is the surficial expression of the water table. Increasing the height of the Green River causes a localized

increase in the water table compared with the surrounding karst basins. For this reason, stable reverse flows can be considered events where the river is temporarily pirated into the cave system. In this case, River Styx Spring acts as a sink that receives overflow from the Green River. During the winter months, the water table is higher, and the River Styx receives water from the Green River most of the time. Therefore, stable reverse flow conditions can be considered the normal flow regime and an overflow mechanism of the water table during the winter months.

Site elevations to determine changes in the hydraulic gradient during flow reversals and spring discharge were not collected for this study. However, future studies on this phenomenon would benefit from this information to understand the cause of flow reversals. Structural irregularities in the lithology, facies changes, or speleological variabilities may influence changes in the hydraulic gradient. Another influence might be vegetation, as multiple studies have shown. Local cones of depression, caused by significant transpiration from the overlying vegetation, affect groundwater flow direction (LaBaugh and Rosenberry 2008). This is unlikely in the case of MCNP, as most flow reversals occur during those seasons when vegetation is dormant. Echo River karst basin is nearly ten times the size of River Styx karst basin, so analyzing differences in discharge rates between the two basins would contribute to the understanding of how variable hydrologic flow regimes affect spring flow reversals.
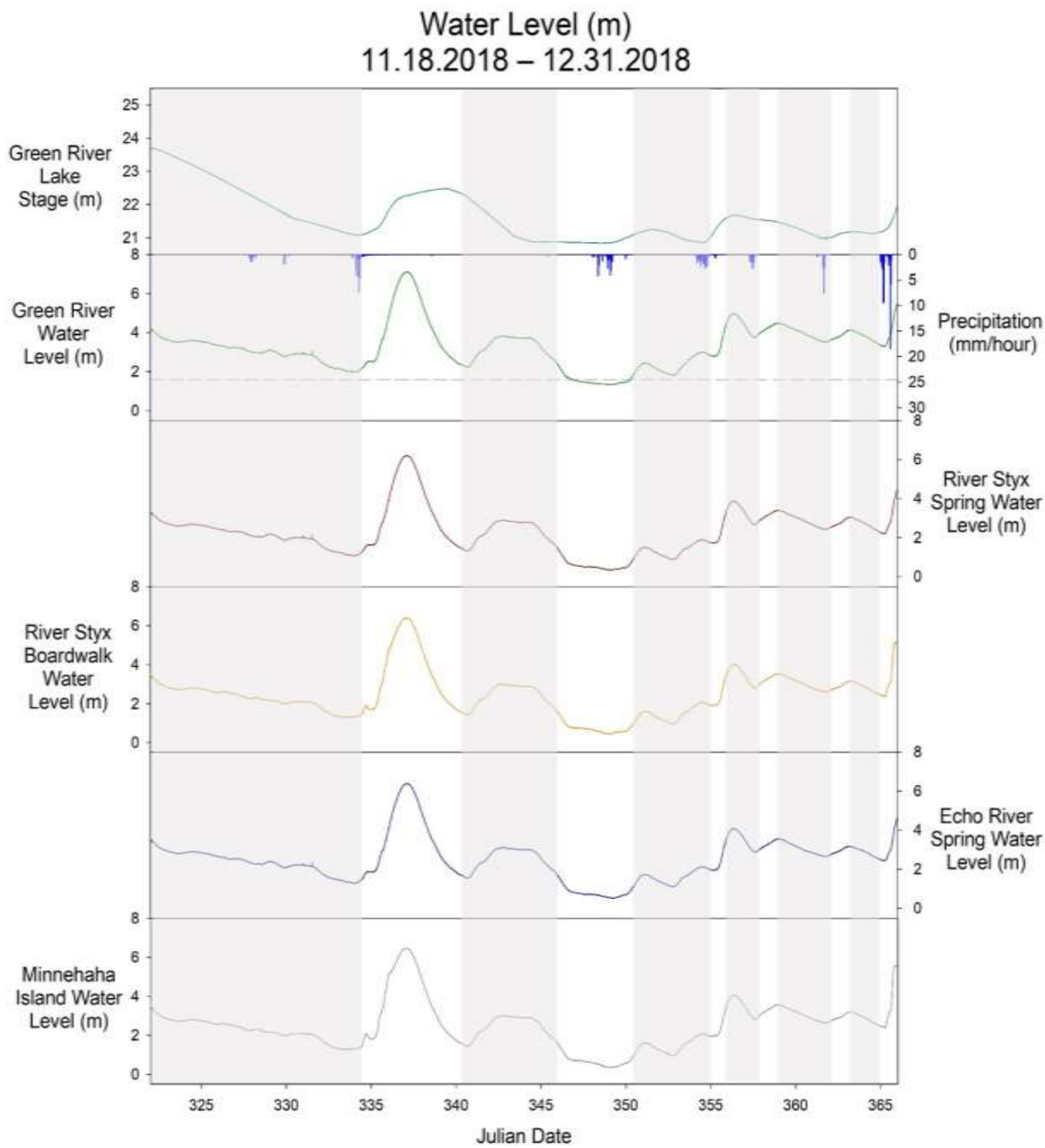
Figure 3.20 Green River Lake and MCNP water levels
During the winter season (JD 322-365), stage never reached base flow conditions, due to
frequent dam releases caused by precipitation events and reduction to winter pool.

3.4 Conclusions

The major mechanisms that influence spring flow reversals include rainfall intensity and duration, antecedent soil moisture conditions, and evapotranspiration. But the primary mechanism that regulates spring flow reversals in Mammoth Cave National Park is anthropogenic: dam control. Even though rainfall affects the head gradient between the groundwater basins and the Green River, intense precipitation events may actually induce normal flow conditions during a reversal, as was seen during the winter season of 2018.

Because the Green River had low-flow conditions throughout much of the summer, flow was normal. During the summer, precipitation events do not usually significantly influence flow conditions. This is likely due to high rates of evapotranspiration, which prevents deep infiltration of meteoric water. During the summer, evapotranspiration rates are high, so precipitation events rarely overwhelm lake levels. Additionally, water is held back from the Green River by the dam in order to keep lake levels at summer pool. For these reasons, there was only one stable reverse flow during the summer.

Flow reversals are largely sustained by the releasing of water from the Green River Lake reservoir. Increased discharge from the dam raises the stage of the Green River downstream for extended periods of time. During the fall transitional season, evapotranspiration rates decline, precipitation increases, and discharge from the dam increases as the lake is reduced to winter pool. The combination of these factors causes an increase in the frequency and duration of stable reverse flows.

High-resolution monitoring of temperature, SpC, and pH in Mammoth Cave National Park can be used to identify when spring flow reversals occur, as well as their frequency and their duration. During most of the year, temperature is the clearest indicator of flow reversals, due to the consistency of cave water temperatures during normal flow conditions; however, temperature is less useful during seasonal transitions. For this reason, SpC and pH can be used to provide additional data regarding flow reversals. Because transitional flow periods may last up to several days, the installation of high-resolution instrumentation to record flow direction is recommended for future studies, in order to better understand the precise timing of spring flow reversals. Further analysis of high-resolution data will provide insights into how flow reversal affects dissolution in a telogenetic karst aquifer.

3.5 Literature Cited

Akindele, E.O., Indabawa, I.I., 2015. A review of the effects of dams on the hydrology, water quality and invertebrate fauna of some Nigerian freshwaters. *The Zoologist* 13, 28-35.

Albéric̓, P., 2004. River backflooding into a karst resurgence (Loiret, France). *Journal of Hydrology* 286(1), 194-202.

Brookfield, A.E., Macpherson, G.L., Covington, M.D., 2016. Effects of changing meteoric precipitation patterns on groundwater temperature in karst environments. *Groundwater* 55(2), 227-236.

Brown, R.F., 1966. Hydrology of the cavernous limestones of the Mammoth Cave Area Kentucky. U.S. Department of Interior, Geological Survey Water-Supply Paper 1837: Denver, CO.

Cane, G., Clark, I.D., 1999. Tracing ground water recharge in an agricultural watershed with isotopes. *Groundwater* 37(1), 133-139.

Compton, M.C., Yahn, B.D., Phelps, L.T., 2017. Preliminary ecological assessment of the Green and Nolin rivers in Mammoth Cave National Park, Kentucky, following the removal of lock and dam #6. Kentucky State Nature Preserves Commission report to the U.S. Fish and Wildlife Service.

Constantz, J.E., Niswonger, R.G., Stewart, A.E., 2008. Analysis of temperature gradients to determine stream exchanges with ground water. In: Rosenberry, D.O., LaBaugh, J.W., ed. *Field Techniques for Estimating Water Fluxes Between Surface Water and Ground Water.* U.S. Geological Survey, Techniques and Methods 4–D2: Reston, VA.

Cushman, R. V., Krieger, R.A., McCabe, J.A., 1965. Present and future water supply for Mammoth Cave National Park, KY. U.S. Geological Survey, Water Supply Paper 1475-Q.

Drever, J.I., 1997. The geochemistry of natural waters: surface and groundwater environments. Upper Saddle River, NJ: Prentice Hall.

Edwards, A., 2009. The hydrochemistry of surface water backflooding into a karst spring and into cave stream passages in Mammoth Cave, KY USA. Report on NPS Permit MACA-2007-SCI-0011.

Francis, B.A., Francis, L.K., Bayani Cardenas, M., 2010. Water table dynamics and groundwater–surface water interaction during filling and draining of a large fluvial island due to dam-induced river stage fluctuations. *Water Resources Research* 46(7), 1-5.

Graf, W.L, 2006. Downstream hydrologic and geomorphic effects of large dams on American rivers. *Geomorphology* 79(3-4), 336-360.

Granger, D.E., Fabel, D., Palmer, A.N., 2001. Pliocene-Pleistocene incision of the Green River, Kentucky, determined from radioactive decay of cosmogenic [26]Al and [10]Be in Mammoth Cave sediments. *GSA Bulletin*, 133(7), 825-836.

Grubbs, S.A., Taylor, J.M., 2004. The influence of flow impoundment and river regulation on the distribution of riverine macroinvertebrates at Mammoth Cave National Park, Kentucky, U.S.A. *Hydrobiologia* 520 (1-3), 19-28.

Gulley, J., Martin, J. B., Screaton, E. J., Moore, P. J., 2011. River reversals into karst springs: A model for cave enlargement in eogenetic karst aquifers. *GSA Bulletin* 123(3-4), 457-467.

Gulley, J.D., Martin, J.B., Moore, P.J., Murphy, J., 2013. Formation of phreatic caves in an eogenetic karst aquifer by CO_2 enrichment at lower water tables and subsequent flooding by sea level rise. *Earth Surface Processes and Landforms* 38(11), 1210-1224.

Helf, K. L., Olson, R.A., 2017. Subsurface aquatic ecology of Mammoth Cave. In: Hobbs, H.H., Olson, R.A., Winkler, E.G., Culver, D.C., ed. *Mammoth Cave: A human and natural history.* Springer Online

Hendrickson, G.E., 1961. Sources of water in Styx and Echo rivers, Mammoth Cave, Kentucky. U.S. Geological Survey Professional Paper, 424-D:D41-D43.

Hess, J.W., Wells, S.G., Quinlan, J.F., White, W.B., 1989. Hydrogeology of the South-central Kentucky karst. In: White, W.B., White, E.L. ed. *Karst hydrology: concepts from the Mammoth Cave area.* New York, NY: Van Nostrand Reinhold.

Hess, J.W., White, W.B., 1989a. Water budget and physical hydrology. In: White, W.B., White, E.L. ed. *Karst hydrology: concepts from the Mammoth Cave area.* New York, NY: Van Nostrand Reinhold.

Huawert, N.M., Sharp, J.M., 2014. Measuring autogenic recharge over a karst aquifer utilizing eddy covariance evapotranspiration. *Journal of Water Resource and Protection* 6, 869-879.

Jackson, L., 2017. Epikarst hydrogeochemical changes in telogenetic karst systems in South-central Kentucky. Master's thesis. Bowling Green: Western Kentucky University, Department of Geography and Geology.

LaBaugh, J.W., Rosenberry, D.O., 2008. Introduction and characteristics of flow. In: Rosenberry, D.O., LaBaugh, J.W., ed. *Field Techniques for Estimating Water Fluxes Between Surface Water and Ground Water.* U.S. Geological Survey, Techniques and Methods 4–D2: Reston, VA.

Lawhon, N., 2014. Investigating telogenetic karst aquifer processes and evolution in south-central Kentucky, U.S., using high-resolution storm hydrology and geochemistry monitoring. Master's thesis. Bowling Green: Western Kentucky University, Department of Geography and Geology.

McClanahan, K., 2014. Carbon Cycling Dynamics Inferred from Carbon Isotope Sourcing in a Mid-Latitude Karst-Influenced River. Master's thesis. Bowling Green: Western Kentucky University, Department of Geography and Geology.

Meiman, J., 2006. Water resources management plan, MCNP, Kentucky. Technical Report: United States Department of the Interior, National Park Service.

Musgrove, M., Stern, L.A., Banner, J.L., 2010. Springwater geochemistry at Honey Creek State Natural Area, central Texas: Implications for surface water and groundwater interaction in a karst aquifer. *Journal of Hydrology* 388, 144-156.

Nimick, D.A., Gammons, C.H., Cleasby, T.E., Madison, J.P., Skaar, D., Brick, C.M., 2003. Diel cycles in dissolved metal concentrations in streams: Occurrence and possible causes. *Water Resources Research* 39(9), 1247-1264.

NOAA (National Oceanic and Atmospheric Administration), 2019. NPS and USCRN in the Eastern United States. Accessed June 29, 2019 from https://www.ncdc.noaa.gov/news/nps-and-uscrn-eastern-united-states.

Palmer, A.N., 1981. *A geological guide to MCNP.* Teaneck, NJ: Zephyrus Press.

Palmer, A.N., 2007. *Cave geology*. Dayton, OH: Cave Books.

Paylor, R.L., Currens, J.C., 2001. Karst Occurrence in Kentucky. Kentucky Geological Survey Map and Chart 35. Accessed October 15, 2019 from https://uknowledge.uky.edu/kgs_mc/35.

Ruhl, M., 2005. Flow reversal events increase the abundance of nontroglobitic fish in the subterranean rivers of Mammoth Cave National Park, Kentucky. Master's thesis. Bowling Green: Western Kentucky University, Department of Geography and Geology.

Shelley, J.A., 2019. Monitoring and evaluating the influences of class V injection wells on urban karst hydrology. Master's thesis. Bowling Green: Western Kentucky University, Department of Geography and Geology.

Taylor, C.J., Greene, E.A., 2008. Hydrogeologic characterization and methods used in the investigation of karst hydrology. In: Rosenberry, D.O., LaBaugh, J.W., ed. *Field Techniques for Estimating Water Fluxes Between Surface Water and Ground Water.* U.S. Geological Survey, Techniques and Methods 4–D2: Reston, VA.

Toomey, R.S., Hobbs, H.H., Olson, R.A., 2017. An Orientation to Mammoth Cave and This Volume In: Hobbs, H.H., Olson, R.A., Winkler, E.G., Culver, D.C., ed. *Mammoth Cave: A human and natural history.* Springer Online

Trimboli, S.R., Weber, K., Ryan, S., Toomey, R.S., 2016. An overview of the reverse flow patterns of River Styx in Mammoth Cave, Kentucky: 2009-2012, in Proceedings, Mammoth Cave Research Symposia, MCNP, 128-129.

Trimboli, S. R., Toomey, R.S., 2019. Temperature and reverse-flow patterns of the River Styx, Mammoth Cave, Kentucky. *Journal of Cave and Karst Studies* 81(3), 174-187.

U.S. Army Corps of Engineers (USACE), 2011. Green River Watershed Section 729 Initial Watershed Assessment. Watershed Study Report: Louisville District.

Wagner, R.J., Boulger Jr., R.W., Oblinger, C.J., Smith, B.A., 2006. *Guidelines and standard procedures for continuous water-quality monitors: Station operation, record computation, and data reporting.* Techniques and Methods 1–D3. Reston, VA: U.S. Geological Survey. Accessed November 21, 2017 from https://pubs.usgs.gov/tm/2006/tm1D3/pdf/TM1D3.pdf

White, W.B., 1989. Introduction to the karst hydrology of the Mammoth Cave area. In: White, W.B., White, E.L. ed. *Karst hydrology: concepts from the Mammoth Cave area.* New York, NY: Van Nostrand Reinhold.

White, W.B., 1993, Analysis of karst aquifers. In: Alley, W.M., ed. *Regional groundwater quality.* New York, NY: Van Nostrand Reinhold.

White, W.B., White, E.L., 2017. Hydrology and hydrogeology of Mammoth Cave. In: Hobbs, H.H., Olson, R.A., Winkler, E.G., Culver, D.C., ed. *Mammoth Cave: A human and natural history.* Springer Online.

Wilde, F.D., Radtke, D.B., Gibs, J., and Iwatsubo, R.T., 2004. Processing of water samples. In *USGS Techniques of Water-Resources Investigations, Book 9.* Reston, VA: U.S. Geological Survey. Accessed November 19, 2017 from https://water.usgs.gov/owq/FieldManual/chapter5/html/Ch5_contents.html

Wilde, F.D., Sandstrom, M.W., Skrobialowski, S.C. 2015. National field manual for the collection of water-quality data. U.S. Geological Survey Techniques of Water-Resources Investigations, Book 9. Reston, VA: U.S. Geological Survey. Accessed November 19, 2017 from https://water.usgs.gov/owq/FieldManual/

4. Dissolution dynamics in Mammoth Cave's River Styx and Echo River karst basins

4.1 Introduction

Karst aquifers are dynamic systems in which groundwater and surface water can be studied as a unified system. The rapid infiltration of meteoric water, short groundwater residence times, and interconnectedness of the surface to subsurface through a variety of geomorphic features allows for the movement of meteoric water through soils, where it becomes enriched with CO_2, and enters the karst system below. Because CO_2 is the primary driver of calcite dissolution, these enriched waters enlarge fractures, joints, and conduits to form cave systems (White 1988; Ford and Williams 2007).

The Mammoth Cave System is the longest cave system in the world with 668 kilometers of mapped passages and a vertical extent of nearly 124 meters (Gulden 2019). The Mammoth Cave System lies on the edge of the Chester Upland and Illinois Basin in South Central Kentucky. The speleogenesis of Mammoth Cave has been directly influenced by the evolution of the Green River through multiple stages of deposition and erosion (Palmer 1981; Granger et al. 2001; Palmer 2017). The Green River is a tributary of the Ohio River. Due to the relationship between the Ohio River, Green River, and Mammoth Cave System, glacial episodes during the Pliocene and Pleistocene that affected the evolution of the Ohio River have been linked to the speleogenesis of Mammoth Cave (Granger et al. 2001). The initial development of the Mammoth Cave System is believed to have occurred over ten million years ago as the Green River carved through the sandstone caprock, exposing limestone at the surface, and created an outlet for subsurface flow through the Girkin formation (Palmer 2017). Later development of

multiple levels of cave passages occurred due to rapid incision and aggradation episodes from about 3.25 to 0.7 million years ago in the Green River. These episodes were linked to changes in the regional hydrology and water supply caused by glacial advances and retreats (Granger et al. 2001). The most recent aggradation event deposited 15 m of sediment in the Green River valley, flooding the lowest levels of the cave, and establishing the current regional base level at which dissolution occurs today (Palmer 2017).

In this study, the dissolution dynamics of River Styx and Echo River groundwater basins in Mammoth Cave National Park (MCNP) were analyzed in order to determine current processes affecting dissolution in these base level conduits. These basins experience a phenomenon known as stable reverse flow, where water from the Green River enters the cave system through River Styx Spring, crosses a drainage divide between the River Styx and Echo River karst basins, and exits Echo River Spring. Stable reverse flows in River Styx and Echo River can last from days to weeks at a time. Stable reverse flows are caused by changes in hydraulic head between the karst basins and the Green River, commonly related to precipitation events in the Green River basin and water level controls by the Green River Lake Dam, 169 kilometers upstream (Meiman 2006; Trimboli et al. 2016; Trimboli and Toomey 2019). In Florida, river reversal in springs have been found to be a significant contributor to eogenetic conduit enlargement (Gulley 2011). However, no investigations attempted to quantify the effects of flow reversals on dissolution in telogenetic karst systems prior to this study.

4.2 Study Area

The Western Pennyroyal karst area of South Central Kentucky, including MCNP (Figure 4.1), is one of the most explored and most studied karst regions in the world (Palmer 1981; White 1989). The park is located 145 kilometers south of Louisville and 30 kilometers northeast of Bowling Green, in one of the most cave dense areas of the state. MCNP is characterized as a deciduous forest in a humid sub-tropical climate (Hess and White 1989; Meiman 2006). MCNP became a World Heritage Site in 1981 and an International Biosphere Reserve in 1990. Fifty-two troglobitic species, those that are adapted to cave environments and spend their whole lives in caves, are present in Mammoth Cave (Toomey et al. 2017).

South Central Kentucky is underlain by Mississippian age sedimentary rocks (Figure 4.2), that gently dip, less than one degree, northwest toward the center of the Illinois Basin (Palmer 1981). The numerous passages of Mammoth Cave developed in an approximately 100-meter-thick section of the St. Louis, St. Genevieve, and Girkin Limestones, which contain minor beds of chert and dolomite. The average porosity of the limestones that make up Mammoth Cave is 2.4% (Worthington et al. 2000). The Big Clifty Sandstone, a 15 to 18-meter-thick formation consisting of interbedded sandstone, siltstone, and shale, acts as a weathering-resistant caprock that protects the Mammoth Cave from rapid denudation (Palmer 1981).
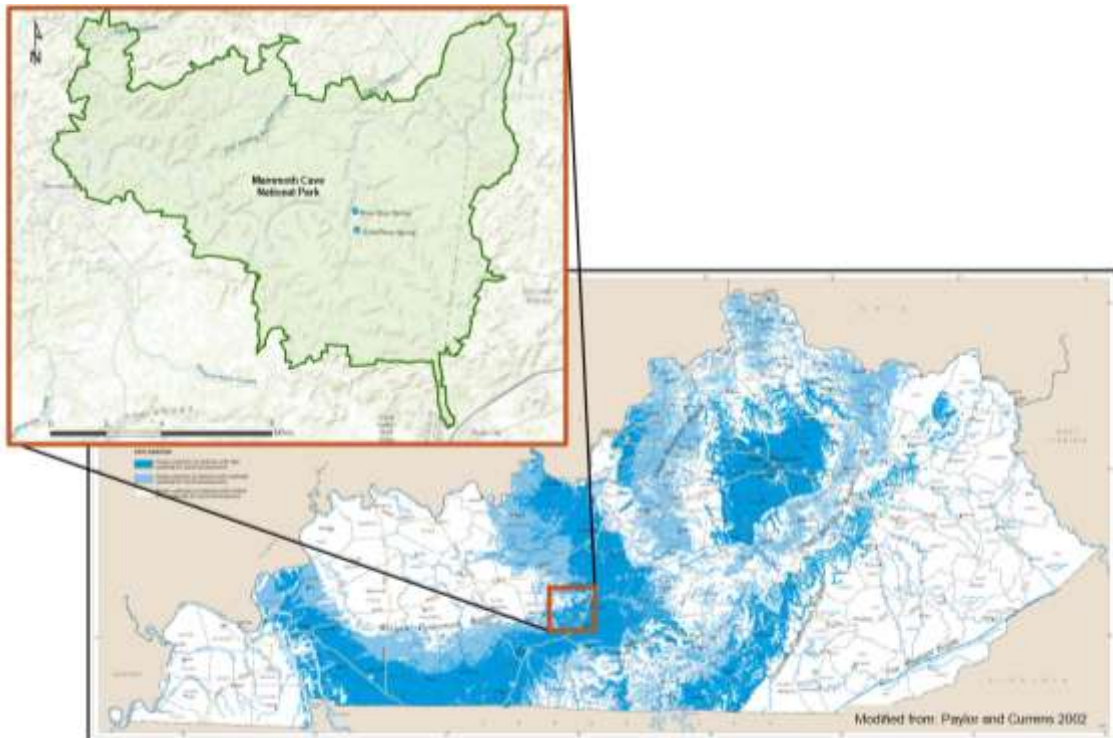
Figure 4.1 Mammoth Cave National Park
located in the Western Pennyroyal karst region
(Modified from Paylor and Currens 2001).

System	Series	Formation	Lithology	Thickness
Mississippian	Chesterian	Hardinsburg		18 m
		Haney		12 m
		Big Clifty		15-18 m
		Girkin		40-43 m
	Meramecian	St. Genevieve		34-37 m
		St. Louis		53-60 m

Sandstone   Limestone   Gypsum   Shale   Chert   Dolomite

Figure 4.2 South Central Kentucky geology
(Modified from Hess et al. 1989).

The Mammoth Cave Karst Aquifer is located in the upper Green River drainage basin (Hess et al. 1989; McClanahan 2014). Conduit development at Mammoth Cave is directly influenced by the Green River, the regional base level of the Mammoth Cave Aquifer. The multiple levels of the cave can be attributed to changes in the base level of the Green River during past glacial conditions (Granger et al. 2001).

The River Styx (2.2 km^2) and Echo River (21.7 km^2) groundwater basins (Figure 4.3) discharge groundwater from the Mammoth Cave Ridge and neighboring karst valleys and are adjacent to one another, separated by a low sandbar (White and White 2017, Trimboli and Toomey 2019). During stable reverse flow, water flows from the Green River into River Styx Spring. This reverse flow, opposite to the normal flow direction, moves along the path of River Styx, then passes over a drainage divide between River Styx and Echo River, flows into the Echo River, and is discharged back into the Green River at Echo River Spring (Figure 4.4).
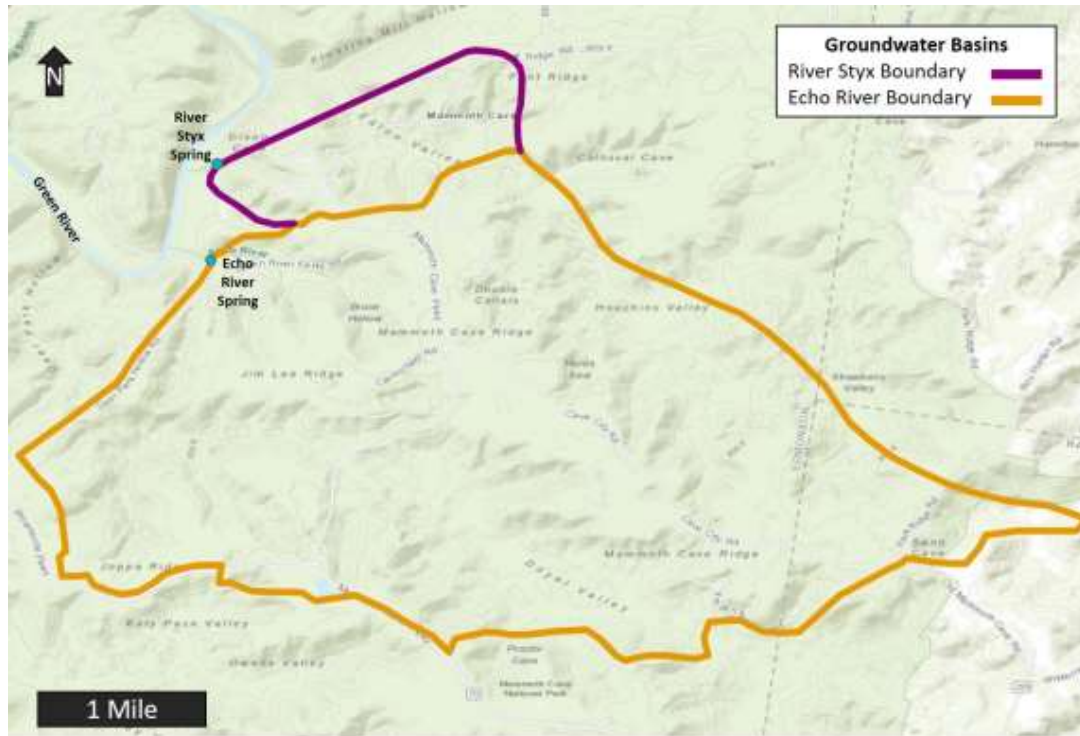
Figure 4.3 River Styx and Echo River groundwater basins
(Modified from Mammoth Cave International Center for Science and Learning 2012).
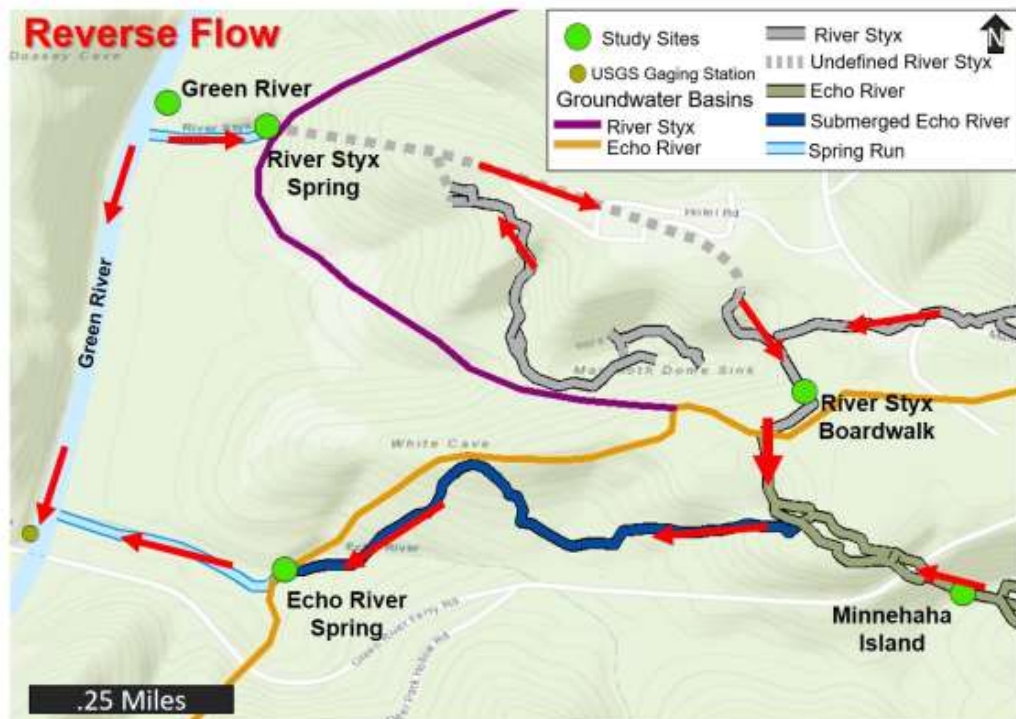
Figure 4.4 Map displaying site locations and the reverse flow route
(Modified from Mammoth Cave International Center for Science and Learning 2012).

4.3 Methods

4.3.1 Site Selection and Setup

Five sites were chosen for data collection: Green River, River Styx Spring, the River Styx Boardwalk (River Styx, in cave), Echo River Spring, and Minnehaha Island (Figure 4.4). Two PVC stilling wells were installed at each of the five sites. All stilling wells were drilled with multiple holes to allow water flow. The Green River stilling wells were screened with wire mesh to prevent sediment buildup. Due to limited access to vertical surfaces, diagonal stilling wells were installed at River Styx Spring, Echo River Spring, Minnehaha Island, and the Green River. T-posts and trees were used as anchor points at these four sites. Vertical stilling wells were installed at River Styx Boardwalk and were anchored to an existing walkway structure. A YSI EXO II was installed at the River Styx Boardwalk in a 7.6 mm stilling well. YSI 6920 V2 multiparameter sondes were installed at River Styx Spring, Echo River Spring, Minnehaha Island, and the Green River in 7.6 mm PVC stilling wells. HOBO pressure transducers were installed in 3.2 mm PVC stilling wells at all five sites.

4.3.2 Data Collection

A YSI multiparameter sonde and a HOBO pressure transducer were both deployed at each of the five sites on June 9, 2018. The YSI multiparameter sondes were used to collect high-resolution data for pH, SpC, and temperature at ten-minute intervals. The HOBO pressure transducers were used to collect high-resolution water level and temperature data at a two-minute resolution. Two additional pressure transducers were installed in-air: one on the surface at River Styx Spring and the other in-cave at

103

Minnehaha Island. The in-air pressure transducers were used to collect barometric pressure data at a two-minute resolution. Sites (when accessible) were visited weekly for maintenance, to resolve any issues with the sites and to download data. The sondes (when accessible) were calibrated once per month to maintain accurate data collection and to minimize drift. Precipitation rates (mm/hour) were collected from the National Park Service's gaseous pollutant and meteorological station located at Houchin Meadow. The stage height of the Green River was obtained from USGS gauging stations on the Green River at the Green River Lake (03305990), the Green River near Campbellsville (03306000), Greensburg (03306500), Munfordville (03308500), Mammoth Cave (03309000), and Brownsville (03311505). Data from these gauging stations were used as a proxy to determine when water was released from an upstream dam on Green River Lake.

A YSI ProDSS multiparameter sonde and an Oakton PCTSTestr 35 were used to collect pH, SpC, and temperature data at each site during sample collection. Handheld multiparameter monitors were calibrated before each field day to ensure the accuracy of the grab samples. Sampling sites were adjusted during storm events if the normal collection site became inaccessible due to increased stage of the Green, River Styx, or Echo Rivers. On a few occasions, samples were not collected due to complete site inaccessibility.

4.3.3 Sample Collection and Analysis

Weekly water samples were collected for analysis starting on June 15, 2018, at all five sites. Both cation and anion samples were collected in 60 mL plastic bottles. The pH of the cation samples was lowered to ≤ 2 using 7 drops of nitric acid (HNO_3) for

preservation purposes (Wilde et al. 2004). All samples were filtered to remove organic

matter using a syringe and 0.45 μm filter paper, as recommended for major-ion analysis

(Wilde et al. 2004). Cation and anion samples were sealed with no headspace; wrapped

with parafilm in order to prevent outgassing and fractionation; and then stored in a

refrigerator at 4 °C until analysis (Wilde et al. 2004). Alkalinity was measured at each

site using the Orion Total Alkalinity test. Sample collection and sonde maintenance

followed the standard guidelines presented in the USGS's National Field Manual for the

Collection of Water-Quality Data (Wilde et al. 2015).

Cation samples were analyzed for calcium (Ca^{2+}), magnesium (Mg^{2+}), potassium

(K^+), sodium (Na^+), and Iron (Fe^{2+}). Cation concentrations in ppm were determined using

inductively coupled plasma optical emission spectroscopy (ICP-OES), method EPA

200.7 revision 4.4, at Western Kentucky University's Advanced Materials Institute.

Anion samples were analyzed for fluoride (F^-), chloride (Cl^-), bromide (Br^-), nitrite

(NO_2^-), nitrate (NO_3^-), phosphate (PO_4^{3-}), and sulfate (SO_4^{2-}). Anion concentrations in

ppm were determined using Ion Chromatography (IC), method 4110 B, at Western

Kentucky University's HydroAnalytical Laboratory.

4.3.4 Data Processing

All data were compiled in Excel and SigmaPlot spreadsheets. High-resolution

water levels were calculated from pressure transducer data using HOBOware software.

Initial water levels, used as a reference, were measured with a tape measure. Barometric

pressure data were removed from the total pressure data to increase the accuracy and

reduce noise within the calculated water levels. The two-minute resolution was chosen

because responses in the karst system occur rapidly, as shown in other studies (Lawhon

2014; Shelley 2019). Hydrochemical data obtained from the sondes (i.e. pH and SpC) were corrected for calibration drift and fouling using calibration values and grab sample data in accordance with the *USGS's Guidelines and Standard Procedures for Continuous Water-Quality Monitors: Station Operation, Record Computation, and Data Reporting* (Wagner et al. 2006). Graphs of high-resolution data regarding temperature, pH, and SpC were analyzed to identify trends and relationships between sites.

Charge balance errors were determined using cation, anion, and alkalinity concentrations. Charge balance errors ranged from 0.3 to 35.1%, with an average of 11.5%. Large errors were associated with storm events, likely caused by dilution, the influence of organic acids causing an overestimation of alkalinity, or temperature variations leading to imprecise pH readings (Palmer 2007; Gulley et al. 2013). A statistical relationship between grab sample SpC data and weekly concentrations of Ca^{2+}, Mg^{2+}, and HCO_3^- was established for each site using linear regression. R^2 values range from 0.13 to 0.79, with Ca-SpC having the strongest relationship and Mg-SpC having the weakest relationship overall (

Table 4.1). P values show that most relationships are statistically robust, with the exception of Mg^{2+} at River Styx Spring. When considering only summer concentrations the R^2 value for River Styx Spring is 0.47. Low R^2 values in the fall and winter at River Styx Spring are likely caused by stable reverse flows. During the winter season, River Styx Spring receives overflow from the Green River most of the time (as was discussed in Chapter 3). Overall, the robustness of the R^2 and P values indicate that most ionic constituents that contribute to SpC are accounted for. Comparison to raw ionic analyses data show low values of other ions (graphs show in Appendix II). Slope equations for

these relationships were applied to the high resolution SpC data to calculate changes in

Ca^{2+}, Mg^{2+}, and HCO_3^- over time. Though the slope equations are based on statistically

robust relationships, it should be noted that calculating dissolution from derived values

can cause minor errors in dissolution rates.

Sampling Sites	Ca^{2+} - SpC		HCO_3^- - SpC		Mg^{2+} - SpC	
	R^2	P	R^2	P	R^2	P
Green River	0.45	0.04666136	0.42	0.00149866	0.79	0.00000004
River Styx Spring	0.68	0.00000686	0.44	0.00080769	0.13	0.15247802
River Styx Boardwalk	0.72	0.00000003	0.61	0.00000033	0.36	0.00747231
Echo River Spring	0.49	0.00569203	0.65	0.00000777	0.41	0.01216316
Minnehaha Island	0.77	0.00000046	0.59	0.00000623	0.62	0.00000697

Table 4.1 Statistical regressions between Ca^{2+}, Mg^{2+}, and HCO_3^-

Dissolution of limestone was calculated using various methods or proxies.

Because CO_2 is the main driver of calcite dissolution, pCO_2 values were calculated to

understand seasonal and storm event changes. The pCO_2 was determined using the

equation (White 1988):

$$P_{CO_2} = \frac{\alpha_{HCO_3^-}\alpha_{H^+}}{K_1 K_{CO_2}}$$
(Eq. 4.1)

Where $\alpha_{HCO_3^-}$ is alkalinity, α_{H^+} is the pH, and K_1 and K_{CO_2} are temperature dependent

constants. Temporal changes in the saturation of calcite (SI_{cal}) was determined using the

equation (Palmer 2007):

$$SI_{cal} = \log \frac{(Ca^{2+})(CO_3^{2-})}{K_{cal}}$$
(Eq. 4.2)

where (Ca^{2+}) is the activity of calcium in solution, (CO_3^{2-}) is the activity of carbonate in

solution, and K_{cal} is the temperature-dependent equilibrium constant of $CaCO_3$ in

solution. SI_{cal} was calculated over the length of the study period using high-resolution

temperature and calculated Ca^{2+} and HCO_3^- concentrations. Wall retreat was calculated using the equation (Palmer 1991):

$$S = \frac{31.56k(1-SI_{cal})^n}{Pr} \qquad\qquad \text{(Eq. 4.3)}$$

Where S is rate of wall retreat, k is a temperature dependent rate constant, n is the reaction order, and Pr is the density of limestone. These values were graphed to show changes in the aggressiveness of water during flow reversal events. The ten-minute interval calculations were summed and averaged over specific periods of time as a method of characterizing seasonal and storm driven dissolution rates.

4.4 Results and Discussion

4.4.1 CO_2 Dynamics

Dissolved CO_2 is the primary factor that influences carbonate dissolution — increasing the concentration of dissolved CO_2 in water decreases the pH and increases the water's ability to dissolve calcite (White 1988; Ford and Williams 2007). Additionally, understanding CO_2 flux on the different scales provides insight into carbonate dissolution rates and how dissolution varies temporally. CO_2 concentrations are derived using equilibrium constants for carbonate reactions in conjunction with measured temperature, pH, and alkalinity. CO_2 concentrations are presented here as $EpCO_2$, the ratio of CO_2 concentration in the water compared with the atmospheric CO_2 concentration of 400 ppm (Figure 4.5).

In waters discharging from River Styx and Echo River Springs, average $EpCO_2$ values are greater in the summer than in the fall and winter. During the summer, the average baseflow $EpCO_2$ was 9.26 at River Styx Spring and 13.18 at Echo River Spring; during the winter, it was 6.44 at River Styx Spring and 11.80 at Echo River Spring. Higher averages in the summer is likely due higher rates of soil CO_2 production and lower antecedent moisture conditions during the summer months. In the warm, summer months, vegetation and microbial processes in the soil are more active and produce more CO_2 (White 1989; Liu et al. 2007; Jackson 2017). High rates of evapotranspiration during the summer limit the amount of infiltration of precipitation into soils. Evapotranspiration combined with more biologic activity cause the antecedent moisture conditions to be low during the summer. Water content in soil limits diffusion of CO_2; therefore, low soil

moisture conditions allow for vertical diffusion of soil CO_2 during the summer (Bouma and Bryla 2000; Loisy et al. 2013).

EpCO$_2$ in River Styx Spring and Echo River Spring are comparable to CO_2 trends from other studies in the Mammoth Cave area (White 1989; Groves and Meiman 2005; Hatcher 2013). For example, Groves and Meiman (2005) calculated EpCO$_2$ values between five and ten times atmospheric background in a downstream section of the Logsdon River (a base level subsurface river in the neighboring Turnhole Basin). Further upstream in Logsdon River, EpCO$_2$ values ranged from fifteen to forty times atmospheric background (Hatcher 2013). Spatial changes (from upstream to downstream) causing a decrease pCO_2 along the flow path of the nearby Logsdon River are attributed to long residence times in which CO_2 to dissolution processes (Anthony 1998; Hatcher 2013). Lower CO_2 concentrations at River Styx Spring compared with River Styx Boardwalk suggests the same process (of CO_2 utilization in the dissolution process) is occurring during normal flow conditions in the River Styx Basin. Higher CO_2 concentrations at Echo River Spring compared with Minnehaha Island suggests other influences on CO_2. This increase can may be attributed to a high CO_2 inputs closer to the spring. The increase of soil CO_2 may be attributed to the oxidation of organics along the flow path or an epikarstic infeeder. Rapid increases in temperature and decreases in SpC following precipitation events in Echo River Spring prior to the actual storm flow response suggests a shallower, rapid epikarstic input (Figure 4.8). The recharge of this epikarstic input may be from the numerous swallets in the organic-rich flood plain where the Echo River Spring lies. These swallets could quickly transport meteoric water and mobilizing soil

CO_2 which is rapidly discharged from Echo River Spring, causing higher $EpCO_2$ values and variability year-round.

The use of carbon isotopes, discussed in chapter 3, identified soil CO_2 as the major source of DIC in groundwater in both the River Styx and Echo River karst basins. Soil CO_2 levels were measured in different karst areas in the Mammoth Cave region. The volume of CO_2 in soils at Echo River Spring was at least double the volume of CO_2 in soils sampled at the nearby Cedar Sink and Flint Ridge areas (Miotke 1975). Additionally, soil thickness is a major factor in soil CO_2 production. Soils in the sinkhole plain are thicker and produce more CO_2 than soils in the karst valleys (i.e. River Styx and Echo River karst basins) (White 1989). However, during high flow events, Echo River receives overflow from the Turnhole Basin, which receives recharge from the Sinkhole Plain (Meiman and Ryan 1993; Meiman 2006). The subsurface distribution of pCO_2 is heterogenous in nature and can vary by an order of magnitude within a distance of 30 m (Gulley et al. 2015). When comparing seasonal averages, as well as storm event response, Echo River Spring has higher $EpCO_2$ values than River Styx Spring, suggesting that soil CO_2 concentrations in the Echo River basin are also higher than the River Styx basin (Figure 4.5 and Figure 4.8).

Storm events cause more variability on a much shorter time scale than seasonal shifts. High precipitation events can saturate soils to the point where soil CO_2 can dissolve and then be transported into the karst system (Groves and Meiman 2005; Vesper and White 2004; Jackson 2017). Following storm events, $EpCO_2$ values were observed to increase of up to four times their normal values in cave rivers, springs, and the Green River (Figure 4.5). The greatest variability was seen in Echo River Spring, where an

October storm event increased $EpCO_2$ by forty times that of the atmosphere. $EpCO_2$ concentrations at Echo River Spring were higher than at Minnehaha Island, suggesting high CO_2 inputs closer to the spring. Storm response does vary depending on season. Changes in $EpCO_2$ following storm events in the summer depend on the antecedent moisture conditions and evapotranspiration. Summer storms aren't able to transport as much soil CO_2 as fall and winter storms due to limited infiltration. During the fall and winter, high soil moisture contents allows for deeper infiltration of meteoric water and mobilization of soil CO_2. The primary mode of transport for soil CO_2 into the karst system during the summer is downward migration through gaseous diffusion. Due to the change in the hydrologic regime in the fall and winter, the mode of transport for soil CO_2 changes. During this time, CO_2 transported by two possible modes: One mode of transport is the piston effect, where the pressure of infiltrating meteoric water forces gaseous CO_2 downward through air-filled pores. The other possible mode of transport is the dissolution of CO_2 into the meteoric water and downward migration in the aqueous state (Loisy et al. 2013). Seasonal changes in the mode of transport of CO_2 helps to explain why $EpCO_2$ is consistently elevated during the summer, as soil CO_2 is continually diffused downward, and why $EpCO_2$ is more variable during the fall and winter, as soil CO_2 is mobilized in pulses associated with storm events.

During the fall and winter, $EpCO_2$ concentrations are lower at all sites following the initial storm pulse than concentrations during stable reverse flows or normal flow conditions (Figure 4.9Figure 4.10). During stable reverse flows, the Green River water that is entering the cave system is diluted with respect to CO_2 compared to the epikarstic and soil waters recharging the River Styx and Echo River basins. Antecedent moisture

conditions and evapotranspiration rates are key to CO_2 transport during storm events, as seen when comparing late summer storms to fall and winter storms. Soils during the fall and winter are generally more saturated than summer soils due to less evapotranspiration, greater soil infiltration of precipitation, and generally greater amounts of precipitation. Increases in water content limit diffusion and increase microbial activity in the soil which can cause soil CO_2 to accumulate when the soils are saturated (Bouma and Bryla 2000; Loisy et al. 2013). Due to limited diffusion, soil CO_2 is transported during pulses following storm events when the antecedent moisture conditions are high. Therefore, fall and winter storms can infiltrate further into soils and can transport more CO_2 into the karst system than normal flow conditions in the River Styx and Echo River karst basins. Larger $EpCO_2$ values within the River Styx and Echo River basin seem to be more strongly influenced by seasonal shifts in the hydrologic regime (increased water levels, low evapotranspiration rates, and increased precipitation) rather than seasonal soil CO_2 production, as was found within the neighboring Turnhole Spring Basin (Groves and Meiman 2001).
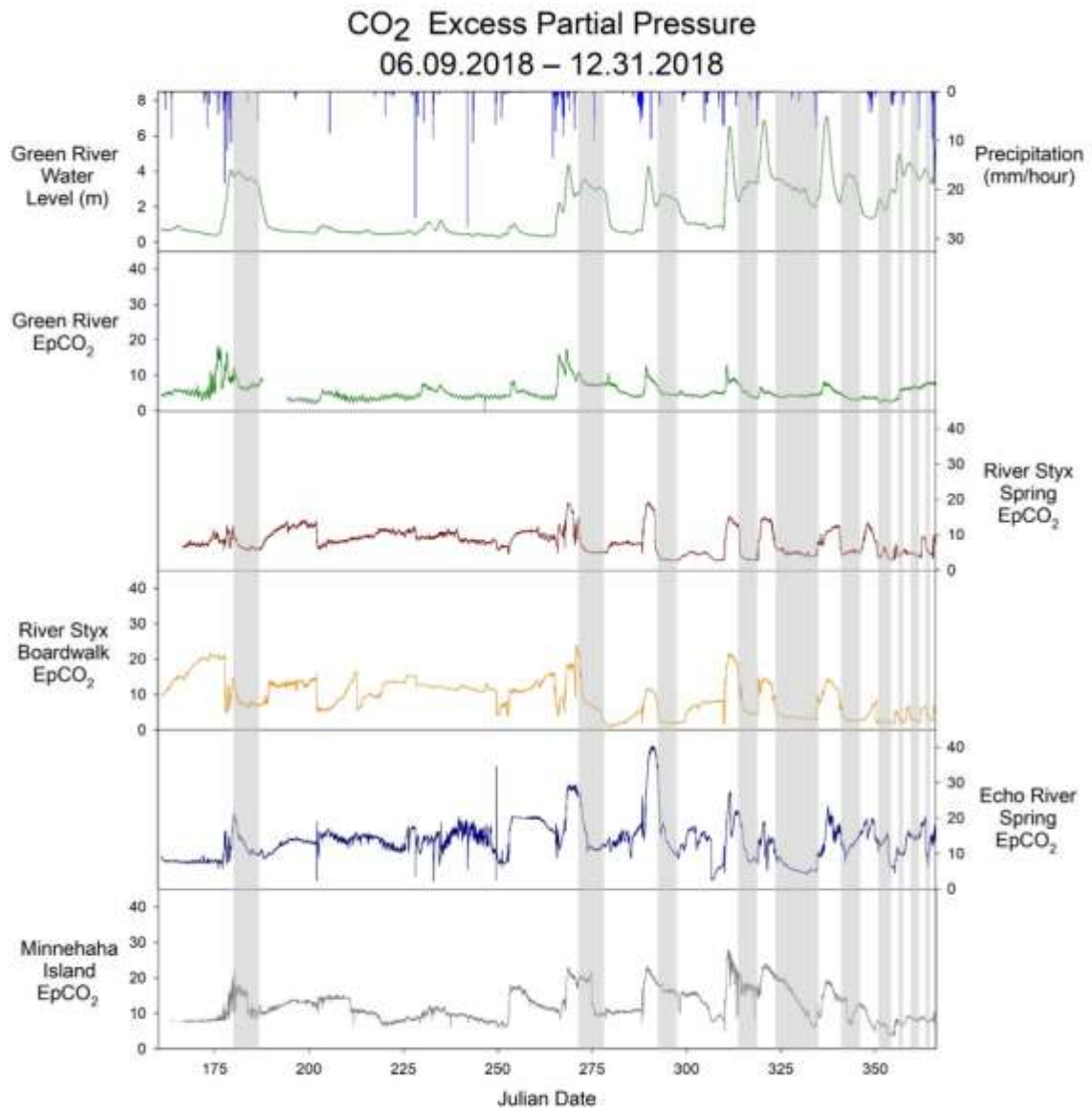
Figure 4.5 EpCO$_2$

EpCO$_2$ shows the influence of seasonal shifts in soil production rates, antecedent moisture conditions, and evapotranspiration on CO$_2$ transport in the River Styx and Echo River basins. Additionally, EpCO$_2$ values during flow reversals are generally lower than normal flow conditions. Stable reverse flows are indicated by gray shading.

4.4.2 SI$_{cal}$

Karst waters are rarely in equilibrium with respect to calcite. To determine whether a karst water is capable of dissolving or is more apt to precipitate calcite, saturation indices (SI$_{cal}$) are used (White 1988). SI$_{cal}$ is derived using equilibrium constants for carbonate reactions in conjunction with measured temperature, pH, Ca^{2+}, and alkalinity. As negative or undersaturated SI$_{cal}$ values approach 0, dissolution slows considerably as reactions are kinetically limited by microbial activities, interactions with other ions in solution, and imperfections and reaction inhibitors at the mineral surface (White 1997; Drever 1997). Dissolution rates are slow when saturation indices are between -0.3 and 0 (White 1997).

Past studies found that waters discharging from Echo and River Styx springs were consistently undersaturated, with SI$_{cal}$ of about -0.2 to -0.3, suggesting that, although the water is aggressive, dissolution is slow (White 1989). During this study period, River Styx Spring ranged between -0.5 and zero for 81.0% of the time. Waters discharging from Echo River Spring ranged between -0.5 and zero for 84.4% of the time. Overall, River Styx Spring was undersaturated, below zero, 83.1% of the time and Echo River Spring was undersaturated for 98.7% of the time. Most waters recharging the River Styx and Echo River groundwater basins likely lose their aggressiveness near the surface with their initial contact with limestone. There is little variability in the seasonal average SI$_{cal}$ of the cave rivers and springs. However, increased precipitation and lower evapotranspiration rates in the fall and winter months causes more storm event variability in SI$_{cal}$ values (Figure 4.6). Echo River Spring does show variability in the summer, likely attributed to the possible epikarstic infeeder.

The Green River was only undersaturated 42.5% of the time. On a seasonal scale, the Green River is supersaturated with respect to calcite during most of the summer and only becomes undersaturated following a major storm event or after a release from the upstream dam at the Green River Lake resevoir. The geology underlying the Green River Lake is dominated by siliciclastics (Osterhoudt 2014). In combination with higher discharges after dam release, the calcite saturation of lake water is lower than low flow Green River water due to lack of carbonate dissolution. During periods of low flow (usually in the summer), karst rivers are typically supersaturated with respect to calcite (White 1989; Gulley 2011). As the seasons transition from fall into winter, increases in precipitation discharge into the river, causing SI_{cal} values to often fall below zero, increasing the variability in saturation of calcite in the Green River.

During stable flow reversals at MCNP, saturation indices were lower at River Styx Boardwalk than River Styx Spring during six of the ten reversals (Figure 4.9Figure 4.10). This suggests that River Styx basin water, with its higher pCO_2 than the Green River, is contributing to the aggressiveness of the mixture. A significant increase in saturation occurs near the end of the reversal at River Styx Boardwalk in Figure 4.9. This was the only time that the water became supersaturated following a reversal and was likely due to low flow conditions causing dissolution in the River Styx conduit as the hydraulic head was slowly returning to normal. In three of the remaining reversals, the saturation indices were either nearly the same or higher at River Styx Boardwalk. This is may be to the length of the reversal, during which there was not enough residence time for the Green River and basin waters to sufficiently mix, thus the SI_{cal} of the water was unaffected by mixing corrosion. Another possibility for the increase in SI_{cal} along the

reversal route is dissolution of calcite or degassing of CO_2. But measured calcium and bicarbonate values do not significantly increase along the flow path during reversals and $EpCO_2$ during these reversals doesn't significantly decrease along the flow path. Calcium and bicarbonate values variability between sites was often within 1 or 2 mg/L, suggesting that the Green River water was not aggressive enough to lead to significant dissolution (Figure 4.7, Figure 4.9Figure 4.10). The Green River is an outlet for many karst springs in the area, so the Green River and cave waters are geochemically similar. Additionally, high-resolution monitoring of geochemical parameters show that the Green River water exits Echo River Spring within twenty-four hours after initially entering River Styx Spring, so the water does not have time to sufficiently mix (Figure 4.9 Figure 4.10). An investigation of mixing corrosion in an eogenetic setting showed similar results — the residence times were not long enough for the effects of mixing; and the primary driver of cave enlargement was diffuse sources of CO_2 (Gulley et al. 2014). Mixing corrosion was not significant driver of dissolution during stable reverse flows due to the geochemical similarities of the waters and their often short residence times.

Figure 4.6 Calcite Saturation Index
The Green River is generally supersaturated with respect to
calcite during the summer but shifts to generally undersaturated during the winter.
Changes in saturation are attributed seasonal shifts in the hydrologic regime.
Stable reverse flows are indicated by shading.
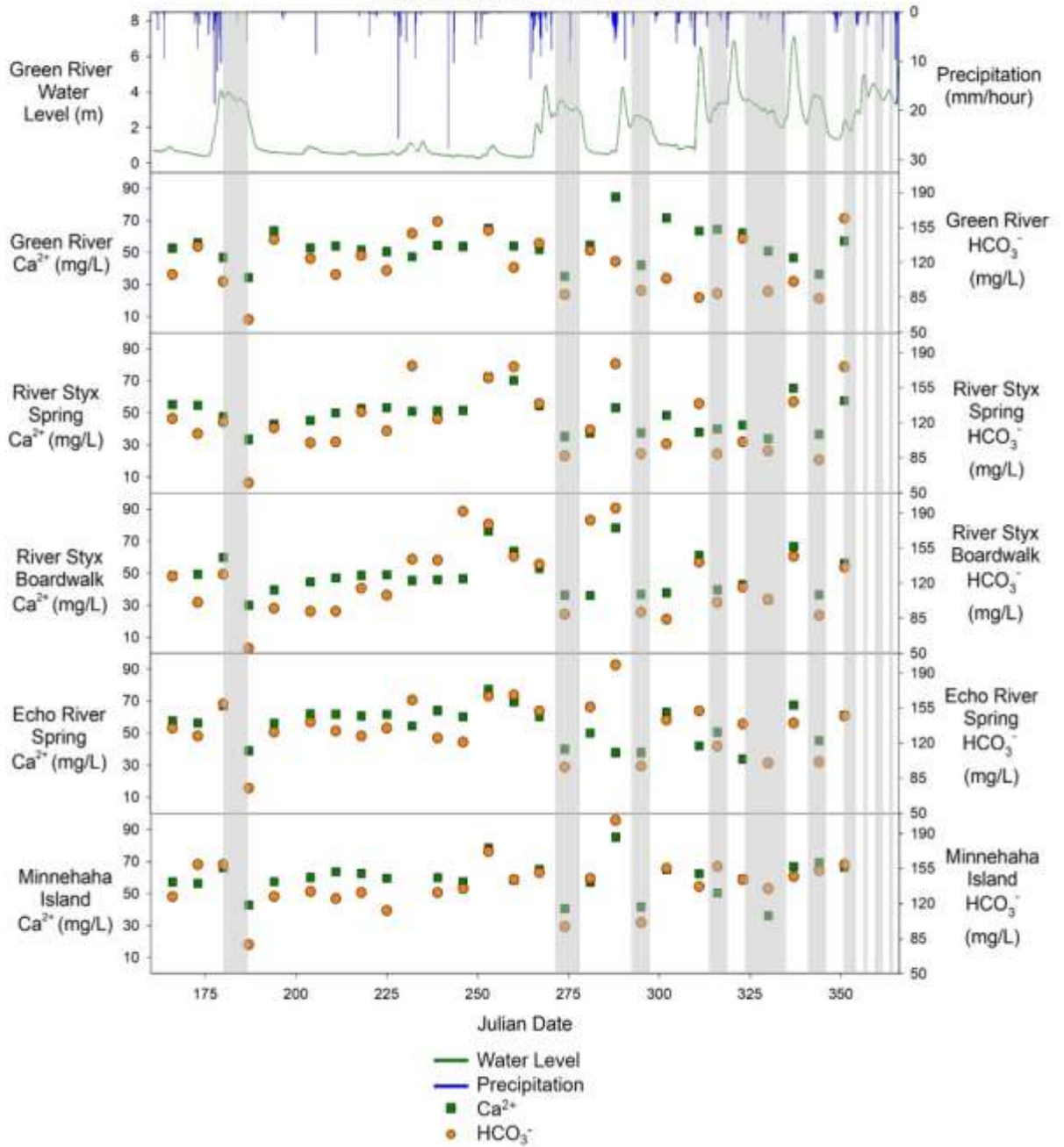
Figure 4.7 Calcium and alkalinity concentrations along the flow reveral route.
Calcium and alkalinity concentrations along the flow reversal route show little change,
suggesting flow reversals do not increase dissolution. Stable reverse flows are indicated
by shading.
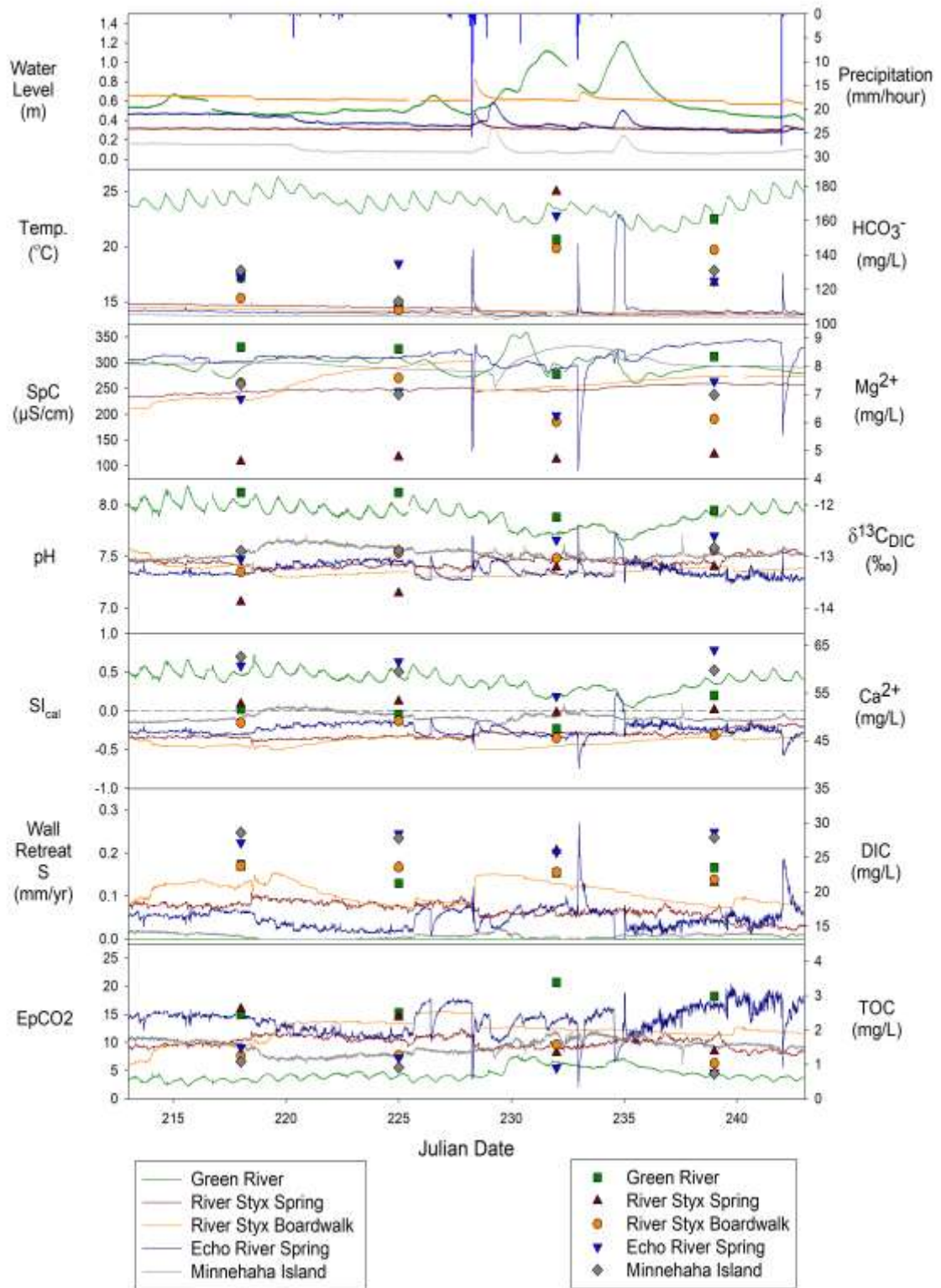
Figure 4.8 August (JD 213-243) geochemical results
No stable reverse flows occurred during this time.
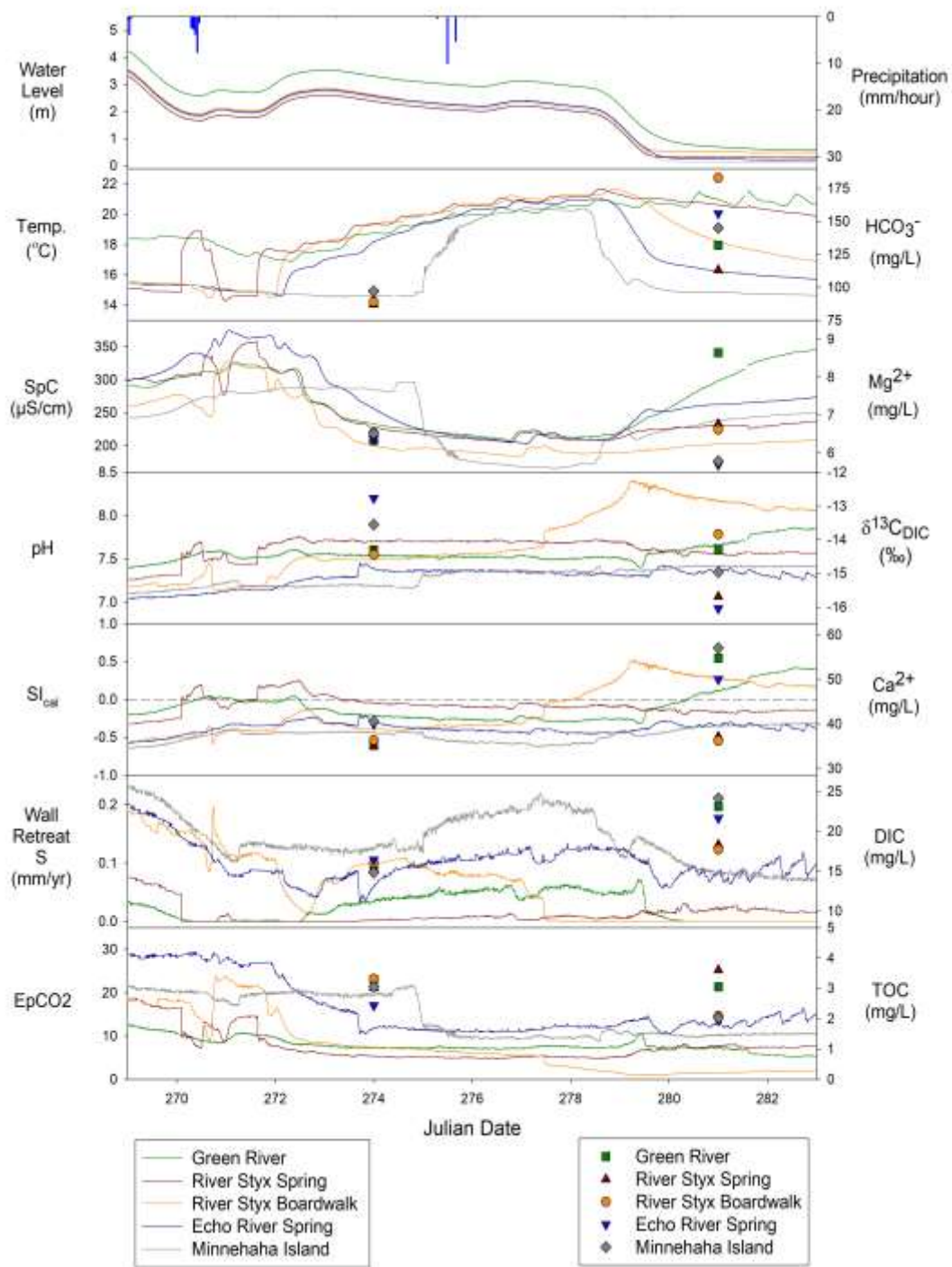
Figure 4.9 Geochemical changes during a stable reverse flow (JD 269-283)
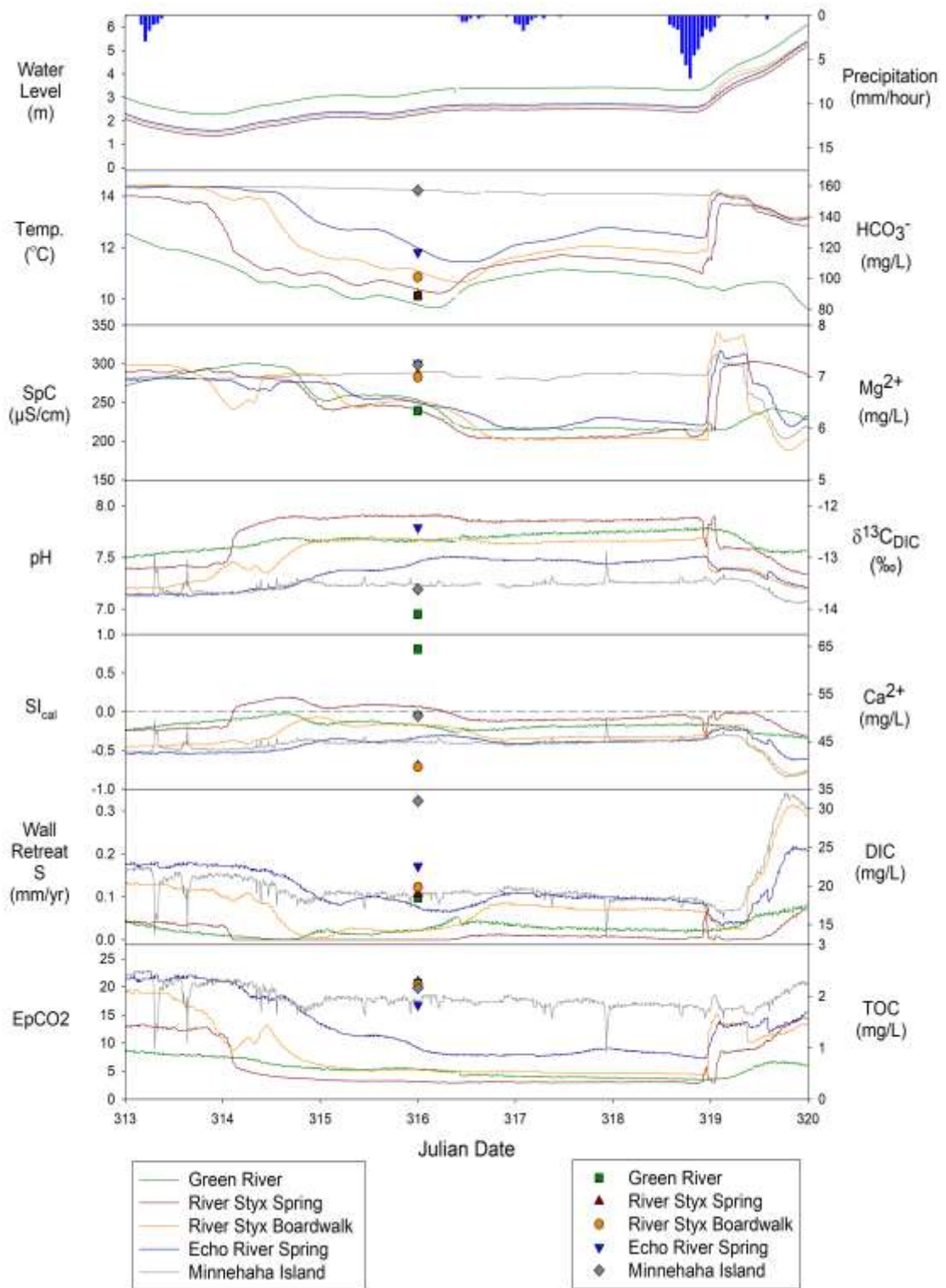
Figure 4.10 Geochemical changes during a stable reverse flow (JD 313-320)

4.4.3 Estimation of Dissolution Rates

Dissolution rates were calculated using Equation 4.3 for wall retreat at ten-minute intervals (Figure 4.11). Dissolution rates show the calculated rate based on conditions at each ten-minute interval in mm per year and do not represent the total dissolution that occurred within the year. Averages of the rates are used as estimations to show the effects that seasonal changes and storm events have on dissolution.

During the summer season, waters discharging from the River Styx Basin had a predicted annual maximum dissolution rate of 0.12 mm per year, a predicted annual minimum dissolution rate of 0 mm per year, and a predicted annual average dissolution rate of 0.05 mm per year. Waters discharging from the Echo River Basin also had a predicted annual average dissolution rate of 0.05 mm per year, but the predicted annual maximum dissolution rate was 0.27 mm per year, following a mid-August precipitation event. This spike in dissolution is associated with high-CO_2 inputs during large precipitations events. During normal flow conditions, dissolution slightly decreases in the fall and winter months, as soil CO_2 production decreases. However, increases in dissolution rates follow large precipitation events, as soils become saturated and soil CO_2 is flushed through the system. These large precipitation events cause more dissolution than normal base flow during the summer period. For example, the calculated amount of wall retreat at Echo River Spring during the summer period (JD 160-265), 105 days, was 0.014 mm; during the fall and winter period (266-365), 99 days, it was 0.033 mm. Factors influencing dissolution rates are: seasonal CO_2 supply; and (most importantly) seasonal shifts in the hydrologic regime, including intensity and duration of precipitation events, evapotranspiration, and antecedent moisture conditions.

In this study, flow reversals did not increase dissolution rates more than normal flow conditions most of the time (Figure 4.11). During stable reverse flows, the average dissolution rates typically were nearly equal, or less than, the average seasonal rate. One exception was at Echo River Spring during the stable reverse flow from Julian Dates 340-345, where a dissolution rates were twice the seasonal average. It was expected that stable reverse flows would increase dissolution rates, as was seen in an eogenetic karst system in Florida (Gulley et al. 2011); however, that was not the case in this telogenetic karst system in Kentucky. An investigation into spring flow reversals in an eogenetic karst system in Florida found that a single flow reversal event could dissolve, in terms of wall retreat in a phreatic tube, up to 3.4 mm. (Gulley et al. 2011). The maximum amount of wall retreat calculated during a reversal in MCNP was 0.003 mm, which was derived by multiplying the average rate of wall retreat by the fraction of the year that the stable reverse flow lasted. Better estimates of wall retreat could be made with the addition of discharge data and passage volumes.

Several key differences account for the difference in dissolution rates between these two settings: river chemistry, spring and conduit morphology, limestone porosity and permeability, and residence time. Reversing river water entering conduits in Florida is significantly more aggressive than in Mammoth Cave. The pH of rivers in Florida's Suwannee River Watershed ranges between 4.0 – 7.5 (Crandall et al. 1999; Gulley et al. 2011). During the study period, The Green River was more alkaline, ranging from 7.29 to 8.3. Five years earlier, high-resolution pH monitoring at sites upstream of Mammoth Cave also recorded Green River pH values ranging between 7.0-8.0 (Osterholdt 2014). Florida rivers have more organic acid and CO_2 inputs, due to an abundance of swamps

and milder climate, which allows for longer growing seasons (Crandall et al. 1999). River

water that enters springs in Florida must discharge from the same spring mouth, so there

are no through flow conditions, as seen in MCNP. River water in Florida reversals can

only move up-conduit or laterally through the matrix porosity of the limestone (Gulley et

al. 2011), resulting in increased contact with the limestone, and providing more time for

dissolution reactions to occur. In the Mammoth Cave system, the stable flow reversal

phenomenon between River Styx and Echo River allows river water to move through the

system with little impediment — water is free to flow along the path of least resistance,

with little residence time, back into the Green River.

In addition to the hydrologic, climatic, and geochemical differences, the

limestones of Mammoth Cave have lower matrix porosity than the young limestones of

Florida. Also, the conduit floor and lower walls of River Styx and Echo River are often

covered in clay, silts, and sands; it is unlikely that much (if any) of the river water

infiltrates the bedrock; however, the function of sediment in speleogenesis is debatable.

Does sediment inhibit or enhance dissolution? Paragenesis is a speleogenetic theory that

suggests limestone dissolution occurs in the upward direction due to sediment cover on

conduit floors. Sediment inhibits dissolution in the downward direction by covering the

water-rock reaction surface (Renault 1970; Ford and Ewers 1978; Farrant and Smart

2011). Paragenesis is a term reserved for phreatic conduits and sediment deposition in

vadose conduits inhibits dissolution of the conduit floor and causes dissolution laterally,

not vertically (Farrant and Smart 2011). In contrast, Vaughn (1998) demonstrated that

dissolution in cave sediment at the base of Charon's Cascade (a waterfall discharging into

the River Styx) was occurring and that pCO_2 values in the sediment were an order of

magnitude higher than water of the River Styx. The high pCO_2 values in the sediment were attributed to the decomposition of organics delivered into the cave through sinkholes in the basin and flow reversal events. Therefore, it is possible that flow reversals can increase dissolution, not through river water or mixing corrosion, but through longer-term processes of organic decomposition within deposited surface sediments into the conduits. Further study is necessary to show the effects of sediment on speleogenesis, and thus how flow reversals may increase dissolution through this process in the River Styx and Echo River. Despite the role of sediment in dissolution, Groves and Meiman (2005) found that most of conduit enlargement (63% - 100%) occurred during high magnitude flows, which only occurred 5% of the time during their study of dissolution in the nearby Logsdon River.

Estimated dissolution in this study is limited due to the lack of discharge data. Estimation of dissolution rates do not account for water-rock contact. Although low flow conditions have similar estimated dissolution rates as stable reverse flows, the actual amount of dissolution may be lower due to low water levels compared with higher water levels during stable reverse flows. The high water levels or pipe-full conditions of stable reverse flows increase the amount of water-rock contact, thus increasing the surface area of calcite that can be dissolved. Discharge data would allow for calculations of the amount of dissolved calcite discharging from the River Styx and Echo River basins, which can then be used to better compare dissolution rates during normal, base flow conditions; normal, storm flow conditions, and reverse flow conditions.
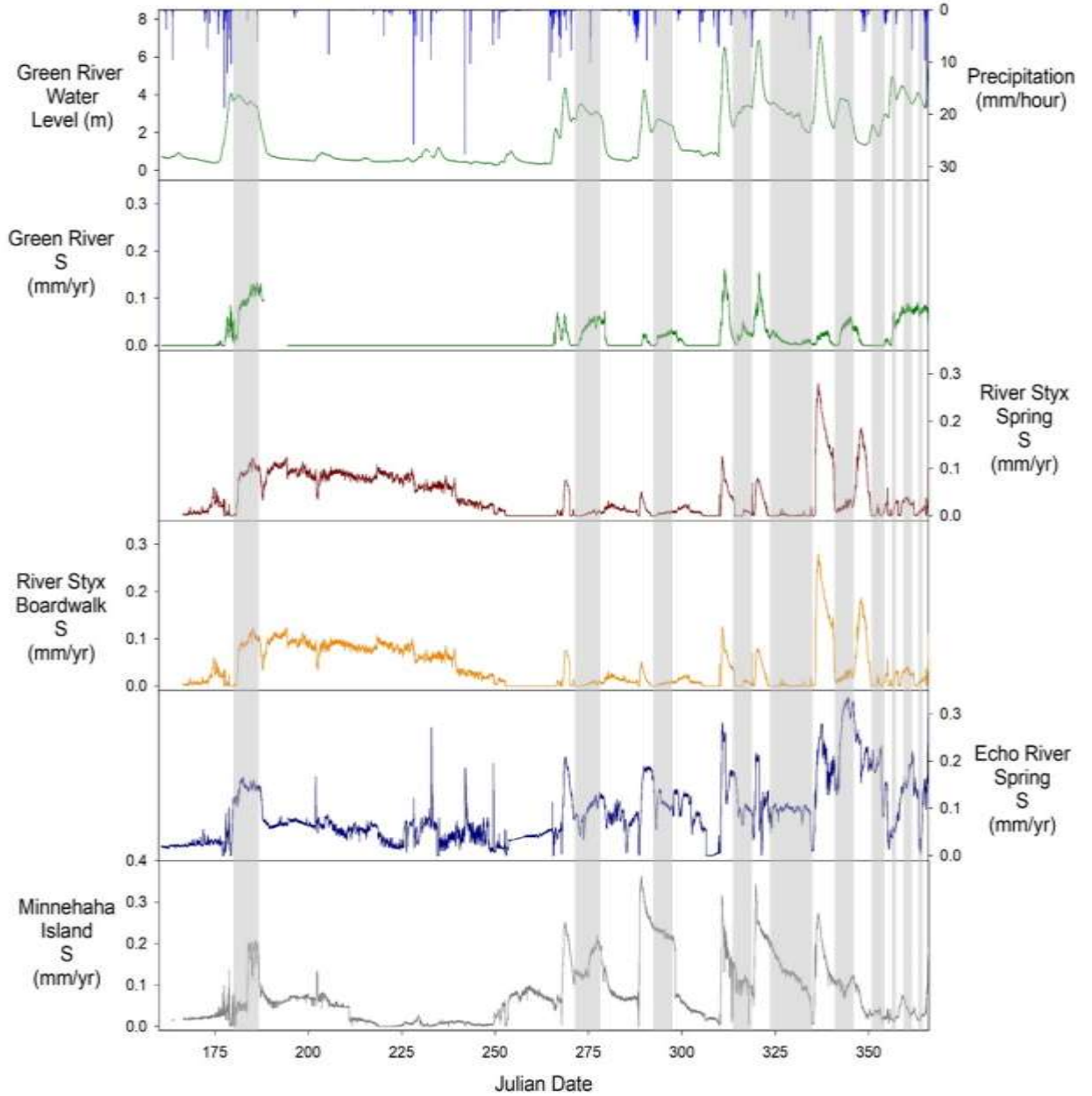
Figure 4.11 Wall retreat calculations
show that the highest rates of wall retreat typically occur during the initial storm pulse.
Flow reversals are indicated by shading.

4.5 Conclusions

Calculations of pCO_2, SI_{cal}, and dissolution rates show that dissolution in the River Styx and Echo River Basin are mostly dominated by large precipitation events and seasonal shifts in the hydrologic regime, rather than normal base flow conditions and stable reverse flows. Estimates of wall retreat show that over twice as much wall retreat occurred at Echo River Spring in the fall and winter months than during the summer period. Although soil CO_2 production is lower in the winter, seasonal increases in precipitation and decreases in evapotranspiration allow for infiltration of more water into soils and the mobilization of soil CO_2.

Stable reverse flows in MCNP are not significant contributors to dissolution, contrary to what was found in Florida. This is likely due to the similarity of the Green River water to base flow cave waters, the lack of aggressiveness of the Green River water, and short residence times that do not allow for mixing of the waters or infiltration in the limestone matrix. Also, the Green River deposits sediment into the karst system during flow reversals, which may limit dissolution by reducing water-rock contact or it may increase dissolution through the input of organic matter CO_2 into the system. Further study is needed to understand the influence of sediment cover on dissolution in the River Styx and Echo River. Additionally, discharge data are needed to calculate better estimates of dissolution in low flow conditions versus pipe-full conditions.

By further understanding dissolution dynamics under different flow regimes and how these processes are dependent on climatic conditions, a larger perspective of past and future speleogenesis in the Mammoth Cave area can be derived. Because the Green River has been a major control of cave development in the past, understanding how the

river affects present-day speleogenetic processes can be applied to the past formation of

Mammoth Cave's large, multiple levels and extensive conduit network.

4.6 Literature Cited

Anthony, D., 1998. Seasonal effects on the geochemical evolution of the Logsdon River, Mammoth Cave, Kentucky. Master's thesis. Bowling Green: Western Kentucky University, Department of Geography and Geology.

Bouma, T.J., Bryla, D.R., 2000. On the assessment of root and soil respiration for soils of different textures: interactions with soil moisture contents and soil CO_2 concentrations. *Plant and Soil* 227, 215-221.

Crandall, C.A., Katz, B.G., Hirten, J.J., 1999. Hydrochemical evidence for mixing of river water and groundwater during high-flow conditions, lower Suwanee River basin, Florida, USA. *Hydrogeology Journal* 7, 454-467.

Drever, J.I., 1997. The geochemistry of natural waters: surface and groundwater environments. Upper Saddle River, NJ: Prentice Hall.

Farrant, A.R., Smart, P.L., 2011. Role of sediment in speleogenesis; sedimentation and paragenesis. *Geomorphology* 134(1-2), 79-93.

Ford, D.C., Ewers, R.O., 1978. The development of limestone cave systems in the dimensions of length and depth. *Canadian Journal of Earth Sciences* 15(11), 1783-1798.

Ford, D.C., Williams, P.W., 2007. *Karst hydrogeology and geomorphology.* 2nd ed. West Sussex, England: John Wiley and Sons Ltd.

Granger, D.E., Fabel, D., Palmer, A.N., 2001. Pliocene-Pleistocene incision of the Green River, Kentucky, determined from radioactive decay of cosmogenic ^{26}Al and ^{10}Be in Mammoth Cave sediments. *GSA Bulletin* 133(7), 825-836.

Groves, C., Meiman, J., 2001. Weathering, geomorphic work, and karst landscape evolution in the Cave City groundwater basin, Mammoth Cave, Kentucky. *Geomorphology* 67, 115-126.

Gulden, B., 2019. World's longest caves. Accessed on November 5, 2019 from http://www.caverbob.com/wlong.htm

Gulley, J., Martin, J. B., Screaton, E. J., Moore, P. J., 2011. River reversals into karst springs: A model for cave enlargement in eogenetic karst aquifers. *GSA Bulletin* 123(3-4), 457-467.

Gulley, J.D., Martin, J.B., Moore, P.J., Murphy, J., 2013. Formation of phreatic caves in an eogenetic karst aquifer by CO_2 enrichment at lower water tables and subsequent flooding by sea level rise. *Earth Surface Processes and Landforms* 38(11), 1210-1224.

Gulley, J.D., Martin, J.B., Moor, P.J., 2014. Vadose CO_2 gas drives dissolution at water tables in eogenetic karst aquifers more than mixing dissolution. *Earth Surface Processes and Landforms* 39(13), 1833-1846.

Gulley, J.D., Martin, J.B., Moore, P.J., Brown, A., Spellman, P.D., Ezell, J. 2015. Heterogeneous distributions of CO_2 may be more important for dissolution and karstification in coastal eogenetic limestone than mixing dissolution. *Earth Surface Processes and Landforms* 40, 1057-1071.

Hatcher, B.E., 2013. Sources of CO_2 controlling the carbonate chemistry of the Logsdon River, Mammoth Cave, Kentucky. Master's thesis. Bowling Green: Western Kentucky University, Department of Geography and Geology.

Hess, J.W., Wells, S.G., Quinlan, J.F., White, W.B., 1989. Hydrogeology of the South-central Kentucky karst. In: White, W.B., White, E.L. ed. *Karst hydrology: concepts from the Mammoth Cave area.* New York, NY: Van Nostrand Reinhold.

Hess, J.W., White, W.B., 1989. Water budget and physical hydrology. In: White, W.B., White, E.L. ed. *Karst hydrology: concepts from the Mammoth Cave area.* New York, NY: Van Nostrand Reinhold.

Jackson, L., 2017. Epikarst hydrogeochemical changes in telogenetic karst systems in South-central Kentucky. Master's thesis. Bowling Green: Western Kentucky University, Department of Geography and Geology.

Lawhon, N., 2014. Investigating telogenetic karst aquifer processes and evolution in south-central Kentucky, U.S., using high-resolution storm hydrology and geochemistry monitoring. Master's thesis. Bowling Green: Western Kentucky University, Department of Geography and Geology.

Liu, Z., Qiang, L., Hailong, S., Wang, J., 2007. Seasonal, diurnal and storm-scale hydrochemical variations of typical epikarst springs in subtropical karst areas of SW China: Soil CO_2 and dilution effects. *Journal of Hydrology* 337, 207-223.

Loisy, C., Cohen, G., Laveuf, C., Le Roux, O., Delaplace, P., Magnier, C., Rouchon, V., Cerepi, A., Garcia, B., 2013. The CO_2-vadose project: Dynamics of the natural CO_2 in a carbonate vadose zone. *International Journal of Greenhouse Gas Control* 14, 97-112.

McClanahan, K., 2014. Carbon Cycling Dynamics Inferred from Carbon Isotope Sourcing in a Mid-Latitude Karst-Influenced River. Master's thesis. Bowling Green: Western Kentucky University, Department of Geography and Geology.

Meiman, J., 2006. Water resources management plan, MCNP, Kentucky. Technical Report: United States Department of the Interior, National Park Service.

Meiman, J., Ryan, M.T., 1993. The Echo River – Turnhole Bend overflow route. *Cave Research Foundation Newsletter* 21(1), 16-18

Miotke, F. -D., 1975. Der Karst im zentralen Kentucky bei Mammoth Cave, Jahrbuch der Geographischen Gesellschaft zu Hannover für.

Osterhoudt, L.L., 2014. Impacts of carbonate mineral weathering on hydrochemistry of the Upper Green River Basin, Kentucky. Master's thesis. Bowling Green: Western Kentucky University, Department of Geography and Geology.

Palmer, A.N., 1981. *A geological guide to MCNP*. Teaneck, NJ: Zephyrus Press.

Palmer, A.N., 1991. Origin and morphology of limestone caves. *GSA Bulletin* 103, 1-21.

Palmer, A.N., 2007. *Cave geology*. Dayton, OH: Cave Books.

Palmer, A. N., 2017. Geologic history of Mammoth Cave. In: Hobbs, H.H., Olson, R.A., Winkler, E.G., Culver, D.C., ed. Mammoth Cave: A human and natural history. Springer Online.

Paylor, R.L., Currens, J.C., 2001. Karst occurrence in Kentucky. Kentucky Geological Survey Map and Chart 35. Accessed October 15, 2019 from https://uknowledge.uky.edu/kgs_mc/35.

Renault, P., 1970. *The formation of caves*. Paris, France: Presses Univeritaires de France.

Shelley, J.A., 2019. Monitoring and evaluating the influences of class V injection wells on urban karst hydrology. Master's thesis. Bowling Green: Western Kentucky University, Department of Geography and Geology.

Toomey, R.S., Hobbs, H.H., Olson, R.A., 2017. An Orientation to Mammoth Cave and This Volume In: Hobbs, H.H., Olson, R.A., Winkler, E.G., Culver, D.C., ed. *Mammoth Cave: A human and natural history.* Springer Online

Trimboli, S. R., Toomey, R.S., 2019. Temperature and reverse-flow patterns of the River Styx, Mammoth Cave, Kentucky. *Journal of Cave and Karst Studies* 81(3), 174-187.

Trimboli, S.R., Weber, K., Ryan, S., Toomey, R.S., 2016. An overview of the reverse flow patterns of River Styx in Mammoth Cave, Kentucky: 2009-2012, in Proceedings, Mammoth Cave Research Symposia, MCNP, 128-129.

Vaughn, K., 1998. A quantitative analysis of interstitial fluid-chemistry and limestone dissolution rates within the clastic sediment of a karst aquifer conduit, Mammoth Cave, Kentucky. Master's thesis. Bowling Green: Western Kentucky University, Department of Geography and Geology.

Vesper, D.J., White, W.B., 2004. Storm pulse chemographs of saturation index and carbon dioxide pressure: implications for shifting recharge sources during storm events in the karst aquifer at Fort Campbell, Kentucky/Tennessee, USA. *Hydrogeology Journal* 12(2), 135-143.

Wagner, R.J., Boulger Jr., R.W., Oblinger, C.J., Smith, B.A., 2006. *Guidelines and standard procedures for continuous water-quality monitors: Station operation, record computation, and data reporting.* Techniques and Methods 1–D3. Reston, VA: U.S. Geological Survey. Accessed November 21, 2017 from https://pubs.usgs.gov/tm/2006/tm1D3/pdf/TM1D3.pdf

White. W.B., 1988. *Geomorphology and hydrology of karst terrains.* New York, NY: Oxford University Press.

White, W.B., 1989. Introduction to the karst hydrology of the Mammoth Cave area. In: White, W.B., White, E.L. ed. *Karst hydrology: concepts from the Mammoth Cave area.* New York, NY: Van Nostrand Reinhold.

White, W. B., 1997. Thermodynamic equilibrium, kinetics, activation barriers, and reaction mechanisms for chemical reactions in karst terrains. *Environmental Geology* 30(1-2), 46-58.

White, W.B., White, E.L., 2017. Hydrology and hydrogeology of Mammoth Cave. In: Hobbs, H.H., Olson, R.A., Winkler, E.G., Culver, D.C., ed. *Mammoth Cave: A human and natural history.* Springer Online.

Wilde, F.D., Radtke, D.B., Gibs, J., and Iwatsubo, R.T., 2004 (rev. 2009). Processing of water samples. In *U.S. Geological Survey Techniques of Water-Resources Investigations, Book 9.* Reston, VA: U.S. Geological Survey. Accessed November 19, 2017 from https://water.usgs.gov/owq/FieldManual/chapter5/html/Ch5_contents.html

Wilde, F.D., Sandstrom, M.W., Skrobialowski, S.C. 2015. National field manual for the collection of water-quality data. U.S. Geological Survey Techniques of Water-Resources Investigations, Book 9. Reston, VA: U.S. Geological Survey. Accessed November 19, 2017 from https://water.usgs.gov/owq/FieldManual/

Worthington, S.R.H., Ford, D.C., Beddows, P.A., 2000. Porosity and permeability enhancement in unconfined carbonate aquifers as a result of solution. In: Klimchouck, A.B., Ford, D.C., Palmer, A.N., Dreybodt, W., ed. *Speleogenesis: evolution of karst aquifers.* Huntsville, AL: National Speleological Society.

5. Carbon sources in Mammoth Cave's River Styx and Echo River karst basins

5.1 Introduction

Karst landscapes play an important role in carbon cycling between atmospheric, biological, and terrestrial carbon reservoirs. Studies have suggested that karst landscapes contribute to climate change mitigation due to the consumption of atmospheric CO_2 in carbonate dissolution reaction (Liu et al. 2010; Zhang et al. 2015). Stable carbon isotope analyses are useful in determining the sources of carbon in water, understanding carbonate weathering reactions, and characterizing the transfer of carbon (carbon flux) between Earth's carbon reservoirs in karst settings.

Carbon has two naturally occurring stable isotopes: ^{12}C and ^{13}C. In nature, approximately 98.8% of stable carbon is ^{12}C and 1.2% of carbon is ^{13}C. For this reason, its isotopes are expressed as ratios. The ratio of ^{13}C to ^{12}C in a sample is compared with the universal standard, written as the following equation (Clark and Fritz 1997; Palmer 2007; Fetter 2013):

$$\delta^{13}C\text{\textperthousand} = \frac{R_{sample} - R_{std}}{R_{std}} \times 1000 \qquad \text{(Eq. 5.1)}$$

where δ^{13}C is the apparent ratio of carbon isotopes in a sample (R_{sample}) compared with the standard (R_{std}) measured in parts per thousand ($^0/_{00}$). These values are multiplied by 1000 in order to represent differences in concentrations more easily; the differences in isotopic ratios are generally small. For carbon isotopes, the universal standard is the Vienna Pee Dee Belemnite (VPDB) of the Pee Dee Formation in South Carolina (Doctor et al. 2008; Fetter 2013). The VPDB standard is used as a relative benchmark, where its ratio represents the zero value. Therefore, samples enriched in ^{13}C with respect to the

VPDB have positive $\delta^{13}C$ values. Samples depleted in ^{13}C with respect to the VPDB have negative $\delta^{13}C$ values. The VPDB is the standard for $\delta^{13}C$ in all carbon compounds, including: carbonate minerals, CO_2, dissolved inorganic carbon (DIC), dissolved organic carbon (DOC), organic liquids, cellulose, and hydrocarbons (Clark and Fritz 1997).

Dissolved inorganic carbon (DIC) includes carbon from dissolution of carbonate minerals and dissolved CO_2 from multiple sources: the atmosphere, microbial and root respiration in soils, and oxidation of organic material. The $\delta^{13}C$ values of DIC ($\delta^{13}C_{DIC}$) is controlled by contributions from these various sources. DIC sourced from carbonate dissolution will cause $\delta^{13}C_{DIC}$ values to become more enriched in ^{13}C, because carbonate rocks typically have $\delta^{13}C_{DIC}$ values between 0‰ to 5‰ (Clark and Fritz 1997; Bullen and Kendall 1998; Fetter 2013). DIC sourced from soil CO_2 will cause $\delta^{13}C_{DIC}$ values to be depleted in ^{13}C, because photosynthetic processes preferentially use the lighter carbon isotope (^{12}C). The $\delta^{13}C_{DIC}$ of soil CO_2 ranges between -28‰ and -5‰ and is affected by: the exchange of CO_2 between the atmosphere and the upper 30 cm of the soil, root respiration, microbial activities, decomposition of organic matter, and plant type (Boutton 1991; Schulte et al. 2011). DIC sourced from the atmosphere will also cause $\delta^{13}C_{DIC}$ values to be depleted in ^{13}C, because the atmosphere contains $\delta^{13}C_{DIC}$ values between -9‰ to -7‰ (Zhang et al., 1995; Clark and Fritz 1997; Zhang et al., 2015; Graven et al. 2017).

The Mammoth Cave National Park (MCNP) in South Central Kentucky contains one of the most studied cave systems in the world, but little research has been applied the study of carbon sourcing in the Green River, River Styx karst basin, and Echo River karst basin. Ballard (2016) sampled for carbon isotopes on multiple occasions in the River Styx

and Echo River karst basins, prior to the removal of Lock and Dam Number Six. Groves and Meiman (2001) estimated that 57% of the carbon flux from the nearby Cave City basin was derived from carbonate dissolution and 42% was biologically derived. These estimates of sourcing are based on ionic concentrations in the water and not carbon isotopes. Carbon isotope analyses of the Green River upstream of Mammoth Cave showed seasonal averages of $\delta^{13}C_{DIC}$ between -14.88‰ and -11.2‰ suggesting soil CO_2 and groundwater DIC were the major sources of carbon in this section of the river (McClanahan 2014). This study examines the seasonal changes in carbon sourcing and dissolution mechanisms during reverse flows between the Green River and River Styx and Echo River karst basins.

5.2 Study Area

The Western Pennyroyal karst area of south-central Kentucky, including MCNP (Figure 5.1), is one of the most explored and studied karst regions in the world (Palmer 1981; White 1989). MCNP is located 145 kilometers south of Louisville and 30 kilometers northeast of Bowling Green, in one of the most cave dense areas of the state. MCNP became a World Heritage Site in 1981 and an International Biosphere Reserve in 1990. Fifty-two troglobitic species, those that are adapted to cave environments and spend their whole life inside caves, are present in Mammoth Cave (Toomey et al. 2017). MCNP is characterized as a deciduous forest in a humid sub-tropical climate (Hess and White 1989; Meiman 2006).

South Central Kentucky is underlain by Mississippian age sedimentary rocks (Figure 5.2), that gently dip, less than one degree, northwest toward the center of the Illinois Basin (Palmer 1981). The numerous passages of Mammoth Cave developed in a

section approximately 100 meters thick in the St. Louis, St. Genevieve, and Girkin

Limestones, which contain minor beds of chert and dolomite. The average porosity of the

limestones that make up Mammoth Cave is 2.4% (Worthington et al. 2000). The Big

Clifty Sandstone, a formation 15 to 18 meters thick consisting of interbedded sandstone,

siltstone, and shale, acts as a weathering-resistant caprock that protects the Mammoth
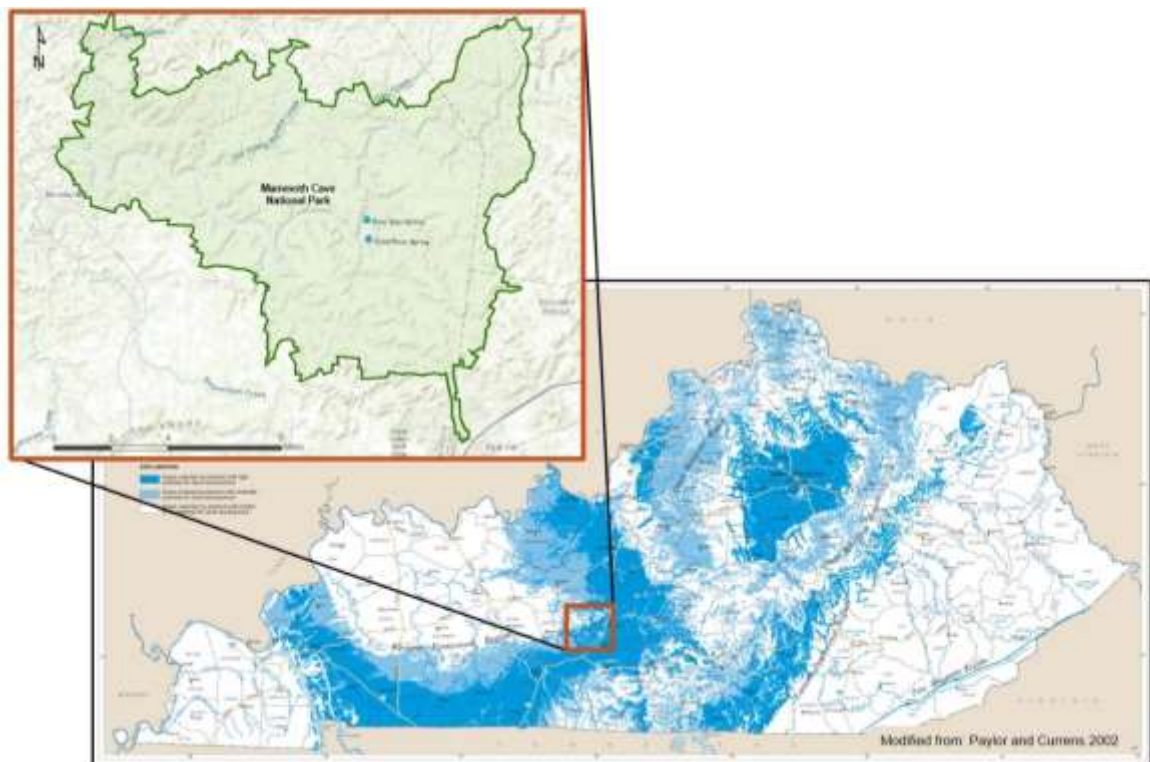
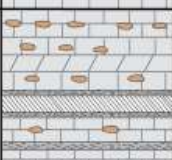Cave from rapid denudation (Palmer 1981).

Figure 5.1 Mammoth Cave National Park
located in the Western Pennyroyal karst region
(Modified from Paylor and Currens 2002).

System	Series	Formation	Lithology	Thickness
Mississippian	Chesterian	Hardinsburg		18 m
		Haney		12 m
		Big Clifty		15-18 m
		Girkin		40-43 m
	Meramecian	St. Genevieve		34-37 m
		St. Louis		53-60 m
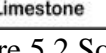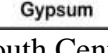
Sandstone   Limestone   Gypsum   Shale   Chert   Dolomite

Figure 5.2 South Central Kentucky geology
(Modified from Palmer 1981).

The Mammoth Cave Karst Aquifer is located in the Upper Green River drainage

basin (Hess et al. 1989; McClanahan 2014). Conduit development at Mammoth Cave is

directly influenced by the Green River, the regional base level of the Mammoth Cave

Aquifer. The multiple levels of the cave can be attributed to changes in the base level of

the Green River during past glacial conditions (Granger et al. 2001).

Mammoth Cave's River Styx and Echo River Springs are both rise pools that

resurge beneath limestone ledges and flow into the Green River by short, silt-floored

spring runs. Echo River Spring and River Styx Spring formed in response to glacially

induced changes in base level of the Green River. The Green River was lower than its

present elevation when Echo River Spring and River Styx Spring formed. As base level

rose, sediment was deposited, causing the Green River to be currently underlain by

approximately 5-10 meters of silt (White and White 2017). Additionally, sediment has

filled the springs' channels, causing River Styx and Echo River Springs to become

alluviated springs (Palmer 1981). The groundwater basins of River Styx and Echo River

Springs (Figure 5.3) are adjacent to one another and discharge groundwater from the

Mammoth Cave Ridge and neighboring karst valleys (White and White 2017). During the

stable reverse flow phenomenon, water flows from the Green River into River Styx

Spring. Water flows opposite to the normal flow direction along the path of River Styx,

then passes a basin divide between River Styx and Echo River, and then flows along the

Echo River. The reverse-flow water is discharged at Echo River Spring and flows back

into the Green River (Figure 5.4).
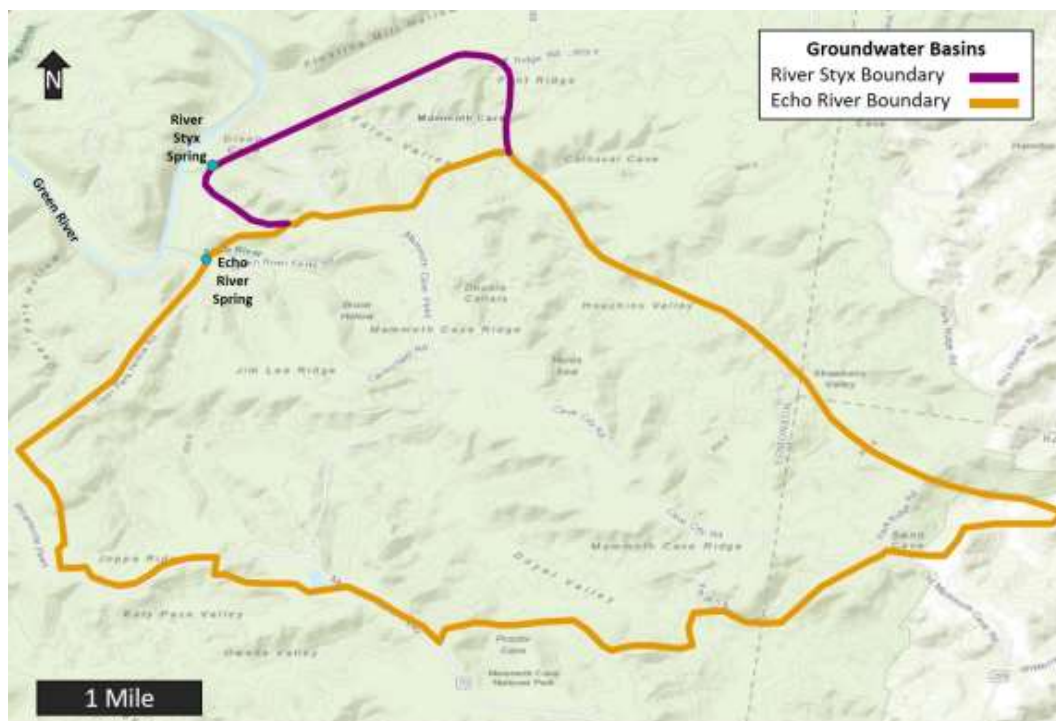
Figure 5.3 River Styx (2.2 km^2) and Echo River (21.7 km^2) groundwater basins
(Modified from Mammoth Cave International Center for Science and Learning 2012).
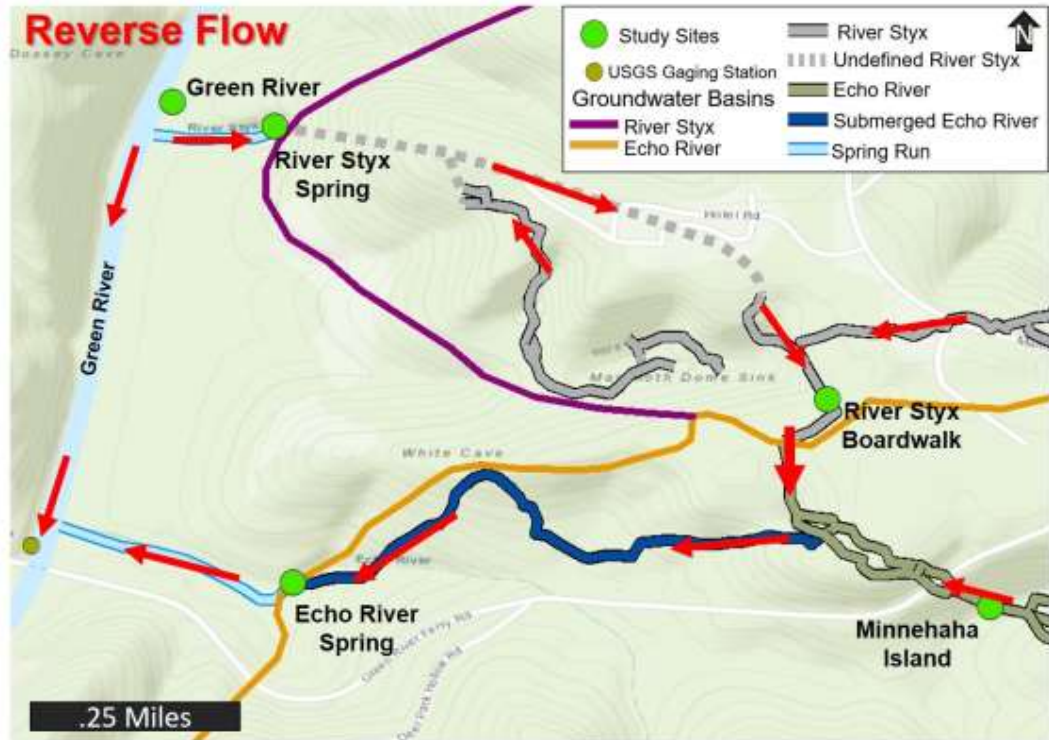
Figure 5.4 Map displaying site locations and stable reverse flow route
(Modified from Mammoth Cave International Center
for Science and Learning 2012).

5.3 Methods

5.3.1 Site Selection and Setup

Five sites were chosen for data collection: Green River, River Styx Spring, the

River Styx Boardwalk (River Styx, in cave), Echo River Spring, and Minnehaha Island

(Figure 5.4). The Green River, River Styx Spring, the River Styx Boardwalk, and Echo

River Spring are located along the same flow path during stable reverse flows.

Minnehaha Island, located upstream in Echo River, sits outside the stable reverse flow

path.

Two PVC stilling wells were installed at each of the five sites. All stilling wells

were drilled with multiple holes to allow water flow. The Green River stilling wells were

screened with wire mesh to prevent sediment buildup. Due to the limited access to

vertical structures or surfaces, diagonal stilling wells were installed at River Styx Spring, Echo River Spring, Minnehaha Island, and the Green River. T-posts and trees were used as anchor points at these four sites. Vertical stilling wells were installed at River Styx Boardwalk and were anchored to the existing walkway structure. A YSI EXO II was installed at the River Styx Boardwalk in a 7.62 cm stilling well. YSI 6920 V2 multiparameter sondes were installed at River Styx Spring, Echo River Spring, Minnehaha Island, and the Green River in 7.62 cm PVC stilling wells. HOBO pressure transducers were installed in 3.18 cm PVC stilling wells at all five sites.

5.3.2 Data Collection

YSI multiparameter sondes and HOBO pressure transducers were deployed at the five sites on June 9, 2018. The YSI multiparameter sondes were used to collect high-resolution data for pH, SpC, and temperature at ten-minute intervals. The HOBO pressure transducers were used to collect high-resolution water level and temperature data at two-minute intervals. Two additional pressure transducers were installed in-air, one on the surface at River Styx Spring and the other in-cave at Minnehaha Island. The in-air pressure transducers were used to collect barometric pressure data at two-minute intervals. Sites (when accessible) were visited weekly for maintenance, to resolve any issues with the sites and to download data. The sondes (when accessible) were calibrated once per month to maintain accurate data collection and minimize drift. Precipitation rates (mm/week) were collected from the National Park Service's gaseous pollutant and meteorological station located at Houchin Meadow. The stage height of the Green River was obtained from the United States Geological Survey's (USGS) gauging stations on the Green River at the Green River Lake (03305990), the Green River near Campbellsville

(03306000), Greensburg (03306500), Munfordville (03308500), Mammoth Cave (03309000), and Brownsville (03311505). Data from these gauging stations were used as a proxy to determine when water was released from the dam on Green River Lake.

A YSI ProDSS multiparameter sonde and an Oakton PCTSTestr 35 were used to collect pH, SpC, and temperature data at each site during sample collection. Handheld multiparameter monitors were calibrated before each field day to ensure accuracy of the grab sample. Sampling sites were adjusted during storm events, if the normal collection site became inaccessible due to increased stage of the Green, River Styx, or Echo Rivers. On a few occasions, samples were not collected due to site inaccessibility.

5.3.3 Sample Collection and Analysis

The collection of weekly water samples for analysis started on June 15, 2018, at all five sites. Carbon isotope samples for $\delta^{13}C_{DIC}$ were collected in 25 mL glass vials; DIC samples were collected in 40 mL amber vials with septa caps; and calcium ion samples were collected in 60 mL plastic bottles. DIC samples were preserved using ~0.5 mL of sulfuric acid(H_2SO_4). The pH of the calcium ion samples was lowered to ≤ 2 using 7 drops of nitric acid (HNO_3) for preservation purposes (Wilde et al. 2004). All samples were filtered to remove organic matter using a syringe and 0.45μm filter paper, as recommended for major-ion analysis (Wilde et al. 2004). All samples were sealed with no headspace; wrapped with parafilm in order to prevent outgassing and fractionation and then stored in a refrigerator at 4°C until analysis (Wilde et al. 2004). Sample collection and sonde maintenance followed the standard guidelines presented in the USGS's National Field Manual for the Collection of Water-Quality Data (Wilde et al. 2015).

$\delta^{13}C_{DIC}$ were analyzed using the Thermo GasBench II interface with the Thermo Finnigan DELTA^{plus} XP isotope ratio mass spectrometer at the University of Kentucky's Stable Isotope Geochemistry Laboratory. DIC concentrations were measured by determining the total carbon and total organic carbon concentrations of each sample using method SM 5310 B-2011 at the Western Kentucky University's (WKU's) HydroAnalytical Laboratory. Calcium ion concentrations in ppm were determined using inductively coupled plasma optical emission spectroscopy (ICP-OES), method EPA 200.7 revision 4.4, at WKU's Advanced Materials Institute.

5.3.4 Data Processing

All data were compiled in Excel and SigmaPlot spreadsheets. High-resolution water levels were calculated from the pressure transducer data using HOBOware software. Initial water levels were measured with a tape measure, used as a reference. Barometric pressure data was removed from the total pressure data to increase the accuracy and reduce noise within the calculated water levels. Hydrochemical data obtained from the sondes (i.e. pH) were corrected for calibration drift and fouling in accordance with the *USGS's Guidelines and Standard Procedures for Continuous Water-Quality Monitors: Station Operation, Record Computation, and Data Reporting* using calibration values and grab sample data (Wagner et al. 2006). Graphs of high-resolution temperature and pH data were analyzed, along with $\delta^{13}C_{DIC}$ and DIC to identify trends and relationships between sites and seasonal trends.

The EPA's stable isotope mixing model for estimating source proportions, IsoSource, was used to determine possible carbon contributions to water samples. IsoSource finds all mathematical solutions that creates isotopic mass balance based on the

isotopic signature of all possible contributing carbon sources. Solutions were derived using a 1% increment with a mass balance tolerance of 0.05%. The range of contributions were broad because the model calculated every contribution solution from 1-100% at 1% increments, therefore, the average is used to simplify the output and provide a relative view of the distribution of carbon sources. Average is derived by calculating the contribution sum from a single source divided by the number of solutions that satisfy the isotopic mass balance. Three carbon sources were considered in the model: soil CO_2, atmospheric CO_2, and carbon from carbonate mineral dissolution. Source values were -23.0‰ for soil, -7.00‰ for atmosphere, and 3.80‰ for limestone bedrock. These values were derived from literature (Clark and Fritz 1997; Zhang et al. 2015; Jackson 2017). Mean contributions of the carbon sources for each site were graphed and analyzed to identify seasonal changes in carbon sourcing.

5.4 Results and Discussion

Samples for $\delta^{13}C_{DIC}$ were collected weekly from June 15 to December 17, 2018. Isotope samples were collected over this six-month period to analyze seasonal influences (summer to winter transition) on carbon sourcing and flux between the Green River, River Styx, and Echo River. The data were analyzed to determine seasonal shifts and changes related to storm events, dam releases, and spring flow reversals. Seasons were defined based on averages and trends in temperature data collected from the Green River and Houchin Meadow's weather station during the study period and not by the seasons' astronomical definitions. Summer was defined as June 9 to September 22 (Julian dates 160-265); fall was defined as September 23 to November 17 (Julian dates 266-321); and winter was defined as November 18 to December 31 (Julian dates 322-365).

5.4.1 Time Series Analysis of $\delta^{13}C_{DIC}$ and pH

During the summer, when water levels are generally under a low flow regime, $\delta^{13}C_{DIC}$ values showed little variability, especially in the cave rivers and springs. The Green River was approximately 1‰ more enriched than the cave waters throughout most of the summer season (Table 5.1). Cave water and spring water $\delta^{13}C_{DIC}$ values are typically close to one another, with summer averages for the four sites ranging from -13.52‰ to -13.12‰. The Green River summer average was -12.39‰. The Green River is slightly more enriched, possibly because the atmosphere contributes more carbon to the Green River than to the subsurface rivers; or because C4 plants (i.e. corn) contribute more to the $\delta^{13}C_{DIC}$ signature than C3 plants (i.e. trees) (Clark and Fritz 1997; Cane and Clark 1999). The latter is likely, as the drainage area of the Green River upstream of MCNP is dominated by agricultural land use. On the other hand, Green River $\delta^{13}C_{DIC}$ values were closer to the cave waters' values following precipitation events. This likely due to the flushing of soil CO_2 from C3 plants (which is isotopically light compared with atmospheric, carbonate-derived CO_2, and C4-derived soil CO_2), which causes the $\delta^{13}C_{DIC}$ of the Green River to become more depleted. Additionally, Green River and cave river $\delta^{13}C_{DIC}$ values were similar during the one stable reverse flow that occurred from June 29 to July 5 (Julian Dates 180-186), because water from the Green River is flowing into the cave during this time, making the water sampled in cave a mixture of river water and basin water (Figure 5.5).

145

	$\delta^{13}C_{DIC}$ (‰ VPDB)		
	Average	Min	Max
Green River			
Summer	-12.39	-13.20	-11.72
Fall	-13.54	-14.30	-12.15
Winter	-12.70	-13.98	-11.99
River Styx Spring			
Summer	-13.52	-14.25	-13.03
Fall	-14.17	-15.69	-13.48
Winter	-12.98	-14.76	-11.53
River Styx Boardwalk			
Summer	-13.12	-13.39	-12.82
Fall	-13.65	-14.76	-12.14
Winter	-13.02	-13.99	-11.76
Echo River Spring			
Summer	-13.17	-14.56	-12.60
Fall	-13.69	-16.04	-12.42
Winter	-13.30	-14.39	-12.46
Minnehaha Island			
Summer	-13.21	-14.32	-12.75
Fall	-13.85	-15.05	-12.51
Winter	-13.79	-14.23	-13.01

Table 5.1 Statistics for seasonal $\delta^{13}C_{DIC}$ values
Basic statistics for seasonal $\delta^{13}C_{DIC}$ values from June to December 2018. Average $\delta^{13}C_{DIC}$ between in-cave and spring sites showed little variability from one another throughout the study period. The Green River is typically less depleted than the other sites due to atmospheric exchange of CO_2.

During the fall and winter transition, when the hydrology of the study area becomes dominated by a high flow regime, $\delta^{13}C_{DIC}$ values become more variable (Figure 5.5). SI_{cal} of River Styx and Echo River were below zero for most of the study, suggesting calcite precipitation isn't a major process affecting fractionation in this system. Spikes in pCO_2 and ^{13}C depleted cave waters suggest that the antecedent moisture conditions in the soil greatly contribute to the mobilization of soil CO_2 into the cave system. Higher moisture content in soil has been shown to inhibit winter CO_2 from migrating to the atmosphere in humid temperate forests (Contosta et al. 2016), making soil CO_2 available to be flushed from the soil by high volume precipitation during winter months. Studies have shown declines in soil CO_2 production in the winter due to decreases in temperatures, suggesting that lower concentrations of CO_2 are available

146

during this time (Richter and Markewitz 1995; Andrews and Schlesinger 2001; Oh et al. 2005); however, soil CO_2 production had been found to be unaffected by seasonal temperature changes in secondary forests (Yang et al. 2015). Soil CO_2 remained elevated during the winter period, likely due to several factors: the lack of ground disturbance (i.e. tillage) that causes CO_2 to diffuse upwards into the atmosphere; dense leaf litter that retains heat and moisture; and the presence of decaying organic matter that replenishes the soil CO_2 reservoir (Yang et al. 2015). Thus, even as seasonal weather patterns change, other forests in karst regions have shown continued soil CO_2 production. The data also suggest that the soil overlying these basins contain a high-CO_2 epikarstic reservoir that is slowly depleted as the seasons transition. The effects of the slowing of soil CO_2 production during the winter months on DIC and the high-CO_2 epikarstic reservoir remain a topic for future study.
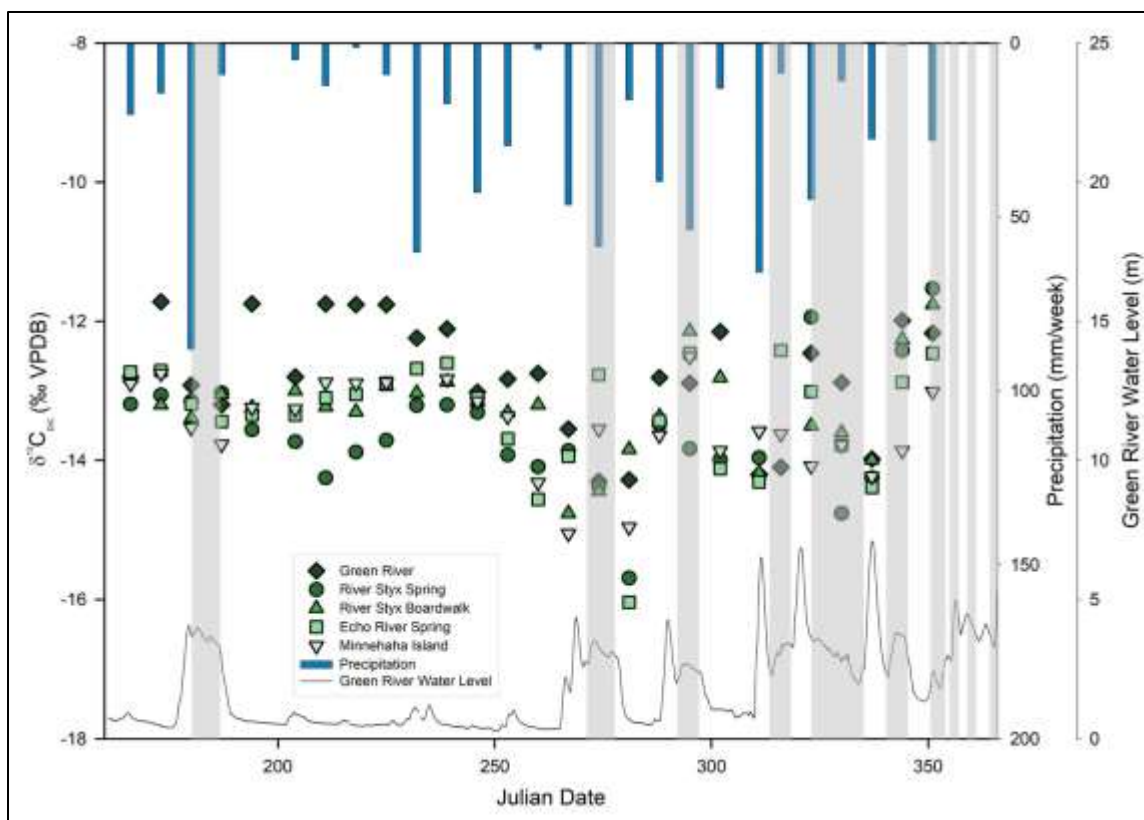
Figure 5.5 $\delta^{13}C_{DIC}$ values

$\delta^{13}C_{DIC}$ values from June to December 2018 show seasonal changes in weekly variability. Summer $\delta^{13}C_{DIC}$ values remain consistent with gradual changes from week to week. Fall and winter $\delta^{13}C_{DIC}$ values were more erratic and reflected changes in temperature and the hydrologic flow regime. (Stable reverse flows indicated by gray bars).

No statistical relationships between pH and $\delta^{13}C_{DIC}$ were found ($r^2<0.15$; $P>0.06$), with the exception of the Green River. The $\delta^{13}C_{DIC}$ was positively correlated ($r^2=0.52$; $P<0.00003$) to pH in the Green River throughout the study period. Brunet et al. (2009) found a similar correlation ($r^2=0.57$) between pH and $\delta^{13}C_{DIC}$ in a tropical watershed. They suggested this correlation may be attributed to biological activities (i.e. carbon uptake into physical structure and decomposition of organics) in the river and carbon dioxide exchange with the atmosphere. This study was conducted in a siliciclastic-dominated watershed with no carbonates; therefore, carbonate dissolution did not contribute to DIC concentrations. Although the Green River is isotopically enriched

148

compared with the groundwater, the correlation of $\delta^{13}C_{DIC}$ with pH suggests that the

atmosphere and biological processes in river ecosystems are more influential on carbon

flux in the Green River than in the cave streams. This correlation may be attributed to the

consistent $\delta^{13}C_{DIC}$ values measured during the summer in the Green River. No correlation

between pH and $\delta^{13}C_{DIC}$ was found in the cave waters, likely due to the lack of exposure

to atmospheric processes on the surface, such as diurnal changes in biological activity in

the river and direct meteoric inputs (Brunet et al. 2009). However, spring flow reversals

introduce organic matter that oxidizes and releases CO_2 into the cave system, including in

basal sediments deposited as flood water recedes (Vaughn 1998). One study on sediment

CO_2 concentrations in River Styx found pCO_2 values an order of magnitude greater in

sediment deposit than in the water from River Styx (Vaughn 1998). Localized maximum

in pCO_2 of cave air has been observed near sediment accumulations due to oxidation of

organic matter in another cave system (Baldini et al. 2006). Increases in pCO_2 related to

the oxidation of organic matter likely occurs on timescales larger and more consistent

than stable reverse flows, and therefore are unlikely to cause short term variability in

$\delta^{13}C_{DIC}$.

Increases in pH in cave waters do not always coincide with enriched $\delta^{13}C_{DIC}$

values, suggesting that increases in pH are not always associated with dissolution. During

the fall and winter, increases in pH coincide with flow reversals (Figure 5.6). Analysis of

high-resolution geochemical parameters and ionic sampling suggest that dissolution

during flow reversals is minimal compared with dissolution during storm events and the

normal flow regime. The $\delta^{13}C_{DIC}$ values also suggest that dissolution during flow

reversals is not significant; there does not appear to be a consistent change in $\delta^{13}C_{DIC}$

values along the reversal flow path that would be reflective of contributions from a ^{13}C-enriched calcite source; however, dissolution is slow, and the flow path is short, so the sample resolution is unable to detect minor changes in chemistry associated with stable reverse flow. Measured DIC values during reversals are typically lower than values during normal flow conditions (Figure 5.7). The low DIC values may be attributed to dilution by river water and not indicative of dissolution rates. No statistical relationships were found between DIC and $\delta^{13}C_{DIC}$. Multiple other studies also found no statistical relationships between DIC and $\delta^{13}C_{DIC}$ (Cane and Clark 1999; Li et al. 2005; Li et al. 2008). The lack of correlation is understandable, as DIC is an actual concentration, where $\delta^{13}C_{DIC}$ is a ratio that is used to identify source; therefore, high DIC values can be from a combination of sources. A scenario in which a relationship would occur between DIC and $\delta^{13}C_{DIC}$ would be in cases were increases in DIC are associated with flushing of a carbon reservoir dominated by a single carbon source. For example, ^{13}C-enriched storage water with large concentrations of DIC caused by dissolution of calcite in waters with long residence times that is pushed through the system during storm events.

$\delta^{13}C_{DIC}$ of both River Styx and Echo River suggest isotopic homogenization due to the consistent range in values (Table 5.1), independent of season. Rapid isotopic homogenization occurs in the epikarst, as infiltrating meteoric waters mix with epikarst storage water (Williams 2008; Polk et al. 2013). $\delta^{13}C_{DIC}$ of epikarst (-13.6‰) and soil waters (-14.7‰) in a phreatic cave system in Indiana were shown to be more depleted than the baseflow (-11.8‰), suggesting soil CO_2 is the major control of $\delta^{13}C_{DIC}$ in the epikarst (Lee and Krothe 2001). $\delta^{13}C_{DIC}$ of karst groundwater should be close to -14‰ under open conditions, where soil CO_2 is the dominant carbon source (Zhang et al. 1995;

Li et al. 2008). Contributions along the flow path can be complex, with hydrological inputs from different areas under variable flow regimes, but $\delta^{13}C_{DIC}$ within River Styx and Echo River groundwater basins demonstrate the rapid homogenization of epikarst waters and dominance of soil CO_2 despite variable hydrologic conditions.
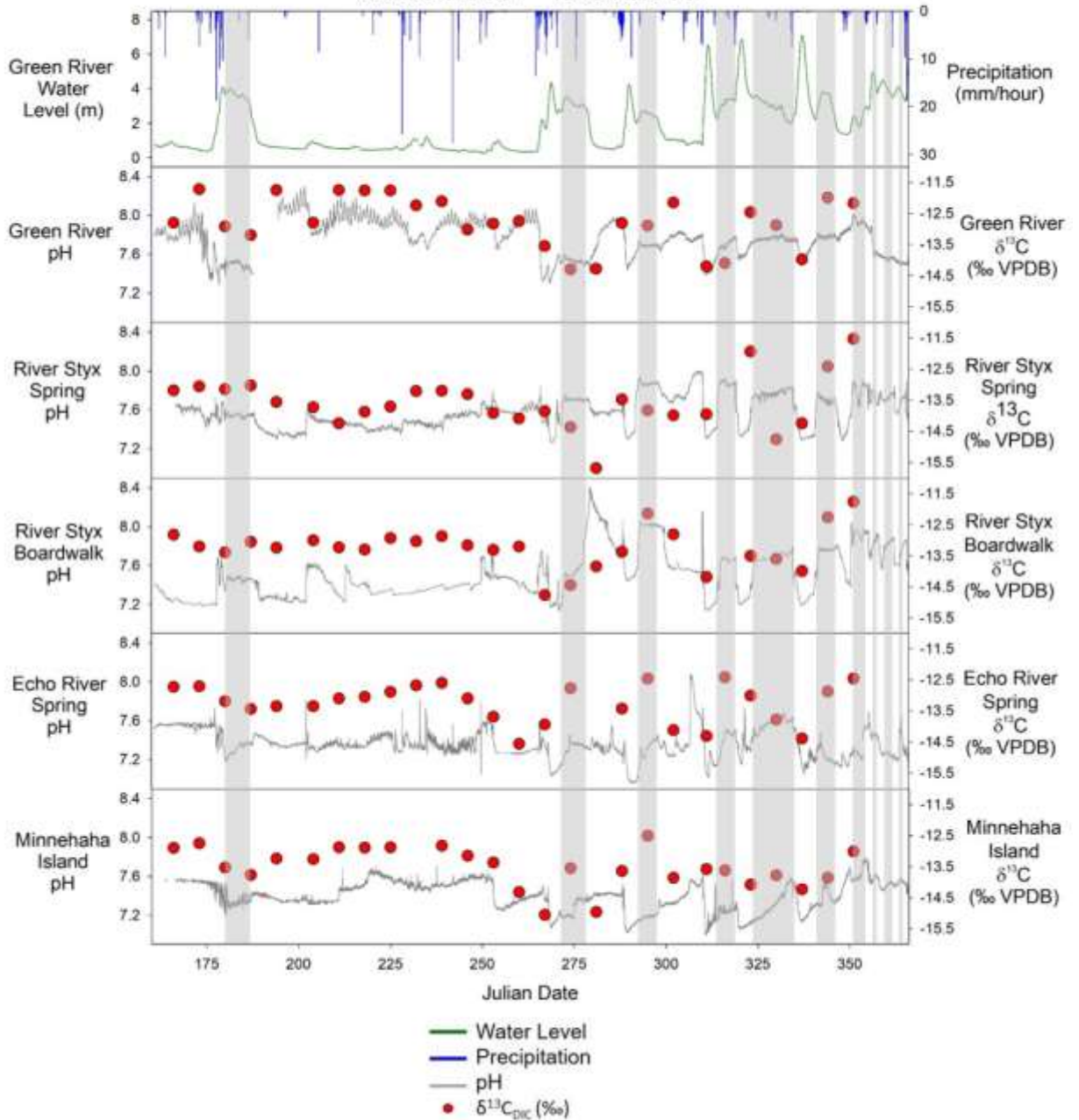
Figure 5.6 pH and $\delta^{13}C_{DIC}$
The lack of correlation between pH and $\delta^{13}C_{DIC}$ values suggests that dissolution does not contribute to increases in pH and that dissolution is minimal during stable reverse flows (reverse flows indicated by gray bars).
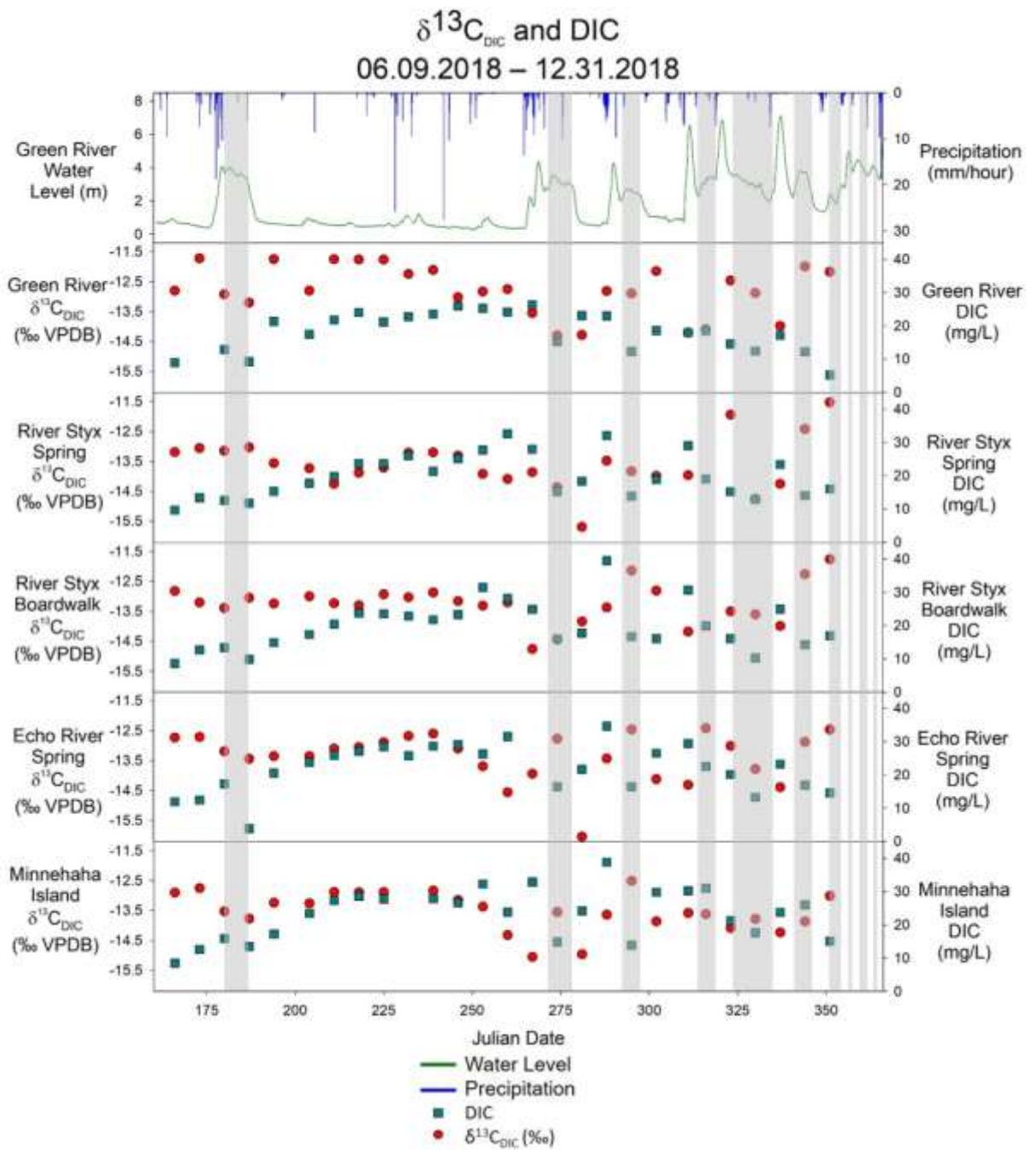
Figure 5.7 DIC and $\delta^{13}C_{DIC}$
Low DIC concentrations along the stable reverse flow (indicated by gray bars) route
suggest that flow reversals are not significant to speleogenesis in the River Styx and Echo
River portions of Mammoth Cave.

5.4.2 Mixing Model Result

IsoSource was used to generate a mixing model that represents the percent of carbon contributions from three different sources: atmospheric CO_2, calcite dissolution, and soil CO_2. IsoSource uses mathematical operations to show the range of possible contributions from each defined source. For this reason, the absolute percentage of carbon source contribution to the mixture was not determined. However, the mean contribution from each source was used to show how carbon sources may change over time. The range of mean contributions for each site from June to December 2018 are summarized in Table 5.2.

The mixing model results show a homogenized system where soil CO_2 is the main contributor to DIC at all sites and throughout the year, with mean contributions ranging from 42.4% to 64.9%. The Green River and River Styx and Echo River groundwater basins are part of an open system, where soil CO_2 is not fully consumed in carbonate dissolution and controls $\delta^{13}C_{DIC}$ values independent of season (Cane and Clark 1999). Atmospheric CO_2 is also a significant contributor to the DIC at sites throughout the year, with mean contributions ranging from 25.5% to 36.6%. Carbon derived from carbonate mineral dissolution contributes the least at all sites throughout the year, with mean contributions ranging 12.6% to 21.6%.

There are no seasonal shifts in the dominant carbon source, as has been previously found in the Green River upstream from Mammoth Cave (McClanahan 2014). However, the previous study included a fourth carbon source (groundwater) in the mixing model. This resulted in a distinct shift in the dominant carbon source from soil CO_2 to groundwater during late winter. As seen in the trend of $\delta^{13}C_{DIC}$ values, the seasonal

influence appears to manifest as variability, rather than a distinct shift in values (Figure

5.8). The range of mean contributions becomes more variable from week to week in the

fall and winter, while the weekly contributions during the summer show more gradual

increases and decreases over time. This variability may be attributed to three factors:

decrease in surface temperatures leading to increased fractionation; increases in

precipitation rates that bring more soil CO_2 into the basin waters, contributing to

isotopically depleted $\delta^{13}C_{DIC}$ values; and changes in the hydrologic regime that cause the

flushing of storage waters.

	Mean Contributions of Carbon Sources		
	Atmosphere	Bedrock	Soil
Green River			
Average	31.95%	19.04%	49.02%
Min	25.60%	16.00%	43.60%
Max	36.00%	21.60%	57.20%
River Styx Spring			
Average	29.61%	17.43%	53.00%
Min	23.20%	13.40%	42.40%
Max	36.60%	20.90%	63.40%
River Styx Boardwalk			
Average	30.83%	18.00%	51.18%
Min	26.20%	15.10%	43.60%
Max	36.00%	20.60%	58.70%
Echo River Spring			
Average	30.69%	17.69%	51.63%
Min	22.50%	12.60%	46.70%
Max	34.70%	19.80%	64.90%
Minnehaha Island			
Average	30.08%	17.44%	52.51%
Min	24.70%	14.60%	47.80%
Max	33.20%	19.80%	60.40%

Table 5.2 Summary of the mixing model results
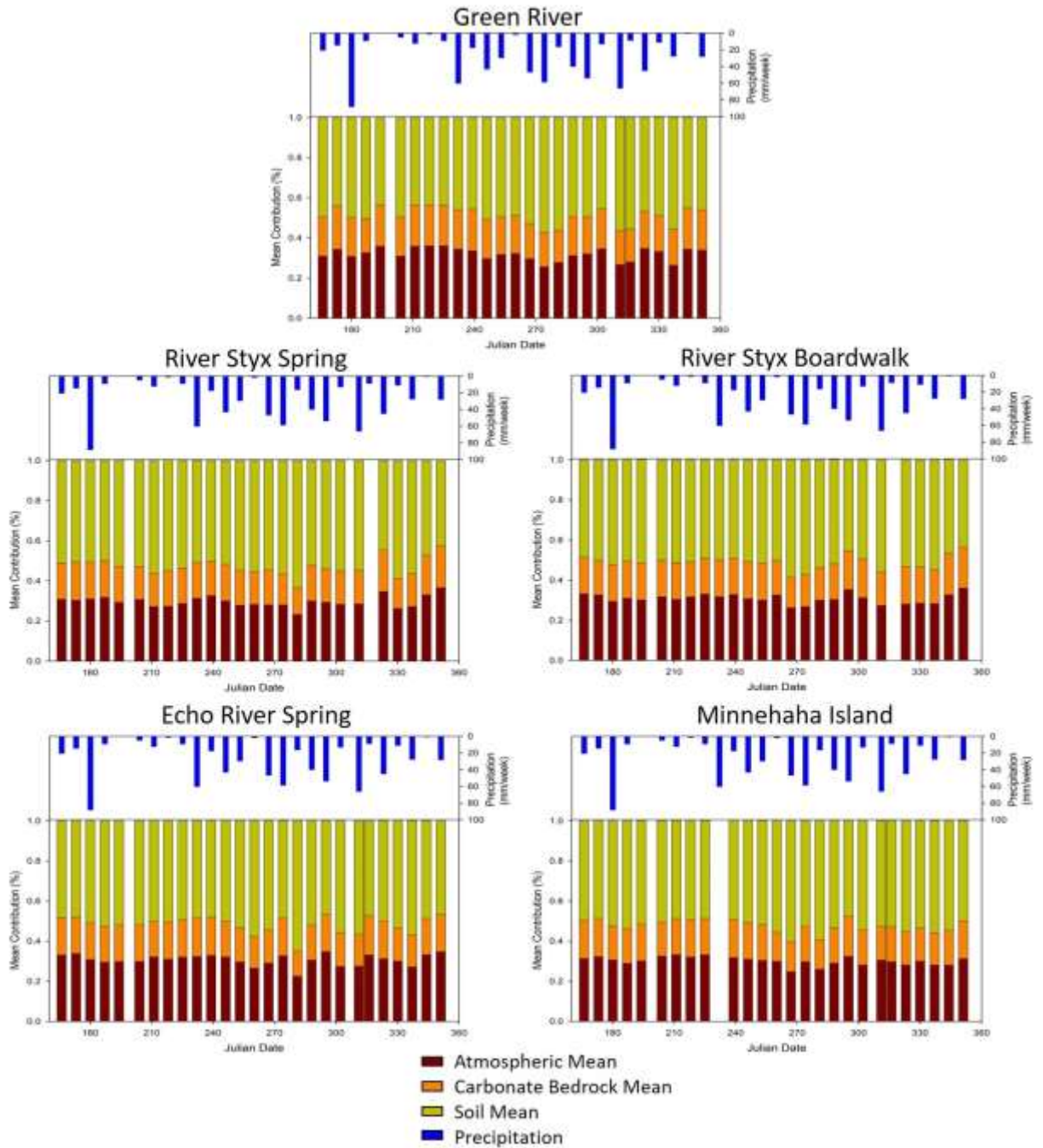The dominant carbon source at all sites throughout the year was soil CO_2.

Figure 5.8 Weekly changes in carbon sourcing in sampled waters
The graphs show only mean contributions based on the IsoSource mixing model and do
not indicate absolute percentages of carbon sources.

5.4.3 Factors Influencing $\delta^{13}C_{DIC}$

Karst groundwater and riverine DIC is influenced by several processes, including soil respiration, atmospheric-water CO_2 exchange, carbonate dissolution, and precipitation (Clark and Fritz 1997; Doctor et al. 2008). Karst groundwater in equilibrium with calcite should have $\delta^{13}C_{DIC}$ values that show equal contributions from dissolved soil CO_2 and dissolved calcite to DIC. For example, Doctor et al. (2008) predicted the $\delta^{13}C_{DIC}$ of groundwater in Sleepers River Watershed in Vermont would be -12‰, because the $\delta^{13}C_{DIC}$ of soil CO_2 in the area was -22‰ and the $\delta^{13}C_{DIC}$ of calcite in the area was -2‰. However, measured $\delta^{13}C_{DIC}$ in the Sleepers River Watershed were found to be lower than expected, with an average of -13.4‰. This suggests that the water was not in equilibrium and that soil CO_2 contributed more to DIC than calcite dissolution. This was also the case in most samples collected from the River Styx and Echo River in this current study. $\delta^{13}C_{DIC}$ of groundwater in equilibrium with soil CO_2 (-23‰) and calcite (3.8‰) was predicted to have values around -9.6‰ in the Mammoth Cave area. However, $\delta^{13}C_{DIC}$ of the River Styx and Echo River were always significantly more depleted than the predicted value. The Green River typically had $\delta^{13}C_{DIC}$ that were more enriched than River Styx and Echo River, likely due to the stronger influence of atmospheric-water CO_2 exchange, yet also more depleted than the predicted value of -8.7‰ (calculated $\delta^{13}C_{DIC}$ of water in equilibrium with soil CO_2, calcite, and the atmosphere).

Carbonate reactions appear to have little influence on the range of $\delta^{13}C_{DIC}$ in the sampled waters. Statistical analyses comparing $\delta^{13}C_{DIC}$ values to Ca^{2+} concentrations did not suggest a strong relationship between carbon sourcing and dissolution ($r^2 < 0.11$; $P > 0.05$). Additionally, no statistical relationship was found between measured DIC

concentrations and $\delta^{13}C_{DIC}$ values ($r^2<0.07$; $P>0.15$). Therefore, the major sources that contributed most to the variability found in $\delta^{13}C_{DIC}$ values were soil and atmospheric CO_2.
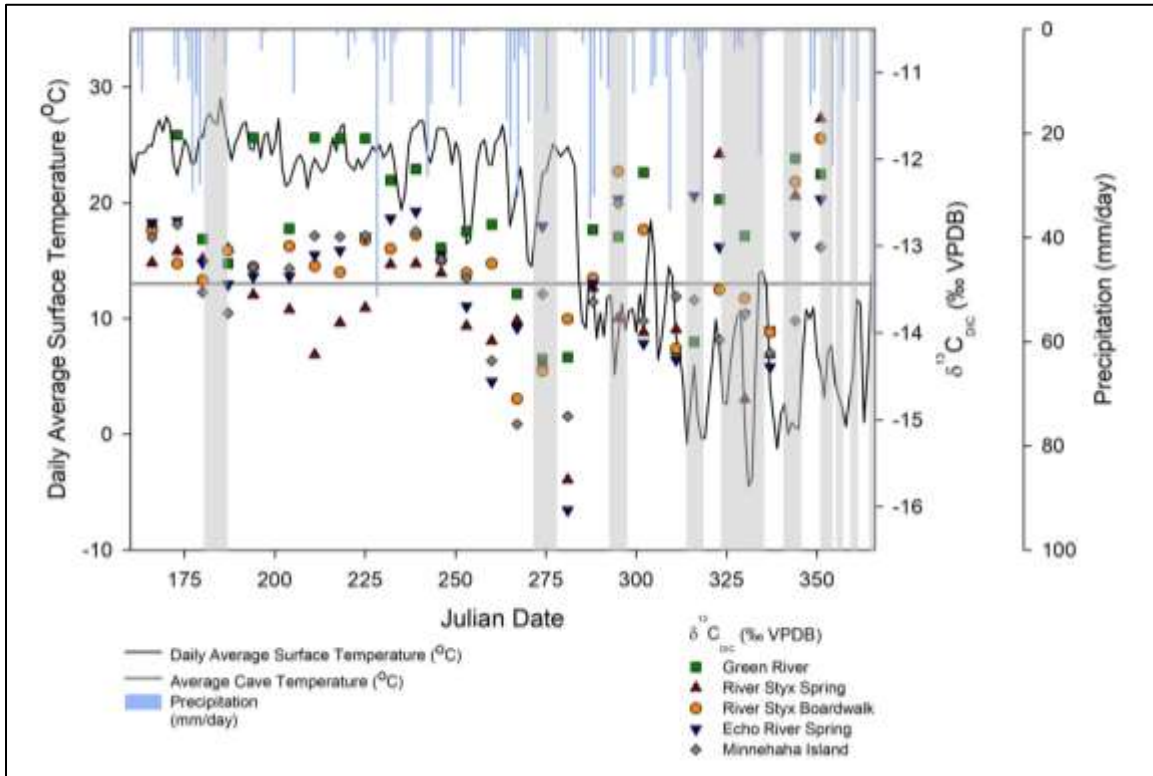
Figure 5.9 Daily average surface temperature
Daily average surface temperature at the Houchin Meadow's weather station overlaid with weekly $\delta^{13}C_{DIC}$.

Increased variability in the fall and winter may be attributed to multiple factors. Changes in the hydrologic regime may cause flushing of storage waters through the epikarst faster than the waters can sufficiently homogenize. This is supported by the wider range of $\delta^{13}C_{DIC}$ in the fall and winter months when precipitation increases, evapotranspiration slows, and the depth to the water table decreases (Figure 5.9). Additionally, stable reverse flows increase in the fall and winter months, causing mixing of river water with cave waters, which can cause increase fractionation. The seasonal shift in variability may be associated with decreasing surface temperatures, which can

158

influence the subsurface through stable reverse flows. Fractionation of ^{13}C is temperature dependent and fractionation processes tend to increase as temperature decreases (Clark and Fritz 1997). Temperature fluctuations and flow reversals may lead to degassing of soil CO_2 or boosts in CO_2 production causing changes in the carbon signature from week to week, thus increasing the range of $\delta^{13}C_{DIC}$ in the fall and winter months.

Seasonal shifts in airflow may also be responsible for the increased variability and $\delta^{13}C_{DIC}$ enrichment in cave waters during late fall and winter. During the winter, cold surface air is pulled into Mammoth Cave's lower surficial openings as warmer cave air flows upward and out of higher entrances (Olson 2017). This phenomenon, known as the "chimney airflow effect," causes air with lower CO_2 concentrations (that is also isotopically enriched) to flow into the cave, displacing air with isotopically lighter CO_2 to the surface (Spötl et al. 2005). Analyses of CO_2 in multiple cave atmospheres show distinct seasonal trends: higher CO_2 concentrations during the summer when soil gas accumulates; and lower CO_2 concentrations during the winter as temperature-driven air flow reversals bring in surface air (Spötl et al. 2005; Knierim et al. 2015; Shindoh et al. 2017). Comparisons of seasonal CO_2 concentrations in cave air and $\delta^{13}C_{DIC}$ in cave waters suggest that seasonal changes in airflow patterns cause a disequilibrium between gaseous CO_2 and aqueous DIC, which can cause degassing of CO_2 and slight $\delta^{13}C_{DIC}$ enrichment of cave waters (Knierim et al. 2015). $\delta^{13}C_{DIC}$ enrichment at River Styx Boardwalk and Minnehaha Island in October and December suggest CO_2 degassing in both River Styx and Echo River associated with changes in airflow patterns or temperature-induced fractionation. Following those days when the surface temperature steeply declined below the average cave temperature, analysis of water samples revealed

enriched $\delta^{13}C_{DIC}$ values (Figure 5.9). However, these values are not consistent throughout

the winter; $\delta^{13}C_{DIC}$ values in November were lighter than $\delta^{13}C_{DIC}$ values during the

summer. The enrichment of $\delta^{13}C_{DIC}$ values at these sites also occurred during almost all

flow reversals, which suggests that temperature changes and mixing with the Green River

water caused enrichment of the sampled values. However, water in the Green River was

more isotopically depleted than water taken from River Styx Boardwalk during two of

the three events. This discrepancy might be attributed to diurnal fluctuations in $\delta^{13}C_{DIC}$ of

river water; a daily variation of 1‰ $\delta^{13}C_{DIC}$ has been observed in a karst river in Florida

(de Montety et al. 2011). However, that variation was associated with photosynthetic

processes, a contribution that, in the case of the Green River in Kentucky during the

winter months, seems an unlikely explanation. The data suggest that changes in the flow

regime and temperatures are the major contributing factors to seasonal variability in

$\delta^{13}C_{DIC}$ values.

5.5 Conclusions

Analysis of $\delta^{13}C_{DIC}$ in Mammoth Cave's Green River, River Styx, and Echo River

shows that DIC is dominated by soil CO_2 and that waters tend to be isotopically

homogenized independent of seasons. Seasonality in $\delta^{13}C_{DIC}$ values and carbon sourcing

manifests, not as distinct shifts in sources, but as changes in variability from summer

(decreased variability) to fall and winter (increased variability). As was found regarding

dissolution in Mammoth Cave's River Styx and Echo River, an analysis of carbon

isotopes reveals that carbon flux is dominated by both large precipitation events and

seasonal shifts in the hydrologic regime, but not necessarily by seasonal changes in CO_2

production. Furthermore, the results from the analysis of $\delta^{13}C_{DIC}$ values support the

findings regarding dissolution, i.e. spring flow reversals do not significantly contribute to dissolution in Mammoth Cave's River Styx and Echo River. However, due to the complexity of carbon sources and water inputs, a future study with higher resolution sampling may uncover even more subtle temporal and seasonal changes in dissolution patterns and carbon flux.

5.6 Literature Cited

Andrews, J.A., Schlesinger, W.H., 2001. Soil CO_2 dynamics, acidification, and chemical weathering in a temperate forest with experimental CO_2 enrichment. *Global Biogeochemical Cycles* 15(1), 149-162.

Baldini, J.U.L., Baldini, L.M., McDermott, F., Clipson, N., 2006. Carbon dioxide sources, sinks, and spatial variability in shallow temperate zone caves: Evidence from Ballynamintra Cave, Ireland. J*ournal of Cave and Karst Studies* 68(1), 4-11.

Ballard, C., Polk, J.S., McClanahan, K., Gulley, J., 2016. Characterizing carbon transport and dissolution processes in a complex karst groundwater reversal system at Mammoth Cave, Kentucky, USA. *Abstracts with Programs, Geological Society of America* 48(7).

Boutton, T.W., 1991. Stable carbon isotope ratios of natural materials: II. Atmospheric, terrestrial, marine, and freshwater environments. In *Carbon isotope techniques*. Coleman, D.C., Fry, B. (Eds). San Diego, CA: Academic Press.

Brunet, F., Dubois, K., Veizer, J., Nkoue Ndondo, G.R., Ndam Ngoupayou, J.R., Boeglin, J.L., Probst, J.L., 2009. Terrestrial and fluvial carbon fluxes in a tropical watershed: Nyong basin, Cameroon. *Chemical Geology* 265(3-4), 563-572.

Bullen, T.D., Kendall, C., 1998. Tracing of weathering reactions and water flowpaths: a multi-isotope approach. In *Isotope Tracers in Catchment Hydrology*. Kendall, C., McDonnell, J.J. (Eds). Amsterdam: Elsevier, 611-646.

Cane, G., Clark, I.D., 1999. Tracing ground water recharge in an agricultural watershed with isotopes. *Groundwater* 37(1), 133-139.

Clark, I., Fritz, P., 1997. *Environmental isotopes in hydrogeology*. Boca Raton, FL: CRC Press LLC.

Contosta, A.R., Burakowski, E.A., Varner, R.K., Frey, S.D., 2016. Winter soil respiration in a humid temperate forest: The roles of moisture, temperature, and snowpack. *Journal of Geophysical Research: Biogeosciences* 121, 3072-3088.

de Montety, V., Martin, J.B., Cohen, M.J., Foster, C., Kurz, M.J. 2011. Influence of diel biogeochemical cycles on carbonate equilibrium in a karst river. *Chemical Geology* 283, 31-43.

Doctor, D.H., Kendall, C., Sebestyen, S.D., Shanley, J.B., Ohte, N., Boyer, E.W., 2008. Carbon isotope fractionation of dissolved inorganic carbon (DIC) due to outgassing of carbon dioxide from a headwater stream. *Hydrological Processes* 22, 2410-2423.

Drever, J.I., 1997. *The geochemistry of natural waters: surface and groundwater environments.* Upper Saddle River, NJ: Prentice Hall.

Fetter, C.W., 2013. *Applied hydrogeology.* London, England: Pearson Education Limited.

Frisia, S., Fairchild, I.J., Fohlmeister, J., Miorandi, R., Spötl, C., Borsato, A., 2011. Carbon mass-balance modelling and carbon isotope exchange processes in dynamic caves. *Geochimica et Cosmochimica Acta* 75, 380-400.

Granger, D.E., Fabel, D., Palmer, A.N., 2001. Pliocene-Pleistocene incision of the Green River, Kentucky, determined from radioactive decay of cosmogenic ^{26}Al and ^{10}Be in Mammoth Cave sediments. *GSA Bulletin* 133(7), 825-836.

Graven, H., Allison, C.E., Etheridge, D.M., Hammer, S., Keeling, R.F., Levin, I., Meijer, H.A.J., Rubino, M., Tans, P.P., Trudinger, C.M., Vaughn, B.H., White, J.W.C., 2017. Compiled records of carbon isotopes in atmospheric CO_2 for historical simulations in CMIP6. Geoscientific Model Development 10, 4405-4417.

Groves, C., Meiman, J., 2001. Weathering, geomorphic work, and karst landscape evolution in the Cave City groundwater basin, Mammoth Cave, Kentucky. *Geomorphology* 67, 115-126.

Hess, J.W., Wells, S.G., Quinlan, J.F., White, W.B., 1989. Hydrogeology of the South-central Kentucky karst. In: White, W.B., White, E.L. ed. *Karst hydrology: concepts from the Mammoth Cave area.* New York, NY: Van Nostrand Reinhold.

Hess, J.W., White, W.B., 1989. Water budget and physical hydrology. In: White, W.B., White, E.L. ed. *Karst hydrology: concepts from the Mammoth Cave area.* New York, NY: Van Nostrand Reinhold.

Jackson, L., 2017. Epikarst hydrogeochemical changes in telogenetic karst systems in South-central Kentucky. Master's thesis. Bowling Green: Western Kentucky University, Department of Geography and Geology.

Knierim, K.J., Pollock, E.D., Hays, P.D., Khojasteh, J., 2015. Using stable isotopes of carbon to investigate the seasonal variation of carbon transfer in a northwestern Arkansas cave. *Journal of Cave and Karst Studies* 77(1), 12–27.

Lee, E., Krothe, N.C., 2001. A four-component mixing model for water in a karst terrain in south-central Indiana, USA. Using solute concentration and stable isotopes as tracers. *Chemical Geology* 179(1), 129-143.

Li, S., Liu, C., Tao, F., Lang, Y., Han, G., 2005. Carbon biogeochemistry of ground water, Guiyang, Southwest China. *Groundwater* 43(4), 494-499.

Li, S., Liu, C., Lang, Y., Tao, F., Zhao, Z., Zhou, Z., 2008. Stable carbon isotope biogeochemistry and anthropogenic impacts on karst ground water, Zunyi, Southwest China. *Aquatic Geochemistry* 14, 211-221.

Liu, Z., Dreybrodt, W., Wang, H. 2010. A new direction in effective accounting for the atmospheric CO_2 budget: Considering the combined action of carbonate dissolution, the global water cycle and photosynthetic uptake of DIC by aquatic organisms. *Earth-Science Reviews* 99, 162-172.

McClanahan, K., 2014. Carbon Cycling Dynamics Inferred from Carbon Isotope Sourcing in a Mid-Latitude Karst-Influenced River. Master's thesis. Bowling Green: Western Kentucky University, Department of Geography and Geology.

Meiman, J., 2006. Water resources management plan, MCNP, Kentucky. Technical Report: United States Department of the Interior, National Park Service.

Oh, N-H, Kim, H-S., Richter, Jr., D.D., 2005. What Regulates Soil CO_2 Concentrations? A Modeling Approach to CO_2 Diffusion in Deep Soil Profiles. *Environmental Engineering Science* 22(1), 38-45.

Olson, R.A., 2017. Mammoth Cave meteorology. In: Hobbs, H.H., Olson, R.A., Winkler, E.G., Culver, D.C., ed. *Mammoth Cave: A human and natural history.* Springer Online.

Palmer, A.N., 1981. *A geological guide to MCNP.* Teaneck, NJ: Zephyrus Press.

Palmer, A.N., 2007. *Cave geology.* Dayton, OH: Cave Books.

Paylor, R.L., Currens, J.C., 2001. Karst occurrence in Kentucky. Kentucky Geological Survey Map and Chart 35. Accessed October 15, 2019 from https://uknowledge.uky.edu/kgs_mc/35.

Polk, J.S., Vanderhoff, S., Groves, C., Miller, B., Bolster, C., 2013. Complex epikarst hydrogeology and contaminant transport in a South-central Kentucky karst landscape. Proceedings of the 16th International Congress of Speleology, Brno, Czeck Republic 110-115.

Richter, D.D., Markewitz, D., 1995. How deep is the soil? *Bioscience* 45(9), 600-609.

Schulte, P., van Geldern, R., Freitag, H., Karim, A., Négrel, P., Petelet-Giraud, E., Probst, A., Probst, J., Telmer, K., Veizer, J., Barth, J.A.C., 2011. Applications of stable water and carbon isotopes in watershed research: weathering, carbon cycling, and water balances. Earth-Science Reviews 109, 20-31.

Shindoh, T., Mishima, T., Watanabe, Y., Ohsawa, S., Tagami, T., Seasonal cave air ventilation controlling variation in cave air pCO_2 and drip water geochemistry at Inazumi Cave, Oita, northeastern Kyushu, Japan. *Journal of Cave and Karst Studies* 79(2), 100-112

Spötl, C., Fairchild, I.J., Tooth, A.F., 2005. Cave air control on dripwater geochemistry, Obir Caves (Austria): Implications for speleothem deposition in dynamically ventilated caves. *Geochimica et Cosmochimica Acta* 69, 2451–2468.

Toomey, R.S., Hobbs, H.H., Olson, R.A., 2017. An Orientation to Mammoth Cave and This Volume In: Hobbs, H.H., Olson, R.A., Winkler, E.G., Culver, D.C., ed. *Mammoth Cave: A human and natural history.* Springer Online.

Vaughn, K., 1998. A quantitative analysis of interstitial fluid-chemistry and limestone dissolution rates within the clastic sediment of a karst aquifer conduit, Mammoth Cave, Kentucky. Master's thesis. Bowling Green: Western Kentucky University, Department of Geography and Geology.

Wagner, R.J., Boulger Jr., R.W., Oblinger, C.J., Smith, B.A., 2006. *Guidelines and standard procedures for continuous water-quality monitors: Station operation, record computation, and data reporting.* Techniques and Methods 1–D3. Reston, VA: U.S. Geological Survey. Accessed November 21, 2017 from https://pubs.usgs.gov/tm/2006/tm1D3/pdf/TM1D3.pdf

White, W.B., 1989. Introduction to the karst hydrology of the Mammoth Cave area. In: White, W.B., White, E.L. ed. *Karst hydrology: concepts from the Mammoth Cave area.* New York, NY: Van Nostrand Reinhold.

White, W.B., White, E.L., 2017. Hydrology and hydrogeology of Mammoth Cave. In: Hobbs, H.H., Olson, R.A., Winkler, E.G., Culver, D.C., ed. *Mammoth Cave: A human and natural history.* Springer Online.

Wilde, F.D., Radtke, D.B., Gibs, J., and Iwatsubo, R.T., 2004 (rev. 2009). Processing of water samples. In *U.S. Geological Survey Techniques of Water-Resources Investigations, Book 9*. Reston, VA: U.S. Geological Survey. Accessed November 19, 2017 from https://water.usgs.gov/owq/FieldManual/chapter5/html/Ch5_contents.html

Wilde, F.D., Sandstrom, M.W., Skrobialowski, S.C. 2015. National field manual for the collection of water-quality data. U.S. Geological Survey Techniques of Water-Resources Investigations, Book 9. Reston, VA: U.S. Geological Survey. Accessed November 19, 2017 from https://water.usgs.gov/owq/FieldManual/

Williams, P.W., 2008. The role of the epikarst in karst and cave hydrogeology: a review. *International Journal of Speleology* 37(1), 1-10.

Worthington, S.R.H., Ford, D.C., Beddows, P.A., 2000. Porosity and permeability enhancement in unconfined carbonate aquifers as a result of solution. In: Klimchouck, A.B., Ford, D.C., Palmer, A.N., Dreybodt, W., ed. *Speleogenesis: evolution of karst aquifers.* Huntsville, AL: National Speleological Society.

Yang, R., Zhao, M., Zeng, C., Chen, B., Liu, Z., 2015. Spatiotemporal Variations of Soil CO_2 in Chenqi, Puding, SW China: The Effects of Weather and LUCC. In: Andreo, B., Carrasco, F., Duran, J.J., Jiménez, P., LaMoreaux, J.W., ed., *Hydrogeological and Environmental Investigations in Karst Systems*. Verlag Berlin Heidelberg: Springer.

Zhang, J., Quay, P.D., Wilbour, D.O. 1995. Carbon isotope fractionation during gaswater exchange and dissolution of CO_2. *Geochemica et Cosmochemica Acta* 59, 107-114.

Zhang, L., Qin, X., Liu, P., Huang, Q., Lan, F., Ji, H. 2015. Estimation of carbon sink fluxes in the Pearl River basin (China) based on a water-rock-gas-organism interaction model. *Environmental Earth Science* 74, 945-952.

6. Conclusions

Spring flow reversals are common occurrences in Mammoth Cave's River Styx and Echo River Springs. This study determined that flow in River Styx Spring was reversing 34% of the time from June 2018 to December 2018. This is significantly higher than was found in the study by Trimboli and Toomey (2019) for the period between October 2009 and October 2012; they concluded that River Styx Spring was experiencing reverse flow 20% of the time. The contrast in these results can be attributed differences in the length of the studies, precipitation patterns, or Green River Dam discharge.

The control of spring flow reversals is hydraulic head differences of the river and karst basins. Hydraulic head variability is heavily influenced by upstream dam control, located on the Green River Lake. All ten stable reverse flows identified in this study coincided with dam releases at Green River Lake Dam. Other factors that influence the frequency and duration of spring flow reversals are: rainfall intensity and duration, rainfall location (upstream Green River basin vs. Mammoth Cave karst basins), antecedent soil moisture conditions, and evapotranspiration. These factors influence seasonal hydrologic regimes, dissolution dynamics, and carbon sourcing. Increased rainfall, higher soil moisture, and lower evapotranspiration rates during the winter raise the water table and causes changes in the hydraulic head, establishing stable reverse flows for most of the season. During the winter, the stable reverse flow phenomenon was the normal flow regime, as Green River overflowed into River Styx Spring 72.5% of the time. Normal flow direction from River Styx Spring can be induced during the winter season by intense precipitation events in the Mammoth Cave karst basins, which may temporarily reverse the hydraulic head gradient between the basins and the Green River.

Calculations of pCO_2, SI_{cal}, and dissolution rates show that dissolution in the River Styx and Echo River Basin are not enhanced during stable reverse flows. Dissolution during stable reverse flows is often lower or equal to normal baseflow conditions. Stable reverse flows were expected to contribute significantly to dissolution, as was found in Florida. Dissolution calculations during a stable reverse flow estimated the maximum amount of wall retreat at Echo River Spring was 0.003, significantly lower than the 3.4 mm estimated in Florida (Gulley et al. 2011). These results are likely due to differences in pH, residence time, and porosity. pH values of the Green River were more basic in the river than the base flow cave waters. Shorter residence times, caused by throughflow of the river water from River Styx Spring to Echo River Spring, do not allow for complete mixing of the waters. Finally, telogenetic karst has low matrix porosity that limits infiltration by aggressive waters.

Analysis of $\delta^{13}C_{DIC}$ shows that DIC is controlled by soil CO_2 in the River Styx and Echo River groundwater basins. There were no seasonal shifts in sources, just increases in variability, as the hydrologic regime changed in the fall and winter. Despite this slight shift in variability, the waters were isotopically homogenized throughout the study period. This suggests a concentrated soil CO_2 reservoir that is slowly depleted through the seasons.

Future studies should examine the role that flow reversals play in the contribution of CO_2 from organic matter. Previous studies have shown increased pCO_2 caused by decay of organics in sediment deposits of the River Styx, suggesting that flow reversals may increase dissolution, but not during the reversal itself. Additionally, higher resolution carbon isotope sampling and discharge measurements could provide further

insight into carbon sourcing dynamics, carbon flux, and dissolution in other karst regions. Future studies would also find value in discharge measurements. Discharge data could be used to further understand hydraulic head dynamics between the Green River, the River Styx Karst Basin, and the Echo River Karst Basin. The Echo River Karst Basin is nearly ten times the area of the River Styx Karst Basin; therefore, precipitation events cause large volumes of water to flow through the basin. Because hydraulic head in the karst basins is controlled by the volume of water moving through them, measurements of this volume (discharge) would be useful in determining why stable reverse flows occur. Additionally, discharge could be used to calculate more precise calcite dissolution under the varying flow regimes. Lastly, discharge data form the Green River Dam could be used to better understand the effects that water level control of the Green River Lake has on stable reverse flows.

Literature Cited

Allaby, M., 2013. Mineral saturation index. In *A Dictionary of Geology and Earth Sciences*, Oxford University Press. Accessed November 20, 2017 from http://www.oxfordreference.com/view/10.1093/acref/9780199653065.001.0001/acref-9780199653065

Anaya, A. A., Padilla, I., Macchiavelli, R., Vesper, D.J., Meeker, J.D., Alshawabkeh, A.N., 2014. Estimating preferential flow in karstic aquifers using statistical mixed models. *Groundwater* 52(4), 584-596.

Anthony, D., 1998. Seasonal effects on the geochemical evolution of the Logsdon River, Mammoth Cave, Kentucky. Master's thesis. Bowling Green: Western Kentucky University, Department of Geography and Geology.

Ballard, C., Polk, J.S., McClanahan, K., Gulley, J., 2016. Characterizing carbon transport and dissolution processes in a complex karst groundwater reversal system at Mammoth Cave, Kentucky, USA. *Abstracts with Programs, Geological Society of America* 48(7).

Boutton, T.W., 1991. Stable carbon isotope ratios of natural materials: II. Atmospheric, terrestrial, marine, and freshwater environments. In *Carbon isotope techniques*. Coleman, D.C., Fry, B. (Eds). San Diego, CA: Academic Press.

Bullen, T.D., Kendall, C., 1998. Tracing of weathering reactions and water flowpaths: a multi-isotope approach. In *Isotope Tracers in Catchment Hydrology*. Kendall, C., McDonnell, J.J. (Eds). Amsterdam: Elsevier, 611-646.

Brown, A.L., Martin, J.B., Screaton, E.J., Gulley, J., 2014. Bank storage in karst aquifers: The impact of temporary intrusion of river water on carbonate dissolution and trace metal mobility. *Chemical Geology* 385, 56-69.

Choquette, P.W., Pray, L.C., 1970. Geologic nomenclature and classification of porosity in sedimentary carbonates. *American Association of Petroleum Geologist Bulletin* 54(2), 207-250.

Clark, I., Fritz, P., 1997. *Environmental isotopes in hydrogeology.* Boca Raton, FL: CRC Press LLC.

Crandall, C.A., Katz, B.G., Hirten, J.J., 1999. Hydrochemical evidence for mixing of river water and groundwater during high-flow conditions, lower Suwanee River basin, Florida, USA. *Hydrogeology Journal* 7, 454-467.

Cuezva, S., Fernandez-Cortes, A., Benavente, D., Serrano-Ortiz, P., Kowalski, A.S., Sanchez-Moral, S., 2010. Short-term CO_2(g) exchange between a shallow karstic cavity and the external atmosphere during summer: role of the surface soil layer. *Atmospheric Environment* 45, 1418-1427.

Doctor, D.H., Kendall, C., Sebestyen, S.D., Shanley, J.B., Ohte, N., Boyer, E.W., 2008. Carbon isotope fractionation of dissolved inorganic carbon (DIC) due to outgassing of carbon dioxide from a headwater stream. *Hydrological Processes* 22, 2410-2423.

Drever, J.I., 1997. *The geochemistry of natural waters: surface and groundwater environments.* Upper Saddle River, NJ: Prentice Hall.

Edwards, A., 2009. The hydrochemistry of surface water backflooding into a karst spring and into cave stream passages in Mammoth Cave, KY USA. Report on NPS Permit MACA-2007-SCI-0011.

Fetter, C.W., 2013. *Applied hydrogeology*. London, England: Pearson Education Limited.

Florea, L.J., 2013. Isotopes of carbon in a karst aquifer of the Cumberland Plateau of Kentucky, USA. *Acta Carsologica* 42, 277-289.

Florea, L.J., Vacher, H.L., 2006. Spring flow hydrographs: eogenetic vs. telogenetic karst. *Groundwater* 44(3), 352-361.

Fogel, M.L., Cifuentes, L.A., 1993. Isotope fractionation during primary production. In *Organic Geochemistry*. Engel, M.H., Macko, S.A. (Eds). New York: Plenum Press, 73-98.

Ford, D.C., Williams, P.W., 2007. *Karst hydrogeology and geomorphology.* 2nd ed. West Sussex, England: John Wiley and Sons Ltd.

Freeze, R.A., Cherry, J.A., 1979. *Groundwater.* Upper Saddle River, NJ: Prentice Hall.

Fry, B., 2006. *Stable isotope ecology*. New York, NY: Springer.

Geye, M., 2000. Groundwater: Saturated and unsaturated zone. In *Environmental isotopes in the hydrological cycle: principles and applications*. Mook, W.G. (Ed). Paris: UNESCO Technical Documents in Hydrology.

Glennon, J.A., 2001. Application of morphometric relationships to active flow networks within the Mammoth Cave Watershed. Master's thesis. Bowling Green: Western Kentucky University, Department of Geography and Geology.

Goldscheider, N., Drew, D., 2007. *Methods in karst hydrogeology.* London, UK: Taylor and Francis Group.

Granger, D.E., Fabel, D., Palmer, A.N., 2001. Pliocene-Pleistocene incision of the Green River, Kentucky, determined from radioactive decay of cosmogenic [26]Al and [10]Be in Mammoth Cave sediments. *GSA Bulletin*, 133(7), 825-836.

Graven, H., Allison, C.E., Etheridge, D.M., Hammer, S., Keeling, R.F., Levin, I., Meijer, H.A.J., Rubino, M., Tans, P.P., Trudinger, C.M., Vaughn, B.H., White, J.W.C., Compiled records of carbon isotopes in atmospheric CO2 for historical simulations in CMIP6. *Geoscientific Model Development* 10, 4405-4417.

Grimes, K.G., 2002. Syngenetic and eogenetic karst: an Australian viewpoint. In: Gabrovšek, F., ed. *Evolution of Karst: from Prekarst to Cessation*. Ljubljana, Slovenia: Inštitut za raziskovanje krasa, ZRC SAZU.

Groves, C., Meiman, J., 2001. Weathering, geomorphic work, and karst landscape evolution in the Cave City groundwater basin, Mammoth Cave, Kentucky. *Geomorphology* 67, 115-126.

Gulley, J., Martin, J. B., Screaton, E. J., Moore, P. J., 2011. River reversals into karst springs: A model for cave enlargement in eogenetic karst aquifers. *GSA Bulletin* 123(3-4), 457-467.

Gulley, J.D., Martin, J.B., Moore, P.J., Murphy, J., 2013. Formation of phreatic caves in an eogenetic karst aquifer by CO_2 enrichment at lower water tables and subsequent flooding by sea level rise. *Earth Surface Processes and Landforms* 38(11), 1210-1224.

Helf, K.L., Olson, R.A., 2017. Subsurface aquatic ecology in Mammoth Cave. In: Hobbs, H.H., Olson, R.A., Winkler, E.G., Culver, D.C., ed. *Mammoth Cave: A human and natural history*. Springer Online.

Hendrickson, G.E., 1961. Sources of water in Styx and Echo rivers, Mammoth Cave, Kentucky. U.S. Geological Survey Professional Paper, 424-D:D41-D43.

Hensley, R.T., Cohen, M.J., 2017. Flow reversals as a driver of ecosystem transition in Florida's springs. *Freshwater Science* 36(1), 14-25.

Herczeg, A.L., Fairbanks, R.G., 1987. Anomalous carbon isotope fractionation between atmospheric CO_2 and dissolved inorganic carbon induced by intense photosynthesis. *Geochimtca et Cosmochrmica Acta* 51, 895-899.

Hess, J.W., Wells, S.G., Quinlan, J.F., White, W.B., 1989. Hydrogeology of the South-central Kentucky karst. In: White, W.B., White, E.L. ed. *Karst hydrology: concepts from the Mammoth Cave area.* New York, NY: Van Nostrand Reinhold.

Hess, J.W., White, W.B., 1989a. Water budget and physical hydrology. In: White, W.B., White, E.L. ed. *Karst hydrology: concepts from the Mammoth Cave area.* New York, NY: Van Nostrand Reinhold.

Hess, J.W., White, W.B., 1989b. Chemical hydrology. In: White, W.B., White, E.L. ed. *Karst hydrology: concepts from the Mammoth Cave area.* New York, NY: Van Nostrand Reinhold.

Hess, J.W., White, W.B., 1993. Groundwater geochemistry of the carbonate karst aquifer, southcentral Kentucky, USA. *Applied Geochemistry* 8(2), 189-204.

Hiscock, K.M., 2005. *Hydrogeology: principles and practices.* Malden, MA: Blackwell Publishing.

Hoefs, J., 2018. *Stable isotope geochemistry*. Cham, Switzerland: Springer International.

Hovey, H.C.,1912. *The Mammoth Cave of Kentucky.* Louisville, KY: John P. Morton and Company.

Hull, R.W., Dysart, J.E., Mann IV, W.B., 1981. Quality of surface water in the Suwannee River Basin, Florida, August 1968 through December 1977. U.S. Geological Survey, Water-Resources Investigations Report 80-110: Tallahassee, FL.

Jackson, L., 2017. Epikarst hydrogeochemical changes in telogenetic karst systems in South-central Kentucky. Master's thesis. Bowling Green: Western Kentucky University, Department of Geography and Geology.

Jones, W.K., 2013. Physical structure of the epikarst. *Acta Carsologica* 42(2-3), 311-314.

Kentucky Geological Survey, 2013. Where Is Karst Located in Kentucky? Accessed November 5, 2017 from https://www.uky.edu/KGS/water/general/karst/where_karst.htm

Khadka, M.B., Martin, J.B., Jin, J., 2014. Transport of dissolved carbon and CO_2 degassing from a river system in a mixed silicate and carbonate catchment. *Journal of Hydrology* 513, 391-402.

Kincaid, T., 1998. River water intrusion to the unconfined Floridan aquifer. *Environmental and Engineering Geoscience* 4(3), 361-374.

Kolata, D.R., Nelson, W.J., 1990. Tectonic history of the Illinois Basin. In: Leighton, M.W., Kolata, D.R., Oltz, D.T., Eidel, J.J., ed. *M 51: Interior Cratonic Basins.* Tulsa, OK: The American Association of Petroleum Geologists.
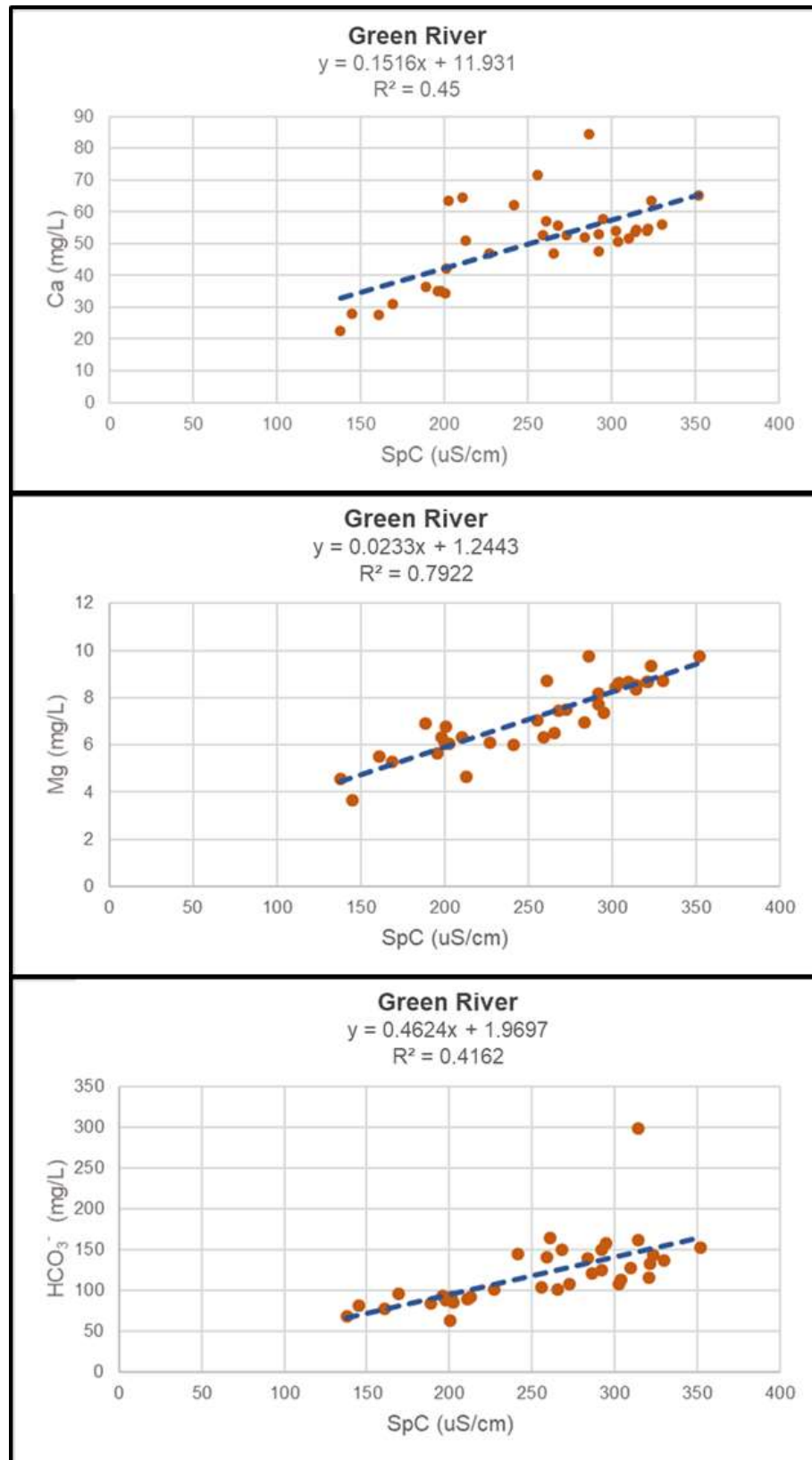
Lawhon, N., 2014. Investigating telogenetic karst aquifer processes and evolution in south-central Kentucky, U.S., using high-resolution storm hydrology and geochemistry monitoring. Master's thesis. Bowling Green: Western Kentucky University, Department of Geography and Geology.

Lindsey, R., 2017. Climate change: atmospheric carbon dioxide. National Oceanic and Atmospheric Administration (NOAA). Accessed March 25, 2018 from https://www.climate.gov/news-features/understanding-climate/climate-change-atmospheric-carbon-dioxide.

MACA (Mammoth Cave National Park), 2017. *Green and Nolin Rivers reopen in park*. Mammoth Cave, KY: NPS. Accessed October 8, 2017, from https://www.nps.gov/maca/learn/news/rivers-open-april.htm.

Martin, J, Screaton, E., 2012. Reversals of karst springs: Implications for water budgets, water quality, and speleogenesis. Award Abstract #0910794, National Science Foundation. Accessed September 9, 2017, from https://nsf.gov/awardsearch/showAward?AWD_ID=0910794.

May, M.T., Kuehn, K.W., Groves, C.G., Meiman, J., 2005. Karst geomorphology and environmental concerns of the Mammoth Cave Region, Kentucky. AIPG Field trip guide: Kentucky Section of the American Institute of Professional Geologists.

McClanahan, K., 2014. Carbon Cycling Dynamics Inferred from Carbon Isotope Sourcing in a Mid-Latitude Karst-Influenced River. Master's thesis. Bowling Green: Western Kentucky University, Department of Geography and Geology.

Meiman, J., 2006. Water resources management plan, MCNP, Kentucky. Technical Report: United States Department of the Interior, National Park Service.

Meiman, J., Groves, C., Herstein, S., 2001. In-cave dye tracing and drainage basin divides in the Mammoth Cave karst aquifer, Kentucky. In Kuniansky, E.L. ed. *U.S. Geological Survey Karst Interest Group Proceedings, Water-Resources Investigations Report 01-4011*, 179-185.

Miller, R.L., Bradford, W.L., Peters, N.E., 1988. Specific conductance: theoretical considerations and application to analytical quality control. U.S. Geological Survey, Water-Supply Paper 2311: Denver, CO.

Mook, W.G., Bommerson, J.C., Staverman, W.H., 1974. Carbon isotope fractionation between dissolved bicarbonate and gaseous carbon dioxide. *Earth and Planetary Science Letters* 22, 169-176.

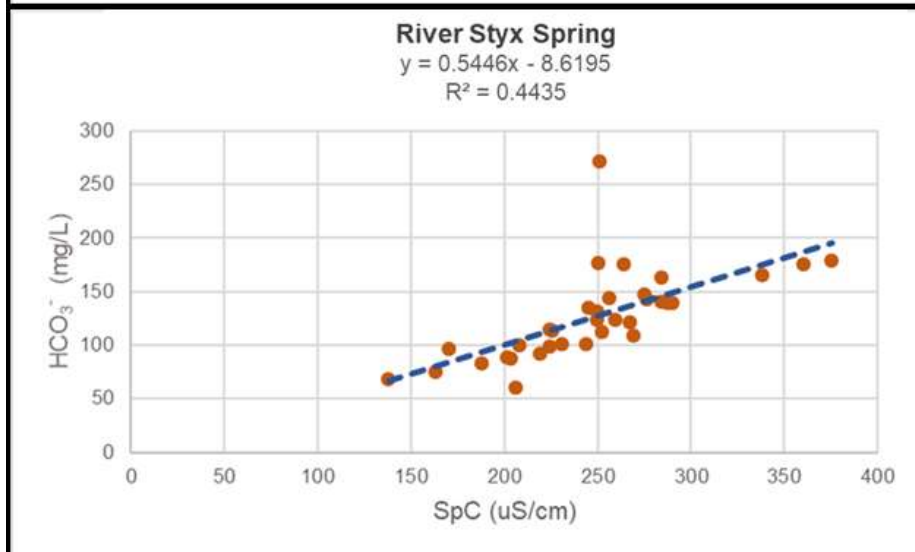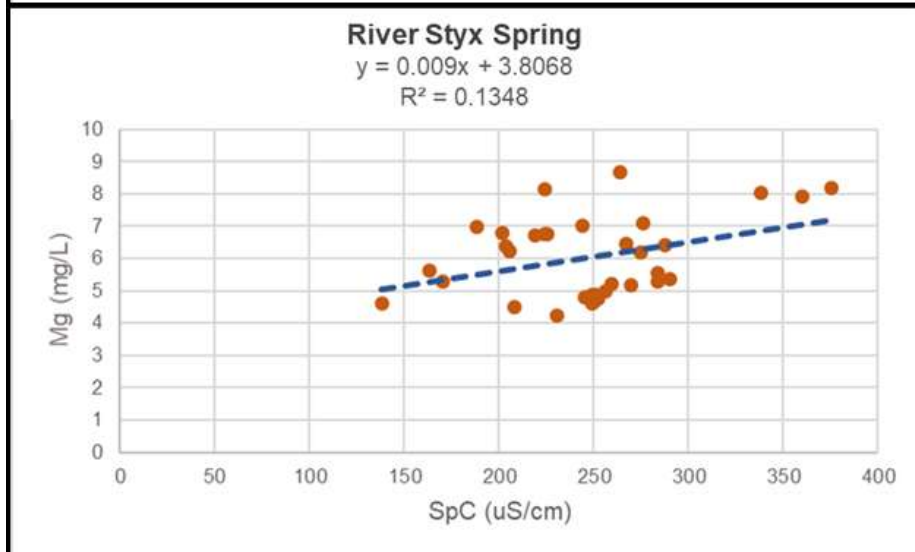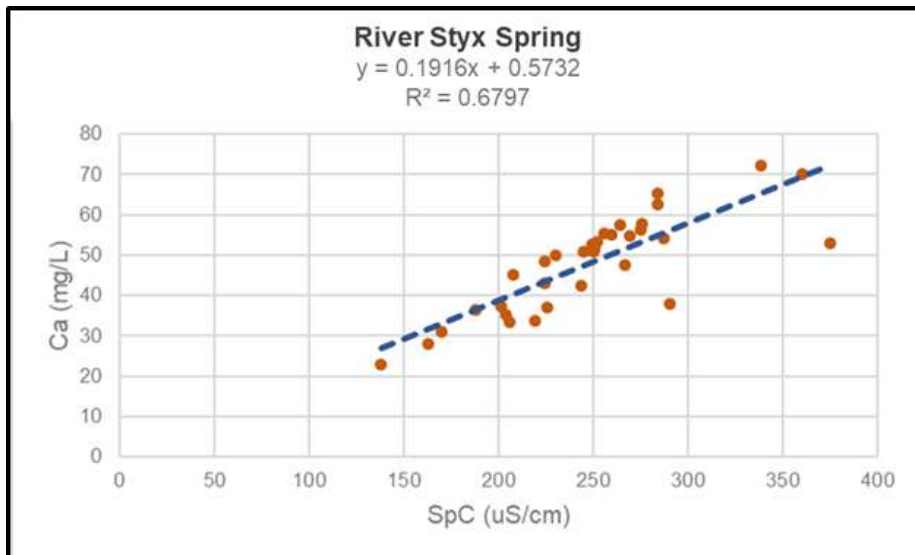Moore, C.H., 1989. Carbonate diagenesis and porosity. Amsterdam, The Netherlands: Elsevier.

National Oceanic and Atmospheric Administration (NOAA), 2019. Global carbon dioxide growth in 2018 reached 4th highest on record. Accessed June 20,2019 from https://www.noaa.gov/news/global-carbon-dioxide-growth-in-2018-reached-4th-highest-on-record

Opsahl, S.P., Chapal, S.E., Wheeler, C.C., 2005. Using stream gauge data to quantify surface water/groundwater exchange between the Upper Floridan Aquifer and the Lower Flint River, Georgia, USA, 1989-2003, in Proceedings of the 20053 Georgia Water Resources Conference.

Osterhoudt, L.L., 2014. Impacts of carbonate mineral weathering on hydrochemistry of the Upper Green River Basin, Kentucky. Master's thesis. Bowling Green: Western Kentucky University, Department of Geography and Geology.

Palmer, A.N., 1981. *A geological guide to MCNP.* Teaneck, NJ: Zephyrus Press.

Palmer, A.N., 2007. *Cave geology*. Dayton, OH: Cave Books.

Palmer, A. N., 2016. The Mammoth Cave system, Kentucky, USA. *Boletín Geológico y Minero,* 127(1), 131-145.

Palmer, A. N., 2017. Geologic history of Mammoth Cave. In: Hobbs, H.H., Olson, R.A., Winkler, E.G., Culver, D.C., ed. Mammoth Cave: A human and natural history. Springer Online.

Quinlan, J.F., 1989. Ground-water monitoring in karst terranes: recommended protocols and implicit assumptions. U.S. Environmental Protection Agency, Las Vegas, NV.

Quinlan, J.F., Ewers, R.O., 1989. Subsurface drainage in the Mammoth Cave area. In: White, W.B., White, E.L. ed. *Karst hydrology: concepts from the Mammoth Cave area.* New York, NY: Van Nostrand Reinhold

Richey, J.E., Melack, J.M., Aufdenkampe, A.K., Ballester, V.M., Hess, L.L., 2002. Outgassing from Amazonian rivers and wetlands as a large tropical source of atmospheric CO_2. *Nature* 416, 617-620.

Schulte, P., van Geldern, R., Freitag, H., Karim, A., Négrel, P., Petelet-Giraud, E., Probst, A., Probst, J., Telmer, K., Veizer, J., Barth, J.A.C., 2011. Applications of stable water and carbon isotopes in watershed research: weathering, carbon cycling, and water balances. *Earth-Science Reviews* 109, 20-31.
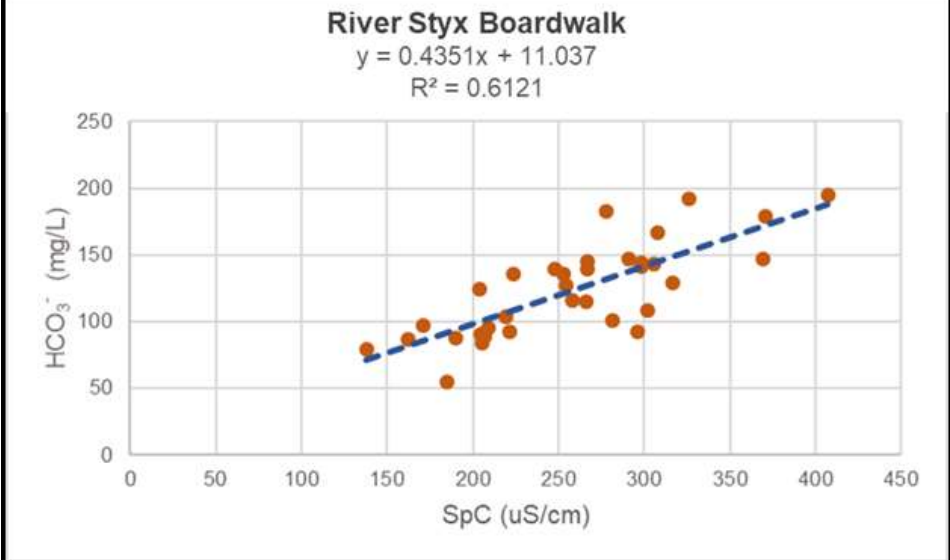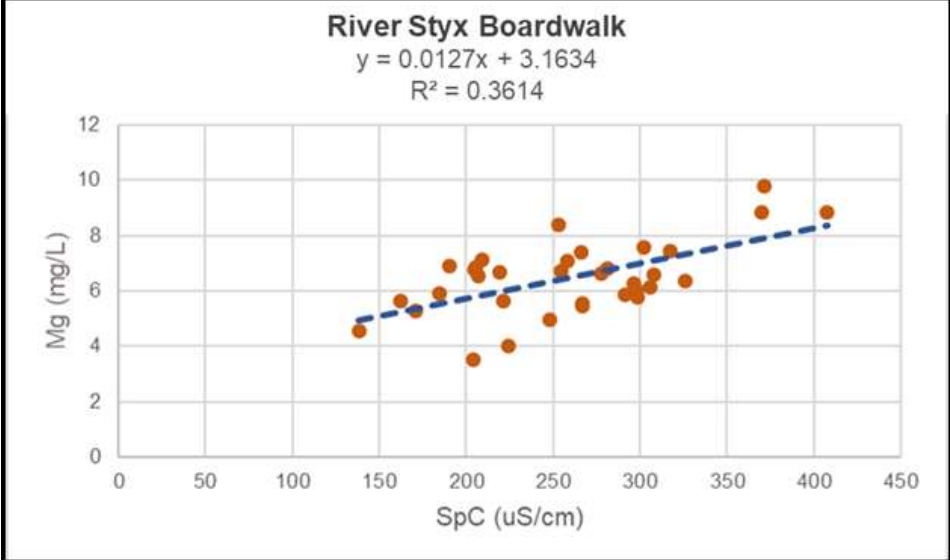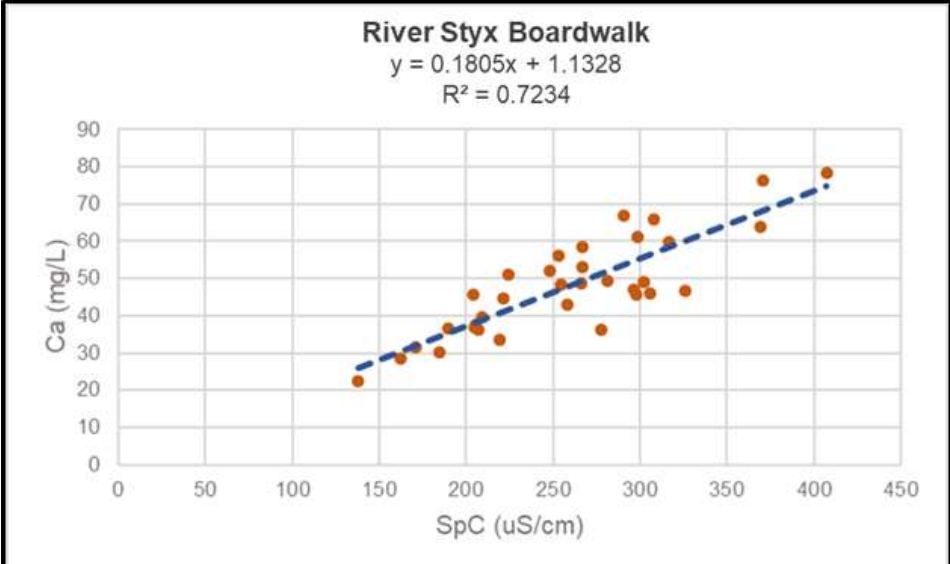
Schwalb, H.R., Wilson, E.N., 1972. Greensburg consolidated oil pool, Green and Taylor Counties, Kentucky: case histories. In: King, R.E., *Stratigraphic oil and gas fields--Classification, exploration methods, and case histories*. AAPG Special Volumes, Memoir 16.

Shelley, J.A., 2019. Monitoring and evaluating the influences of class V injection wells on urban karst hydrology. Master's thesis. Bowling Green: Western Kentucky University, Department of Geography and Geology.

Shuster, E.V., White, W.B., 1971. Seasonal fluctuations in the chemistry of limestone springs: a possible means for characterizing carbonate aquifers. *Journal of Hydrology* 14, 93-128.

Soto, L., Pate, D.L., 2016. Cave and karst resources summary: Mammoth Cave National Park, Kentucky. Report, National Park Service: Geologic Resources Division.

Sutherland, C., 2017. Kentucky Caves – 2017. Unpublished map. Accessed November 4, 2017 from http://chuck-sutherland.blogspot.com/2017/10/kentucky-cave-distribution-map-2017.html.

Thrailkill, J., 1985. Flow in a limestone aquifer as determined from water tracing and water levels in wells. *Journal of Hydrology* 78(1-2), 123-136.

Toomey, R.S., Hobbs, H.H., Olson, R.A., 2017. An Orientation to Mammoth Cave and This Volume In: Hobbs, H.H., Olson, R.A., Winkler, E.G., Culver, D.C., ed. *Mammoth Cave: A human and natural history.* Springer Online.

Trimboli, S. R., Toomey, R.S., 2019. Temperature and reverse-flow patterns of the River Styx, Mammoth Cave, Kentucky. *Journal of Cave and Karst Studies* 81(3), 174-187.

Trimboli, S.R., Toomey, R.S., Weber, K., Ryan, S., 2011. The misbehaving spring: studying unique underground river flow patterns with advanced middle school science students, in Proceedings, George Wright Society Conference on Parks, Protected Areas, and Cultural Sites, 311-316.

Trimboli, S.R., Weber, K., Ryan, S., Toomey, R.S., 2016. An overview of the reverse flow patterns of River Styx in Mammoth Cave, Kentucky: 2009-2012, in Proceedings, Mammoth Cave Research Symposia, MCNP, 128-129.

Wagner, R.J., Boulger Jr., R.W., Oblinger, C.J., Smith, B.A., 2006. *Guidelines and standard procedures for continuous water-quality monitors: Station operation, record computation, and data reporting.* Techniques and Methods 1–D3. Reston, VA: U.S. Geological Survey. Accessed November 21, 2017 from https://pubs.usgs.gov/tm/2006/tm1D3/pdf/TM1D3.pdf
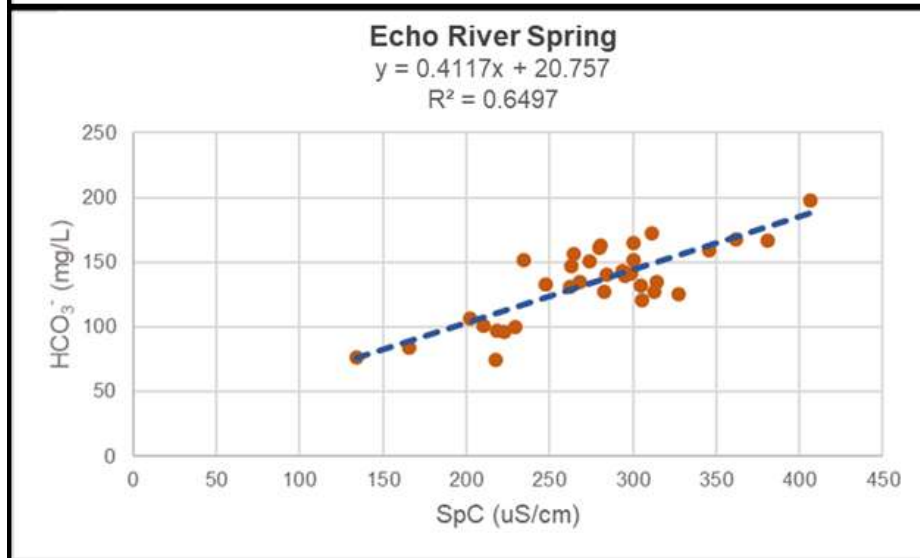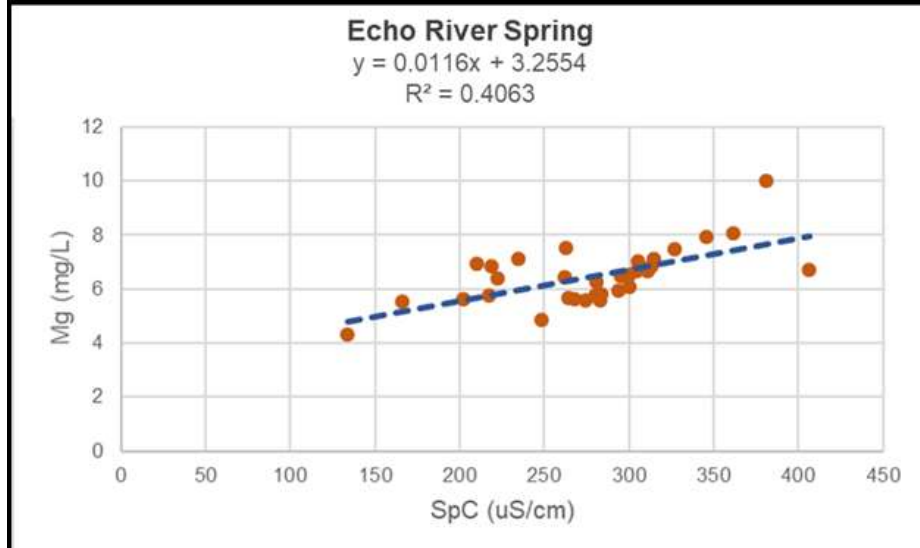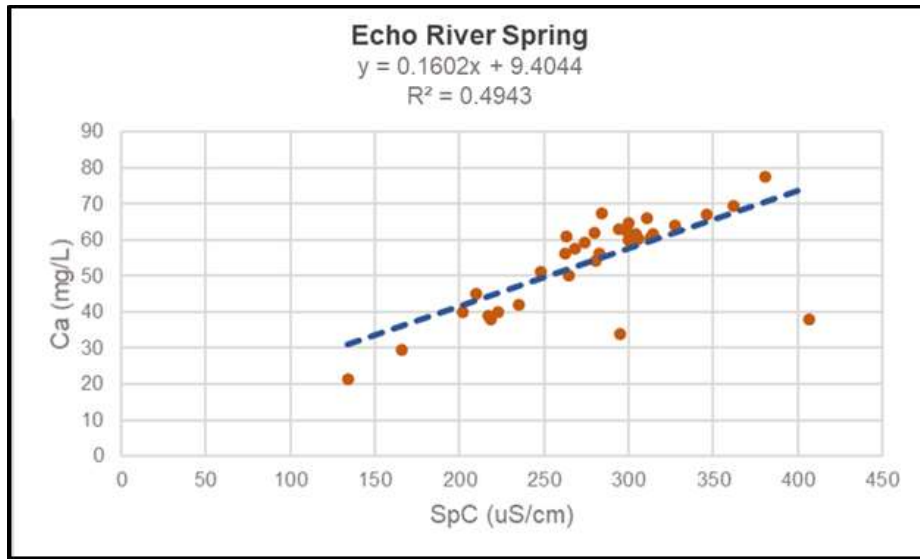
White. W.B., 1988. *Geomorphology and hydrology of karst terrains.* New York, NY: Oxford University Press.

White, W.B., 1989. Introduction to the karst hydrology of the Mammoth Cave area. In: White, W.B., White, E.L. ed. *Karst hydrology: concepts from the Mammoth Cave area.* New York, NY: Van Nostrand Reinhold.

White, W.B., Deike, III, G.H., 1989. Hydraulic geometry of cave passages. In: White, W.B., White, E.L. ed. *Karst hydrology: concepts from the Mammoth Cave area.* New York, NY: Van Nostrand Reinhold.

White, W.B., White, E.L., 2017. Hydrology and hydrogeology of Mammoth Cave. In: Hobbs, H.H., Olson, R.A., Winkler, E.G., Culver, D.C., ed. *Mammoth Cave: A human and natural history.* Springer Online.

Wilde, F.D., Radtke, D.B., Gibs, J., and Iwatsubo, R.T., 2004 (rev. 2009). Processing of water samples. In *USGS Techniques of Water-Resources Investigations, Book 9.* Reston, VA: U.S. Geological Survey. Accessed November 19, 2017 from https://water.usgs.gov/owq/FieldManual/chapter5/html/Ch5_contents.html

Wilde, F.D., Sandstrom, M.W., Skrobialowski, S.C. 2015. National field manual for the collection of water-quality data. U.S. Geological Survey Techniques of Water-Resources Investigations, Book 9. Reston, VA: U.S. Geological Survey. Accessed November 19, 2017 from https://water.usgs.gov/owq/FieldManual/

Worthington, S.R.H., Ford, D.C., Beddows, P.A., 2000. Porosity and permeability enhancement in unconfined carbonate aquifers as a result of solution. In: Klimchouck, A.B., Ford, D.C., Palmer, A.N., Dreybodt, W., ed. *Speleogenesis: evolution of karst aquifers.* Huntsville, AL: National Speleological Society.

Yang, R.Y., Liu, Z., Min Zhao, C.Z., 2012. Response of epikarst hydrochemical changes to soil CO_2 and weather conditions at Chenqi, Puding, SW China. *Journal of Hydrology* 468-469 , 151-158.

Yang, R., Zhao, M., Zeng, C., Chen, B., Liu, Z., 2015. Spatiotemporal variations of soil CO_2 in Chenqi, Puding, SW China: The effects of weather and LUCC. In: Andreo, B., Carrasco, F., Duran, J.J., Jiménez, P., LaMoreaux, J.W., ed., *Hydrogeological and Environmental Investigations in Karst Systems*. Verlag Berlin: Springer.

Zhang, J., Quay, P.D., Wilbour, D.O. 1995. Carbon isotope fractionation during gaswater exchange and dissolution of CO_2. *Geochemica et Cosmochemica Acta* 59, 107-114.

Zhang, L., Qin, X., Liu, P., Huang, Q., Lan, F., Ji, H. 2015. Estimation of carbon sink fluxes in the Pearl River basin (China) based on a water-rock-gas-organism interaction model. *Environmental Earth Science* 74, 945-952.
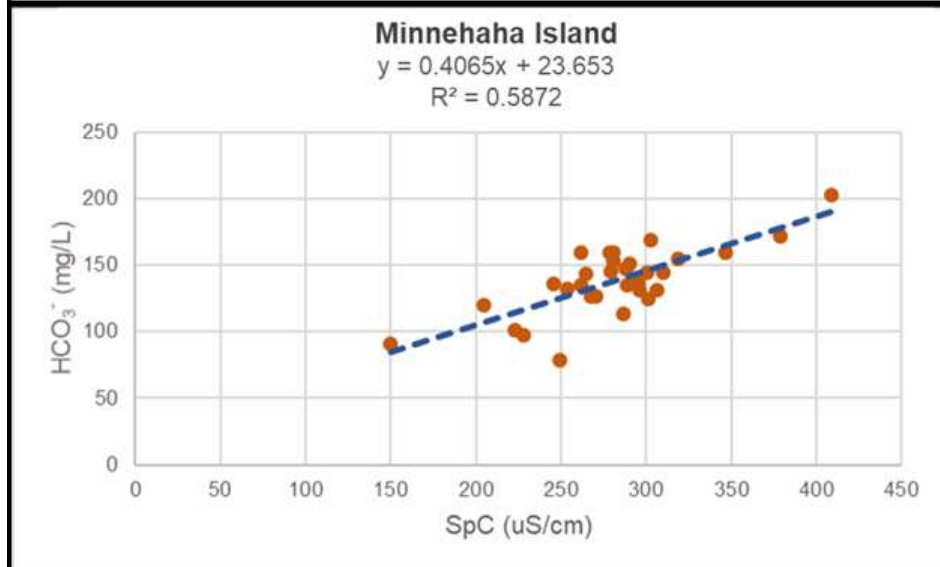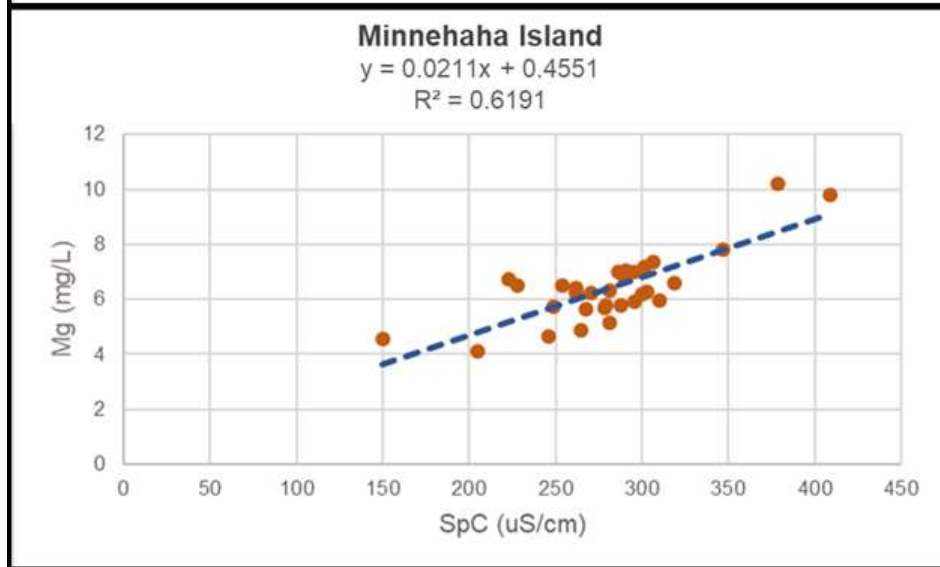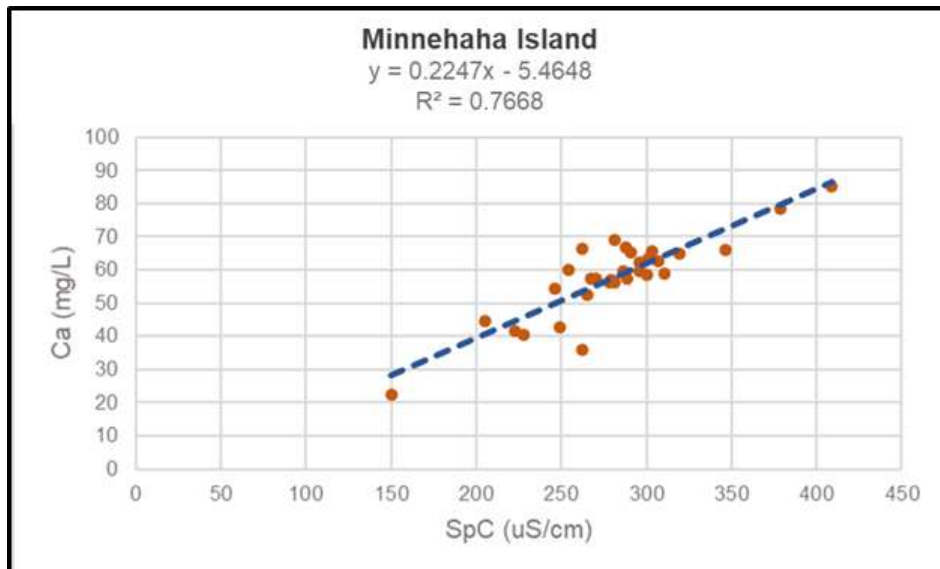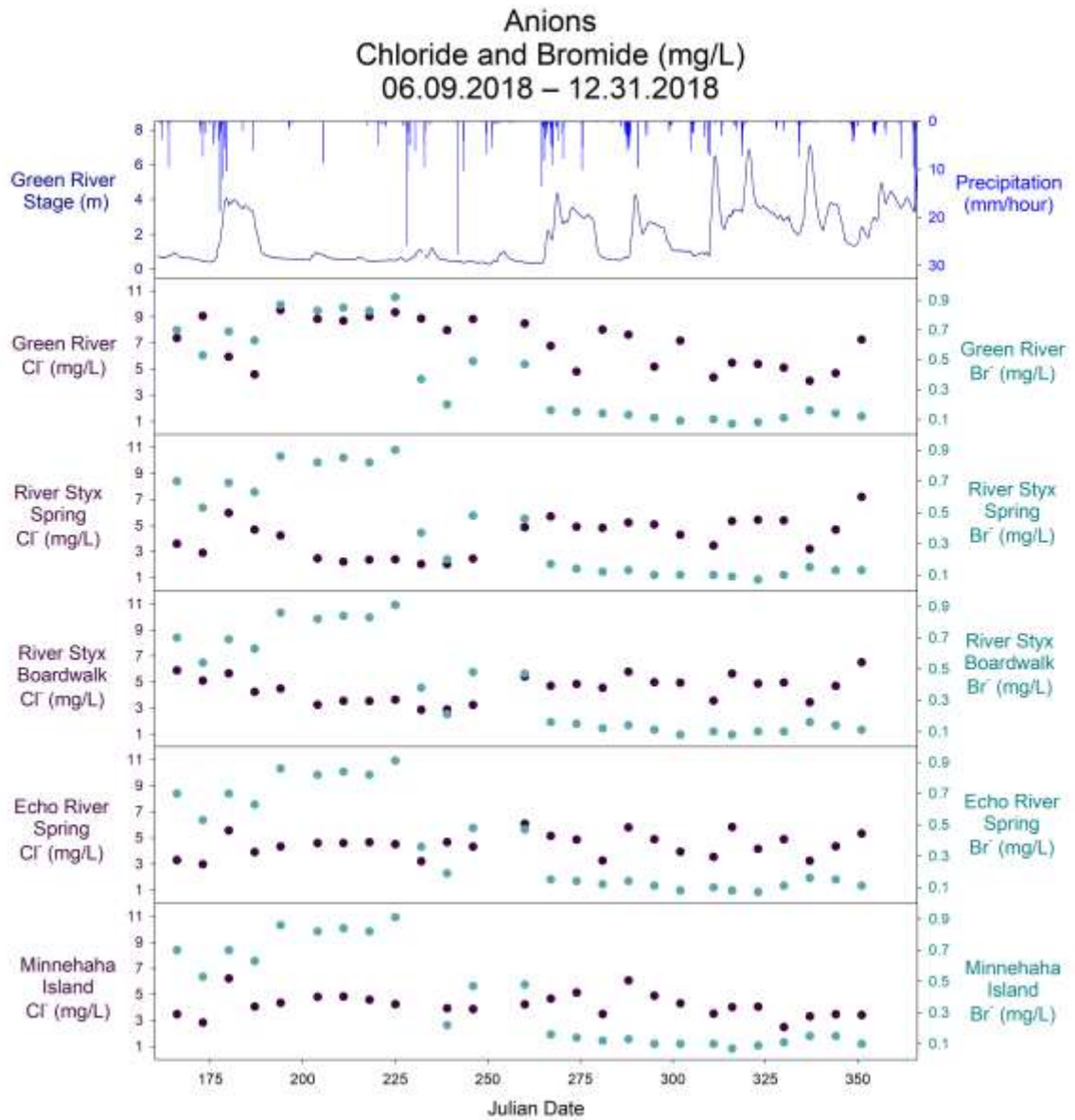
Appendix I: SpC Statistical Relationships

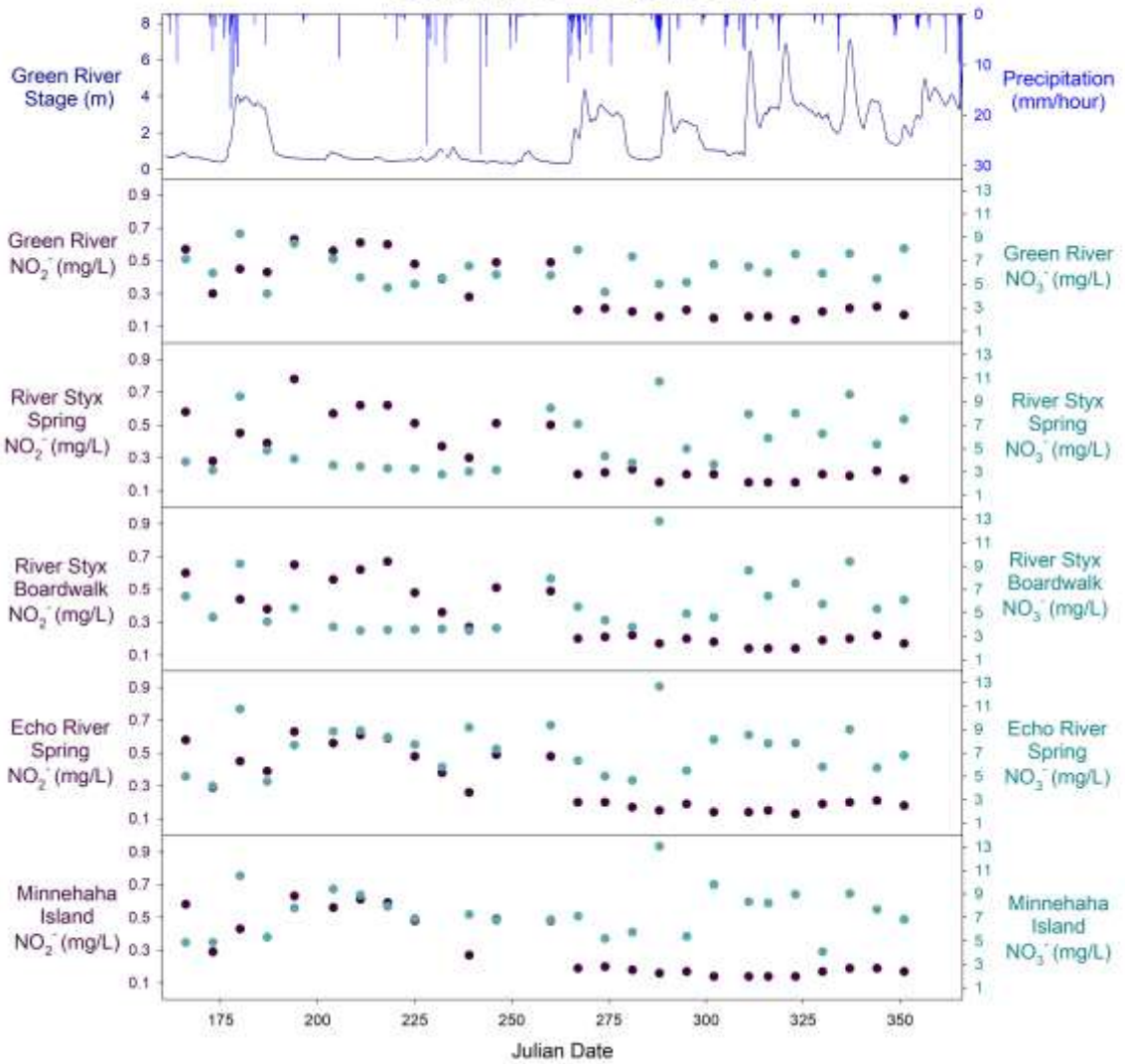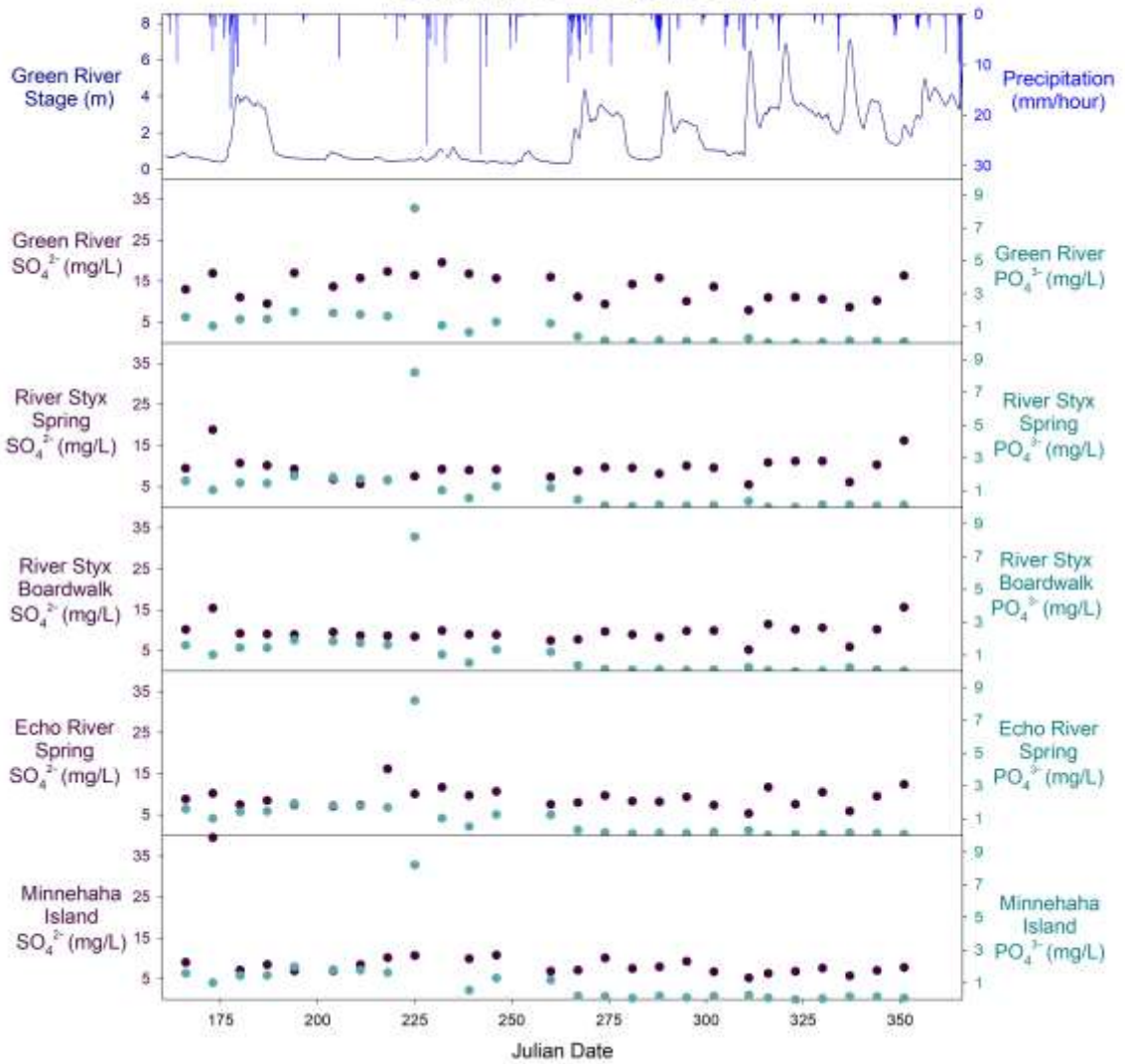**Green River**
$$y = 0.1516x + 11.931$$
$$R^2 = 0.45$$

Green River
$$y = 0.0233x + 1.2443$$
$$R^2 = 0.7922$$

Green River
$$y = 0.4624x + 1.9697$$
$$R^2 = 0.4162$$

178

River Styx Spring
y = 0.1916x + 0.5732
R² = 0.6797

River Styx Spring
y = 0.009x + 3.8068
R² = 0.1348

River Styx Spring
y = 0.5446x - 8.6195
R² = 0.4435

179

River Styx Boardwalk
y = 0.1805x + 1.1328
R² = 0.7234

River Styx Boardwalk
y = 0.0127x + 3.1634
R² = 0.3614

River Styx Boardwalk
y = 0.4351x + 11.037
R² = 0.6121

180

Echo River Spring
y = 0.1602x + 9.4044
R² = 0.4943

Echo River Spring
y = 0.0116x + 3.2554
R² = 0.4063

Echo River Spring
y = 0.4117x + 20.757
R² = 0.6497

181

Minnehaha Island

y = 0.2247x - 5.4648

$R^2 = 0.7668$

Minnehaha Island

y = 0.0211x + 0.4551

$R^2 = 0.6191$

Minnehaha Island

y = 0.4065x + 23.653

$R^2 = 0.5872$

Appendix II: Other Water Analyses Data

Anions
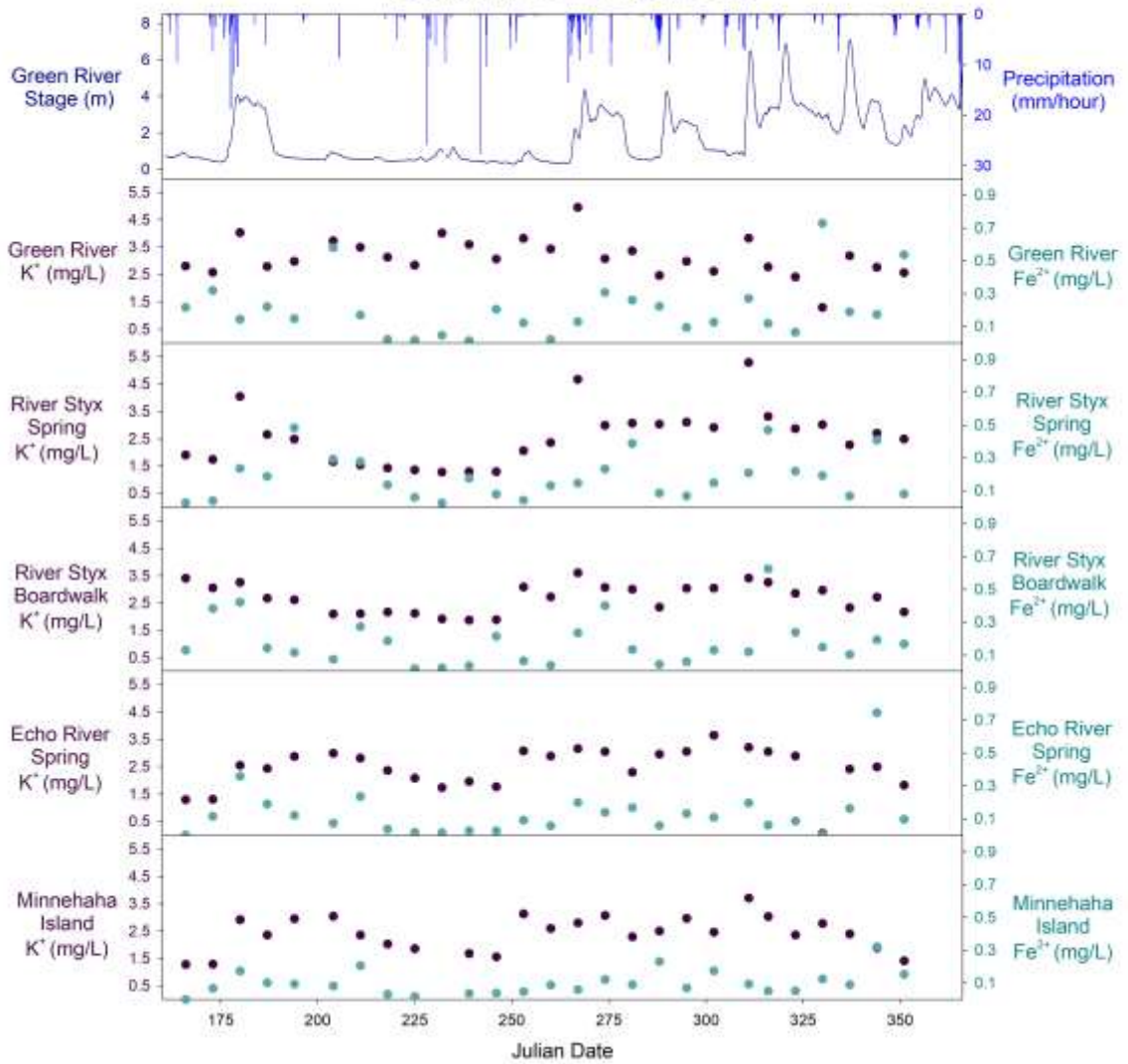Chloride and Bromide (mg/L)
06.09.2018 – 12.31.2018

Anions
Nitrite and Nitrate (mg/L)
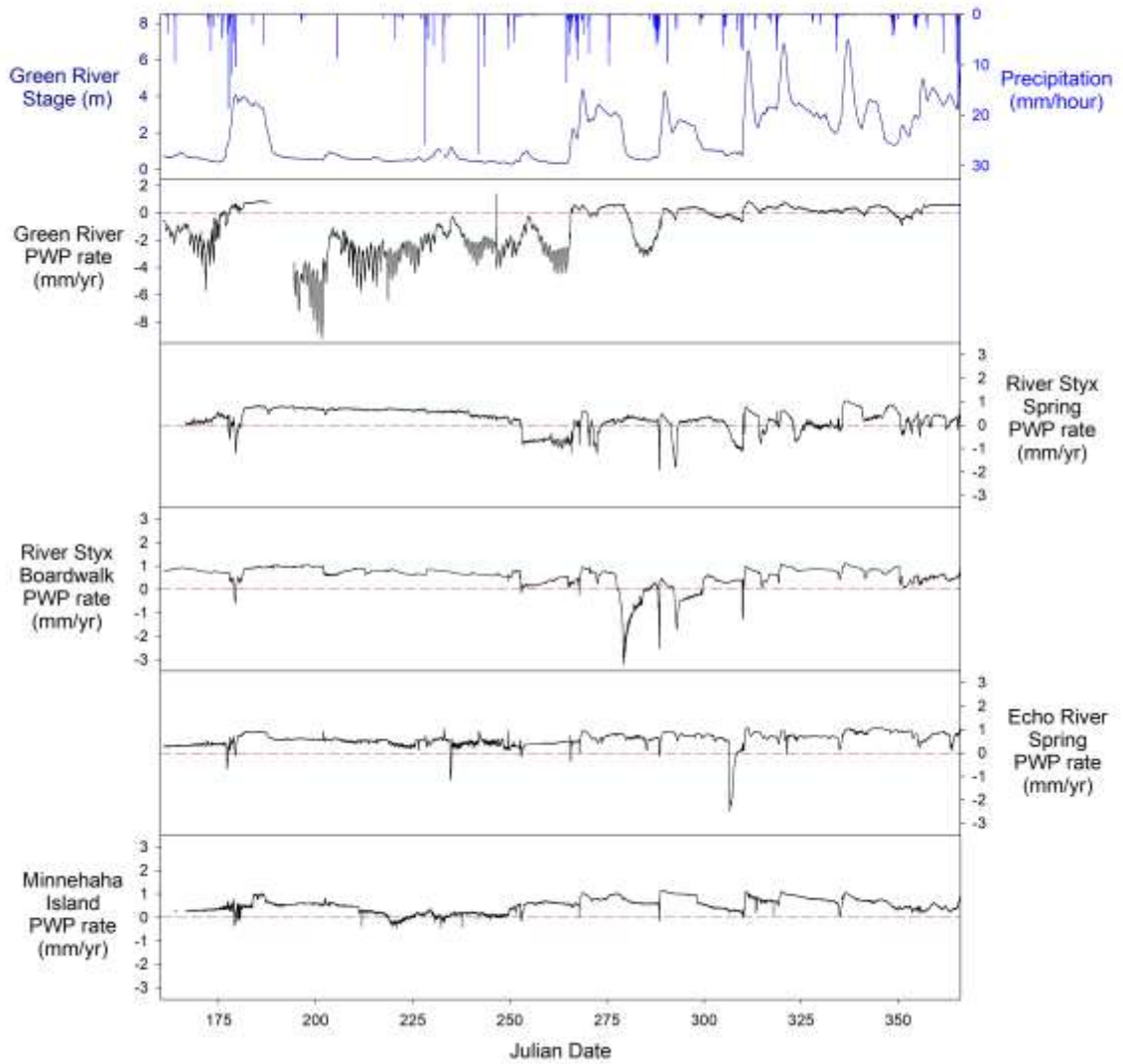06.09.2018 – 12.31.2018

184

Anions
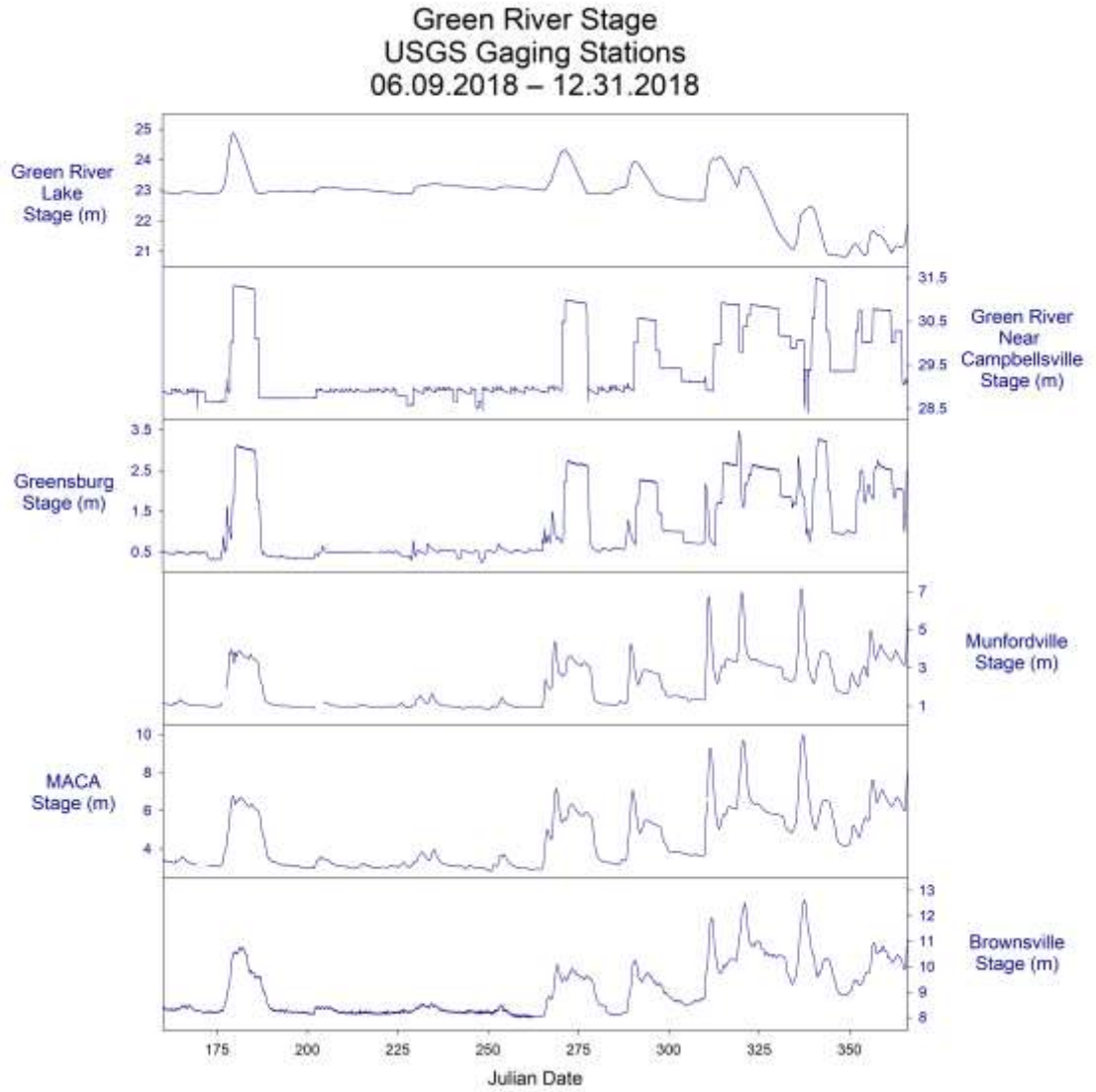## Sulfate and Phosphate (mg/L)
06.09.2018 – 12.31.2018

Cations
Potassium and Iron (mg/L)
06.09.2018 – 12.31.2018

Calcite Dissolution
Plummer-Wigley-Parkhurst
06.09.2018 – 12.31.2018

Appendix III: Green River Stage and Discharge Data

Green River Stage
USGS Gaging Stations
06.09.2018 – 12.31.2018

Green River Discharge
06.09.2018 – 12.31.2018

Green River Q-SI$_{cal}$ Relationship

$y = -0.294\ln(x) + 0.2357$
$R^2 = 0.7637$

189